Beyond the Standard Higgs at the LHC: present constraints on Little Higgs models and future prospects

Dissertation

zur Erlangung des Doktorgrades
an der Fakultät für Mathematik,
Informatik und Naturwissenschaften
Fachbereich Physik
der Universität Hamburg

vorgelegt von

MARCO TONINI

aus

BOLZANO, ITALIEN

Hamburg

2014

Gutachter/in der Dissertation:	Dr. Jürgen Reuter Prof. Dr. Gudrid Moortgat–Pick
Gutachter/in der Disputation:	Prof. Dr. Alessandro Mirizzi Prof. Dr. Peter Schleper Dr. Frank Tackmann
Datum der Disputation:	13. Oktober 2014
Vorsitzender des Prüfungsausschusses:	Prof. Dr. Michael Rübhausen
Vorsitzende des Promotionsausschusses:	Prof. Dr. Daniela Pfannkuche
Dekan des Fachbereichs Physik:	Prof. Dr. Heinrich Graener

Abstract

This thesis discusses the consistency of different Little Higgs models with the collected collider data as of the summer of 2013. Moreover, future prospects for possible discoveries and mass measurement methods of new physics signals at the foreseen LHC run II with increased center–of–mass energy are presented. Little Higgs models belong to a class of extensions of the Standard Higgs model, predicting a strong interaction regime at a compositeness scale $\Lambda = 4\pi f$ above the electroweak scale v. The Higgs boson arises as a pseudo–Goldstone boson of an approximate global symmetry spontaneously broken at the scale f. A natural hierarchy between the compositeness and the electroweak scale is introduced by the Collective Symmetry Breaking mechanism: one–loop diagrams generating the Higgs mass term are forced to be at most logarithmically sensitive to Λ. A naturally light Higgs boson can thus be accommodated, consistently with a perturbative theory until a scale of order 10 TeV. We have probed the parameter space of three prominent examples of Little Higgs models, namely the Simplest Little Higgs model, the Littlest Higgs model, and the Littlest Higgs model with T–parity, against electroweak precision observables and the collected LHC data concerning both Higgs properties and direct searches for new particles, with $\sqrt{s} = 7,\ 8\,\mathrm{TeV}$ and up to $25\,\mathrm{fb}^{-1}$ of integrated luminosity. Lower bounds on the scale f are set, within a certain degree of confidence level, which allow to draw conclusions on the "naturalness" of the different models. Optimisations of the existing direct searches setups, assuming a Little Higgs signal, as well as dedicated mass measurement methods designed for the foreseen LHC runs with $\sqrt{s} = 13,\ 14\,\mathrm{TeV}$ are thoroughly discussed and proposed in this thesis. Special attention will be dedicated to final states including either a large or negligible fraction of missing transverse momentum. In particular, we will propose a dedicated collider search tailored for the discovery and mass measurement of a top partner, exploiting jet–substructure techniques and optimised kinematical selection cuts, as well as a mass measurement method for the topology of semi–invisibly decaying particles, pair produced from the decay of a resonance.

Zusammenfassung

Die vorliegende Arbeit erörtert die Übereinstimmung verschiedener Little–Higgs–Modelle mit den bis Sommer 2013 an Teilchenbeschleunigern gesammelten Daten und die Aussicht auf mögliche Entdeckungen von und Massenbestimmungsmethoden für Anzeichen neuer Physik durch den geplanten Betrieb des LHC mit einer höheren Schwerpunktsenergie. Little–Higgs–Modelle gehören zu einer Klasse von Erweiterungen des Standard–(Higgs–) Modells, die oberhalb der elektroschwachen Skala v ein Regime starker Wechselwirkung bei einer Skala $\Lambda = 4\pi f$ vorhersagt. Das Higgs Boson geht als Pseudo–Goldstone Boson aus einer approximativen globalen Symmetrie hervor, die bei der Skala f spontan gebrochen wird. Der kollektive Symmetrie–Brechungs–Mechanismus bewirkt dabei eine natürliche Hierarchie zwischen den Skalen Λ und v: Die Ein–Schleifen–Diagramme, die den Higgs–Massen–Term generieren, sind zwangsläufig höchstens logarithmisch abhänging von Λ. Dadurch kann ein natürlicherweise leichtes Higgs Boson innerhalb einer bis zu einer Skala von der Ordnung 10 TeV perturbativen Theorie konsistent verwirklicht werden. Der Parameterraum von drei prominenten Beispielen von Little–Higgs–Modellen, nämlich des Simplest Little Higgs Modells, des Littlest Higgs Modells und des Littlest Higgs Modells mit T–Parität wurde auf Übereinstimmung mit elektroschwachen Präzisionsobservablen und den LHC Daten bezüglich Higgs-Eigenschaften und der direkten Suche nach neuen Teilchen (bei $\sqrt{s} = 7, 8\,\mathrm{TeV}$ und bis zu $25\,\mathrm{fb}^{-1}$ integrierter Luminosität) untersucht. Mit einer festgelegten statistischen Genauigkeit werden untere Grenzen für die Skala f ermittelt, die es erlauben, die Natürlichkeit der verschiedenen Modelle zu beurteilen. Ausserdem werden in dieser Arbeit Optimierungsmöglichkeiten für die direkte Suche nach neuen Teilchen unter Annahme eines Little–Higgs–Signals sowie geeignete Methoden zur Massenbestimmung, die auf den $\sqrt{s} = 13, 14\,\mathrm{TeV}$ Betrieb des LHC zugeschnitten sind, vorgeschlagen und ausführlich diskutiert. Besondere Aufmerksamkeit wird Endzuständen mit entweder sehr grossem oder verschwindend geringem Anteil von fehlendem Transversal–Impuls geschenkt. Insbesondere wird eine eignens für die Entdeckung und Massenbestimmung eines Top–Partners optimierte Suche an Beschleunigern, die auf Jet-Substruktur-Methoden und optimierten kinematischen Selektionsschnitten basiert, sowie eine Methode zur Massenbestimmung für die Topologie von semi–unsichtbar zerfallenden Teilchen, die paarweise durch den Zerfall einer Resonanz produziert wurden, vorgeschlagen.

Acknowledgements

The first thanks to Elisa: the daily love and company have been and will always be a gift for which be grateful every day. Thanks for supporting me with patience and love, correcting me when needed, and for your smile that drives away the clouds!

Together with Elisa a special thanks to my whole family: Stefano, Giuliano, Marina, grandpa Nino & friends. The trial of the distance has proven again how the roots of our family allow the trees to grow and the fruit to ripen. Thanks to your sacrifices and willingness I have been given the possibility to undertake this exciting learning adventure, from Trento to Padova and Hamburg, and I will always be grateful to you. Together with you a big thanks to all my uncles, aunts and cousins!

I would like to thank my supervisor, Jürgen Reuter, for the opportunity he has granted me to work at DESY: it has been a joy learning to do research and enjoying this work. Thanks for the work together during these three years and for the comments on my thesis. I would like to thank Gudi for her willingness to be co–referee of my work, and Andreas Weiler for his enlightening lectures on BSM Physics. Also fundamental for me have been all my research collaborators, which I would like to thank sincerely, and all people who answered with patience lots of my questions, in particular Jürgen, Maikel, Kazuki, Lucian and Maxim Perelstein.

A big thanks to my DESY friends: the discovery of a friendship is even more valuable than a scientific discovery! Maikel: thanks for all I have learnt from you, I became not only a much better physicist than I was three years ago, but most of all a better person. Thanks for the research we have been doing together, and for your brotherly friendship: it has been an experience that I will always remember with gratitude. We will meet then one day to see again the *Lost*–finale ;-) Martin: your intelligence and dedication have inspired me since the first day I have met you. It is a privilege to be your friend! Paolo Gunnellini: thanks for a friendship that has grown till becoming fundamental in every aspect of life, from work to friendship, from faith to love. The seniors of our group, Francisco, Marco & Sara with Mattia, and then the experimental friends, Marco Filipuzzi and Francesco Costanza: the time we spent together made the experience in Hamburg even more brilliant! Last but not least, Stefano: we arrived together in Hamburg as good friends, we finish our PhD as brothers. Thanks for being the engine and glue of our group, and for teaching us *the rules* for a healthy life as PhD students ;-)

Thanks to the friends of Building 1b, starting from Kazuki, a person of rare intelligence, kindness and helpfulness, for the work together and for your friendship, which is very important to me. To my office–mates Peter, Shireen and Lisa: thanks for your kindness, for the physics discussions, and for the laughs which have made the office a place both productive and welcoming! Then: Martin Vollmann, Stefan Liebler, Tomas Kasemets, Florian Domingo, Andrew Papanastasiou, Max Stahlhofen, Stefan Prestel, Jo Gaunt, Andreas Goudelis, Moritz McGarrie, Frank Tackmann & Markus Diehl for the friendship, physics discussions and lunches together. And of course a thanks to Heidi for the nice chats in German on Fridays after lunch!

My Hamburg "family" deserves the final thanks. The experience to meet again the friendship with Jesus through your faces has been as liberating as decisive. So many are the friends with whom I walked this path, and since all of you know what ties us together, I will just write down your names: Elisabeth, Sara and Tommaso Mazza with their children Francesca, Pietro, Giovanni and Lucia, don Romano, Ralf, Tommaso Cardani, Marco Berci, Andrea, Matteo Pezzi, Miriam, Lucia, Chiara, Giorgia, Benno, Rosario, Antonio, Benedetta, Luca, Enrico Suzzani, the sisters of Mother Teresa, Points Coeur Berlin, Piero Ferrarese for his friendship without borders, and the great families Spee, Carcano, Bachstein & Lenke all around Germany. The Pfarrgemeinde St. Bonifatius is a continuous discovery, too, in particular Pfarrer Johannes Peter Paul, Schwester Monika Maria, Robert with Carmen, Tobias, and Dominik with family. But the biggest thanks to Paolo, Laura and children Bolzoni, and Matteo Pasi, with the gratitude for having recognised especially with you that, in the end, it is Him who is taking the initiative.

Ringraziamenti

Il primo grazie ad Elisa: l'amore e compagnia quotidiani sono stati e continuano ad essere un regalo di cui ringraziare ogni giorno. Grazie per avermi sempre sostenuto con pazienza ed amore, corretto quando ce n'era bisogno, e per il tuo sorriso che scaccia le nubi!

Insieme ad Elisa un ringraziamento speciale a tutta la mia famiglia: Stefano, Giuliano, Marina, nonno Nino & friends. La prova della lontananza ha dimostrato ancora una volta come le radici della nostra famiglia permettano agli alberi di crescere e ai frutti di maturare. Grazie anche ai vostri sacrifici e disponibilità mi è stata data la possibilità di intraprendere questa entusiasmante avventura di studio, da Trento a Padova fino ad Amburgo, di cui vi sarò sempre grato. Insieme con voi un grande grazie agli zii e cugini tutti!

Vorrei ringraziare il mio supervisor, Jürgen Reuter, per l'opportunità che mi ha concesso di lavorare a DESY: è stata una gioia poter imparare a fare ricerca e godere di questo lavoro. Grazie per il lavoro insieme in questi tre anni, e per i commenti alla tesi. Ringrazio Gudi per la sua continua disponibilità ad essere co–supervisor del mio lavoro, ed Andreas Weiler per il suo illuminante corso di BSM Physics. Sono stati fondamentali per me poi tutti i collaboratori di ricerca, che ringrazio sinceramente, e le persone che con pazienza hanno risposto a molte mie domande, in particolare Jürgen, Maikel, Kazuki, Lucian e Maxim Perelstein.

Un grande grazie ai miei amici di DESY: la scoperta di un'amicizia vale anche più di una scoperta scientifica! Maikel: grazie a quello che ho imparato da te, non solo posso dirmi un fisico molto migliore di quello che ha iniziato tre anni fa, ma soprattutto una persona migliore. Grazie per la ricerca fatta insieme e per la tua amicizia fraterna: è stata un'esperienza che ricorderò sempre con gratitudine. Ci ritroveremo poi un giorno a vedere di nuovo il finale di *Lost* ;-) Martin: la tua intelligenza e dedizione mi hanno ispirato fin dal primo giorno che ti ho conosciuto, è un privilegio essere tuo amico! Paolo Gunnellini: grazie per un'amicizia che è cresciuta nel tempo fino a diventare fondamentale per ogni ambito della vita, dal lavoro all'amicizia, dalla fede al voler bene. I senior del gruppo, Francisco, Marco & Sara con Mattia, e poi gli amici sperimentali, Marco Filipuzzi e Francesco Costanza: il tempo passato insieme ha reso ancora più bella l'esperienza ad Amburgo! Last but not least, Stefano: siamo arrivati insieme ad Amburgo da buoni amici, finiamo il dottorato da fratelli. Grazie per essere stato il motore e il collante dell'amicizia del nostro gruppo, e per averci insegnato *le regole* per una sana vita da dottorandi ;-)

Grazie agli amici del Building 1b, a partire da Kazuki, persona di rara intelligenza, bontà e disponibilità, per il lavoro insieme e per la tua amicizia per me molto importante! I miei compagni di ufficio Peter, Shireen e Lisa: grazie per la vostra gentilezza, per le discussioni di fisica, e per le risate che hanno reso il posto di lavoro un luogo sia produttivo che accogliente! E poi: Martin Vollmann, Stefan Liebler, Tomas Kasemets, Florian Domingo, Andrew Papanastasiou, Max Stahlhofen, Stefan Prestel, Jo Gaunt, Andreas Goudelis, Moritz McGarrie, Frank Tackmann & Markus Diehl per l'amicizia, le discussioni di fisica e i pranzi insieme. E ovviamente un grazie a Heidi per le belle chiacchierate in tedesco del venerdì dopo pranzo!

La mia "famiglia" di Amburgo merita poi il grazie finale. L'esperienza di incontrare di nuovo l'amicizia di Gesù attraverso i vostri volti è stata tanto liberante quanto decisiva. Tanti sono gli amici con cui si è fatto un pezzo di strada insieme, ed ognuno ha presente ciò che ci unisce, per cui mi limito a scrivere i vostri nomi: Elisabeth, Sara e Tommaso Mazza con i figli Francesca, Pietro, Giovanni e Lucia, don Romano, Ralf, Tommaso Cardani, Marco Berci, Andrea, Matteo Pezzi, Miriam, Lucia, Chiara, Giorgia, Benno, Rosario, Antonio, Benedetta, Luca, Enrico Suzzani, le suore di Madre Teresa, Points Coeur Berlin, Piero Ferrarese per la sua amicizia senza confini, e le grandi famiglie Spee, Carcano, Bachstein & Lenke in giro per la Germania. Una scoperta continua è poi la parrocchia di St. Bonifatius, in particolare Pfarrer Johannes Peter Paul, Schwester Monika Maria, Robert con Carmen, Tobias, e Dominik con famiglia. Il grazie più grande però a Paolo, Laura e figli Bolzoni, e Matteo Pasi, con la gratitudine di aver riconosciuto soprattutto con voi che, in fondo, ha preso Lui l'iniziativa.

List of publications

This thesis is based on the following publications:

[1] J. Reuter and M. Tonini, *Can the 125 GeV Higgs be the Little Higgs?*, JHEP **1302** (2013) 077, [arXiv:1212.5930].

[2] J. Reuter, M. Tonini and M. de Vries, *Little Higgs Model Limits from LHC - Input for Snowmass 2013*, arXiv:1307.5010.

[3] J. Reuter, M. Tonini and M. de Vries, *Littlest Higgs with T–parity: Status and Prospects*, JHEP **1402** (2014) 053, [arXiv:1310.2918].

[4] L. A. Harland–Lang, C.–H. Kom, K. Sakurai and M. Tonini, *Sharpening* m_{T2} *cusps: the mass determination of semi–invisibly decaying particles from a resonance*, JHEP **1406** (2014) 175, [arXiv:1312.5720].

[5] J. Reuter and M. Tonini, *Top Partner Discovery in the* $T \to tZ$ *channel at the LHC*, arXiv:1409.6962.

Declaration on oath

I hereby declare, on oath, that I have written the present dissertation by my own and have not used other than the acknowledged resources and aids.

Hamburg, the 18th August 2014

Marco Tonini

Eidesstattliche Erklärung

Hiermit erkläre ich an Eides statt, dass ich die vorliegende Dissertationsschrift selbst verfasst und keine anderen als die angegebenen Quellen und Hilfsmittel benutzt habe.

Hamburg, den 18. August 2014

Marco Tonini

Contents

Chapter 1

Introduction

If I have seen further it is by standing on the shoulders of giants.

Bernard of Chartres

On the shoulders of giants

The story of the Standard Model of particle physics is a long and impressive sequence of theoretical and experimental milestones, where the effort of scientists in the 20th century contributed to formulate one of the most remarkable and well–established scientific theories describing an aspect of Nature, namely the interactions between (massive) elementary particles.

From the theoretical side, the modern formulation of particle physics has its roots in the development of quantum field theory in the late 1920s: in particular, a quantum mechanical formulation compatible with Einstein's special relativity has been realised thanks to the work of physicists including Bohr, Dirac, Heisenberg, Pauli and Schrödinger. This led to the proposal of Quantum Electrodynamics as a relativistic quantum field theory of the electromagnetic field and fermionic charges, describing many processes at lowest order of the perturbative expansion in the electromagnetic coupling.

It was however only in the 1950s that the theoretical community was able to provide predictions of remarkable precision within the framework of Quantum Electrodynamics, namely only after proposing a consistent treatment of the otherwise puzzling divergences appearing at higher orders in the aforementioned perturbative expansion. This has been the great contribution of physicists like Tomonaga, Schwinger, Dyson and Feynman.

In the 1950s, a consistent formulation of Quantum Electrodynamics as a $U(1)$ gauge theory, and a further generalisation to non–abelian gauge groups like $SU(2)$, has been developed thanks to the work of e.g. Yang and Mills. However, troubles involving the generation of mass terms for otherwise massless gauge bosons were still plaguing the proposed theories.

The discovery by Nambu, Goldstone and others in the early 1960s that spontaneous symmetry breaking introduces additional scalar degrees of freedom in a quantum field theory (Nambu–Goldstone bosons), provided the final boost for the modern formulation of the Standard Model of weak interactions. Indeed in 1964 three different collaborations independently proposed the generalisation of spontaneous symmetry breaking to relativistic gauge theories, namely by R. Brout and F. Englert [1], by G. Gouralnik, C. R. Hagen and T. Kibble [2], and by P. Higgs [3,4]. The crucial idea is that the Nambu–Goldstone bosons of a spontaneously broken gauge quantum theory become unphysical and take over the role of the "cancellon" fields in the BRST quartets, while the longitudinal polarisations of the gauge bosons become now physical. This allows to consistently describe a gauge quantum theory of massive gauge bosons.

In 1967 Glashow, Salam and Weinberg formulated a model of electroweak interactions in terms of an $SU(2) \otimes U(1)$ gauge theory, unifying the QED electromagnetic theory with the weak interactions previously described by Fermi's contact interaction Lagrangian. The mechanism of spontaneous symmetry breaking allowed for the consistent introduction of mass terms for weak $W^{\pm}, Z$ gauge bosons, accounting for the weakness of weak interactions at low energies, while leaving massless the QED photon. This was indeed achieved by introducing a scalar field, namely the Higgs field, whose vacuum expectation value triggers the spontaneous breaking of the electroweak $SU(2) \otimes U(1)$ gauge symmetry to the residual QED $U(1)_{\text{em}}$ symmetry. Couplings of the Higgs field to fermion fields, called Yukawa couplings, furthermore provide a consistent mechanism to generate masses and mixings of quarks and leptons. It is important to note that the introduction of the Z boson via the $SU(2) \otimes U(1)$ gauge symmetry was only a speculative statement at that point, since no experimental sign of short–distance neutral interactions was observed.

A parallel development was carried out for a quantum description of the spectrum of different hadrons, especially during the 1960 thanks to the work of e.g. Gell–Mann among others. This led to the introduction of the concept of quarks as particles transforming as a vector under a flavour symmetry, as well as being charged under an additional quantum number in order to be consistent with Pauli's exclusion principle, namely the colour charge. The quantum theory of strong interactions was formulated as Quantum Chromodynamics with the quarks charged under an $SU(3)$ colour quantum number, and the gluons as the $SU(3)$ gauge bosons. The discovery of asymptotic freedom by Gross, Wilczek and Politzer in 1973 then allowed to make precise predictions for the behaviour of QCD at high–energy experiments, as well as providing a plausible understanding of the confining behaviour of the strong force at low–energies, where bound states of quarks are created generating the observed hadronic spectrum.

We also need to mention the crucial work of 't Hooft and Veltman in 1971, too: by proving the renormalisability of Yang–Mills theories, as well as introducing the tool of dimensional regularisation for consistently calculating divergent integrals in quantum field theory, they provided another step towards the established Standard formulation of the electroweak and strong interactions.

From the experimental side, spectacular achievements have always been going along the theoretical steps. Without aiming for a comprehensive list of relevant experimental investigations of the Standard Model, we have to remember for example the 1956 experiment carried out by the group led by C.–S. Wu proving CP violation in weak interactions; the measurement proving left–handedness of weak interactions in 1957 by M. Goldhaber; deep inelastic scattering experiments at SLAC in 1969 and later e^+e^- experiments at PETRA and LEP, spectacularly confirming the structure of the strong interactions; the discovery of neutral weak currents and the determination of the weak mixing angle in 1973 via a neutrino experiment at the Gargamelle bubble chamber at CERN, confirming the $SU(2) \otimes U(1)$ gauge structure of weak interactions; the charm quark discovery in 1974 at SLAC/BNL; the discovery of the electroweak $W^{\pm}, Z$ bosons with the UA1, UA2 detectors of the CERN Super Proton Synchrotron in 1983, as well as the countless precision experiments at LEP which have explored the nature of the gauge interactions with extremely high precision. More recently, the confirmation of the top quark in 1995 at the Tevatron collider has further consolidated the validity of the Standard Model.

One of the few "missing pieces" of the Standard Model, waiting for a direct experimental confirmation for nearly 50 years and only recently obtained at the LHC, has been ironically enough the most important one, namely the Higgs boson. The Higgs boson is indeed the quantum excitation of the Higgs field responsible for the mechanism of electroweak symmetry breaking: while the spontaneous symmetry breaking was satisfyingly proved by the discovery of the predicted electroweak gauge bosons, its explicit realisation through an $SU(2)$–doublet scalar field had evaded so far the attempts for an experimental confirmation.

The Large Hadron Collider era

Nowadays, with the advent of the Large Hadron Collider (LHC), a whole new range of energies is opening up for experimental particle physics, namely the range from the electroweak scale up to the multi–TeV regime. Within the first 2010–2012 run of the LHC crucial results have been already collected, most notably indeed the discovery of a (light) Higgs boson with mass $m_h \sim 125\,\mathrm{GeV}$, publicly announced on the 4th of July 2012 [5, 6]. The discovery of the Higgs boson in the range of mass allowed by precision tests of LEP can be regarded as another success of the theory. Also remarkable are the (preliminary) measurements of the Higgs couplings and production modes, which are turning out to be as predicted by the Standard Model: no significant sign of new phenomena has been observed so far. This is starting to provide severe constraints on possible theories that differ significantly from the Standard Model at the probed energies.

Despite this enormous success, we know that the Standard Model cannot describe all phenomena we have observed so far. In particular, the absence of a possible candidate to describe the Dark Energy and Dark Matter components as observed in various cosmological and astrophysical observations, and the observation of neutrino oscillations proving that neutrinos cannot be massless as in the minimal Standard Model, represent the main experimental results without a “standard” description.

Furthermore, different theoretical motivations are considered as issues of the actual Standard Model formulation above the electroweak scale. In particular we can mention: the flavour puzzle of the Standard Model, namely the absence of a dynamical explanation or a symmetry argument to describe the huge hierarchy among the particle masses and peculiar mixing structure; the matter–antimatter asymmetry, since the sources of CP–violation in the Standard Model (e.g. the phase of the CKM matrix) cannot account for a sufficient contribution for a primordial matter–antimatter asymmetry; the absence of a consistent formulation for the inclusion of gravitational interactions in a single unified theory at higher energies; and last but not least, the fine–tuning problem: a light (fundamental) Higgs boson implies large accidental cancellations between different and in principle uncorrelated physical quantities, due to its large radiative sensitivity to possible higher scales in the theory. In a “natural” theory, large cancellations among uncorrelated terms should either not be present, or explained by means of symmetry arguments.

The issue of a necessary fine–tuning to account for a light Higgs boson has always been the main guideline for possible model building of Beyond the Standard Model Physics:

suitable new phenomena should appear around the TeV energy scale in order to suppress the large radiative corrections to the Higgs mass. The most sought–after solution of the fine–tuning problem at the LHC is Supersymmetry (SUSY). In supersymmetric extensions, the Higgs mass is protected against high–energy radiative corrections by the non–renormalisability of an unbroken supersymmetric theory, while at low energies the Higgs mass gets contributions which are sensitive at most to the SUSY–breaking scale. Another appealing aspect of minimal SUSY is that it is a weakly coupled theory at any scale, assuring perturbative calculability for any possible process.

An alternative solution is given by strongly–coupled extensions of the Standard Model. In this class of models, a new strong interaction sector in assumed at some energy above the electroweak scale, making the Higgs a composite object above the compositeness scale. Since it does not make sense to speak of an elementary scalar Higgs boson above the compositeness scale, at low energies the Higgs mass is thus at most sensitive to the value of the compositeness scale. In this sense, assuming a strong sector as UV–completion of the Standard Model prevents dangerous fine–tuning requirements to account for the observed Higgs mass. In a generic strongly interacting extension of the Standard Model, the compositeness scale would be however close to the Higgs mass, causing a conflict with electroweak precision observables and direct searches for heavy resonances.

A consistent way to implement a strong UV–completion of the Standard Model has been discovered to be represented by models in which the Higgs arises as Goldstone boson of some spontaneously broken global symmetry of the strong sector. In particular, a branch of these strongly coupled theories Beyond the Standard Model is represented by Little Higgs models, with their Collective Symmetry Breaking mechanism generating a “natural” hierarchy between the compositeness scale and the electroweak scale.

Measurements of the Higgs mass and its couplings represent a completely new source of constraints which have to be satisfied by possible extensions of the Standard Model. The more data are collected at the LHC, the more precise these observables can be measured, increasing their discrimination power. In general, these constraints set lower bounds on the compositeness scale, similar to usual electroweak constraints. Consequently, Higgs precision constraints might yield lower bounds on the masses of the additional resonances predicted by Standard Model extensions.

Analogous constraints can be obtained via direct searches for the aforementioned new particles. An important observation is that decay chains involving new particles generate final states which might be mimicked by different (reducible or irreducible) Standard Model processes. The latter represent thus possible backgrounds concealing signatures from Beyond the Standard Model signals: the experimental collaborations usually define several search strategies (cut–and–count analyses) aiming at reducing the Standard Model backgrounds while being sensitive to match possible new physics signals. In the best case scenario for a Beyond the Standard Model point of view, excesses above the Standard Model background should be observed such that evidence or discovery of new physics might be claimed. In the null–result scenario, the direct search analysis is completely consistent with the Standard Model prediction within the experimental uncertainties: in this case, one could only set lower bounds on the masses and/or couplings of the assumed signal spectrum, as with Higgs precision measurements.

Even in the absence of discrepancies with respect to Standard Model predictions, it is of high interest to probe the parameter space of different Beyond the Standard Model extensions by including the latest LHC data, including Higgs searches and direct searches for new particles. If naturalness and fine–tuning have been the main motivation to develop "natural" extensions of the Standard Model, then pushing the scale of new physics (either compositeness– or SUSY–breaking scale or similar) to higher values should analogously provide an indication for the validity of these models, even if the inconsistency of a model through fine–tuning arguments can only be a qualitative statement.

The second run of the LHC with higher center–of–mass energy $\sqrt{s} = 13,\, 14\,\text{TeV}$ and increased integrated luminosity up to several hundreds of fb^{-1}, will certainly shed further light on the question of whether naturalness is the paradigm explaining the physics above the electroweak scale. Also exciting is the possibility to probe the electroweak scale within a completely different experimental environment, namely with possible future Linear Colliders exploiting e^+e^- collisions at much higher center–of–mass energies than the previous LEP and LEP2 experiments at CERN. The foreseen International Linear Collider (ILC), for example, is currently proposed to be built in Japan and performing up to $\sqrt{s} = 500\,\text{GeV}$. Additional kinematic information from e.g. the fixed and known center–of–mass energy of the hard–scattering, represents one of the main advantages by developing a lepton collider, together with many different processes which can be probed thanks to the leptonic initial state not accessible at hadron colliders. A new era of particle physics experiments is therefore already quickly approaching.

Structure of the thesis

The main focus of this thesis is the interpretation of LHC results within the framework of Little Higgs models, and the proposal of several dedicated analyses at the foreseen LHC run II. In **Chapter 2** we will discuss the main features of the $SU(2) \otimes U(1)$ electroweak theory, underlying crucial aspects which led to the introduction of the Higgs boson for the formulation of a phenomenologically consistent theory. The Higgs Model is introduced, as well as a discussion of its shortcomings which represent the main motivation to study possible extensions Beyond the Standard Model. In **Chapter 3** we will first present the general idea of a strong sector as UV–completion of the Standard Model, and then we will focus on the Collective Symmetry Breaking mechanism introduced in Little Higgs models as an attempt of realising a natural strongly coupled electroweak theory. A detailed discussion of Little Higgs models which have been considered in this thesis is also presented. In **Chapter 4** we will present our main results and findings which have been published in refs. [7–9], on the interpretation of existing experimental data within the context of different Little Higgs models. In particular, we included in our analysis measurements of electroweak precision observables, specific Higgs precision observables, and direct searches for new particles. A final section describes a possible optimisation of LHC direct searches targeting Little Higgs topologies. In **Chapter 5** we turn our attention to future experimental searches, namely considering the foreseen LHC run with increased center–of–mass energy at $\sqrt{s} = 13,\ 14\,\text{TeV}$. This part of our results have been published in refs. [10,11]. First, a direct search for a top partner involving top–tagging techniques and optimised selection cuts is presented, and the sensitivity of a top partner mass measurement method is discussed. Secondly, a mass determination method for final states involving large fraction of missing transverse momentum is presented. The discussed method focuses on the topology where a semi–invisibly decaying particle with unknown mass is pair produced from the decay of an s–channel particle. A summary of the results and possible further developments are finally discussed in **Chapter 6**.

Chapter 2

The Standard Model and Beyond

This chapter provides an introduction to the Standard Model of Particle Physics, focussing on the theoretical and experimental evidence which led to the prediction of the Higgs boson. Particular interest will be given to the issues related to perturbative unitarity violation in longitudinal vector boson scattering, and the presence of divergent contributions to precisely measured observables in the electroweak theory without the Higgs boson. We will then describe the shortcomings of the Standard Model including the Higgs boson, giving thus a plausible motivation for different Beyond the Standard Model extensions. We will further present the formalism to describe a quantum theory of Goldstone bosons arising from a spontaneous symmetry breaking, and the example of the low–energy QCD Lagrangian will be given. The main topic of the thesis is indeed concerned with strongly interacting Beyond the Standard Model theories of the Little Higgs type, where the Higgs boson arises as a (pseudo–) Goldstone boson of a spontaneously broken enlarged symmetry. The formalism detailed in this chapter will be of use when describing the structure of the models under consideration. The resources I used for this chapter are refs. [12–17].

2.1 A scalar particle ancestor

Before addressing the concepts that led to the prediction of the Higgs boson, it is worth briefly describing the theoretical modeling of another existing scalar particle, discovered long before the Higgs boson, namely the pion. In terms of modern quantum field theory concepts, the pion is the lightest meson composed of first–generation quarks with mass of roughly 135 MeV and spin 0. The impressive consistency of the low–energy QCD Lagrangian as the correct model describing the experimental properties of the pion might be indeed considered as a useful guideline to understand the physics of other "light" scalar particles such as the Higgs boson.

The crucial idea will be to consider the pion as an emerging Goldstone boson from spontaneous breaking of an approximate global symmetry. In this way, the scalar nature of the pion as well as its relatively light mass compared to the other observed resonances will be straightforward to understand and to describe mathematically. We will start in section 2.1.1 with a rather formal review of Goldstone's theorem and its natural formalism in quantum field theory language, namely the Callan–Coleman–Wess–Zumino (CCWZ) formalism. The pion Lagrangian will arise as the application of the CCWZ formalism to the case of the spontaneous breaking of the (approximate) $SU(3)_{\rm L} \otimes SU(3)_{\rm R}$ global symmetry of QCD. The explicit formulation of the low–energy QCD Lagrangian, as well as its phenomenological consequences, are discussed in section 2.1.2.

We will eventually use the discussed formalism in the context of Electroweak Symmetry Breaking (EWSB) in section 2.2.

2.1.1 CCWZ formalism for Goldstone bosons

Consider a classical field theory with n scalar fields ϕ^A, $A = 1 \dots n$, with a Lagrangian

$$\mathcal{L} = \mathcal{L}_{\rm kin} - V(\phi^A) \tag{2.1}$$

invariant under a Lie group G acting on the scalar fields. Let $\langle \phi^A \rangle$ be the minimum-energy configuration of the potential, and assume there is only a subgroup H of G under which the vacuum configuration is invariant, i.e. $h\langle \phi^A \rangle = \langle \phi^A \rangle \ \forall\ h \in H$. The global symmetry group G is said to be spontaneously broken to the subgroup H in the vacuum configuration. Goldstone's theorem states that there is a zero eigenvalue of the scalar mass matrix for each generator of the coset G/H, namely $\dim({\rm G}) - \dim({\rm H})$ zero eigenvalues.

These flat directions of the potential define the so–called vacuum manifold made of physically equivalent vacua: the excitations along this flat directions are called *Goldstone bosons*, and in a quantum interpretation we identify these excitations as massless scalar particles $\pi(x)$.

It is therefore useful to introduce a parametrisation of the Goldstone bosons for a generic spontaneous symmetry breaking pattern G/H. This prescription is given by the CCWZ formalism [18, 19], which we will review in the following.

Let $\phi(x)$ be a set of scalar fields transforming linearly under the continuous global symmetry group G:

$$g : \phi \to g\,\phi\,. \tag{2.2}$$

If T^a are the generators of H, and X^a are the generators of the coset G/H, the CCWZ prescription is to parametrise $\phi(x)$ as

$$\phi(x) = \xi(x)\,\langle\phi\rangle = e^{i\pi^a(x)\cdot X^a/f}\,\langle\phi\rangle\,, \tag{2.3}$$

where $\pi^a(x)$ are the Goldstone bosons fields, $\langle\phi\rangle$ is the vacuum expectation value which realises the breaking $G \to H$, and f is a mass–dimension one parameter which sets the scale of the symmetry breaking. Notice that the CCWZ definition is independent of the particular representation of ϕ under G.

Naïvely one might say that even $\xi(x)$ transforms linearly as $\phi(x)$ under the action of $g \in G$, but this is not generically true: under a global symmetry transformation g, the matrix $\xi(x)$ is transformed to a new matrix $g\,\xi(x)$, which is in general no longer in standard form, namely

$$g : \xi(x) \to g\,\xi(x) \neq e^{i\pi'(x)\cdot X^a/f}\,. \tag{2.4}$$

In order to have a well-defined linear transformation law for $\phi(x)$, one can use the fact that the vacuum $\langle\phi\rangle$ is invariant under H transformations, namely

$$h\,\langle\phi\rangle = \langle\phi\rangle \quad \forall\, h \in H \tag{2.5}$$

to find a matrix $U_H \in H$ such that $g\,\xi(x)\,U_H^\dagger(g,\pi)$ is in standard form:

$$g\,\phi(x) = g\,[\xi(x)\,\langle\phi\rangle] = g\,\xi(x)\,U_H^\dagger(g,\pi)\,U_H(g,\pi)\,\langle\phi\rangle = g\,\xi(x)\,U_H^\dagger(g,\pi)\,\langle\phi\rangle \overset{!}{=} \xi'(x)\,\langle\phi\rangle\,. \tag{2.6}$$

The matrix $U_H^\dagger(g,\pi)$ depends on g and ξ: therefore, under a transformation $g \in G$ the Goldstone boson fields transform non-linearly as

$$g : \xi(x) \to g\,\xi(x)\,U_H^\dagger(g,\pi)\,. \tag{2.7}$$

On the other hand, ξ transforms linearly under transformations of the unbroken group H

$$h : \xi(x) \to h\,\xi(x)\,h^{-1}\,. \tag{2.8}$$

An explicit example will show the main features of the CCWZ parametrisation. Consider a theory of a single scalar field ϕ where the symmetry breaking pattern $SU(N) \to$

$SU(N-1)$ is realised: following the CCWZ prescription, we parametrise ϕ as

$$\phi = \xi\,\langle\phi\rangle = e^{i\pi^a X^a/f}\,\langle\phi\rangle = \exp\left[\frac{i}{f}\left(\begin{array}{ccc|c} \pi^0 & & & \pi_1 \\ & \ddots & & \vdots \\ & & \pi^0 & \pi_{N-1} \\ \hline \pi_1^* & \dots & \pi_{N-1}^* & -(N-1)\pi_0 \end{array}\right)\right]\begin{pmatrix} 0 \\ \vdots \\ 0 \\ 1 \end{pmatrix}, \tag{2.9}$$

where $\bar{\pi} = (\pi_1, \dots, \pi_{N-1})$ are complex fields, while π_0 is real, representing the $2N-1$ Goldstone bosons of the theory.

We will focus now on the transformation properties of the complex Goldstone boson fields under the broken and unbroken symmetry groups. Under the unbroken $SU(N-1)$ group, ϕ transforms as

$$\phi \xrightarrow{T^a} U_{N-1}\,\phi = \left(U_{N-1}\,e^{i\pi^a X^a/f}\,U_{N-1}^\dagger\right)U_{N-1}\,\langle\phi\rangle = e^{i/f\left(U_{N-1}\,\pi^a X^a\,U_{N-1}^\dagger\right)}\,\langle\phi\rangle \tag{2.10}$$

where in the second equality we used the fact that the vacuum $\langle\phi\rangle$ is invariant under unbroken U_{N-1} transformations. Therefore the Goldstone bosons transform linearly under the unbroken $SU(N-1)$ group:

$$\pi^a X^a \xrightarrow{T^a} U_{N-1}\,\pi^a X^a\,U_{N-1}^\dagger\,. \tag{2.11}$$

Explicitly, a generic $SU(N-1) \subset SU(N)$ transformation can be written as

$$U_{N-1} = \left(\begin{array}{c|c} \hat{U}_{N-1} & 0 \\ \hline 0 & 1 \end{array}\right) \tag{2.12}$$

and we can see that the $N-1$ complex Goldstone bosons transform in the fundamental representation of $SU(N-1)$:

$$\left(\begin{array}{c|c} 0 & \bar{\pi} \\ \hline \bar{\pi}^\dagger & 0 \end{array}\right) \to U_{N-1}\left(\begin{array}{c|c} 0 & \bar{\pi} \\ \hline \bar{\pi}^\dagger & 0 \end{array}\right)U_{N-1}^\dagger = \left(\begin{array}{c|c} 0 & \hat{U}_{N-1}\bar{\pi} \\ \hline \bar{\pi}^\dagger\hat{U}_{N-1}^\dagger & 0 \end{array}\right). \tag{2.13}$$

Under a symmetry transformation of the coset G/H we have on the other hand

$$\begin{aligned} U_{G/H}\,e^{i\pi^a X^a/f}\,\langle\phi\rangle &= \exp\left[i\begin{pmatrix} 0 & \bar{\alpha} \\ \bar{\alpha}^\dagger & 0 \end{pmatrix}\right]\exp\left[\frac{i}{f}\begin{pmatrix} 0 & \bar{\pi} \\ \bar{\pi}^\dagger & 0 \end{pmatrix}\right]\langle\phi\rangle \\ &= \exp\left[i\begin{pmatrix} 0 & \bar{\alpha} \\ \bar{\alpha}^\dagger & 0 \end{pmatrix}\right]\exp\left[\frac{i}{f}\begin{pmatrix} 0 & \bar{\pi} \\ \bar{\pi}^\dagger & 0 \end{pmatrix}\right]U_H^\dagger(\alpha,\pi)\langle\phi\rangle \\ &\overset{!}{=} \exp\left[\frac{i}{f}\begin{pmatrix} 0 & \bar{\pi}' \\ \bar{\pi}'^\dagger & 0 \end{pmatrix}\right]\langle\phi\rangle \end{aligned} \tag{2.14}$$

defining a non–linear transformation law for the Goldstone bosons, as already discussed in the general case. One notices that, to linear order in α, the transformation (2.14) reduces to a shift transformation:

$$\bar{\pi} \xrightarrow{X^a} \bar{\pi}' = \bar{\pi} + \bar{\alpha} \cdot f + \mathcal{O}(\alpha^2)\,. \tag{2.15}$$

The prescription to construct the most general effective field theory for only Goldstone boson degrees of freedom (with all other heavy fields integrated out), is to write down all Lorentz– and G–invariant terms with increasing number of derivatives of the Goldstone boson matrix. However, for general G and H, this is not trivial. Consider for example the two–derivatives term. Naïvely one would write a two–derivatives term using the field $\xi(x)$ in the parametrisation (2.3), i.e.

$$f^2\,\mathrm{Tr}\,|\partial_\mu \xi|^2\,, \tag{2.16}$$

but in general this term is not G–invariant

$$f^2\,\mathrm{Tr}\,|\partial_\mu \xi|^2 \to f^2\,\mathrm{Tr}\left|\partial_\mu\left(g\,\xi(x) U^\dagger(x)\right)\right|^2 \neq f^2\,\mathrm{Tr}\,|\partial_\mu \xi|^2 \tag{2.17}$$

because of the x–dependence in $U(g,\pi) \in H$. Using a bit of algebra one obtains

$$\mathrm{Tr}\;|\partial_\mu \xi|^2 = \mathrm{Tr}\left[(\partial_\mu \xi^\dagger)\xi\xi^\dagger(\partial^\mu \xi)\right] = \mathrm{Tr}\left[\left(\xi^\dagger \partial_\mu \xi\right)^\dagger\left(\xi^\dagger \partial^\mu \xi\right)\right]\,. \tag{2.18}$$

It can be shown that the object $\xi^\dagger \partial_\mu \xi$ decomposes as

$$\xi^\dagger \partial_\mu \xi = v^a_\mu T^a + p^a_\mu X^a\,, \tag{2.19}$$

with the objects $v_\mu \equiv v^a_\mu T^a$ and $p_\mu \equiv p^a_\mu X^a$ transforming as

$$v_\mu \to U(v_\mu + \partial_\mu)U^\dagger\,, \tag{2.20}$$

$$p_\mu \to U\,p_\mu\,U^\dagger\,. \tag{2.21}$$

The field v_μ transforms like a connection, while p_μ is suitable to construct a G–invariant two–derivatives term: the only non-trivial term is given by

$$\mathcal{L}_2 = f^2\,\mathrm{Tr}\left[p^\mu p^\dagger_\mu\right]\,. \tag{2.22}$$

However the form of p_μ and v_μ heavily depends on the specific groups G and H.

Everything simplifies if the Lie algebra G/H is a symmetric space. A symmetric space is a coset space endowed with an involutive automorphism on the generators

$$T^a \to T^a\,, \qquad X^a \to -X^a\,. \tag{2.23}$$

Applying the automorphism to eq. (2.19) we find that p_μ is simply given by

$$p_\mu = \frac{1}{2}\left(\xi^\dagger \partial_\mu \xi - \xi \partial_\mu \xi^\dagger\right) . \tag{2.24}$$

If we then define a field $\Sigma(x)$ as

$$\Sigma(x) = \xi \tilde{\xi}^\dagger = e^{2i\pi^a X^a/f} , \tag{2.25}$$

where $\tilde{\xi}$ is the image of ξ under (2.23), we can rewrite the two–derivative term of eq. (2.22) as

$$\mathcal{L}_2 = \frac{f^2}{4} \text{Tr} \left|\partial_\mu \Sigma\right|^2 , \tag{2.26}$$

which indeed contains the Goldstone boson kinetic term canonically normalised.

From eq. (2.7) we see that Σ transforms as

$$\Sigma \to g\, \Sigma\, \tilde{g}^\dagger , \tag{2.27}$$

where $\tilde{g}$ is the image of g under (2.23). Therefore, for symmetric spaces we can construct a Goldstone boson matrix Σ as an element of G/H but transforming linearly under G.

The most general effective field theory for G/H–Goldstone bosons can then be constructed by writing all Lorentz and G–invariant terms involving p_μ and v_μ, or $\partial_\mu \Sigma$ in case of symmetric spaces, with increasing number of derivatives.

However, one should take care to correctly identify the finite cut–off up to which the theory is valid. A good estimate can be obtained by naïve dimensional analysis, yielding a relation between the cut–off Λ and the scale f of the G/H spontaneous breaking as [20]

$$\Lambda \sim 4\pi f . \tag{2.28}$$

The effective theory should then be trusted only for energies well below this scale.

2.1.2 Low–energy QCD: the Pion Lagrangian

The whole CCWZ machinery acquires relevance once we observe the spectrum of hadrons with masses in the $\mathcal{O}(100\,\text{MeV})$ range. The lightest hadronic particles are pseudo-scalar particles ($J^P = 0^-$, i.e. particles with total spin 0 and odd parity), with masses between $130 - 550\,\text{MeV}$, namely the eight light mesons ($\pi^\pm, \pi^0, K^\pm, K^0, \bar{K}^0, \eta$). At higher masses, different spin structures appear, namely the ρ vector meson ($J^P = 1^-$) with mass 770 MeV, and the first spin 1/2 particles, the nucleons p and n ($J^P = 1/2^+$) with masses of roughly 940 MeV.

There is clearly a mass gap between the eight light mesons and the other resonances. This observation led to identify the light scalar mesons, in the limit where one neglects their masses, with Goldstone bosons of a spontaneously broken symmetry described by a coset G/H, with G containing at least eight more generators than the unbroken group H.

The other particles with masses in the range of $\mathcal{O}(1\,\mathrm{GeV})$ cannot be identified as (scalar) Goldstone bosons. However, as long as we consider energies much smaller than $\mathcal{O}(1\,\mathrm{GeV})$, these massive resonances cannot be excited and therefore produced on–shell. Therefore, we would expect that an effective theory of light mesons should break down at the scale $\mathcal{O}(1\,\mathrm{GeV})$.

Let us now consider the low-energy limit of QCD, in order to identify the global symmetry breaking which could give rise to the eight light mesons as Goldstone bosons. Defining the flavour vector $q_i = (u, d, s)$, we can write the three–flavour $SU(3)_C$-invariant quark Lagrangian for u, d, s quarks as

$$\mathcal{L}_{\text{QCD, 3 fl.}} \supset \bar{q}^i_L\, i\not{D} q^i_L + \bar{q}^i_R\, i\not{D} q^i_R + m_i(\bar{q}^i_L q^i_R + \bar{q}^i_R q^i_L)\,. \tag{2.29}$$

It is clear that the mass terms for the quarks mix left– and right–chiralities, but if we set the three quark masses to zero, a large $SU(3)_L \otimes SU(3)_R$ symmetry is restored. Equivalently, in terms of vector and axial transformations of the flavour multiplet, the chiral symmetry of the three–flavour Lagrangian can be expressed as $SU(3)_V \otimes SU(3)_A$.

The crucial point now is that we have a tremendous amount of phenomenological and theoretical evidence (e.g. from lattice QCD) that the $SU(3)_A$ axial symmetry is spontaneously broken. The origin of this spontaneous symmetry breaking can be found in the QCD dynamics: at low energies QCD is a strongly coupled theory, with the phenomenon of confinement allowing the creation of bound states of quarks.

The vacuum expectation value of a quark condensate is therefore not vanishing:

$$\langle 0|\bar{q}q|0\rangle = \langle 0|\bar{q}_L q_R + \bar{q}_R q_L|0\rangle \neq 0\,, \tag{2.30}$$

forcing the chiral symmetry to be spontaneously broken to the vector $SU(3)_V$ subgroup

$$SU(3)_L \otimes SU(3)_R \to SU(3)_V\,, \tag{2.31}$$

under which the left– and right– chiralities transform in the same way.

We thus expect eight new Goldstone bosons associated to the symmetry breaking, which can be identified with the eight light meson fields. $SU(3)_L \otimes SU(3)_R \to SU(3)_V$ is therefore the symmetry breaking we want to describe using the CCWZ formalism.

Notice that the coset $G/H = SU(3)_L \otimes SU(3)_R/SU(3)_V$ is a symmetric space: the automorphism defining the symmetric space just interchanges the left– and right– generators. Following the CCWZ prescription we introduce a Σ field

$$\Sigma(x) = e^{2i\pi^a X^a/f} \cdot \mathbb{1}_{3\times 3}\,, \tag{2.32}$$

where X^a are $SU(3)$ generators, f is a mass dimension one parameter, and $\mathbb{1}_{3\times 3}$ is the three–dimensional identity matrix. The explicit representation of the Goldstone boson matrix is given by

$$\pi^a X^a = \begin{pmatrix} \frac{1}{\sqrt{2}}\pi^3 + \frac{1}{\sqrt{6}}\eta_8 & \pi^+ & K^+ \\ \pi^- & -\frac{1}{\sqrt{2}}\pi^3 + \frac{1}{\sqrt{6}}\eta_8 & K^0 \\ K^- & \bar{K}^0 & -\frac{2}{\sqrt{6}}\eta_8 \end{pmatrix}, \tag{2.33}$$

where we have already identified the different Goldstone boson combinations with the eight light meson fields.

By identifying the Σ field with the quark condensate, one can infer its quantum numbers under $SU(3)_L \otimes SU(3)_R$, namely

$$\Sigma \sim (3, \bar{3}), \quad \Sigma \to L\Sigma R^\dagger\,. \tag{2.34}$$

The first non–trivial derivative term is given by eq. (2.26), namely

$$\mathcal{L}_2 = \frac{f^2}{4}\,\mathrm{Tr}\,|\partial_\mu \Sigma|^2\;, \tag{2.35}$$

where the pre–factor $f^2/4$ assures the correct normalisation for the pion kinetic term.

A possible way to identify the value of the dimensionful parameter f is by explicitly calculating the decay width of the leptonic pion decay $\pi^+ \to \mu^+\nu_\mu$ through the W^+ gauge boson. After introducing the $SU(2)_L \otimes U(1)_Y$ gauge structure as an embedding in the $SU(3)$ chiral symmetry

$$SU(2)_L \subset SU(3)_L\,, \qquad U(1)_Y = T_{3R}\,, \tag{2.36}$$

one can calculate the decay rate of the aforementioned process. Restoring the pion mass in the kinematic calculations, and with G_F as the Fermi coupling constant, the result reads

$$\Gamma_{\pi^+\to\mu^+\nu_\mu} = \frac{G_F^2}{4\pi} f^2 m_\mu^2 m_\pi \left(1 - \frac{m_\mu^2}{m_\pi^2}\right)^2\,. \tag{2.37}$$

This allows to identify f with the pion decay constant with a measured value of

$$f \sim 93\,\mathrm{MeV}\,. \tag{2.38}$$

This is exactly the value we were expecting, since our effective theory is consistent only for energies below $\Lambda \sim 4\pi f \sim 1\,\mathrm{GeV}$, which is indeed the Λ_{QCD} scale.

A final remark which is worth mentioning, is that the $SU(2)_L \otimes U(1)_Y$ gauging is another source of chiral symmetry breaking: loop diagrams involving a photon and the charged meson propagator are responsible for a (small) contribution to the charged meson masses, which is indeed consistent with the observed phenomenology.

The phenomenological success of the low–energy description of QCD gives us the confidence to consider the CCWZ formalism as a good candidate to describe the effective theory of Goldstone bosons associated to other spontaneous symmetry breaking patterns. As we will discuss in the next section, the most notable example will be the $SU(2)_L \otimes U(1)_Y \to U(1)_{\mathrm{em}}$ electroweak symmetry breaking (EWSB).

2.2 Electroweak Chiral Lagrangian

2.2.1 Hidden symmetries and Electroweak Symmetry Breaking

The entire physics discovered in high–energy experiments before the start of the LHC could be compactly described by the Lagrangian

$$\begin{aligned}
\mathcal{L} &= \mathcal{L}_{\mathrm{int}} + \mathcal{L}_{\mathrm{mass}}\,, \\
\mathcal{L}_{\mathrm{int}} &= -\frac{1}{4}W^a_{\mu\nu}W^{a\,\mu\nu} - \frac{1}{4}B_{\mu\nu}B^{\mu\nu} - \frac{1}{4}G_{\mu\nu}G^{\mu\nu} + \sum_{j=1}^{3}\left(\bar{\Psi}^{(j)}_L i\not{D}\Psi^{(j)}_L + \bar{\Psi}^{(j)}_R i\not{D}\Psi^{(j)}_R\right)\,, \\
\mathcal{L}_{\mathrm{mass}} &= m_W^2 W^+_\mu W^{-\,\mu} + \frac{1}{2}m_Z^2 Z^\mu Z_\mu \\
&\quad - \sum_{i,j}\left(\bar{u}^{(i)}_L M^u_{ij} u^{(j)}_R + \bar{d}^{(i)}_L M^d_{ij} d^{(j)}_R + \bar{e}^{(i)}_L M^e_{ij} e^{(j)}_R + \bar{\nu}^{(i)}_L M^\nu_{ij} \nu^{(j)}_R\right) + \text{h.c.} \\
&\equiv m_W^2 W^+_\mu W^{-\,\mu} + \frac{1}{2}m_Z^2 Z^\mu Z_\mu + \sum_{i,j}\bar{\Psi}^{(i)}_L M_{ij}\Psi^{(j)}_R\,.
\end{aligned} \tag{2.39}$$

In particular, Ψ is a collective index for the SM fermions and i, j are generation (flavour) indices. A remarkable property of $\mathcal{L}$ is that while all the fundamental interactions among the particles are symmetric under a local $SU(2)_L \otimes U(1)_Y$ symmetry, the observed mass spectrum is not. In other words, the electroweak $SU(2)_L \otimes U(1)_Y$ symmetry is hidden by spontaneously breaking of the vacuum.

Focussing first on the $SU(2)_L \otimes U(1)_Y$ transformation properties of the fermion fields, we can show how to restore the gauge invariance to the whole Lagrangian. In particular, under a $SU(2)_L$ transformation defined as $U = \exp\left(i\alpha^a(x)\cdot\sigma_a/2\right)$, where σ^a are the three

Pauli matrices, the different fermion chiralities transform as

$$\Psi_L \xrightarrow{\mathrm{SU(2)}} U\,\Psi_L\,, \tag{2.40}$$

$$\Psi_R \xrightarrow{\mathrm{SU(2)}} \Psi_R\,. \tag{2.41}$$

On the other hand, under a $U(1)_Y$ transformation $\exp\Big(i\beta(x)\,y/2\cdot\mathbb{1}\Big)$, which can be expressed in terms of the electric charge q and the isospin transformations as

$$\exp\Big(i\beta(x)\frac{y}{2}\cdot\mathbb{1}\Big) = \exp\Big(i\beta(x)\,q\cdot\mathbb{1}\Big)\,\exp\Big(-i\beta(x)\cdot\frac{\sigma^3}{2}\Big) \equiv \exp\Big(i\beta(x)\,q\cdot\mathbb{1}\Big)\,V^\dagger\,, \tag{2.42}$$

the different fermion chiralities transform as

$$\Psi_L \xrightarrow{\mathrm{U(1)}} \exp\Big(i\beta(x)\,q\cdot\mathbb{1}\Big)\,V^\dagger\,\Psi_L \tag{2.43}$$

$$\Psi_R \xrightarrow{\mathrm{U(1)}} \exp\Big(i\beta(x)\,q\cdot\mathbb{1}\Big)\,\Psi_R\,. \tag{2.44}$$

If we now introduce a new field Σ with the $SU(2)_L\otimes U(1)_Y$ transformation property

$$\Sigma \xrightarrow{\mathrm{SM}} U\,\Sigma\,V^\dagger\,, \tag{2.45}$$

it is easy to show that the term $\bar\Psi_L\,\Sigma\,M\,\Psi_R$ is gauge invariant under the full SM group defined by eq. (2.40), (2.41), (2.43) and eq. (2.44). To obtain the correct fermion masses as in eq. (2.39), we need to assume that Σ acquires a finite expectation value $\langle\Sigma\rangle$, and the simplest way is to assume

$$\langle\Sigma\rangle = \mathbb{1}\,. \tag{2.46}$$

The $SU(2)_L\otimes U(1)_Y$ hidden symmetry is therefore now manifest also for the fermion mass terms, while being spontaneously broken when Σ develops its vacuum expectation value. The electroweak symmetry is indeed spontaneously broken to the group which leaves the expectation value $\langle\Sigma\rangle$ invariant under eq. (2.45), namely to the group defined by

$$U\,V^\dagger = \mathbb{1} \quad\Rightarrow\quad U = V\,. \tag{2.47}$$

Eq. (2.47) defines a left–over $U(1)$ symmetry of the Lagrangian which is indeed eventually identified with the QED gauge group.

Turning our attention to the gauge boson masses, we understood from the fermion sector that we should look for a $SU(2)_L\otimes U(1)_Y$ gauge invariant Lagrangian written in terms of the sigma field Σ. In particular, one introduces a $SU(2)_L\otimes U(1)_Y$ covariant derivative acting on the Σ field

$$D_\mu\Sigma = \partial_\mu\Sigma + ig'\Sigma B_\mu\frac{y}{2}\,|_{q=0} + igW^a_\mu\frac{\sigma_a}{2}\Sigma = \partial_\mu\Sigma - ig'\Sigma B_\mu\frac{\sigma_3}{2} + igW^a_\mu\frac{\sigma_a}{2}\Sigma\,. \tag{2.48}$$

Once the Σ field develops the expectation value as in eq. (2.46), one can indeed show that the gauge boson mass terms are generated from the gauge symmetric term

$$\frac{v^2}{4}\mathrm{Tr}\left[D_\mu\Sigma\,(D^\mu\Sigma)^\dagger\right]\,, \tag{2.49}$$

where v is identified as the electroweak scale.

At this stage we have then defined a manifestly $SU(2)_L\otimes U(1)_Y$–invariant electroweak theory, with massive gauge bosons and fermions, described by the Lagrangian

$$\begin{aligned}\mathcal{L}_{\mathrm{EW}\chi} = \mathcal{L}_{\mathrm{int}} + \frac{v^2}{4}\mathrm{Tr}\left[D_\mu\Sigma\,(D^\mu\Sigma)^\dagger\right] - \sum_{i,j}\bar{\Psi}_L^{(i)}\,\Sigma\,M_{ij}\Psi_R^{(j)}\\ - \frac{\mu^2 v^2}{4}\mathrm{Tr}\left[\Sigma^\dagger\Sigma\right] - \frac{\lambda v^4}{16}\left(\mathrm{Tr}\left[\Sigma^\dagger\Sigma\right]\right)^2 + \text{ h.c.}\,.\end{aligned} \tag{2.50}$$

The second line of eq. (2.50) contains additional gauge invariant potential terms for Σ (without derivatives) up to mass–dimension 4, with properly chosen pre–factors μ,λ. Notice that other $SU(2)_L\otimes U(1)_Y$ invariant terms involving the Σ field might be included as well, but for now we will consider only the ones in eq. (2.50). However, the dynamical generation of the vacuum expectation value of Σ is not specified.

Now the resemblance with the low–energy QCD case is manifest, e.g. eq. (2.35), where the $SU(3)_L\otimes SU(3)_R\to SU(3)_V$ spontaneous symmetry breaking is substituted by the EWSB pattern $SU(2)_L\otimes U(1)_Y\to U(1)_{\mathrm{em}}$. Therefore we will now make use of the CCWZ formalism to parametrise the actual form of the sigma field:

$$\Sigma(x) = \exp\left(i\frac{\chi^a(x)\sigma_a}{v}\right) \tag{2.51}$$

where χ^a are the three Goldstone bosons associated with EWSB, and where Σ transforms under $SU(2)_L\otimes U(1)_Y$ as in eq. (2.45).

The *Electroweak Chiral Lagrangian* of eq. (2.50) describes a manifestly $SU(2)_L\otimes U(1)_Y$–invariant field theory of massive and interacting gauge bosons and fermions, and propagating Goldstone bosons. These Goldstone bosons become the longitudinal polarisations of the massive EW gauge bosons in the unitarity gauge defined by eq. (2.46). In a different gauge fixing, the Goldstone boson fields propagate and can be considered as external states of Green functions. In particular, this is an effective field theory which becomes strongly coupled if extrapolated up to energies of the order of a cut–off scale $\Lambda\sim 4\pi v\sim 3\,\mathrm{TeV}$, where one should also include a whole series of operators organised in a chiral expansion in powers of (∂_μ/Λ).

It should be noted that the symmetry group acts non–linearly on the Goldstone bosons, namely

$$\chi^a(x) \xrightarrow{\text{SM}} \chi^a(x) + \frac{v}{2}\alpha^a(x) - \frac{v}{2}\delta^{a3}\beta(x) + \mathcal{O}\left(\chi^2\right) . \tag{2.52}$$

For this reason, the $SU(2)_L \otimes U(1)_Y$ is said to be non–linearly realised in this setup.

This "high–scale" version of the low–energy QCD Lagrangian (where the scale f is now identified with the electroweak scale v) is a prototype of the so–called "Technicolor models", where the longitudinal modes of the massive W and Z bosons are the Goldstone modes of the condensate's symmetry breaking, called *technipions*.

However, three crucial problems arise within this minimal setup, which we will describe in the following, making this theory still inconsistent with the experimental observations.

2.2.2 The need of additional degrees of freedom

The first issue is given by a violation of perturbative unitarity in the elastic scattering of the Goldstone boson $\chi\chi \to \chi\chi$ at energies $E \gg m_W$. This is particularly dangerous since, in the $E \gg m_W$ limit, the aforementioned process corresponds to the physical scattering of longitudinal W bosons, namely $W_L W_L \to W_L W_L$ (Equivalence Theorem). Specifically, the corresponding scattering amplitude grows with E^2,

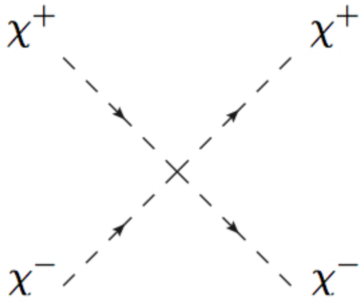

$$\mathcal{A}(\chi^+\chi^- \to \chi^+\chi^-) = \frac{1}{v^2}(s+t) \tag{2.53}$$

due to the derivative interaction among four Goldstone bosons that comes from expanding the kinetic term of Σ,

$$\begin{aligned}\mathcal{L}_{\text{EW}\chi} &\supset \frac{v^2}{4}\text{Tr}\left[\partial_\mu\Sigma\,\left(\partial^\mu\Sigma\right)^\dagger\right] \\ &= \frac{1}{6v^2}\left[\left(\chi^a\partial_\mu\chi^a\right)^2 - \chi^a\chi^a\left(\partial_\mu\chi^b\partial^\mu\chi^b\right)\right] + \frac{1}{2}\left(\partial_\mu\chi^a\right)^2 + \mathcal{O}\left(\chi^6\right) .\end{aligned} \tag{2.54}$$

A partial wave projection of the amplitude in eq. (2.53) would eventually reveal a unitarity violation of the elastic scattering at energies $E \sim 4\pi v$. This issue is therefore ultimately linked to the non–renormalisability of the Lagrangian.

A second issue is related to some $SU(2)_L \otimes U(1)_Y$–invariant operators that we have neglected so far from the Electroweak Chiral Lagrangian (2.50), namely

$$\Delta\mathcal{L}_{\mathrm{EW}\chi} = a_T \frac{v^2}{8}\left(\mathrm{Tr}\left[\Sigma^\dagger\left(D_\mu\Sigma\right)\sigma^3\right]\right)^2 + a_S\,\mathrm{Tr}\left[\Sigma^\dagger W^a_{\mu\nu}\frac{\sigma^a}{2}\Sigma B^{\mu\nu}\frac{\sigma^3}{2}\right] + \ldots \tag{2.55}$$

The LEP experiment sets a strong constraint on both coefficients a_T, a_S at the weak scale [21, 22], parametrised by the well–known S, T parameters [23, 24]

$$\Delta\hat{T} \equiv \Delta\epsilon_1 = a_T(m_Z)\,,$$
$$\Delta\hat{S} \equiv \Delta\epsilon_3 = g^2\,a_S(m_Z)\,. \tag{2.56}$$

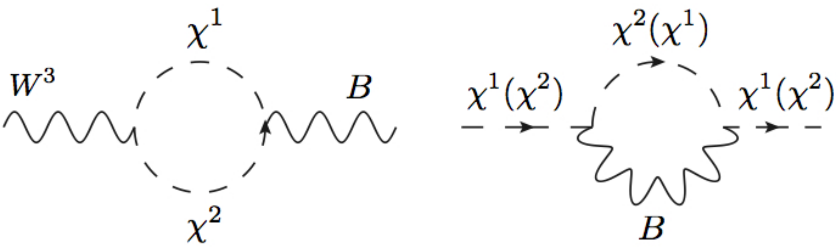

Figure 2.1: *Logarithmically divergent contributions to the S (left diagram) and T (right diagram) parameters from loops of the electroweak Goldstone bosons.*

Even by setting a_T, a_S to zero at the cut–off scale Λ, namely $a_T(\Lambda) = a_S(\Lambda) = 0$, their values run logarithmically at lower scales due to the one–loop exchange of the Goldstone bosons, as depicted in figure 2.1, generating a large contribution to $\epsilon_{1,3}$ as [25]

$$\Delta\epsilon_{1,3}(m_Z) = \Delta\epsilon_{1,3}(\Lambda) + c_{1,3}\log\frac{\Lambda^2}{m_Z^2}\,,$$
$$c_1 = -\frac{3}{16\pi^2}\frac{\alpha_{\mathrm{W}}(m_{\mathrm{Z}})}{\cos^2\theta_{\mathrm{W}}} \qquad c_3 = +\frac{1}{12\pi}\frac{\alpha_{\mathrm{W}}(m_{\mathrm{Z}})}{4\sin^2\theta_{\mathrm{W}}}\,. \tag{2.57}$$

This log–dependence in the cut–off Λ therefore generates a huge tension with the LEP fit, making the minimal Electroweak Chiral Lagrangian inconsistent with the observed data.

At this point it is worth noticing that eq. (2.50) is (approximately) invariant under a larger global $SU(2)_L \otimes SU(2)_R$ symmetry group, under which $\Sigma \to U_L\,\Sigma\,U_R^\dagger$. This $SU(2)_L \otimes SU(2)_R$ group is spontaneously broken to the diagonal $SU(2)_c$ by the vacuum expectation $\langle\Sigma\rangle$, and explicitly broken by g_1 and $M^u_{ij} \neq M^d_{ij}$. In the limit of vanishing g_1, the "custodial" $SU(2)_c$ implies $m_W = m_Z$, which for arbitrary g_1 is replaced by the tree–level relation

$$\rho \equiv \frac{m_W^2}{m_Z^2\cos^2\theta_W} = 1\,. \tag{2.58}$$

The operator proportional to a_T in eq. (2.56) is invariant under $SU(2)_L \otimes U(1)_Y$ but explicitly breaks the global $SU(2)_L \otimes SU(2)_R$: one can therefore conclude that any additional physics UV–completing the Electroweak Chiral Lagrangian should approximately preserve the $SU(2)_c$ custodial symmetry, or have accidental cancellations, in order to avoid additional dangerous contributions to ΔT.

Finally, after July 4th 2012, the (minimal) Electroweak Chiral Lagrangian is ruled out by the discovery of an additional scalar particle which is not predicted by eq. (2.50), namely the *Higgs boson* [5,6].

2.3 Higgs Model

2.3.1 The most general Higgs Lagrangian

The Electroweak Chiral Lagrangian in its minimal setup is inconsistent, but one can clearly extend it by introducing a (real) scalar field $h(x)$, which is a singlet of the custodial symmetry $SU(2)_c$. We will call this new scalar field the *Higgs boson*. Assuming custodial invariance, the most general chiral Lagrangian at the level of two derivatives is the following:

$$\begin{aligned}\mathcal{L}_{\text{EWSB}} = \mathcal{L}_{\text{int}} &+ \frac{v^2}{4}\text{Tr}\left[D_\mu\Sigma\,(D^\mu\Sigma)^\dagger\right]\left(1 + 2a\frac{h}{v} + b\frac{h^2}{v^2} + \dots\right)\\ &- \frac{v}{\sqrt{2}}\sum_{i,j} y_{ij}\,\bar{\Psi}_L^{(i)}\,\Sigma\,\Psi_R^{(j)}\left(1 + c\frac{h}{v} + \dots\right)\\ &- \frac{\mu^2 v^2}{4}\text{Tr}\left[\Sigma^\dagger\Sigma\right] - \frac{\lambda v^4}{16}\left(\text{Tr}\left[\Sigma^\dagger\Sigma\right]\right)^2 + \frac{1}{2}\left(\partial_\mu h\right)^2 + V(h) + \text{ h.c.}\end{aligned} \tag{2.59}$$

where we have expressed the fermion masses in terms of the dimensionless Yukawa couplings y_{ij}, and where $V(h)$ is some potential for $h(x)$, including a corresponding mass term.

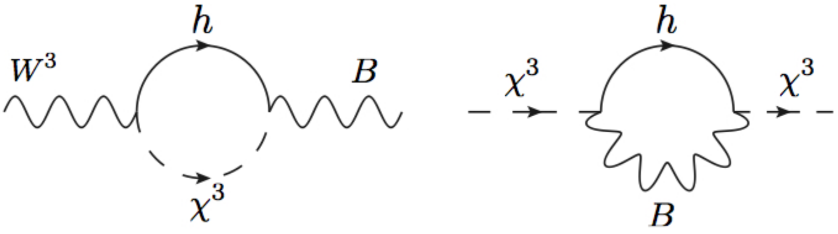

Figure 2.2: *Logarithmically divergent contributions to the S (left diagram) and T (right diagram) parameters from loops involving the Higgs boson.*

The diagrams involving the exchange of the scalar $h(x)$ give rise to two types of effects.

First, virtual corrections to the EW parameters ϵ_1, ϵ_3 are generated, see figure 2.2:

$$\Delta\epsilon_i = -c_i\, a^2 \log\frac{\Lambda^2}{m_h^2} \qquad i = 1, 3\,. \tag{2.60}$$

Combining with eq. (2.57), the net effect in the renormalisation–group running of $a_{T,S}(\mu)$ down to $\mu = m_Z$ therefore becomes

$$\Delta\epsilon_i = c_i \log\frac{m_h^2}{m_Z^2} + \left(1 - a^2\right) c_i \log\frac{\Lambda^2}{m_h^2} \qquad i = 1, 3\,. \tag{2.61}$$

We define an effective value of m_h as

$$m_h\big|_{\text{eff}} = m_h \left(\frac{\Lambda}{m_h}\right)^{1-a^2} \tag{2.62}$$

such that we can express

$$\Delta\epsilon_i \equiv c_i \log\frac{m_h^2\big|_{\text{eff}}}{m_Z^2}\,. \tag{2.63}$$

From this, by setting $m_t = 173.2\,\text{GeV}$ and performing a fit with two degrees of freedom, one obtains that the LEP data require

$$23\,\text{GeV} \leq m_h\big|_{\text{eff}} \leq 280\,\text{GeV} \qquad \text{at } 99\%\text{ CL} \tag{2.64}$$

namely LEP data favor the presence of a light Higgs. In other words, the inclusion of a (light) Higgs boson makes the Electroweak Chiral Lagrangian consistent with the LEP results. In particular, for $\Lambda = 1.2\,\text{TeV}$ and $m_h = 120\,\text{GeV}$, the LEP bound implies that

$$0.63 \leq a^2 \leq 1.72\,. \tag{2.65}$$

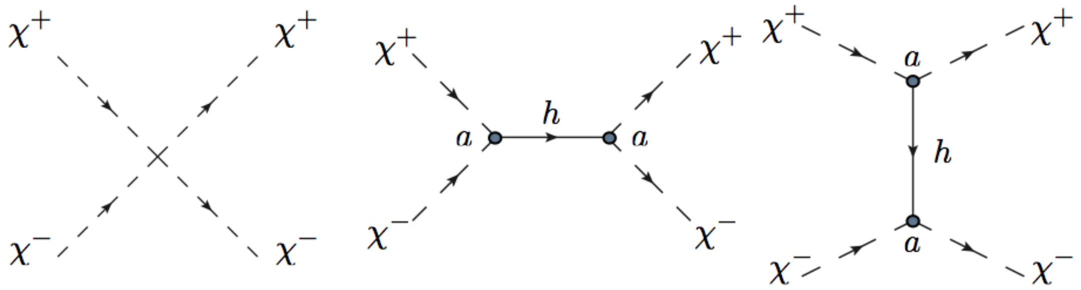

Figure 2.3: *Tree–level diagrams for the elastic $\chi^+\chi^- \to \chi^+\chi^-$ scattering within the Higgs Lagrangian of eq. (2.59).*

The tree–level exchange of the scalar $h(x)$ in the $\chi\chi$ elastic scattering, see figure 2.3, yields a new contribution to the amplitude of eq. (2.53), namely

$$\mathcal{A}(\chi^+\chi^- \to \chi^+\chi^-) = \frac{1}{v^2}\left[s - a^2\frac{s^2}{s - m_h^2} + (s \leftrightarrow t)\right] = \frac{s+t}{v^2}\left(1 - a^2\right) + \mathcal{O}\left(\frac{m_h^2}{E^2}\right)\,, \tag{2.66}$$

implying that the loss of unitarity is delayed up to the scale

$$\Lambda \sim \frac{4\pi v}{\sqrt{|1-a^2|}} \,. \tag{2.67}$$

There are other inelastic processes involving h to check versus unitarity. In particular, the $\chi\chi \to hh$ scattering as depicted in figure 2.4 (equivalent to the process $W_L W_L \to hh$ at high energies), is described by the amplitude

$$\mathcal{A}\left(\chi^+\chi^- \to h\,h\right) = \frac{s}{v^2}\left(b - a^2\right) + \mathcal{O}\left(\frac{m_h^2}{E^2}\right) \,. \tag{2.68}$$

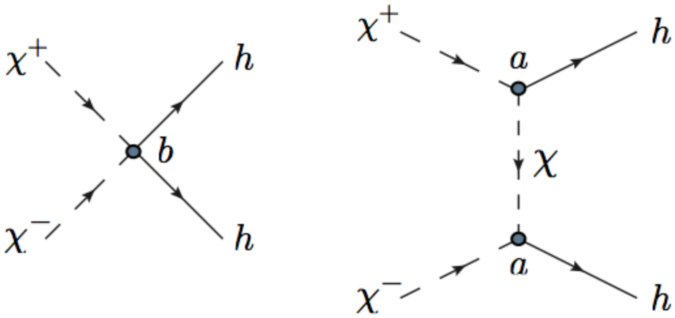

Figure 2.4: *Tree–level diagrams for the* $\chi^+\chi^- \to hh$ *scattering within the Higgs Lagrangian of eq.* (2.59).

Secondly, the $\chi\chi \to \psi\bar{\psi}$ scattering as depicted in figure 2.5 (equivalent to the process $W_L W_L \to \psi\bar{\psi}$ at high energies), generates the following amplitude

$$\mathcal{A}\left(\chi^+\chi^- \to \bar{\psi}\,\psi\right) = \frac{M\sqrt{s}}{v^2}\left(1 - ac\right) + \mathcal{O}\left(\frac{m_h^2}{E^2}\right) \,. \tag{2.69}$$

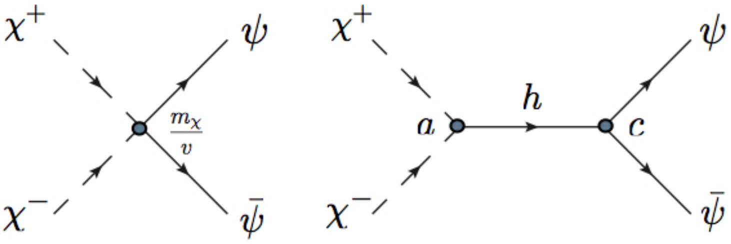

Figure 2.5: *Tree–level diagrams for the elastic* $\chi^+\chi^- \to \psi\bar{\psi}$ *scattering within the Higgs Lagrangian of eq.* (2.59).

Both amplitudes of eq. (2.68) and eq. (2.69) therefore violate perturbative unitarity at a high scale, too, since they are explicitly proportional to $\sqrt{s}$. The actual value of the scale where the loss of perturbative unitarity is observed, depends on the particular values of the a, b, c coefficients. This means that specific values of the Higgs couplings might ameliorate the unitarity issue, by lifting the scale of the strong sector regime.

2.3.2 The renormalisable Higgs Model

At this point we can notice that by tuning the Higgs couplings to

$$a = b = c = 1 \tag{2.70}$$

the theory can be made perturbative up to arbitrary scales, see eq. (2.67), (2.68), (2.69), and that the logarithmic divergences in $a_{T,S}(\mu)$ exactly cancel out, see eq. (2.61), making the contribution to the electroweak parameters finite. Both observations are intimately connected to the fact that a theory with $a = b = c = 1$ is renormalisable. The conditions given in eq. (2.70) indeed match the Electroweak Chiral Lagrangian onto the original Standard Model formulation of the EWSB Lagrangian (from now on simply the *Higgs model*), as we will show in the following.

In the Electroweak Chiral Lagrangian, the explicit parametrisation of the Goldstone bosons was given by the non–linear embedding defined in eq. (2.51) using the CCWZ formalism. However, the correct pattern of EWSB does not depend on the explicit parametrisation of the Σ field: we could therefore choose a different parametrisation for the Goldstone bosons. In particular, for the Higgs model defined by eq. (2.70) one can choose a linear embedding of the Goldstone bosons, which in the basis of the Pauli matrices σ_a can be expressed as

$$\Sigma(x) = \mathbb{1} - \frac{i}{v}\chi^a(x)\sigma_a\,. \tag{2.71}$$

We can now further expand eq. (2.71) by including the scalar Higgs boson as quantum excitation around the vacuum expectation value of Σ:

$$\begin{aligned}\Sigma(x) \to \left(1 + \frac{h(x)}{v}\right)\mathbb{1} - \frac{i}{v}\chi^a(x)\sigma_a &= \frac{1}{v}\begin{pmatrix} v + h - i\chi^3 & -\chi^2 - i\chi^1 \\ \chi^2 - i\chi^1 & v + h + i\chi^3 \end{pmatrix} \\ &\equiv \frac{\sqrt{2}}{v}\left(\tilde{H},\, H\right)\,. \end{aligned} \tag{2.72}$$

In the last step we have rewritten the 2×2 matrix as a bi–doublet in terms of the $SU(2)_L$ complex doublet H

$$H = \frac{1}{\sqrt{2}}\begin{pmatrix} -\chi^2 - i\chi^1 \\ v + h + i\chi^3 \end{pmatrix}, \qquad \tilde{H} = -i\,\sigma_2\,H^* = \frac{1}{\sqrt{2}}\begin{pmatrix} v + h - i\chi^3 \\ \chi^2 - i\chi^1 \end{pmatrix}. \tag{2.73}$$

With this identification, eq. (2.59) simplifies to the well–known form

$$\begin{aligned} \mathcal{L}_{\mathrm{H}} = \mathcal{L}_{\mathrm{int}} + \left|D_\mu H\right|^2 \\ - \sum_{i,j} y_{ij} \left(\bar{\Psi}_L^{(i)}\, H\, \Psi_R^{(j)} + \bar{\Psi}_L^{(i)}\, \tilde{H}\, \Psi_R^{(j)}\right) \\ - \mu^2 H^\dagger H - \lambda\left(H^\dagger H\right)^2 + \text{ h.c.} \\ \text{with } D_\mu H = \left(\partial_\mu - i g W_\mu^a \sigma_a - \frac{i}{2} g' B_\mu\right) H\,, \end{aligned} \tag{2.74}$$

which is now manifestly renormalisable. The unitarity of the Higgs model and the absence of divergences, other than those corresponding to a renormalisation of the Higgs wave function and gauge kinetic terms, can therefore be traced back to its renormalisability. In terms of H, UV–contributions to $\epsilon_{1,3}$ are indeed now parametrised only by dimension–6 operators:

$$\epsilon_1 \leftrightarrow \left(H^\dagger D_\mu H\right)^2, \qquad \epsilon_3 \leftrightarrow \left(H^\dagger W_{\mu\nu} B^{\mu\nu} H\right)\,. \tag{2.75}$$

Finally, if we expand the potential terms for the Higgs doublet of eq. (2.74) in unitarity gauge, we can extract the relations for the mass and self–couplings of the new scalar Higgs field $h(x)$ after minimising the corresponding "Mexican–hat" potential, namely

$$\begin{aligned} \mathcal{L}_H \supset \frac{1}{2} m_h^2\, h^2 - \frac{m_h^2}{2\,v}\, h^3 - \frac{m_h^2}{8\,v^2}\, h^4 \\ \text{with} \quad m_h^2 = 2\,\lambda v^2 = -2\,\mu^2\,. \end{aligned} \tag{2.76}$$

2.4 Shortcomings of the Standard Model

We have seen that explicit mass terms for vector bosons and fermions are forbidden by the $SU(2)_L \otimes U(1)_Y$ gauge symmetry. Since they have to vanish if the symmetry is unbroken, the mass terms have to be proportional to the vacuum expectation value v. This is true at any order in perturbation theory, because the renormalisation procedure preserves all the symmetries. Therefore, the size of any loop correction to fermion and gauge boson masses is controlled by their tree–level values.

This property is not shared by scalar particles. In particular, the mass of the Higgs boson m_h is an arbitrary parameter of the SM, not protected by any approximate symmetry. This means that the Higgs mass is additively renormalised, namely getting radiative corrections proportional to the mass of any particle it couples to.

Suppose now that the SM is a complete description of Nature, with no new phenomena appearing at any higher energy scale.

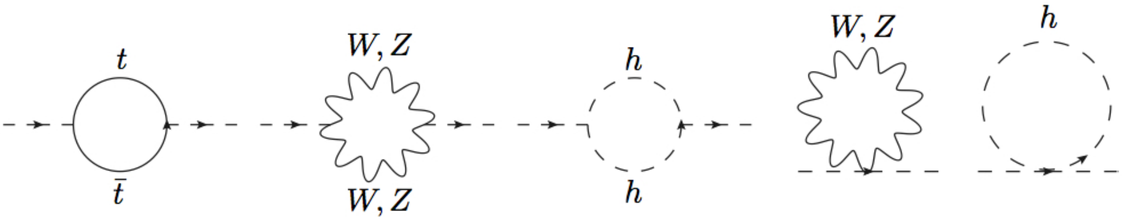

Figure 2.6: *One–loop corrections to the Higgs two–point function involving SM particles.*

The β–function for the running Higgs mass, considering only the one–loop corrections generated by the diagrams in figure 2.6, is given by

$$\beta_{m_h^2} = \frac{3m_h^2}{8\pi^2}\left(2\lambda + y_t^2 - \frac{3g^2}{4} - \frac{g'^2}{4}\right) , \tag{2.77}$$

where λ is the Higgs–self coupling, y_t is the Yukawa coupling of the top quark, and g, g' are the $SU(2)_L \otimes U(1)_Y$ gauge couplings. There would be no reason to set the input for the renormalisation group running at some arbitrary high scale other than the electroweak scale: the renormalised value of the Higgs mass at the electroweak scale would not be predicted, but determined by the experiments in a fully "natural" way. In other words, there would not be any potentially "dangerous" sensitivity of the Higgs mass to other high scales.

However, the SM is usually considered as an effective theory valid within a limited energy range: at least at the Planck–scale quantum gravity effects should become relevant, but there are many other hints of new physics at high energies as mentioned in the introduction.

Suppose now the presence of some new–physics energy scale above the electroweak scale, $\Lambda_{\text{NP}} > v$. If the Higgs boson is coupled to the new–physics sector, then its mass gets a correction from loops of the new heavy particles, and these corrections are quadratic in their mass $M \sim \Lambda_{\text{NP}}$. This is considered as a problem for a UV completion of the SM in which the Higgs mass is a predictable quantity. Considering for example a Dirac fermion with mass M and Yukawa coupling y, the one–loop β–function of the running Higgs mass would be

$$\beta_{m_h^2} \supset \frac{y}{(4\pi)^2}\left(m_h^2 - 6M^2\right) . \tag{2.78}$$

The renormalisation group running thus generates a mass term $m_h^2 \sim M^2$. The boundary conditions for the renormalisation group equation should naturally be fixed at the high scale Λ_{NP}, where one imagines some UV–completion to determine the masses and couplings. The running Higgs mass at the electroweak scale, where one should match the renormalised value with the experimental value, then reads

$$m_h^2\,(\Lambda_{\mathrm{SM}}) \sim m_h^2\,(\Lambda_{\mathrm{NP}}) - c\,\Lambda_{\mathrm{NP}}^2 \log\frac{\Lambda_{\mathrm{NP}}}{\Lambda_{\mathrm{SM}}}\,, \tag{2.79}$$

where c is a numerical factor including the different coupling constants. If the scale Λ_{NP} is much higher than m_h, then the two contributions in (2.79) have to balance each other out with very high accuracy in order to generate a Higgs boson mass much smaller than Λ_{NP}. This non–natural sensitivity of the Higgs boson mass to radiative corrections from higher scales is commonly referred as the *hierarchy* or *fine–tuning problem* of the SM. An accidental cancellation between the initial condition $m_h^2\,(\Lambda_{\mathrm{NP}})$ and the quantum corrections of the order of at most one percent, would imply that the scale of new physics cannot be higher than $\mathcal{O}(\mathrm{TeV})$.

Clearly, one possibility is to ignore the hierarchy problem and accept a fine–tuned SM: in this case one has to find some other guideline other than naturalness to go beyond the SM. If one insists on naturalness, still viewing the SM as an effective theory, then one has to conclude that new Beyond the Standard Model (BSM) physics has to appear at the TeV scale. The models that describe these phenomena can be divided into two classes, depending on whether they are strongly coupled or weakly coupled at higher scales.

Among the weakly interacting theories beyond the SM, the main candidate is Supersymmetry. The non–renormalisation theorem causes all quadratic divergences to cancel out exactly above the scale of supersymmetry–breaking Λ_{soft}. The main corrections to the Higgs mass still come from SM–loops, but proportional to only the cut–off scale $\Lambda_{\mathrm{soft}}^2$.

In strongly coupled models, the Higgs boson is a resonance of some new strongly interacting sector. Since it makes no sense to speak about the Higgs particle above its compositeness scale Λ_{comp}, it is automatically protected from Planck–scale radiative corrections. The Higgs mass is therefore sensitive at most to $\Lambda_{\mathrm{comp}}^2$.

The main topic of the thesis is concerned with strongly interacting Beyond the Standard Model theories, in particular of the Little Higgs type. For this reason, in the next chapters we will focus only on the strongly coupled UV–completion of the SM, assuming the naturalness of EWSB as a guiding principle for model building of TeV–scale physics.

Chapter 3

The Little Higgs model setup

This chapter describes the relevant ideas of a class strongly coupled models Beyond the Standard Model, namely Little Higgs models. We will first discuss how the Higgs boson can arise as a (pseudo–) Goldstone boson of an enlarged global symmetry, and then show how the Collective Symmetry Breaking mechanism of Little Higgs models prevents the appearance of a dangerous quadratic–sensitivity to the compositeness scale at one–loop in the Higgs potential. The main focus of the chapter will be devoted to phenomenological consequences of the most common implementations of the Little Higgs ideas. The resources used for this chapter are refs. [15, 17, 26–40].

3.1 The Higgs as a pseudo–Goldstone boson

Technicolor–like models without a light Higgs scalar as the Electroweak Chiral Lagrangian (2.50) described in the previous chapter, where the electroweak symmetry is broken dynamically in the same way as the $SU(3)_L \otimes SU(3)_R$ chiral symmetry in low–energy QCD, can be safely said to be ruled out by the direct observation of a Higgs–like scalar particle by the ATLAS and CMS collaborations [5, 6].

The radiative instability of the dimension–two operator $H^\dagger H$ in the renormalisable Higgs Model (2.74) however gives us the confidence to look for Beyond the Standard Model physics appearing at the TeV–scale, corroborated by the fact that perturbative unitarity issues and electroweak precision constraints can be alleviated by a light Higgs boson even with *non–standard* couplings (2.59).

Between the weekly coupled and the strongly coupled extension of the SM, let us focus for now on the latter, namely assuming that the Higgs boson is part of a composite sector.

This means that its couplings differ from the ones of a standard $SU(2)_L$ doublet, and above the compositeness scale $\Lambda = 4\pi f$ the theory becomes strongly interacting. In general, unless some mechanism is generating a separation of scales, one would expect the scale f to coincide with the electroweak scale v, and the vector and fermion resonances appearing below this energy scale to have masses comparable with the Higgs mass. However, direct searches for new particles at the LHC have shown neither signs of new fermions up to masses of $600 - 800\,\text{GeV}$ [41–44], nor signs of new vector bosons up to a few TeV [45, 46].

The Higgs boson has therefore to be much lighter than other possible states of the composite sector. This situation has still a convincing connection with the low–energy QCD description, where the pions arise as a set of scalar states naturally lighter than the compositeness scale Λ_{QCD}, with all other resonances at higher masses. This is possible because the pions are the Goldstone bosons associated with the spontaneous breaking of the approximate $SU(3)_L \otimes SU(3)_R$ chiral symmetry of QCD. One can assume that also the Higgs is a (pseudo–) Goldstone boson associated to a global symmetry breaking of the strong sector, not necessarily the full electroweak group as in Technicolor models.

If we want to construct a viable EWSB theory including the Higgs as Goldstone boson of a G/H spontaneous symmetry breaking, a few precautions are necessary. In particular, at least four Goldstone bosons are needed to reproduce the $SU(2)_L$ Higgs doublet, and the symmetry group G has to embed the SM gauge group $SU(2)_L \otimes U(1)_Y \equiv G_{\text{SM}}$, since the Higgs must couple to the gauge fields. Notice that if $G_{\text{SM}} \subset H$, then EWSB cannot be triggered at tree–level, since H is an unbroken symmetry group. On the other hand, if a misalignment between G_{SM} and H is generated, as it will be at loop–level, the $G \to H$ breaking triggers EWSB as well. Finally, one usually needs to impose that the strong sector respects a custodial $SU(2)_L \otimes SU(2)_R$ symmetry in order to avoid large contributions to the T–parameter.

These are the basic requirements to construct a generic *Composite Higgs* model, and we can depict its symmetry structure as in figure 3.1. The minimal group satisfying these requirements is $SO(5) \otimes U(1)_X$, see [13] for a review. In this minimal model there are exactly four Goldstone bosons, namely only the Higgs doublet, living in the coset $SO(5)/SO(4)$. The extra $U(1)_X$ group is needed in order to correctly assign the hypercharge for all the SM fields, with $Y = T_{3R} + X$, and does not take part in the breaking.

However, if the symmetry group G would be an exact symmetry, the Higgs potential would vanish because of the shift symmetry acting on it. As a consequence, one would have

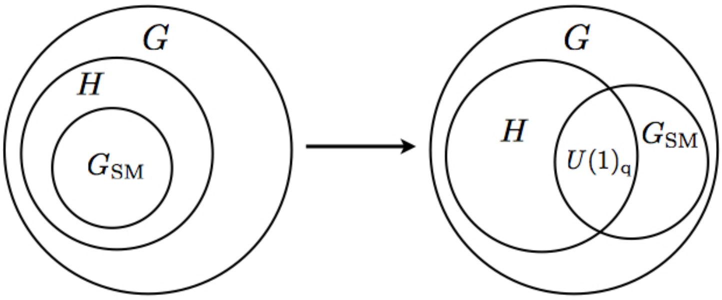

Figure 3.1: *Diagrammatic representation of the global/gauge structure of generic G/H Composite Higgs models. At tree–level (diagram on the left), the SM gauge group $G_{SM} \subset H$ remains unbroken. The Higgs doublet is identified among the G/H massless Goldstone bosons. A misalignment is generated at one–loop level from explicit breaking of the global symmetry (diagram on the right), such that a potential for the Higgs is introduced and EWSB is triggered, with only the $U(1)_q$ as remaining unbroken gauge subgroup. The SM gauge bosons acquire a mass of order v.*

no EWSB and a perfectly massless Higgs boson. For this reason, the global symmetry G has to be only approximate, making the Higgs a massive pseudo–Goldstone boson. Its explicit breaking comes from the gauging of only a subgroup of G and by symmetry–breaking Yukawa couplings: the effective potential of the Higgs field, which will not respect the full symmetry group G, is therefore generated through radiative corrections involving SM fields, e.g. vector bosons and top quark.

In a model with generic order one parameters, the EW scale would be again expected to be generated at the same order of the only other scale in the theory, namely the scale f, up to some model–dependent factor. In order to have a significant splitting between f and the EW scale, a certain amount of fine–tuning between different terms in the potential has to be introduced. This is the so–called *little hierarchy problem*.

A *Little Higgs* model can be generically considered as a Composite Higgs model, in the sense that the Higgs boson arises as a pseudo–Goldstone boson of an approximate global symmetry of a strong sector. The additional structure introduced in Little Higgs models tries to overcome the issue of a natural separation between the electroweak scale v and the compositeness scale Λ, namely forcing the electroweak symmetry to be broken *collectively*.

Heuristically, one needs to explicitly break two different symmetries to allow for mass and potential terms for the Higgs: breaking only one of these symmetries leaves the respective other one as a global symmetry under which the Higgs field transforms non–linearly. Because the original global symmetry group is explicitly broken, the Higgs still develops a quadratically-sensitive mass term in the compositeness scale, due to gauge boson or fermion loops, but with a two–loop suppression factor. Larger global symmetry groups are therefore required, such that residual symmetries generate a Higgs potential of the form

$$V(h) \sim \left[\begin{array}{c} \text{small} \\ \text{w.r.t. } f^2 \end{array} \right] \cdot h^\dagger h + \mathcal{O}(1) \cdot |h^\dagger h|^2 \,. \tag{3.1}$$

We will discuss now how a shift–symmetry associated to additional pseudo–Goldstone bosons can forbid $h^\dagger h$ while allowing $|h^\dagger h|^2$, as exploited in the *Collective Symmetry Breaking* mechanism.

3.2 Collective Symmetry Breaking

Little Higgs theories [47, 48] avoid quadratic divergences in the Higgs potential at one–loop level through the Collective Symmetry Breaking (CSB) mechanism. This mechanism has to be appropriately introduced for each Higgs–coupling contributing with a quadratic sensitivity to the Higgs mass, namely into the scalar–, gauge– and fermion–sectors.

3.2.1 Generation of a collective quartic

Let us start with the collective generation of the quartic coupling of the Higgs. Assuming that the Higgs is a pseudo–Goldstone boson, we have seen that the shift symmetry

$$h \to h + \epsilon \tag{3.2}$$

forbids any potential for the Higgs. But suppose there is an additional degree of freedom ϕ, such that the scalar potential consists of two operators (included by hand or induced radiatively as in the Coleman–Weinberg potential):

$$V \supset \lambda_1 f^2 \left| \phi + \frac{h^2}{f} \right|^2 + \lambda_2 f^2 \left| \phi - \frac{h^2}{f} \right|^2 \,. \tag{3.3}$$

We see that this potential generates a mass term for ϕ, namely

$$m_\phi = f \sqrt{\lambda_1 + \lambda_2} \tag{3.4}$$

but the question is whether a viable potential for h can be generated as well. One should notice that each term in the scalar potential would be invariant under the Higgs shift–symmetry of eq. (3.2) by requiring ϕ to transform respectively as

$$\lambda_1 : \begin{cases} h \to h + \epsilon \\ \phi \to \phi - \dfrac{h\epsilon + \epsilon h}{f} \end{cases} \quad \text{or} \quad \lambda_2 : \begin{cases} h \to h + \epsilon \\ \phi \to \phi + \dfrac{h\epsilon + \epsilon h}{f} \,. \end{cases} \tag{3.5}$$

Furthermore, one can observe that, taken alone, neither λ_i term would generate a physical Higgs quartic, since each individual quartic could be removed by a field redefinition

$$\lambda_1 : \ \phi_+ \equiv \phi + \frac{h^2}{f} \qquad \lambda_2 : \ \phi_- \equiv \phi - \frac{h^2}{f} \,. \tag{3.6}$$

However, both shift symmetries of ϕ defined in eq. (3.5) cannot be simultaneously required, and collectively the two operators yield a Higgs quartic term after ϕ is integrated out:

$$V_{\text{eff}} \supset \frac{4\lambda_1\lambda_2}{\lambda_1+\lambda_2}\, h^4 \equiv \lambda_{\text{eff}}\, h^4 \,. \tag{3.7}$$

For this reason, only diagrams involving both couplings λ_1, λ_2 can contribute to radiatively generate a Higgs–mass, with a mild logarithmic sensitivity to the scale Λ:

$$\Delta m_h^2 \sim \frac{1}{16\pi^2} \lambda_{\text{eff}}\, m_\phi^2 \,\log \frac{\Lambda^2}{m_\phi^2} \,. \tag{3.8}$$

Therefore, the resulting potential allows for a parametric separation between the electroweak scale v and the scale f, as in (3.1). The degree(s) of freedom ϕ responsible for canceling quadratically–divergent contributions to the Higgs mass from Higgs–self interaction diagrams are called *quarticons* (or generically *cancellons*).

The quantum numbers of the quarticon field $\phi \sim h^2$ are not specified at this point. The possible $SU(2)_L$ representations for h^2 are determined by

$$\mathbf{2} \otimes \mathbf{2} = \mathbf{3}_S \otimes \mathbf{1}_A \qquad \mathbf{2} \otimes \mathbf{2^*} = \mathbf{3} \otimes \mathbf{1} \,, \tag{3.9}$$

where the S/A subscript refers to the representation being symmetric or antisymmetric. In a one–Higgs doublet model, the $\mathbf{1}_A$ representation vanishes, and the quarticon can be a complex triplet, a real triplet, or a real singlet carrying no charges:

$$h^i h^j \to \phi^{ij} \qquad (\mathbf{3}_S) \tag{3.10}$$

$$h^\dagger \sigma^a h \to \phi^a \qquad (\mathbf{3}) \tag{3.11}$$

$$h^\dagger h \to \eta \qquad (\mathbf{1}) \tag{3.12}$$

A complex triplet is used in the $SU(5)/SO(5)$ Littlest Higgs [49], a real triplet is present in the $SO(9)/(SO(5) \otimes SO(4))$ model [50], while the $[SU(3) \otimes U(1)]^2/[SU(2) \otimes U(1)]^2$ Simplest Little Higgs [51, 52] predicts a real singlet scalar.

However, a real singlet field η is potentially “dangerous”: having no non–trivial quantum numbers, a quadratically divergent η tadpole cannot be prevented by the shift symmetries, and is necessarily accompanied by a quadratically–divergent Higgs mass at one–loop. A certain amount of fine–tuning or a non–minimal setup are therefore required in models predicting dangerous singlets. Furthermore, triplet scalars usually get vacuum expectation values after EWSB, inducing a large correction to the T–parameter. For this reason, one–Higgs doublet models with triplet scalars require a discrete symmetry named *T–parity* in order to forbid a triplet tadpole [53–55], or extending G such that H includes a custodial symmetry as in the already mentioned ref. [50]. The latter model is however not viable, since it includes a dangerous singlet among the quarticon fields.

Alternatively, G/H could be expanded to include a second Higgs doublet: this permits non–dangerous (real and complex) singlet scalars, alleviating the issue of triplet vevs without introducing T–parity. If h_1 and h_2 carry the same hypercharge, the quarticon can be a complex singlet with or without hypercharge:

$$h_1^i h_2^j \epsilon_{ij} \to \phi \qquad\qquad (\mathbf{1}_A) \tag{3.13}$$

$$h_1^\dagger h_2 \to \phi \qquad\qquad (\mathbf{1})\,. \tag{3.14}$$

It should be noted that only the hypercharge neutral complex quarticon (3.14) can generate a viable quartic potential, and has been used in the $SU(6)/Sp(6)$ antisymmetric condensate model [56]. As mentioned before, the quarticon can be a real singlet, too, as long as an extra $\mathbb{Z}_2$ symmetry is included, forbidding a ϕ tadpole

$$\mathrm{Re}\left[h_1^\dagger h_2\right] \to \phi \qquad (\mathbf{1})\,, \tag{3.15}$$

as exploited in the $SO(6)^2/SO(6)$ Bestest Little Higgs [57].

The recent $SO(10)/SO(5)^2$ model [28] is finally an example of a two–Higgs doublet model predicting a scalar triplet among the quarticon fields, with a built–in custodial symmetry to prevent strong constraints from electroweak precision measurements.

3.2.2 Gauge collective interactions

We will present now a pedagogical example on how to introduce gauge and fermion interactions without introducing quadratic sensitivity to compositeness scale Λ at one–loop. The (toy) model we are going to consider realises the spontaneous symmetry breaking pattern $SU(3)/SU(2)$.

Following the CCWZ prescription, we can write the Goldstone boson matrix as

$$\pi \equiv \pi^a X^a = \left(\begin{array}{cc|c} -\frac{\sqrt{2}}{3}\eta & & \mathrm{h} \\ & -\frac{\sqrt{2}}{3}\eta & \\ \hline \multicolumn{2}{c|}{h^\dagger} & \frac{2\sqrt{2}}{3}\eta \end{array}\right) \tag{3.16}$$

with $\Sigma = \exp(i\pi/f)\,(0,0,1)^T$. At the two–derivative level, the Lagrangian of our low–energy theory can be written as usual as $\mathcal{L}_2 = f^2/4\,\mathrm{Tr}\,[\partial_\mu \Sigma]$. For simplicity, in the following we will not consider the quarticon field η in the Goldstone boson matrix (3.16).

Let us start with the gauge interactions. At first, two options seem available, either gauging only the $SU(2)$ subgroup within the global $SU(3)$ symmetry, or gauging the whole $SU(3)$ group. The $SU(2)$–gauging however is an explicit breaking of the global symmetry structure, and we expect an introduction of a quadratically–divergent contribution to the Higgs mass, as in the SM. To do so, we promote ∂_μ to a covariant derivative

$$\partial_\mu \Sigma \to \left(\partial_\mu - ig\, W_\mu^a \frac{\sigma^a}{2}\right)\Sigma \equiv \left(\partial_\mu - ig\, W_\mu\right)\Sigma\,, \tag{3.17}$$

where σ^a are the $SU(2) \subset SU(3)$ generators. Using the formalism we have introduced in section A.1, namely eq. (A.1.13), we can write the quadratic contribution to the scalar effective potential from the gauge–boson interaction at one–loop as

$$\begin{aligned} V_{1\text{–loop}}(\Sigma) \supset \frac{3}{64\pi^2}\Lambda^2\,\mathrm{Tr}\left[M_\mathrm{g}(\Sigma)^\dagger M_\mathrm{g}(\Sigma)\right] &= \frac{3}{64\pi^2}\Lambda^2\,\mathrm{Tr}\left[\left|-i\frac{g}{2}\left(\begin{array}{c|c} \sigma^a & \\ \hline & \end{array}\right)\Sigma\right|^2\right] \\ \sim g^2\Lambda^2\,\mathrm{Tr}\left[\Sigma^\dagger\left(\begin{array}{c|c} \mathbb{1} & \\ \hline & \end{array}\right)\Sigma\right] &= g^2\Lambda^2\, h^\dagger h + \dots \end{aligned} \tag{3.18}$$

which generates a non–vanishing quadratic–divergent contribution to the Higgs mass.

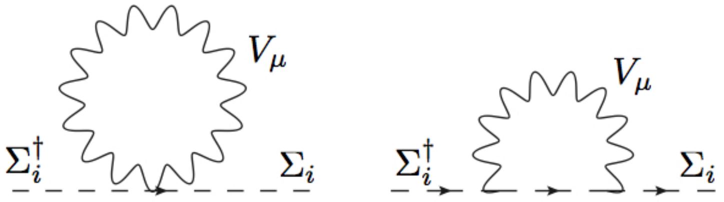

Figure 3.2: *Quadratically divergent one–loop contributions to the Coleman–Weinberg scalar potential from EW gauging.*

On the other hand, if we gauge the entire $SU(3)$ group, we would use the covariant derivative

$$\partial_\mu \Sigma \to \left(\partial_\mu - ig\, G_\mu^a \frac{\lambda^a}{2}\right)\Sigma \equiv \left(\partial_\mu - ig\, G_\mu\right)\Sigma\,, \tag{3.19}$$

where λ^a are the $SU(3)$ generators. We would thus obtain the following Λ^2–contribution

$$\begin{aligned} V_{1\text{–loop}}(\Sigma) \supset \frac{3}{64\pi^2}\Lambda^2\,\mathrm{Tr}\left[M_\mathrm{g}(\Sigma)^\dagger M_\mathrm{g}(\Sigma)\right] &= \frac{3}{64\pi^2}\Lambda^2\,\mathrm{Tr}\left[\left|-ig\frac{\lambda^a}{2}\Sigma\right|^2\right] \\ \sim g^2\Lambda^2\,\mathrm{Tr}\left[\Sigma^\dagger\,\mathbb{1}\,\Sigma\right] &= g^2\Lambda^2 f^2 + \dots \end{aligned} \tag{3.20}$$

which is independent on $h^\dagger h$. In this case, all massless Goldstone bosons have been absorbed to become the longitudinal degrees of freedom of the massive $SU(3)$ gauge bosons. Therefore, if we include only $SU(2)$ covariant derivatives we re–introduce the SM quadratic divergence, while gauging the full $SU(3)$ turns the Higgs into a Goldstone boson which gives mass of order f to the heavy gauge bosons: what we need is clearly a way to mix an extended $SU(3)$ gauge sector and a global symmetry where the Goldstone modes are not eaten.

As a third attempt, we finally introduce the gauge couplings in a collective manner. First we introduce two copies of the sigma field, $\Sigma_{j=1,2}$, assuming for simplicity aligned vacuum expectation values ($f_1 = f_2 \equiv f$). The global symmetry is therefore extended to $SU(3)_1 \otimes SU(3)_2$. We then gauge the vector (diagonal) subgroup $SU(3)_{\mathrm{V}} \subset SU(3)_1 \otimes SU(3)_2$, namely introducing one set of $SU(3)$ gauge bosons and fixing $g_1 = g_2 \equiv g$:

$$\Sigma_j = \exp\left[-\frac{i}{f}\left(\begin{array}{c|c} & h \\ \hline h^\dagger & \end{array}\right)\right]\begin{pmatrix} 0 \\ 0 \\ 1 \end{pmatrix} \qquad j = 1,2$$

$$\mathcal{L}_2 = \frac{f^2}{4}\,\mathrm{Tr}\,|D_\mu \Sigma_1|^2 + \frac{f^2}{4}\,\mathrm{Tr}\,|D_\mu \Sigma_2|^2$$

$$\text{with } D_\mu \Sigma_j = \left(\partial_\mu - ig\, G^a_\mu \frac{\lambda^a}{2}\right)\Sigma_j\,. \tag{3.21}$$

Our theory consists now of two sigma fields, each representing the spontaneous breaking of an $SU(3)_{\mathrm{i}}$ global symmetry to $SU(2)_{\mathrm{i}}$, the coset being thus $[SU(3)]^2 / [SU(2)]^2$. As before, taken alone both $|D_\mu \Sigma_j|^2$ terms do not generate a quadratic–divergent contribution to the Higgs mass at one–loop level as in eq. (3.20):

$$V_{1\text{–loop}}(\Sigma_{1,2}) \sim 2\, g^2 \Lambda^2 f^2 + \ldots \tag{3.22}$$

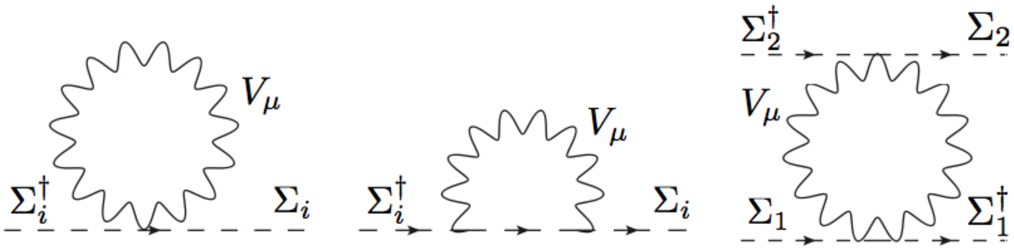

Figure 3.3: *Quadratic and logarithmically divergent one–loop contributions to the Coleman–Weinberg scalar potential from EW gauging within the Little Higgs toy model.*

However, other diagrams do contribute to the radiative generation of a Higgs potential, as in figure 3.3, where both Σ_1 and Σ_2 are directly coupled through a gauge–boson loop.

By counting powers of momentum, we can guess that the third diagram will only be log–divergent, as one could check by an explicit calculation:

$$V_{\text{1–loop}}(\Sigma_{1,2}) \supset -\frac{3g^4}{64\pi^2}\,\text{Tr}\left[\left|\Sigma_1^\dagger\,\Sigma_2\right|^2\right]\log\frac{\Lambda^2}{\mu^2} + \ldots \sim g^4 f^2\, h^\dagger h\,\log\frac{\Lambda^2}{\mu^2} + \ldots \tag{3.23}$$

where we have used

$$\Sigma_1^\dagger\,\Sigma_2 = f^2 - 2h^\dagger h + \frac{2}{3f^2}\left(h^\dagger h\right)^2 + \mathcal{O}\left(\frac{1}{f^2}\right)\,. \tag{3.24}$$

The absence of one–loop quadratic divergences is precisely the aim of the CSB mechanism, which we will understand now using symmetry arguments. First of all, one should notice that the generation of a mass term for the Higgs is possible because we have introduced an explicit breaking of the $SU(3)_1 \otimes SU(3)_2$ global symmetry by gauging only its diagonal subgroup as in eq. (3.21). Without this explicit breaking, the shift symmetries would have prevented its generation. The two $SU(3)_1 \otimes SU(3)_2$ symmetries are indeed broken to the diagonal group $SU(3)_\text{V}$, as one can directly see by checking that the Lagrangian is now invariant only if $\Sigma_{1,2}$ transform in the same way, namely

$$\begin{aligned}\mathcal{L}_2 \sim |g\,G_\mu\Sigma_1|^2 + |g\,G_\mu\Sigma_2|^2 &\xrightarrow{SU(3)^2} g^2\left|\left(UG_\mu U^\dagger\right)(U_1\Sigma_1)\right|^2 + g^2\left|\left(UG_\mu U^\dagger\right)(U_2\Sigma_2)\right|^2 \\ \overset{!}{=} \mathcal{L}_2 \quad &\Longleftrightarrow \quad U_1 = U_2 = U \equiv U_\text{V}\,.\end{aligned} \tag{3.25}$$

We then effectively have only one exact $SU(3)_\text{V}$ global symmetry to start with, and only one set of massless Goldstone bosons arises. On the other hand, the axial $SU(3)_\text{A}$ symmetry is explicitly broken in the gauging process, being thus only an approximate symmetry of the original Lagrangian: the corresponding Goldstone bosons get a mass term from loops involving gauge bosons, namely from the $SU(3)_\text{A}$–breaking operator of eq. (3.23).

If we would set the gauge coupling of Σ_2 to zero, we would restore the two independent $SU(3)_1 \otimes SU(3)_2$ symmetries, one acting on (Σ_1, G_μ), and the other acting on Σ_2. As a result, we would have again two spontaneously broken exact $SU(3)_\text{i}$ groups with a total number of ten massless Goldstone bosons, of which five are eaten via the gauging of $SU(3)_1$, and no mass term radiatively generated for the other five. Similarly, no mass term would be generated by setting the gauge coupling of Σ_1 to zero. Only in the presence of gauge couplings for both Σ_1 and Σ_2, the $SU(3)_1 \otimes SU(3)_2$ global symmetry is explicitly broken to $SU(3)_\text{V}$, and only then the pseudo–Goldstone boson Higgs can develop a potential. Therefore, any diagram which contributes to the Higgs mass has to involve both gauge couplings, being only log–sensitive in the compositeness scale.

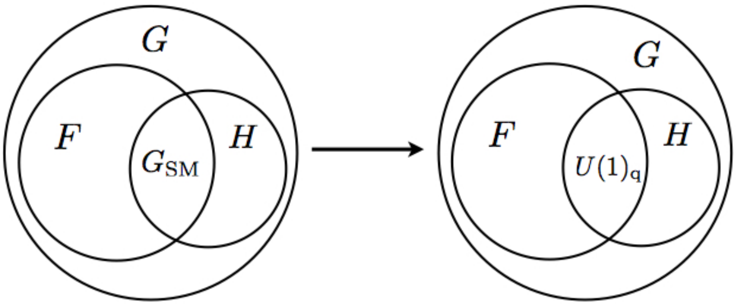

Figure 3.4: *Diagrammatic representation of the global/gauge structure of Little Higgs models. At tree–level (diagram on the left), a set of $F \setminus H$ gauge bosons obtain a mass of order f from the G/H spontaneous symmetry breaking, while the SM gauge group $G_{SM} \subset H$ remains unbroken. The Higgs doublet is identified among the G/H massless Goldstone bosons. At one–loop (diagram on the right), a further misalignment is generated from explicit breaking of the global symmetry, such that a potential for the Higgs is introduced and EWSB gets triggered, with only the $U(1)_q$ as remaining unbroken gauge subgroup. The SM gauge bosons acquire a mass of order v.*

Returning to a generic G/H setup, we have seen that in Little Higgs models the gauge group should not be a subgroup of the unbroken H group, because additional cancellon gauge fields with mass of order f are required to be present in the theory. A diagrammatic view of the global/gauge structure of Little Higgs models can be seen in figure 3.4. On the other hand, in generic Composite Models where no CSB mechanism is implemented, the gauge group of the theory might as well be identified with the SM gauge group and spontaneously broken only at loop–level, see figure 3.1. No additional cancellon gauge fields are indeed introduced, and the SM gauge bosons acquire a mass of order v at the price of additional fine–tuning.

3.2.3 Top–partner as a cancellon field

The other numerically most significant quadratic divergence stems from the top quark loop: at least the top Yukawa coupling should therefore be introduced following the CSB prescription, namely introducing $SU(3)$ symmetries into the Yukawa couplings which are collectively broken. To do so, we enlarge the third generation quark doublet into a triplet, adding a new left–handed fermion T with charge 2/3 which will mix with the SM top

$$\Psi = \begin{pmatrix} t \\ b \\ T \end{pmatrix} \equiv \begin{pmatrix} Q \\ T \end{pmatrix} . \tag{3.26}$$

To construct appropriate Yukawa couplings, we need to include the corresponding right–handed partners t_1^c, b^c, t_2^c, where t_2^c is the Dirac partner of T, so that we can write

$$\begin{aligned}\mathcal{L}_Y &= \lambda_1\, \Sigma_1^\dagger \Psi\, t_1^c + \lambda_2\, \Sigma_2^\dagger \Psi\, t_2^c = (t_1^c,\, t_2^c) \begin{pmatrix} \lambda_1 \Sigma_1^\dagger \\ \lambda_2 \Sigma_2^\dagger \end{pmatrix} \Psi \\ &\supset \lambda f \left(1 - \frac{h^\dagger h}{2f}\right) T^c T + \lambda h^\dagger Q t^c + \ldots \end{aligned} \tag{3.27}$$

For simplicity we have set $\lambda_1 = \lambda_2 \equiv \lambda/\sqrt{2}$, and identified the mass eigenstates

$$T^c = \frac{t_2^c + t_1^c}{\sqrt{2}}, \qquad t^c = \frac{t_2^c - t_1^c}{\sqrt{2}}\,. \tag{3.28}$$

From eq. (3.27) it is clear that we can identify λ with the SM top Yukawa coupling λ_t. Furthermore, the fermion partner T has a Dirac mass $\lambda_t f$ and a coupling to two Higgs fields with coupling constant $\lambda_t/(2f)$.

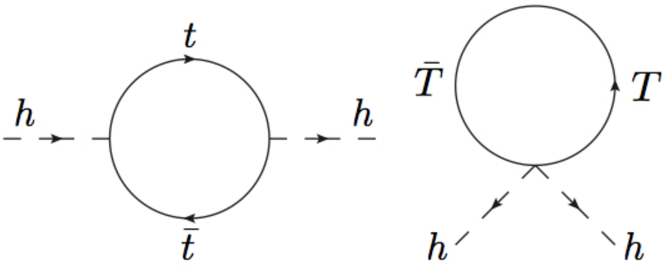

Figure 3.5: *Quadratically divergent one–loop contributions to the Coleman–Weinberg scalar potential from the top sector of the Little Higgs toy model.*

Both diagrams in figure 3.5 might contribute to generate a quadratically divergent Higgs mass, as in the SM for the top quark. This is however prevented by the collective implementation of the Yukawa couplings in (3.27). The quadratic–divergent part of the Coleman–Weinberg effective potential contains indeed only terms which are independent of the Higgs mass

$$\begin{aligned} V_{1\text{-loop}}(\Sigma) &\supset -\frac{2}{64\pi^2} \Lambda^2\, \mathrm{Tr}\left[M_t(\Sigma)^\dagger M_t(\Sigma)\right] \\ &\sim \lambda^2 \Lambda^2 \left(\Sigma_1^\dagger \Sigma_1 + \Sigma_2^\dagger \Sigma_2\right) = 2\lambda^2 \Lambda^2 f^2 + \ldots \end{aligned} \tag{3.29}$$

where the top mass matrix in the background of the Higgs field is

$$M_t(\Sigma) = \begin{pmatrix} \lambda_1 \Sigma_1^\dagger \\ \lambda_2 \Sigma_2^\dagger \end{pmatrix}. \tag{3.30}$$

In other words, the top partner loop quadratic divergence has compensated the contribution coming from the SM loop. It should be noted that this cancellation occurs between same–spin particles, unlike for example in Supersymmetry where new particles with different spin structure are introduced to address the hierarchy problem.

The absence of quadratic divergences from top loops can be again understood analyzing the symmetries of the Lagrangian (3.27) for the Σ_j fields. The term proportional to λ_1 forces Σ_1 and Ψ to transform identically under $SU(3)_1$, while the term proportional to λ_2 forces Σ_2 and Ψ to be aligned as well. Therefore, as in the gauge sector, the effective global symmetry structure is $SU(3)_V/SU(2)_V$, with five Goldstone bosons eaten by the heavy $SU(3)$ gauge bosons. Removing on the other hand one of the two Yukawa couplings restores a residual $SU(3)$ symmetry in the Lagrangian, because $\Sigma_{1,2}$ can transform independently while still leaving (3.27) invariant. Therefore, with either of the λ_i turned off, one would expect two sets of Goldstone bosons: one combination becomes the longitudinal degrees of freedom of the heavy gauge bosons, while the other set is left massless.

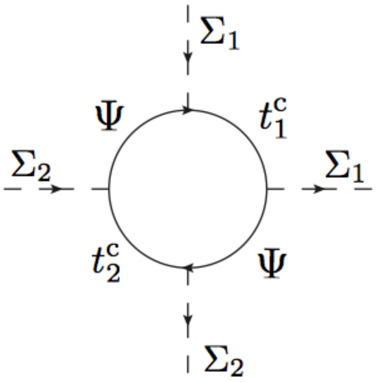

Figure 3.6: *Logarithmically divergent one–loop contribution to the Coleman–Weinberg scalar potential from the top sector of the Little Higgs toy model.*

In this way, a contribution to the Higgs potential can only come from a diagram involving both couplings λ_i. The lowest–order fermion diagram which involves both couplings is the loop as in figure 3.6, which is proportional to $|\lambda_1\lambda_2|^2$ and only log–sensitive to Λ, as a result of the collective introduction of the Yukawa couplings.

3.3 Overview of the considered models

In this section we will discuss in more details the three different Little Higgs models which have been considered as explicit framework for our analyses, namely the Simplest Little Higgs (SLH), the Littlest Higgs (L^{2}H), and the Littlest Higgs with T–parity (LHT). This section should not be thought as a comprehensive review, for which we refer the reader to [17, 26]. We will present separately the scalar, gauge and fermion sectors of the models, in order to underline the relevant phenomenological aspects.

3.3.1 Gauge and scalar sectors

Simplest Little Higgs

As discussed in our toy example, the simplest extension of the SM symmetry structure implementing a collective generation of quartic and gauge interactions requires the extension of the $SU(2)$ gauge group to $SU(3)$. In particular we introduce two different fields $\Sigma_{1,2}$ each parametrising the spontaneous global symmetry breaking $SU(3)_\mathrm{i} \to SU(2)_\mathrm{i}$ in the CCWZ formalism. In order to correctly reproduce the SM hypercharge quantum numbers, the SLH[1] prescription is to assign $SU(3)_\mathrm{i} \otimes U(1)_\mathrm{i}$ quantum numbers

$$\Sigma_\mathrm{i} \sim (\mathbf{3}, -\frac{1}{3}) \tag{3.31}$$

and aligned vacuum expectation values f_1, f_2. Therefore, the global symmetry structure could be expressed as

$$\frac{[SU(3)_\mathrm{i} \otimes U(1)_\mathrm{i}]^2}{[SU(2)_\mathrm{i} \otimes U(1)_\mathrm{i}]^2}\,, \tag{3.32}$$

giving rise to ten Goldstone bosons. The partial gauging of the diagonal subgroup $SU(3)_\mathrm{V} \otimes U(1)_\mathrm{X}$ generates a potential for five Goldstone bosons, among which we can identify the four degrees of freedom of the Higgs complex doublet, and a real scalar field η. The other five Goldstone bosons remain massless and become longitudinal degrees of freedom of five new gauge bosons after the spontaneous symmetry breaking

$$SU(3)_\mathrm{V} \otimes U(1)_\mathrm{X} \to SU(2)_\mathrm{L} \otimes U(1)_\mathrm{Y}\,. \tag{3.33}$$

The radiatively generated Higgs potential further triggers EWSB, such that three of the four degrees of freedom of the Higgs complex doublet become the longitudinal polarisations of the SM massive gauge bosons.

The SLH model belongs to the class of *Simple Group models*, because of the extension of the EW gauge group to an enlarged simple Lie group ($SU(3)$).

In unitarity gauge we can express the sigma fields $\Sigma_{1,2}$ as

$$\Sigma_1(x) = \exp\left(\frac{i\,t_\beta\,\Theta(x)}{f}\right)\begin{pmatrix}0\\0\\f\,c_\beta\end{pmatrix}\,, \qquad \Sigma_2(x) = \exp\left(-\frac{i\,\Theta(x)}{t_\beta\,f}\right)\begin{pmatrix}0\\0\\f\,s_\beta\end{pmatrix}\,, \tag{3.34}$$

---

[1] For the original references see [51, 52]. For detailed reviews see [29–33].

where $t_\beta = s_\beta/c_\beta = f_2/f_1$ is the ratio of the vacuum expectation values of the sigma fields, $f = \sqrt{f_1^2 + f_2^2}$, and $\Theta(x)$ the Goldstone boson matrix

$$\Theta = \pi^a\, X^a = \frac{1}{f}\left[\begin{pmatrix} \mathbb{0}_{2\times 2} & H \\ H^T & 0 \end{pmatrix} + \frac{\eta}{\sqrt{2}}\mathbb{1}_{3\times 3}\right], \qquad H = \begin{pmatrix} h \\ 0 \end{pmatrix}. \tag{3.35}$$

The kinetic term for $\Sigma_{1,2}$ is

$$\mathcal{L}_\Sigma = \sum_{i=1}^{2} |D_\mu \Sigma_i|^2 = \sum_{i=1}^{2}\left|\left(\partial_\mu + igA^a_\mu\lambda^a + \frac{ig_x}{3}B^x_\mu\right)\Sigma_i\right|^2, \tag{3.36}$$

where λ_a are $SU(3)$ generators, while A^a_μ and B^x_μ are the $SU(3)_\mathrm{V}$ and $U(1)_\mathrm{X}$ gauge fields, respectively. The gauge couplings g and g_x are fixed by the SM gauge couplings: the $SU(3)$ coupling g is exactly the SM $SU(2)_\mathrm{L}$ gauge coupling, and

$$g_x = \frac{g'}{\sqrt{1 - \frac{t_\mathrm{W}^2}{3}}} \tag{3.37}$$

with $t_\mathrm{W} \equiv \tan\theta_\mathrm{W}$, θ_W being the weak mixing angle.

The gauge boson mass eigenstates arising from (3.33) include a Z' as a linear combination of A^8_μ and B^x_μ, and a complex $SU(2)$ doublet (Y_0, X^-) with masses

$$m_{Z'} = \sqrt{\frac{2}{3 - t_\mathrm{W}^2}}\, gf\,, \qquad m_{X^\pm} = m_{Y_0} = m_{\bar{Y}_0} = \frac{gf}{\sqrt{2}}. \tag{3.38}$$

The other set of SM $SU(2)_\mathrm{L} \otimes U(1)_\mathrm{Y}$ gauge bosons is left massless at this point. After EWSB, the heavy gauge bosons receive additional mass contributions of order $\mathcal{O}(v^2/f^2)$, and in particular the Z' boson mixes with the analogous SM Z boson, leading to corrections to electroweak precision observables. The SM $W^\pm, Z$ gauge bosons acquire masses of

$$m_Z = \frac{gv}{2c_\mathrm{W}}\left(1 + \frac{v^2}{f^2}\frac{\left(1 - t_\mathrm{W}^2\right)^2}{16} + \mathcal{O}\left(\frac{v^4}{f^4}\right)\right), \tag{3.39}$$

$$m_W = \frac{gv}{2}\left(1 - \frac{1}{12}\frac{v^2}{f^2}\frac{t_\beta^4 - t_\beta^2 + 1}{t_\beta^2} + \mathcal{O}\left(\frac{v^4}{f^4}\right)\right) \tag{3.40}$$

while the photon remains massless. Notice the presence of $\mathcal{O}(v^2/f^2)$ custodial violating terms in eq. (3.39) and (3.40).

It is to be noted that the presence of the pseudo–scalar η and in particular of the coupling h–Z–η is a peculiar and distinguishing feature of the Simple Group models class, as already pointed out in [32, 33].

The vacuum expectation value v of the Higgs field is radiatively generated from the explicit breaking introduced by the gauge and Yukawa interactions. Its value is therefore predicted as a function of the model parameters, and we have the freedom to fix its value to reproduce e.g. the SM prediction for the W–boson mass, namely

$$m_W^{\mathrm{SM}} = \frac{g\, v_{\mathrm{SM}}}{2}\,, \qquad v_{\mathrm{SM}} \sim 246.26 \text{ GeV}\,. \tag{3.41}$$

Comparing eq. (3.40) and eq. (3.41) we can therefore fix

$$v = v_{\mathrm{SM}} \left(1 + \frac{1}{12} \frac{v_{\mathrm{SM}}^2}{f^2} \frac{t_\beta^4 - t_\beta^2 + 1}{t_\beta^2} \right) \tag{3.42}$$

such that

$$m_W = m_W^{\mathrm{SM}} + \mathcal{O}\left(\frac{v_{\mathrm{SM}}^4}{f^4} \right)\,. \tag{3.43}$$

In the Coleman–Weinberg potential up to dimension four operators, it can be shown [30] that only the $\left|\Sigma_1^\dagger \Sigma_2\right|^2$ term generates a non–trivial potential for the pseudo–Goldstone bosons. Another important observation is that $\left|\Sigma_1^\dagger \Sigma_2\right|^2$ does not have any η–dependence:

$$\Sigma_1^\dagger \Sigma_2 = f^2 s_\beta\, c_\beta \exp\left[-i \left(t_\beta + \frac{1}{t_\beta} \right) \frac{\eta}{\sqrt{2} f} \right] \cos\left(\frac{h}{f c_\beta s_\beta} \right)\,, \tag{3.44}$$

leaving the scalar field η massless, while a quartic coupling and a mass term for the Higgs are generated. The presence of a massless scalar field is problematic, and any term in the Coleman–Weinberg potential proportional to $\left|\Sigma_i^\dagger \Sigma_i\right|^{2n}$ or $\left|\Sigma_1^\dagger \Sigma_2\right|^{2n}$ cannot ameliorate the situation. This is the problem of a potentially “dangerous” singlet as already mentioned in section 3.2.1.

A possible solution to the massless η problem is to introduce by hand a new term in the scalar potential, namely

$$-\,\mu^2 \left(\Sigma_1^\dagger \Sigma_2 \,+\, \text{h.c.} \right)\,. \tag{3.45}$$

This term explicitly breaks the $[SU(3)_i]^2$ global symmetry, spoiling the CSB mechanism and reintroducing quadratically divergent corrections to the Higgs mass. However, since this correction turns out to be numerically insignificant, this solution is commonly used in literature and we will adopt this extension, too. But most importantly, it introduces an explicit η dependence, allowing for the generation of a mass term for η.

The scalar potential becomes

$$V_{\text{eff}} = -m^2\, H^\dagger H + \lambda \left(H^\dagger H \right)^2 - \frac{1}{2} m_\eta^2\, \eta^2 + \lambda' H^\dagger H\, \eta^2 + \ldots \tag{3.46}$$

where all parameters have been explicitly evaluated taking into account the one–loop contribution from the gauge and top Yukawa couplings [30], and assuming that the physics at the compositeness scale Λ does not generate additional significant contributions. The important point is that m^2 is generated with only log–sensitivity to Λ at one–loop. Minimising the scalar potential (3.46), one obtains the usual relations determining the value of the vacuum expectation value v of the Higgs field and its mass m_h as

$$v^2 = \frac{m^2}{\lambda}\,, \qquad m_h = \sqrt{2}m\,. \tag{3.47}$$

Including only the explicit one–loop results from the gauge and top Yukawa couplings and the contribution from eq. (3.45), all coefficients of the Coleman–Weinberg potential (3.46) are then known. Therefore, eq. (3.42) and eq. (3.47) represent three constraints to be imposed on the free parameters of the SLH model.

Littlest Higgs

We can move now to the class of *Product Group models*, where the weak gauge group emerges as the unbroken part of a product gauge group.

In our work we have focussed on the well–known Littlest Higgs model[2] ($\mathrm{L}^2\mathrm{H}$). The global structure of the model describes the spontaneous symmetry breaking given by

$$SU(5)/SO(5)\,. \tag{3.48}$$

The group $SU(5)$ has a total of 24 generators, of which 10 (T_a) span the unbroken $SO(5)$ subgroup, while the remaining 14 generators (X_a) span the coset $SU(5)/SO(5)$. Since $SU(5)$ is a symmetric space, with an automorphism related to the complex conjugation of the generators, we can make use of eq. (2.25) and eq. (2.27) to define our sigma field in the CCWZ formalism as

$$\Sigma = \exp\left[2i\frac{\pi^a X_a}{f}\right]\langle\Sigma\rangle\,. \tag{3.49}$$

In here, the vacuum expectation value $\langle\Sigma\rangle$ is given by an $SU(5)$ symmetric tensor field

$$\langle\Sigma\rangle = \begin{pmatrix} \mathbb{0}_{2\times2} & \mathbb{0}_{2\times1} & \mathbb{1}_{2\times2} \\ \mathbb{0}_{1\times2} & 1 & \mathbb{0}_{1\times2} \\ \mathbb{1}_{2\times2} & \mathbb{0}_{2\times1} & \mathbb{0}_{2\times2} \end{pmatrix}, \tag{3.50}$$

and Σ transforms under an $SU(5)$ transformation as [49]

$$\Sigma \to V\,\Sigma\,\tilde{V}^\dagger = V\,\Sigma\,V^{\mathrm{T}}\,, \qquad V \in SU(5)\,. \tag{3.51}$$

---

[2] For the original reference see [49]. For a detailed review see [35].

Since the vacuum is unchanged under an $SO(5)$ transformation $U \in SO(5)$, namely

$$U\langle\Sigma\rangle U^{\mathrm{T}} = \langle\Sigma\rangle\,, \qquad U = \exp\left[i\theta^a T_a\right] \in SO(5)\,, \tag{3.52}$$

by expanding the matrix U up to first order in θ^a we obtain

$$\langle\Sigma\rangle = \langle\Sigma\rangle + i\theta^a\left(T_a\langle\Sigma\rangle + \langle\Sigma\rangle T_a^{\mathrm{T}}\right) + \mathcal{O}\left(\theta^2\right) \tag{3.53}$$

which provides a recipe to identify the unbroken and broken generators T_a, X_a as

$$\{T_a, \langle\Sigma\rangle\} = 0 \tag{3.54}$$

$$[X_a, \langle\Sigma\rangle] = 0\,. \tag{3.55}$$

In order to obtain a collective generation of a Higgs potential, we require two copies of the SM gauge group to be simultaneously gauged within the global symmetry $SU(5)$. For this reason the Littlest Higgs belongs to the class of Product Group models. In particular, we embed the gauge group $\left[SU(2)_i \otimes U(1)_i\right]^2$ in $SU(5)$ such that the generators for the two $SU(2)_i$ are

$$Q_1^a = \frac{1}{2}\begin{pmatrix} \sigma^a & \mathbb{0}_{2\times3} \\ \mathbb{0}_{3\times2} & \mathbb{0}_{3\times3} \end{pmatrix}, \qquad Q_2^a = \frac{1}{2}\begin{pmatrix} \mathbb{0}_{3\times3} & \mathbb{0}_{2\times3} \\ \mathbb{0}_{3\times2} & -\sigma^{a\,*} \end{pmatrix} \tag{3.56}$$

with σ^a the Pauli matrices, while the $U(1)_i$ generators are

$$Y_1 = \frac{1}{10}\begin{pmatrix} -3\cdot\mathbb{1}_{2\times2} & \mathbb{0}_{2\times3} \\ \mathbb{0}_{3\times2} & 2\cdot\mathbb{1}_3 \end{pmatrix}, \qquad Y_2 = \frac{1}{10}\begin{pmatrix} -2\cdot\mathbb{1}_{3\times3} & \mathbb{0}_{2\times3} \\ \mathbb{0}_{3\times2} & 3\cdot\mathbb{1}_{2\times2} \end{pmatrix}. \tag{3.57}$$

It is easy to check that the following linear combinations of gauged generators

$$Q^a = \frac{1}{\sqrt{2}}\left(Q_1^a + Q_2^a\right), \qquad Y = Y_1 + Y_2 \tag{3.58}$$

satisfy eq. (3.54), being identified as the generators of the unbroken SM gauge group $SU(2)_{\mathrm{L}} \otimes U(1)_{\mathrm{Y}}$. On the other hand, the orthogonal combination of gauged generators satisfy eq. (3.55): the vacuum expectation value $\langle\Sigma\rangle$ thus leads to the spontaneous breaking of the gauge group to the SM group at the scale f, namely

$$\left[SU(2)_i \otimes U(1)_i\right]^2 \to SU(2)_{\mathrm{L}} \otimes U(1)_{\mathrm{Y}}\,, \tag{3.59}$$

such that a complete set of $SU(2) \otimes U(1)$ gauge bosons acquires a mass of order f.

Gauge interactions are introduced by a proper definition of the $\left[SU(2)_i \otimes U(1)_i\right]^2$ covariant derivative acting on the sigma field Σ, namely

$$D_\mu\Sigma = \partial_\mu\Sigma - i\sum_{j=1}^{2}\left[g_j\left(W_j\Sigma + \Sigma\,W_j^{\mathrm{T}}\right) + g_j'\left(B_j\Sigma + \Sigma\,B_j^{\mathrm{T}}\right)\right] \tag{3.60}$$

with $W_i = W^a_{i\mu}\, Q^a_i$, $B_i = B_{i\mu}\, Y_i$ $(i = 1, 2)$. The scalar kinetic term in the CCWZ formalism reads

$$\mathcal{L}_\Sigma = \frac{f^2}{8} \mathrm{Tr}\left[|D_\mu \Sigma|^2 \right] . \tag{3.61}$$

Explicitly, the 14 Goldstone bosons arising from the $SU(5)/SO(5)$ spontaneous symmetry breaking are given by

$$\pi^a X_a = \begin{pmatrix} \frac{1}{2} X & \frac{1}{\sqrt{2}} H^\dagger & \Phi^\dagger \\ \frac{1}{\sqrt{2}} H & \frac{2}{\sqrt{5}} \eta & \frac{1}{\sqrt{2}} H^* \\ \Phi & \frac{1}{\sqrt{2}} H^{\mathrm{T}} & \frac{1}{2} X^* \end{pmatrix} \tag{3.62}$$

where

$$X = \begin{pmatrix} \chi^0 - \frac{1}{\sqrt{5}}\eta & \sqrt{2}\chi^+ \\ \sqrt{2}\chi^- & -\chi^0 - \frac{1}{\sqrt{5}}\eta \end{pmatrix} , \quad \Phi = \begin{pmatrix} \phi^{++} & \frac{1}{\sqrt{2}}\phi^+ \\ \frac{1}{\sqrt{2}}\phi^+ & \phi^0 \end{pmatrix} , \quad H^{\mathrm{T}} = \begin{pmatrix} \pi^+ \\ \frac{h + i\pi^0}{\sqrt{2}} \end{pmatrix} . \tag{3.63}$$

In particular, under $SU(2)_{\mathrm{L}} \otimes U(1)_{\mathrm{Y}}$ the Goldstone bosons decompose as

$$\mathbf{1}_0 \oplus \mathbf{3}_0 \oplus \mathbf{2}_{\pm\frac{1}{2}} \oplus \mathbf{3}_{\pm 1} , \tag{3.64}$$

where the real singlet $\mathbf{1}_0$ (η) and the real triplet $\mathbf{3}_0$ (χ) are eaten by the heavy gauge bosons and do not appear in unitary gauge. The complex doublet $\mathbf{2}_{\pm\frac{1}{2}}$ (H) can be identified with the Higgs field, while the complex triplet $\mathbf{3}_{\pm 1}$ (Φ) is the physical quarticon field in the scalar sector.

The gauge boson mass eigenstates before EWSB are linear combinations of W_i, B_i with mixing angles given by

$$c = \frac{g_1}{\sqrt{g_1^2 + g_2^2}} , \qquad c' = \frac{g_1'}{\sqrt{g_1'^2 + g_2'^2}} . \tag{3.65}$$

Only one set of $SU(2) \otimes U(1)$ gauge bosons becomes massive,

$$m_{W^\pm_{\mathrm{H}}} = m_{Z_{\mathrm{H}}} = \frac{gf}{2sc} , \qquad m_{A_{\mathrm{H}}} = \frac{g'f}{2\sqrt{5}s'c'} , \tag{3.66}$$

where we have identified

$$g = g_1 s = g_2 c , \qquad g' = g_1' s' = g_2' c' . \tag{3.67}$$

EWSB induces a further mixing, with an additional contribution of order $\mathcal{O}(v^2/f^2)$ to the masses of the heavy gauge boson, and weak–scale masses for the SM $W^\pm, Z$ gauge bosons:

$$m_Z = \frac{gv}{2}\left[1 - \frac{1}{2}\frac{v^2}{f^2}\left(\frac{1}{6} + \frac{1}{4}\left(c^2 - s^2\right) + \frac{5}{4}\left(c'^2 - s'^2\right)^2\right) + 4\frac{v'^2}{v^2} + \mathcal{O}\left(\frac{v^4}{f^4}\right)\right], \tag{3.68}$$

$$m_{W^\pm} = \frac{gv}{2c_W}\left[1 - \frac{1}{2}\frac{v^2}{f^2}\left(\frac{1}{6} + \frac{1}{4}\left(c^2 - s^2\right)\right) + 2\frac{v'^2}{v^2} + \mathcal{O}\left(\frac{v^4}{f^4}\right)\right]. \tag{3.69}$$

Note again the presence of $\mathcal{O}(v^2/f^2)$ custodial violating terms in the SM gauge boson masses, as well as a contribution proportional to the vacuum expectation value v' of the field $\phi^0 \in \Phi$ which is generated after EWSB.

As for the SLH model, we have the freedom to fix the value of the vacuum expectation value v to reproduce the SM prediction for the W–boson mass (3.41): comparing with (3.69) we obtain the relation

$$v = v_{\rm SM}\left[1 + \frac{1}{2}\frac{v_{\rm SM}^2}{f^2}\left(\frac{1}{6} + \frac{1}{4}\left(c^2 - s^2\right)\right) - 2\frac{v'^2}{v_{\rm SM}^2}\right] \tag{3.70}$$

such that

$$m_W = m_W^{\rm SM} + \mathcal{O}\left(\frac{v_{\rm SM}^4}{f^4}\right). \tag{3.71}$$

Gauge and Yukawa interactions explicitly break the $SU(5)$ symmetry: a potential for the pseudo–Goldstone bosons is radiatively generated at loop–level. As usual, one can calculate the quadratic– and log–divergent contributions of the Coleman–Weinberg potential from the different mass matrices of gauge, fermion and scalar particles in the background of the Σ field. The dominant contribution comes from the quadratically divergent term, which turns out to generate a potential for the Higgs field and the complex triplet as [49]

$$\lambda_1 f^2 \left|\Phi_{ij} + \frac{i}{2f}\left(H_i H_j + H_j H_i\right)\right|^2 + \lambda_2 f^2 \left|\Phi_{ij} - \frac{i}{2f}\left(H_i H_j + H_j H_i\right)\right|^2. \tag{3.72}$$

The coefficient λ_1 includes contributions from both the gauge boson mass matrix as well as from the fermion mass matrix, and its corresponding operator preserves an $SU(3)$ "residual" symmetry (embedded in the lower–right corner of the gauge generators) under which the pseudo–Goldstone bosons shift–transform as

$$\begin{aligned} H_i &\to H_i + \epsilon_i + \dots \\ \Phi_{ij} &\to \Phi_{ij} - i\left(\epsilon_i H_j + \epsilon_j H_i\right) + \dots \end{aligned} \tag{3.73}$$

The coefficient λ_2 includes a contribution only from the gauge boson mass matrix, and its corresponding operator preserves another $SU(3)$ "residual" symmetry (embedded in the upper–left corner of the gauge generators) acting on the pseudo–Goldstone bosons as

$$\begin{aligned} H_i &\to H_i + \eta_i + \dots \\ \Phi_{ij} &\to \Phi_{ij} + i\left(\eta_i H_j + \eta_j H_i\right) + \dots \end{aligned} \tag{3.74}$$

These residual $SU(3)$ symmetries are due to the implementation of the CSB mechanism as detailed in section 3.2.1. A mass term for the triplet Φ of order gf and a quartic interaction for the Higgs field are generated from the quadratic–part of the Coleman–Weinberg potential, but no mass for the Higgs.

On the other hand, a dimension–two operator for the Higgs is generated at one–loop only from the log–divergent part of the Coleman–Weinberg potential, from contributions of gauge, fermion and scalar interactions. This is again a consequence of the CSB mechanism, guaranteeing a natural separation between the electroweak scale and Λ. In particular, a negative contribution to the dimension–two Higgs operator proportional to the heavy fermion mass is generated in the log–divergent part of the Coleman–Weinberg potential: this term dominates over the positive gauge and scalar contributions, such that EWSB can be triggered.

Including all contributions, the scalar potential can be finally expanded as

$$V_{\text{eff}} = \lambda_{\Phi^2} f^2 \,\text{Tr}\left(\Phi^\dagger \Phi\right) + i\lambda_{H\Phi H} f \left(H\Phi^\dagger H^{\text{T}} - H^* \Phi H^\dagger\right) - \mu^2 H H^\dagger + \lambda_{H^4}\left(HH^\dagger\right)^2 \tag{3.75}$$

where the different coefficients are functions of the fundamental parameters of the model, and their explicit values can be found in [35]. Minimisation of the scalar potential (3.75) leads to the generation of a vacuum expectation value for both the neutral components of the Higgs doublet (v) and of the complex triplet (v') as

$$v^2 = \frac{\mu^2}{\lambda_{H^4} - \lambda^2_{H\Phi H}/\lambda_{\Phi^2}}\,, \tag{3.76}$$

$$v' = \frac{\lambda_{H\Phi H}}{2\lambda_{\Phi^2}} \frac{v^2}{f^2}\,. \tag{3.77}$$

The corresponding scalar mass spectrum is given by

$$m_h = \sqrt{2}\mu\,, \tag{3.78}$$

$$m_\Phi = \frac{\sqrt{2} m_h f}{v} \frac{1}{\sqrt{1-x^2}} \tag{3.79}$$

where the masses of the triplet are degenerate at this order, and defining $x \equiv 4v'f/v^2$. Furthermore, the following relation among the vacuum expectation values has to hold in order to obtain a positive triplet mass:

$$\frac{v'^2}{v^2} < \frac{v^2}{16f^2}\,. \tag{3.80}$$

If the coefficients in the CW potential (3.75) can be fully calculated within the model, then eq. (3.70), eq. (3.76) and eq. (3.78) are three constraints to be imposed on the free parameters of the L^{2}H model. However, it is to be noted that there could exist important two–loop contributions to the Higgs potential, in particular of the same order as the log–divergent terms: these two–loop contributions have not been evaluated, and therefore we will treat the μ^2 coefficient of the dimension–two Higgs operator as a free parameter of the theory of order $f^2/16\pi^2$.

Littlest Higgs with T–parity

As we will detail in a following section, the original Littlest Higgs model suffers from severe constraints from electroweak precision tests, which could only be satisfied in rather extreme regions of the parameter space. This is especially important after the discovery of a light Higgs boson, as there could have been a cancellation to precision observables between the gauge states and a heavy Higgs scalar.

The most severe constraints arise from tree–level corrections to precision observables due to the exchange of the heavy gauge bosons, as well as from the small but non–vanishing vacuum expectation value v' of the triplet scalar Φ. These constraints might be evaded either by a different model building approach, including e.g. a custodial symmetry in the theory, or with the introduction of a conserved discrete symmetry called T–parity, such that tree–level contributions to EWPT from heavy gauge bosons and from v' are removed.

The Littlest Higgs model with T–parity[3] (LHT) shares the same global and local symmetry structure of the original L^{2}H model. T–parity is originally inherited from the automorphism of the Lie algebra generators [53, 54], namely

$$T^a \to T^a \tag{3.81}$$

$$X^a \to -X^a\,, \tag{3.82}$$

which in the specific $SU(5)/SO(5)$ case can be expressed as

$$\tau^a \to \langle\Sigma\rangle\,(\tau^a)^T\,\langle\Sigma\rangle \tag{3.83}$$

for any generator τ^a.

In the gauge sector, T–parity is then introduced as an exchange symmetry between the gauge bosons of the two different copies of the SM gauge group as

$$T: \qquad W^a_{1\,\mu} \leftrightarrow W^a_{2\,\mu}\,, \qquad B_{1\,\mu} \leftrightarrow B_{2\,\mu}\,. \tag{3.84}$$

---

[3] For the original references see [53, 54]. For detailed reviews see [36–40].

The gauge kinetic term in the CCWZ formalism (3.61) becomes T–parity invariant for

$$g_1 = g_2 = \sqrt{2}\, g\,, \qquad g_1' = g_2' = \sqrt{2}\, g' \tag{3.85}$$

or equivalently, by fixing the mixing angles in the gauge sector of eq. (3.65) to

$$c = c' = s = s' = \frac{1}{\sqrt{2}}\,. \tag{3.86}$$

The gauge boson masses in eq. (3.66), (3.68), (3.69) are modified accordingly with (3.86). The custodial symmetry violating term in (3.69) vanishes. The crucial point is that the heavy gauge bosons are odd under a T–parity transformation (3.84), while the SM gauge bosons are even. This transformation property holds even after EWSB, which induces a further mixing only between states with equal T–parity.

The action of T–parity in the scalar sector is defined as a transformation acting on the Goldstone boson matrix (3.62)

$$T: \qquad \pi^a X_a \equiv \pi \to -\Omega\, \pi\, \Omega \tag{3.87}$$

$$\Omega = \begin{pmatrix} \mathbb{1}_{2\times 2} & & \\ & -1 & \\ & & \mathbb{1}_{2\times 2} \end{pmatrix}$$

which gives the Higgs doublet H a positive parity, while keeping the triplet Φ odd. Being odd under an exact discrete symmetry, the triplet Φ cannot acquire a vacuum expectation value, namely $v' = 0$, as e.g. the coupling $H^\dagger \Phi H$ in (3.75) is forbidden by T–parity. Such a symmetry can only be broken by anomalies [58]. The scalar triplet mass (3.79) as well as the SM gauge boson masses (3.68), (3.69), and the relation defining the vacuum expectation value for the Higgs doublet (3.70) are modified accordingly.

3.3.2 Fermion sectors

Simplest Little Higgs

As for the simplified model of section 3.2.3, the SM fermion doublets must be expanded into triplets of $SU(3)$ for gauge invariance. The corresponding right–handed components then transform as $SU(3)$ singlets. We will present now the *anomaly–free* embedding of the fermion sector of SLH, which has the upside to define an anomaly–free low–energy theory without additional degrees of freedom [59, 60].

Each lepton family consists of an $SU(3)$ left–handed triplet and two right–handed singlets (no light right–handed neutrino is introduced):

$$L_m^{\mathrm{T}} = (\nu_{\mathrm{L}}, \ell_{\mathrm{L}}, iN_{\mathrm{L}})_m\,, \quad \ell_{\mathrm{R}\,m}\,, \quad N_{\mathrm{R}\,m}\,. \tag{3.88}$$

In the quark sector, the first two generations are required to contain $SU(3)$ left–handed conjugate triplet representations and three right–handed singlets, while the third generation is analogous to the lepton sector:

$$Q_1^{\mathrm{T}} = (d_{\mathrm{L}}, -u_{\mathrm{L}}, iD_{\mathrm{L}})\,, \quad d_{\mathrm{R}}\,, \quad u_{\mathrm{R}}\,, \quad D_{\mathrm{R}} \tag{3.89}$$

$$Q_2^{\mathrm{T}} = (s_{\mathrm{L}}, -c_{\mathrm{L}}, iS_{\mathrm{L}})\,, \quad s_{\mathrm{R}}\,, \quad c_{\mathrm{R}}\,, \quad S_{\mathrm{R}} \tag{3.90}$$

$$Q_3^{\mathrm{T}} = (t_{\mathrm{L}}, b_{\mathrm{L}}, iT_{\mathrm{L}})\,, \quad t_{\mathrm{R}}\,, \quad b_{\mathrm{R}}\,, \quad T_{\mathrm{R}}\,. \tag{3.91}$$

The gauge representations and hypercharges for the fermion sector can be found in [31].

The Yukawa Lagrangian in the anomaly–free embedding for the quarks reads

$$\mathcal{L}_Y \supset i\,(\bar{d}_{\mathrm{R}}^1,\, \bar{d}_{\mathrm{R}}^2)\, Q_1^{\mathrm{T}} \begin{pmatrix} \lambda_1^d \Sigma_1 \\ \lambda_2^d \Sigma_2 \end{pmatrix} + i\,(\bar{s}_{\mathrm{R}}^1,\, \bar{s}_{\mathrm{R}}^2)\, Q_2^{\mathrm{T}} \begin{pmatrix} \lambda_1^s \Sigma_1 \\ \lambda_2^s \Sigma_2 \end{pmatrix} \tag{3.92}$$

$$+ (\bar{t}_{\mathrm{R}}^1,\, \bar{t}_{\mathrm{R}}^2) \begin{pmatrix} \lambda_1^t \Sigma_1^\dagger \\ \lambda_2^t \Sigma_2^\dagger \end{pmatrix} Q_3 + \sum_m \frac{\lambda_b^m}{\Lambda} \bar{d}_{\mathrm{R}\,m}\, \epsilon_{ijk}\, \Sigma_1^i\, \Sigma_2^j\, Q_3^k \tag{3.93}$$

$$+ i \sum_{m,n} \frac{\lambda_u^{mn}}{\Lambda} \bar{u}_{\mathrm{R}\,m}\, \epsilon_{ijk}\, \Sigma_1^{i\,*}\, \Sigma_2^{j\,*}\, Q_n^k \tag{3.94}$$

where $d_{\mathrm{R}}^1, d_{\mathrm{R}}^2$ are linear combinations of $d_{\mathrm{R}}, D_{\mathrm{R}}$ and analogously for $(s_{\mathrm{R}}^1, s_{\mathrm{R}}^2)$, $(t_{\mathrm{R}}^1, t_{\mathrm{R}}^2)$. Furthermore, $d_{\mathrm{R}\,m}$ runs over $(d_{\mathrm{R}}, s_{\mathrm{R}}, b_{\mathrm{R}}, D_{\mathrm{R}}, S_{\mathrm{R}})$, $u_{\mathrm{R}\,m}$ runs over $(u_{\mathrm{R}}, c_{\mathrm{R}}, t_{\mathrm{R}}, T_{\mathrm{R}})$, namely with $m, n = 1, 2$ and $i, j, k = 1, 2, 3$. Dimension–five operators in eq. (3.93), suppressed by one power of the scale Λ, are needed to generate the masses of the light quarks (u, c, b) and to possibly generate flavour mixing effects.

The lepton Lagrangian is analogous to the third generation terms of eq. (3.93) but without a “collective structure”, because of the non–severity of the quadratic divergences due to the small size of the lepton Yukawa couplings:

$$\mathcal{L}_Y \supset i\lambda_N^m\, \bar{N}_{\mathrm{R}m}\, \Sigma_2^\dagger\, L_m + \sum_m \frac{i\lambda_\ell^{mn}}{\Lambda} \bar{\ell}_{\mathrm{R}\,m}\, \epsilon_{ijk}\, \Sigma_1^i\, \Sigma_2^j\, L_n^k\,. \tag{3.95}$$

Before EWSB, the heavy fermion partners get the following mass terms:

$$m_{\rm T} = f\sqrt{\left(\lambda_1^t\right)^2 c_\beta^2 + \left(\lambda_2^t\right)^2 s_\beta^2} \tag{3.96}$$

$$m_{\rm D} = f\sqrt{\left(\lambda_1^d\right)^2 c_\beta^2 + \left(\lambda_2^d\right)^2 s_\beta^2} \tag{3.97}$$

$$m_{\rm S} = f\sqrt{\left(\lambda_1^s\right)^2 c_\beta^2 + \left(\lambda_2^s\right)^2 s_\beta^2} \tag{3.98}$$

$$m_{{\rm N}\,i} = f\, s_\beta\, \lambda_N^i\,. \tag{3.99}$$

After EWSB, the heavy partner masses receive other $\mathcal{O}(v^2/f^2)$ contributions, while the SM fermions get masses proportional to the weak scale v:

$$m_u = -\frac{v}{\sqrt{2}}\frac{f}{\Lambda}\lambda_u^{11}\,, \quad m_c = -\frac{v}{\sqrt{2}}\frac{f}{\Lambda}\lambda_u^{22}\,, \quad m_b = -\frac{v}{\sqrt{2}}\frac{f}{\Lambda}\lambda_b^{3}\,, \quad m_{\ell\,i} = -\frac{v}{\sqrt{2}}\frac{f}{\Lambda}\lambda_\ell^{ii} \tag{3.100}$$

$$m_t = \frac{v}{\sqrt{2}}\frac{\lambda_1^t\lambda_2^t}{\sqrt{\left(\lambda_1^t\right)^2 c_\beta^2 + \left(\lambda_2^t\right)^2 s_\beta^2}} \tag{3.101}$$

$$m_d = -\frac{v}{\sqrt{2}}\frac{\lambda_1^d\lambda_2^d}{\sqrt{\left(\lambda_1^d\right)^2 c_\beta^2 + \left(\lambda_2^d\right)^2 s_\beta^2}} \tag{3.102}$$

$$m_s = -\frac{v}{\sqrt{2}}\frac{\lambda_1^s\lambda_2^s}{\sqrt{\left(\lambda_1^s\right)^2 c_\beta^2 + \left(\lambda_2^s\right)^2 s_\beta^2}}\,. \tag{3.103}$$

With appropriate choices of the free parameters one can recover the mass values as in the SM.

Considering only the third generation, fixing the SM top and bottom masses to their experimental values will fix two free parameters, leaving only f, t_β and $R = \lambda_1^t/\lambda_2^t$ as free parameters. In terms of mass eigenstates we can finally obtain

$$\begin{aligned}\mathcal{L}_Y \supset & -m_{\rm T}\,\bar{T}_{\rm R}\,T_{\rm L} - m_{\rm t}\,\bar{t}_{\rm R}\,t_{\rm L} \\ & + \lambda_t\, h\,\bar{t}_{\rm R}\,t_{\rm L} + \lambda_T\, h\,\bar{T}_{\rm R}\,t_{\rm L} + \frac{\lambda_T'}{2m_{\rm T}}\,h\,h\,\bar{T}_{\rm R}\,T_{\rm L} + {\rm h.c.}\end{aligned} \tag{3.104}$$

where all coefficients can be expressed in terms of the already mentioned free parameters. In particular, the relation

$$\lambda_T' = \lambda_t^2 + \lambda_T^2 \tag{3.105}$$

is guaranteed by the collective structure, and allows for the cancellation of the quadratic divergences to the Higgs mass from loops involving the top fermions. Note also that the top Yukawa coupling (3.101) vanishes if either of the λ_i^t is set to zero, as required again by the CSB mechanism.

Kinetic terms for all fermion fields according to the assigned gauge quantum numbers are introduced, generating interaction terms among the different fermions and gauge bosons of the SLH model [31].

Littlest Higgs

The top partner cancellon field is introduced in the L^{2}H model as a vector–like fermion t_2 with $[SU(2)_i \otimes U(1)_i]^2$ quantum numbers $(\mathbf{3},\mathbf{1})_{\mathrm{Y}_i}$. The explicit $U(1)_i$ quantum numbers can be found in [35]. Being vector–like, the top partner is allowed to get a bare mass chosen to be of order f. The SM third generation quark doublet is then embedded with the top partner t_2 into an incomplete $SU(5)$ multiplet

$$\Psi = \begin{pmatrix} i\, b_{\mathrm{L}} \\ -i\, t_{1\,\mathrm{L}} \\ t_{2\,\mathrm{L}} \\ \mathbb{0}_{2\times 1} \end{pmatrix} \equiv \begin{pmatrix} q_{\mathrm{L}} \\ t_{2\,\mathrm{L}} \\ \mathbb{0}_{2\times 1} \end{pmatrix} . \tag{3.106}$$

The collective and gauge invariant Yukawa Lagrangian for the third generation reads

$$\mathcal{L}_Y \supset \frac{1}{2}\lambda_1 f \left(\epsilon_{ijk}\, \epsilon_{xy}\, \bar{\Psi}_i\, \Sigma_{jx}\, \Sigma_{ky}\, t_{1\,\mathrm{R}}\right) + \lambda_2 f \left(\bar{t}_{2\,\mathrm{L}}\, t_{2\,\mathrm{R}}\right) + \text{h.c.} \tag{3.107}$$

where the indices i,j,k are summed over $1,2,3$, and x,y are summed over $4,5$. This interaction satisfies the collective requirements: the λ_1 operator preserves $SU(3)_1$ and breaks $SU(3)_2$, while the λ_2 term vice–versa.

By expanding the Σ field and including the Higgs vacuum expectation value from EWSB, one obtains the following terms involving the top and top partner fields

$$\mathcal{L}_Y \supset \lambda_1 f \left(\frac{s_\Sigma}{\sqrt{2}}\, \bar{t}_{1\,\mathrm{L}}\, t_{1\,\mathrm{R}} + \frac{1+c_\Sigma}{2}\, \bar{t}_{2\,\mathrm{L}}\, t_{1\,\mathrm{R}}\right) + \lambda_2 f \left(\bar{t}_{2\,\mathrm{L}}\, t_{2\,\mathrm{R}}\right) + \text{h.c.} \tag{3.108}$$

$$= \left(\bar{t}_{1\,\mathrm{L}},\, \bar{t}_{2\,\mathrm{L}}\right) \begin{pmatrix} \lambda_1 f\, s_\Sigma/\sqrt{2} & 0 \\ \lambda_1 f\,(1+c_\Sigma)/2 & \lambda_2 f \end{pmatrix} \begin{pmatrix} t_{1\,\mathrm{R}} \\ t_{2\,\mathrm{R}} \end{pmatrix} + \text{h.c.} \tag{3.109}$$

$$\equiv \left(\bar{t}_{1\,\mathrm{L}},\, \bar{t}_{2\,\mathrm{L}}\right) M_{\mathrm{t}} \begin{pmatrix} t_{1\,\mathrm{R}} \\ t_{2\,\mathrm{R}} \end{pmatrix} + \text{h.c.} \tag{3.110}$$

where $c_\Sigma = \cos\left(\sqrt{2}(h+v)/f\right)$, $s_\Sigma = \sin\left(\sqrt{2}(h+v)/f\right)$. Diagonalisation of the mass matrix leads to the following spectrum for the SM top and top partner, at leading order in the v/f expansion of Σ:

$$m_t = \frac{\lambda_1\, \lambda_2}{\sqrt{\lambda_1^2+\lambda_2^2}}\, v\,, \qquad m_{\mathrm{T}} = f\sqrt{\lambda_1^2+\lambda_2^2}\,. \tag{3.111}$$

Fixing the SM top mass to the experimental value leaves either λ_1 or λ_2 as free parameter besides f.

An explicit calculation of the quadratic divergent term of the Coleman–Weinberg potential from the top mass matrix in eq. (3.109) reveals no dependence on the Higgs mass operator $h^\dagger h$:

$$V_{1\text{-loop}}(\Sigma) \supset -\frac{2}{64\pi^2}\Lambda^2 \,\mathrm{Tr}\left[M_{\mathrm{t}}^\dagger M_{\mathrm{t}}\right] \sim \Lambda^2 f^2 \left(\lambda_1^2 + \lambda_2^2\right) \,. \tag{3.112}$$

This is the result of the CSB mechanism implemented in the top Yukawa coupling. The top partner T plays therefore the role of the cancellon field of the top sector of the L^{2}H model.

The Yukawa interactions for the up–type quarks of the first two generations have the same form as eq. (3.107), except that no extra vector–like quark partners $\left(u^i_{2\,\mathrm{L}}, u^i_{2\,\mathrm{R}}\right)$, $i = 1, 2$, are introduced: no collective interaction is needed for the first two generations, since the quadratic divergent contributions to the Higgs mass are negligible. The Yukawa interactions for the down–type quarks and charged leptons of the three generations are generated by a similar Lagrangian without additional fermion partners:

$$\mathcal{L}_Y \supset \frac{1}{2}\lambda_d f \left(\epsilon_{ijk}\,\epsilon_{xy}\,\bar{\Psi}_i\,\Sigma^*_{jx}\,\Sigma^*_{ky}\,d_{1\,\mathrm{R}}\right) + \text{h.c.} \tag{3.113}$$

Together with the Yukawa interactions, kinetic terms for all fermion fields are introduced accordingly, generating interaction terms among the different fermions and gauge bosons of the L^{2}H model [35].

Littlest Higgs with T–parity

All Lagrangian terms are required to satisfy T–parity. This is achieved in the top sector by introducing a second $SU(5)$ incomplete multiplet

$$\Psi' = \begin{pmatrix} \mathbb{0}_{2\times 1} \\ t'_{2\,\mathrm{L}} \\ i\,b'_{\mathrm{L}} \\ -i\,t'_{1\,\mathrm{L}} \end{pmatrix} \equiv \begin{pmatrix} \mathbb{0}_{2\times 1} \\ t'_{2\,\mathrm{L}} \\ q'_{\mathrm{L}} \end{pmatrix} , \tag{3.114}$$

as well as the right–handed counterparts q'_{R}, $t'_{2\,\mathrm{R}}$, and by assigning the following T–parity transformation properties

$$T : \begin{cases} \Psi \leftrightarrow -\langle\Sigma\rangle\Psi' \quad \left(q_{\mathrm{L}} \leftrightarrow -q'_{\mathrm{L}}\,,\ t_{2\,\mathrm{L}} \leftrightarrow -t'_{2\,\mathrm{L}}\right) \\ t_{1\,\mathrm{R}} \leftrightarrow t_{1\,\mathrm{R}} \\ t'_{2\,\mathrm{R}} \leftrightarrow -t'_{2\,\mathrm{R}} \\ \Sigma \rightarrow \tilde{\Sigma} \equiv \langle\Sigma\rangle\,\Omega\,\Sigma^\dagger\,\Omega\,\langle\Sigma\rangle \end{cases} \tag{3.115}$$

such that a T–parity invariant version of eq. (3.107) can be written as

$$\mathcal{L}_Y \supset \frac{\lambda_1 f}{2\sqrt{2}}\,\epsilon_{ijk}\,\epsilon_{xy}\left(\bar{\Psi}_i\,\Sigma_{jx}\,\Sigma_{ky} - \left(\bar{\Psi}'\langle\Sigma\rangle\right)_i\,\tilde{\Sigma}_{jx}\,\tilde{\Sigma}_{ky}\right) t_{1\,\mathrm{R}} + \lambda_2 f\left(\bar{t}_{2\,\mathrm{L}}\,t_{2\,\mathrm{R}} + \bar{t}'_{2\,\mathrm{L}}\,t'_{2\,\mathrm{R}}\right) + \text{h.c.}\,. \tag{3.116}$$

The T–parity eigenstates of the Lagrangian (3.116) are given by

$$q_{\mathrm{L}\,\pm} = \frac{1}{\sqrt{2}}\left(q_{\mathrm{L}} \mp q'_{\mathrm{L}}\right)\,, \quad t_{2\,\mathrm{L},\pm} = \frac{1}{\sqrt{2}}\left(t_{2\,\mathrm{L}} \mp t'_{2\,\mathrm{L}}\right)\,, \quad t_{2\,\mathrm{R},\pm} = \frac{1}{\sqrt{2}}\left(t_{2\,\mathrm{R}} \mp t'_{2\,\mathrm{R}}\right)\,. \tag{3.117}$$

In terms of these eigenstates, upon expanding the Σ field and including the Higgs vacuum expectation value, one obtains analogous terms as in eq. (3.108)

$$\mathcal{L}_Y \supset \lambda_1 f\left(\frac{s_\Sigma}{\sqrt{2}}\,\bar{t}_{1\,\mathrm{L},+}\,t_{1\,\mathrm{R},+} + \frac{1+c_\Sigma}{2}\,\bar{t}_{2\,\mathrm{L},+}\,t_{1\,\mathrm{R},+}\right) + \lambda_2 f\left(\bar{t}_{2\,\mathrm{L},+}\,t_{2\,\mathrm{R},+} + \bar{t}_{2\,\mathrm{L},-}\,t_{2\,\mathrm{R},-}\right) + \text{h.c.}\,. \tag{3.118}$$

The absence of quadratic divergences to the Higgs mass operator $h^\dagger h$ is therefore preserved, as for the L^{2}H model (3.112). It is to be noted that in eq. (3.118), no mass term for the T–odd combination $t_- \equiv (t_{1\,\mathrm{L},-}, t_{1\,\mathrm{R},-})$ is generated, while the T–odd combination $T_- \equiv (t_{2\,\mathrm{L},-}, t_{2\,\mathrm{R},-})$ obtains a mass $\lambda_2 f$. By diagonalising the T–even mass terms one can obtain the following mass spectrum at leading order in the v/f expansion of Σ:

$$m_{t_+} \equiv m_t = \frac{\lambda_1\,\lambda_2}{\sqrt{\lambda_1^2+\lambda_2^2}}\,v\,, \qquad m_{\mathrm{T}_+} = f\sqrt{\lambda_1^2+\lambda_2^2}\,, \qquad m_{\mathrm{T}_-} = \lambda_2 f\,. \tag{3.119}$$

As in the L^{2}H model, fixing the SM top mass to the experimental value leaves either λ_1 or λ_2 as free parameter besides f.

Analogous Yukawa Lagrangians are introduced for the up–type quarks of the first two generations, but without the addition of vector–like top partners. A T–parity invariant version of eq. (3.113) for down–quarks and charged leptons can be obtained as [38]

$$\mathcal{L}_Y \supset \frac{i\lambda_d f}{2\sqrt{2}}\,\epsilon_{ij}\,\epsilon_{xyz}\left(\bar{\Psi}'_x\,\Sigma_{iy}\,\Sigma_{jz}\,X - \left(\bar{\Psi}\langle\Sigma\rangle\right)_x\,\tilde{\Sigma}_{iy}\,\tilde{\Sigma}_{jz}\,\tilde{X}\right) d_{\mathrm{R}}\,. \tag{3.120}$$

The SM doublet q_{L} is now embedded as $-\sigma_2\,q_{\mathrm{L}}$ in Ψ, and analogously for Ψ'.

The insertion of X is needed for gauge invariance, transforming as a singlet under $SU(2)_{1,2}$ and with $U(1)_{1,2}$ charges $(1/10, -1/10)$. $\tilde{X}$ is the T–parity image of X. Two possible choices for X are used in literature, namely $X = (\Sigma_{33})^{-1/4}$ and $X = (\Sigma_{33})^{1/4}$, called *Case A* and *Case B* respectively, where Σ_{33} is the (3,3) component of the non–linear sigma model field Σ.

It is necessary to introduce new operators in our theory to give rise to a mass term for the T–odd fermion t_-, since no corresponding mass term is generated via the Yukawa interaction eq. (3.116). Another $SO(5)$ multiplet Ψ_c is introduced as

$$\Psi_c = \begin{pmatrix} i\,d_c \\ -i\,u_c \\ \chi_c \\ i\,\tilde{d} \\ -i\,\tilde{u}_c \end{pmatrix} \equiv \begin{pmatrix} q_c \\ \chi_c \\ \tilde{q}_c \end{pmatrix} , \tag{3.121}$$

transforming under T–parity as

$$T: \quad \Psi_c \to -\Psi_c\,. \tag{3.122}$$

Its components are called *mirror fermions*. A viable $SU(5)$ and T–parity invariant Lagrangian is given by

$$\mathcal{L}_\kappa = -\kappa\, f \left(\bar{\Psi}'\, \xi\, \Psi_c + \bar{\Psi}\, \langle\Sigma\rangle\, \Omega\, \xi^\dagger\, \Omega\, \Psi_c \right) + \text{h.c.} \tag{3.123}$$

where one should also add explicit Dirac mass terms for the left–over T–odd states. This Lagrangian induces new Higgs boson interactions with up–type partners as well as the mass terms for all the T–odd fermions $q_{\mathrm{L},-}$ (3.117):

$$\mathcal{L}_\kappa \supset -\sqrt{2}\kappa\, f \left[\bar{d}_{\mathrm{L},-}\, \tilde{d}_c + \frac{1+c_\xi}{2} \bar{u}_{\mathrm{L},-}\, \tilde{u}_c - \frac{s_\xi}{\sqrt{2}} \bar{u}_{\mathrm{L},-}\, \chi_c - \frac{1-c_\xi}{2} \bar{u}_{\mathrm{L},-}\, u_c \right] + \text{h.c.} + \dots \tag{3.124}$$

where $c_\xi = \cos\left((v+h)/\sqrt{2}f\right)$, $s_\xi = \sin\left((v+h)/\sqrt{2}f\right)$. For simplicity, one can assume that the coupling κ is diagonal and flavour independent, forcing the T–odd fermions to be degenerate.

In particular, after EWSB, the following mass spectrum is generated at order $\mathcal{O}(v^2/f^2)$ for each generation of quarks and leptons:

$$m_{u_-} = \sqrt{2}\,\kappa\, f \left(1 - \frac{1}{8}\frac{v^2}{f^2} \right) , \quad m_{d_-} = \sqrt{2}\,\kappa\, f \tag{3.125}$$

for a total of twelve additional T–odd fermions partners.

From the kinetic terms of the fermion fields one can obtain the gauge–fermion interactions, too: a collection of Feynman Rules for the LHT model can be found e.g. in ref. [40].

Chapter 4

Lessons from collected data, so far

This chapter details the results of my research work on constraining the parameter space of the considered Little Higgs models using the available public experimental data. A first section is dedicated to the results obtained including Electroweak Precision observables, which historically have always represented the most severe constraints to be taken into account. A second section details the Little Higgs modifications involving Higgs sector observables: the final aim is indeed the inclusion of the newly collected Higgs data to probe the Little Higgs parameter space. A final section is dedicated to a systematic recasting procedure of LHC direct searches for new particles, under the hypothesis of a Little Higgs signal, to obtain a further and complementary experimental information with respect to Higgs and Electroweak Precision data. An optimisation of the analyses assuming a Little Higgs signal is also proposed, to possibly increase the exclusion power to otherwise unconstrained parameter space regions. The corresponding publications are [7–9]. The main resources used for this chapter are refs. [7–9, 24, 37, 61, 62].

4.1 Electroweak Precision Tests

Not only can new physics appear as detectable external states, either directly as new final state particles, or as intermediate steps of longer decay chains: interaction terms of new physics with SM particles can generate sensible effects even through modifications of SM–like couplings, or by radiative contributions at loop–level.

Precisely measured observables might thus possess a huge discrimination power against new physics effects. In particular, two–point functions of the gauge fields have been tightly constrained by the experiments at LEP, as we will discuss in the following. Let us parametrise the most general $U(1)_{\rm em}$–invariant Lagrangian involving only quadratic terms of SM gauge bosons as

$$\mathcal{L}_{V^2} = -\frac{1}{2} W_3^\mu \, \Pi_{33}(p^2) \, W_{3\,\mu} - W_3^\mu \, \Pi_{3B}(p^2) \, B_\mu - \frac{1}{2} B^\mu \, \Pi_{BB}(p^2) \, B_\mu - W_+^\mu \, \Pi_{+-}(p^2) \, W_{-\,\mu} \,, \tag{4.1}$$

where the different form factors $\Pi(p^2)$, in an effective low–energy point of view, get corrections from both SM and possibly BSM degrees of freedom. The effective Lagrangian (4.1) is in this sense independent of the particular high–energy completion of the SM, since it generically parametrises any possible additional contribution to the quadratic terms.

By expanding the form factors in terms of small momenta p^2 we obtain

$$\Pi(p^2) = \Pi(0) + p^2 \, \Pi'(0) + \frac{p^4}{2} \, \Pi''(0) + \mathcal{O}(p^6) \,, \tag{4.2}$$

for a total of 12 different coefficients parametrising all possible contributions to eq. (4.1) up to $\mathcal{O}(p^6)$. However, some form factors are nothing but the renormalised SM parameters which have to be matched to the experimental values. In particular $\Pi_{+-}(0)', \Pi_{BB}(0)'$ fix the normalisation of the gauge kinetic terms and $\Pi_{+-}(0)$ the renormalised W mass:

$$\Pi'_{+-}(0) = \Pi'_{BB}(0) = 1 \,, \tag{4.3}$$

$$\Pi_{+-}(0) = -m_{\rm W}^2 \,. \tag{4.4}$$

Two additional constraints follow from requiring a massless photon, namely $\Pi_{\gamma\gamma}(0) = \Pi_{Z\gamma}(0) = 0$. In conclusion, seven are the remaining coefficients which enclose possible electroweak corrections, and are expressed in terms of the following *oblique parameters* [24]:

$$\hat{S} = \frac{g}{g'} \, \Pi'_{3B}(0) \,, \qquad \hat{T} = \frac{\Pi_{33}(0) - \Pi_{+-}(0)}{m_{\rm W}^2} \,, \qquad \hat{U} = \Pi'_{+-}(0) - \Pi'_{33}(0) \,, \tag{4.5}$$

$$V = \frac{m_{\rm W}^2}{2} \left(\Pi''_{33}(0) - \Pi''_{+-}(0) \right) \,, \qquad X = \frac{m_{\rm W}^2}{2} \, \Pi''_{3B}(0) \,, \tag{4.6}$$

$$Y = \frac{m_{\rm W}^2}{2} \, \Pi''_{BB}(0) \,, \qquad W = \frac{m_{\rm W}^2}{2} \, \Pi''_{33}(0) \,. \tag{4.7}$$

All these parameters are predicted in the SM: for example, one–loop diagrams involving the exchange of the Higgs boson give a contribution to both $\hat{S}, \hat{T}$ parameters with a log–dependence on the Higgs mass, as we already mentioned in section 2.3.1, see eq. (2.61). From eq. (4.5) it is now easier to see how the $\hat{T}$ parameter gets corrections from custodial symmetry violating effects. Note that the $\hat{S}, \hat{T}, \hat{U}$ parameters are related by simple rescalings to the usual S, T, U parameters defined in [23]:

$$S = \frac{4 s_{\rm W}^2 \, \hat{S}}{\alpha_{\rm W}} \,, \qquad T = \frac{\hat{T}}{\alpha_{\rm W}} \,, \qquad U = -\frac{4 s_{\rm W}^2 \, \hat{U}}{\alpha_{\rm W}} \,. \tag{4.8}$$

A relevant contribution to the oblique parameters in extensions of the SM arises from the modified couplings of the Higgs boson to the SM gauge bosons. In the SM, due to its renormalisability, the one–loop contribution of the Higgs boson to the vector boson self energy exactly cancels the log–divergence arising from loops of would–be Goldstone bosons, see eq. (2.61). As noticed in [63], due to the modified Higgs couplings to the SM gauge bosons, the Higgs loop contribution to the self energy diagrams does not exactly compensate the log–divergence arising from the Goldstone boson diagrams, leading to a contribution to the oblique parameters of

$$S_{\rm h} = -\frac{1}{6\pi}(1-y_{\rm W}^2)\log\frac{m_{\rm h}}{\Lambda}\,, \tag{4.9}$$

$$T_{\rm h} = \frac{3}{8\pi c_{\rm W}^2}(1-y_{\rm W}^2)\log\frac{m_{\rm h}}{\Lambda}\,, \tag{4.10}$$

where $y_{\rm W}$ parametrises the shift in the Higgs–gauge bosons coupling compared to its SM value, and Λ is the usual cut–off of the effective theory.

The main constraints on these effective form factors arise from LEP observables at the Z–pole in e^+e^- annihilation and W mass measurement, from the cross sections and asymmetries in $e^+e^- \to f\bar{f}$ at LEP2 with higher center–of–mass energy $\sqrt{s} \sim (200\,\text{GeV})^2$, and from low–energy measurements like neutrino–nucleon scattering, which we will call collectively Electroweak Precision Tests (EWPT).

In general, both oblique parameters and flavour dependent corrections contribute to the prediction of electroweak observables within a generic theory. Explicitly, flavour dependent corrections to charged– and neutral–current couplings of SM gauge bosons can be parametrised as

$$\mathcal{L}_{\rm cc} = -\frac{g}{\sqrt{2}}\sum_{i,j}\bar{f}_i\,\gamma^\mu\,[(h_{\rm L}+\delta h_{\rm L})\,P_{\rm L} + (h_{\rm R}+\delta h_{\rm R})\,P_{\rm R}]\,f_j\,W_\mu\,, \tag{4.11}$$

$$\mathcal{L}_{\rm nc} = -\frac{g}{c_{\rm W}}\sum_{i}\bar{f}_i\,\gamma^\mu\,[(g_{\rm L}+\delta g_{\rm L})\,P_{\rm L} + (g_{\rm R}+\delta g_{\rm R})\,P_{\rm R}]\,f_i\,Z_\mu\,, \tag{4.12}$$

where $P_{\rm L,R}$ are the chiral projectors, $h_{\rm L/R}$, $g_{\rm L/R}$ correspond to the SM values, and $\delta h_{\rm L/R}$, $\delta g_{\rm L/R}$ enclose possible new contributions.

In our analysis, we will make use of a parametrisation of 21 different EWPT observables in terms of the oblique parameters and flavour dependent corrections as originally proposed in [64]. The explicit experimental values and SM predictions of the 21 EWPT observables used in our analysis are summarised in table B.1. The SM values have been obtained with $m_h = 124.5\,\text{GeV}$ [22].

The consistency test of the Little Higgs prediction with the experimental observations is performed through a χ^2 analysis: we consider the 21 different EWPT as independent measurements to be compared to the corresponding theoretical predictions, functions of the free parameters of the models. In this way, 95% and 99% CL exclusion contour regions for any parameter space can be drawn.

Furthermore, it is useful to define a quantity to measure the degree of "naturalness" of a model with respect to experimental measurements. This is identified with the required fine–tuning necessary to accommodate the experimental measurements: the stricter the fine–tuning required in the consistent region of parameter space, the lower the degree of naturalness of the model. However, the definition of the fine–tuning is sort of arbitrary, and has not an absolute physical meaning: conclusions regarding the validity of a model based on fine–tuning arguments have to be taken with a grain of salt.

The fine–tuning can be quantified by observing how much the radiative contributions from the heavy states to the Higgs mass squared exceed the experimental value $\mu^2_{\rm exp} = m_h^2/2$, as originally proposed in [49]. If we call $\delta\mu^2$ the leading radiative correction to the Higgs mass squared, we can then define the fine–tuning as

$$\Delta = \frac{\mu^2_{\rm exp}}{|\delta\mu^2|}\,. \tag{4.13}$$

Lower values of Δ clearly imply a higher degree of fine–tuning. In particular, the dominant log–divergent contribution to μ^2 arise in Little Higgs models from the top sector, and is generically given as

$$\delta\mu^2 = -\frac{3\,\lambda_t\,m_{\rm T}^2}{8\,\pi^2}\log\frac{\Lambda^2}{m_{\rm T}^2} \tag{4.14}$$

where $\Lambda = 4\pi f$, λ_t is the SM top Yukawa coupling, and $m_{\rm T}$ is the mass of the "cancellon" top partner.

Contours of required fine–tuning will be drawn on top of the exclusion plots, too, and will represent a possible guideline to infer the naturalness of the considered model.

In the following sections, we evaluate the contributions to the oblique parameters and flavour dependent corrections for the three different Little Higgs models discussed in this thesis, and derive exclusion contours from them.

4.1.1 Simplest Little Higgs

The dominant contribution to oblique parameters in SLH stems from the presence of a Z' boson in the spectrum, with a custodial–violating Z–Z' mixing. The corrections arise already at tree–level, and are found to be [52, 65]

$$S_{Z'} = \frac{8s_{\mathrm{W}}^2}{\alpha_{\mathrm{W}}} \frac{m_{\mathrm{W}}^2}{g^2 f^2}\,, \qquad T_{Z'} = \frac{1}{\alpha_{\mathrm{W}}} \frac{v^2}{8f^2} \left(1 - t_{\mathrm{W}}^2\right)^2 . \tag{4.15}$$

Additional contributions follow from the modified Higgs couplings to the electroweak bosons compared to their SM value, see eq. (4.10). Explicitly we evaluate them as [7]

$$S_h = -\frac{1}{18\pi} \frac{t_\beta^4 - t_\beta^2 + 1}{t_\beta^2} \frac{v^2}{f^2} \log \frac{m_h}{\Lambda}\,, \tag{4.16}$$

$$T_h = \frac{1}{8\pi c_{\mathrm{W}}^2} \frac{t_\beta^4 - t_\beta^2 + 1}{t_\beta^2} \frac{v^2}{f^2} \log \frac{m_h}{\Lambda}\,. \tag{4.17}$$

Flavour dependent corrections can be obtained from the fermion–gauge interaction Lagrangian, and we summarise our findings [7] in table 4.1 and table 4.2. In particular,

$$\delta_\nu = -\frac{v}{\sqrt{2} f t_\beta}\,, \qquad \delta_Z = -\frac{(1 - t_{\mathrm{W}}^2)\sqrt{3 - t_{\mathrm{W}}^2}}{8c_{\mathrm{W}}} \frac{v^2}{f^2} \tag{4.18}$$

are two coefficients parametrising the rotation to the mass eigenstate basis in the fermion–sector and neutral gauge boson–sector, respectively [29].

	δh_{L}	δh_{R}
$\nu\ell$	$-\delta_\nu^2/2$	0
ud	$-\delta_\nu^2/2$	0
cs	$-\delta_\nu^2/2$	0
tb	$-\delta_\nu^2\, t_\beta^4 \frac{(1-R^2)^2}{2\left(R^2+t_\beta^2\right)^2}$	0

Table 4.1: *Corrections to the charged–current couplings in the SLH model.*

	δg_{L}	δg_{R}
$\nu\nu$	$-\delta_\nu^2/2 + (1/2 - s_{\mathrm{W}}^2)\delta_Z/\sqrt{3 - 4s_{\mathrm{W}}^2}$	0
$\ell\ell$	$(1/2 - s_{\mathrm{W}}^2)\delta_Z/\sqrt{3 - 4s_{\mathrm{W}}^2}$	$s_{\mathrm{W}}^2\delta_Z/\sqrt{3 - 4s_{\mathrm{W}}^2}$
uu	$(-1/2 + 2/3s_{\mathrm{W}}^2)\delta_Z/\sqrt{3 - 4s_{\mathrm{W}}^2}$	$-2/3s_{\mathrm{W}}^2\delta_Z/\sqrt{3 - 4s_{\mathrm{W}}^2}$
tt	$-\delta_\nu^2\, t_\beta^4 \frac{(1-R^2)^2}{2\left(R^2+t_\beta^2\right)^2} + (1/2 - 1/3s_{\mathrm{W}}^2)\delta_Z/\sqrt{3 - 4s_{\mathrm{W}}^2}$	$-2/3s_{\mathrm{W}}^2\delta_Z/\sqrt{3 - 4s_{\mathrm{W}}^2}$
dd	$\delta_\nu^2/2 + (-1/2 + 2/3s_{\mathrm{W}}^2)\delta_Z/\sqrt{3 - 4s_{\mathrm{W}}^2}$	$1/3s_{\mathrm{W}}^2\delta_Z/\sqrt{3 - 4s_{\mathrm{W}}^2}$
bb	$(1/2 - 1/3s_{\mathrm{W}}^2)\delta_Z/\sqrt{3 - 4s_{\mathrm{W}}^2}$	$1/3s_{\mathrm{W}}^2\delta_Z/\sqrt{3 - 4s_{\mathrm{W}}^2}$

Table 4.2: *Corrections of the neutral-current couplings in* SLH.

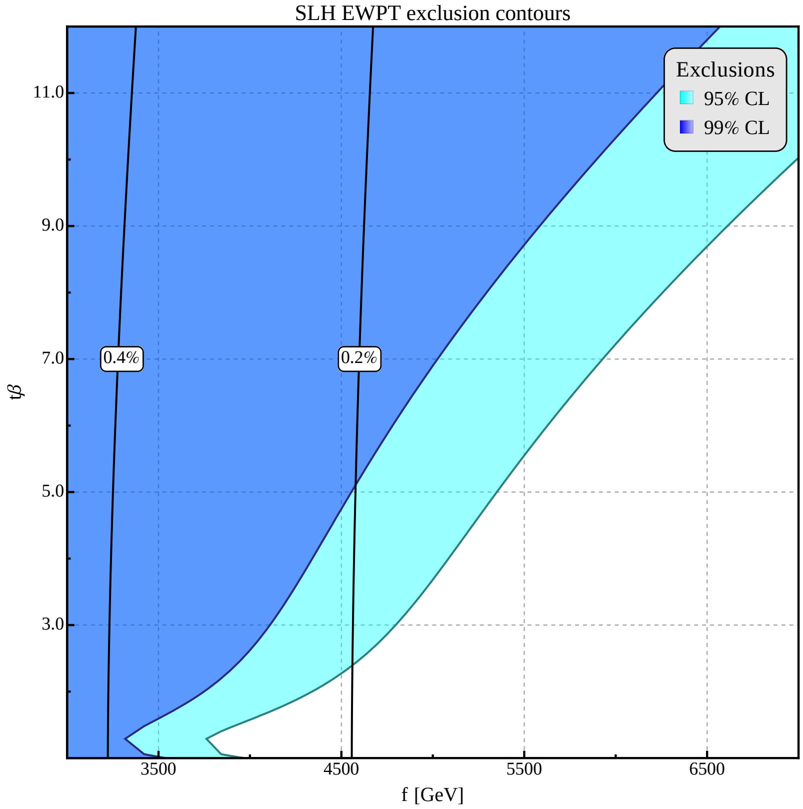

Figure 4.1: *Excluded SLH parameter space regions at 95% and 99% CL from EWPT. The thick black lines enclose regions of required fine–tuning (on the left–hand side of the lines).*

The explicit oblique and flavour–dependent corrections induced by the SLH model can be used to reconstruct the total contribution to electroweak observables, following the EWPT parametrisation of [64]. The result of the χ^2–scan in the (f, t_β) SLH parameter space is shown in figure 4.1. In particular, $f = \sqrt{f_1^2 + f_2^2}$ is the $[SU(3)]^2/[SU(2)]^2$ symmetry breaking scale, while $t_\beta = f_2/f_1$ is the ratio of the vacuum expectation values of the two $\Sigma_{1,2}$ fields. We can finally extract a lower bound on f at 95% CL of

$$(f_{\text{SLH}})_{\text{EWPT}} \gtrsim 3.7\,\text{TeV} \quad (95\%\,\text{CL})\,. \tag{4.19}$$

Large t_β values are disfavoured because of the oblique contribution introduced by the modified Higgs–gauge bosons coupling (4.17). The absence of a custodial symmetry, preventing dangerous tree–level mixings between heavy and SM gauge bosons, clearly pushes the symmetry breaking scale f into the $\mathcal{O}(\text{TeV})$ range. A level of $\mathcal{O}(0.1\%)$ fine–tuning is required in the consistent region.

4.1.2 Littlest Higgs

Historically, the most severe constraints on the parameter space of the L^{2}H model arise from EWPT: due to the absence of a custodial symmetry or a discrete parity like T–parity, tree–level mixing between heavy and light (SM) gauge bosons, as well as a vacuum expectation value for the scalar triplet Φ, cannot be forbidden. The explicit contributions to electroweak observables from gauge mixing and from the triplet vacuum expectation value are known in literature [34, 66]. Additional contributions due to quark loop modifications of the light gauge boson propagators are parametrically much smaller with respect to the aforementioned contributions, as discussed in [66], and we neglect them.

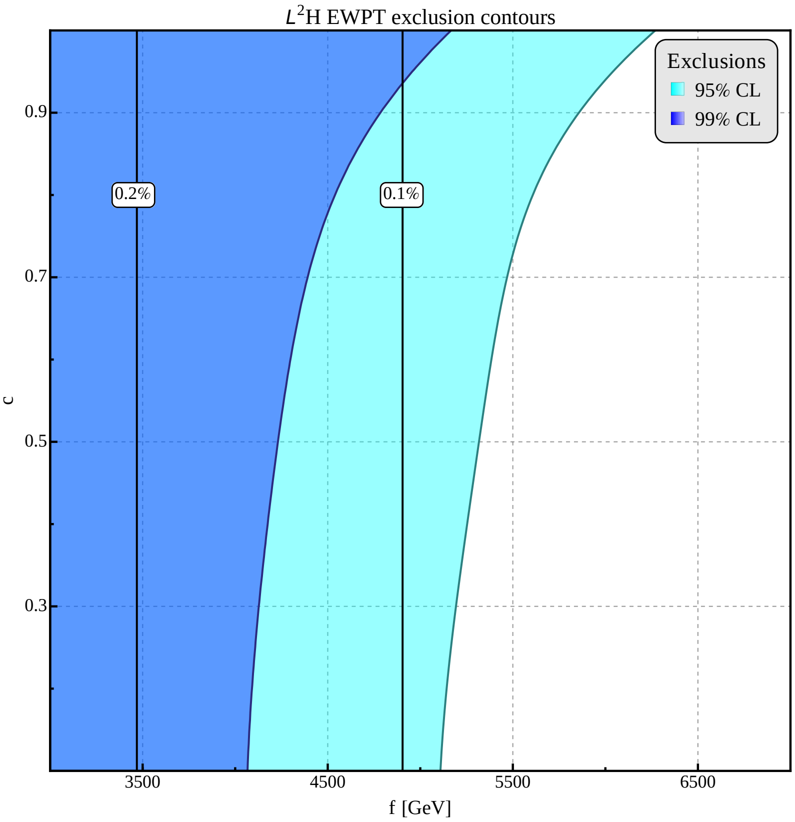

Figure 4.2: *Excluded L^2H parameter space regions at 95% and 99% CL from EWPT. The thick black lines enclose regions of required fine–tuning (on the left–hand side of the lines).*

By analysing the explicit expressions of the 21 electroweak observables in terms of the free parameters of the L^{2}H model as reported in [66], we evaluate the 95% and 99% CL excluded regions within the L^{2}H (f, c) parameter space. In particular, f is the $SU(5)/SO(5)$ symmetry breaking scale, while $c \in (0, 1)$ is one of the mixing angles in the gauge sector (3.65). It is to be noted that the remaining three free parameters, namely the second mixing angle c' in the gauge sector, see eq. (3.65), the ratio R of the two top–Yukawa couplings

λ_1/λ_2, see eq. (3.107) (recalling that either λ_1 or λ_2 can be fixed by the SM top mass), and the vacuum expectation value v' of the triplet scalar $\phi^0 \in \Phi$, are fitted during our χ^2 evaluation, namely fixed for each (f, c) point to the corresponding values which minimise the total χ^2.

The results of our analysis are summarised in figure 4.2, from which we obtain a lower bound on f at 95% CL of

$$(f_{\mathrm{L^2H}})_{\mathrm{EWPT}} \gtrsim 5.1\,\mathrm{TeV} \quad (95\%\,\mathrm{CL})\,. \tag{4.20}$$

As with the SLH model, the presence of dangerous contributions to EWPT pushes the symmetry breaking scale f into the $\mathcal{O}(\mathrm{TeV})$ range, forcing an $\mathcal{O}(0.1\%)$ fine–tuning.

4.1.3 Littlest Higgs with T–parity

In order to overcome the intrinsic tension of the L^{2}H model with electroweak precision data, a discrete T–parity is implemented in all sectors of the model. In this way, no T–odd particle can contribute as external state at tree–level, forbidding all dangerous tree–level contributions which were plaguing the original L^{2}H formulation: no contribution to EWPT arises at tree–level from T–odd particles. The only T–even non–SM particle is the T–even top partner T_+: however, it might contribute at tree–level only to observables which involve the SM top quark, for example its couplings with the SM gauge bosons. Since these couplings are not experimentally well measured yet, no sensible constraints can be obtained from the T_+ partner at tree–level either.

On the other hand, relevant contributions to EWPT arise at loop–level, from processes involving the two top partners $T_\pm$, the T–odd heavy gauge bosons, and the T–odd heavy mirror quarks. The main contributions to EWPT have been obtained from different collaborations [7,37,67,68], and we will collect here the main results.

Oblique corrections to the electroweak gauge bosons propagators induced by loop diagrams involving the SM top and its T–even top partner are given by [37,67]

$$S_{T_+} = \frac{s_\beta^2}{2\pi}\left[\left(\frac{1}{3} - c_\beta^2\right)\log x_{\mathrm{t}} + c_\beta^2\frac{(1+x_{\mathrm{t}})^2}{(1-x_{\mathrm{t}})^2} + \frac{2c_\beta^2 x_{\mathrm{t}}^2(3-x_{\mathrm{t}})\log x_{\mathrm{t}}}{(1-x_{\mathrm{t}})^3} - \frac{8c_\beta^2}{3}\right]\,, \tag{4.21}$$

$$T_{T_+} = \frac{3}{16\pi}\frac{s_\beta^2}{s_{\mathrm{W}}^2 c_{\mathrm{W}}^2}\frac{m_{\mathrm{t}}^2}{m_{\mathrm{Z}}^2}\left[\frac{s_\beta^2}{x_{\mathrm{t}}} - 1 - c_\beta^2 - \frac{2c_\beta^2}{1-x_{\mathrm{t}}}\log x_{\mathrm{t}}\right]\,, \tag{4.22}$$

$$U_{T_+} = -\frac{s_\beta^2}{2\pi}\left[s_\beta^2\log x_{\mathrm{t}} + c_\beta^2\frac{(1+x_{\mathrm{t}})^2}{(1-x_{\mathrm{t}})^2} + \frac{2c_\beta^2 x_{\mathrm{t}}^2(3-x_{\mathrm{t}})\log x_{\mathrm{t}}}{(1-x_{\mathrm{t}})^3} - \frac{8c_\beta^2}{3}\right]\,, \tag{4.23}$$

where s_β is the mixing angle in the right–handed top sector, and $x_{\mathrm{t}} = m_{\mathrm{t}}^2/m_{T+}^2$.

Another relevant one–loop contribution to oblique parameters would have arisen from the heavy gauge boson loops. However, in ref. [68] it has been explicitly shown how the log–divergent contribution to the T–parameter due to the custodial–symmetry violating tree–level W_{H}^3–$W_{\mathrm{H}}^{\pm}$ mass splitting, completely vanishes. The left–over contributions are parametrically much smaller compared to the contribution from the top sector, and are therefore neglected.

The contribution from loops involving the T–odd mirror fermion partners has been first calculated in [37], and can be expressed for each quark partner q_{H} as

$$T_{q_{\mathrm{H}}} = -\frac{\kappa^2}{192\pi^2\alpha_{\mathrm{W}}}\frac{v^2}{f^2}\,, \tag{4.24}$$

assuming for simplicity a diagonal and degenerate coupling matrix κ.

We further evaluate the modifications of the Higgs couplings to the electroweak bosons compared to their SM value, see eq. (4.10), generating another relevant contribution to the oblique parameters [7]:

$$S_{\mathrm{h}} = -\frac{1}{18\pi}\frac{v^2}{f^2}\log\frac{m_{\mathrm{h}}}{\Lambda}\,, \qquad T_{\mathrm{h}} = \frac{1}{8\pi c_{\mathrm{W}}^2}\frac{v^2}{f^2}\log\frac{m_{\mathrm{h}}}{\Lambda}\,. \tag{4.25}$$

Finally, we took into account possible contributions arising from new higher–dimensional operators which parametrise the effect of UV–physics as in ref. [67], namely

$$S_{\mathrm{UV}} = c_{\mathrm{s}}\frac{4m_{\mathrm{W}}^2}{\pi g^2 f^2}\,, \qquad T_{\mathrm{UV}} = -c_{\mathrm{t}}\frac{m_{\mathrm{W}}^2}{2\pi e^2 g^2 f^2}\,. \tag{4.26}$$

The coefficients $c_{\mathrm{s}}, c_{\mathrm{t}}$ have $\mathcal{O}(1)$ values depending on the details of the UV–physics, and are assumed equal to one for simplicity as in [67].

All the different contributions to the oblique parameters S, T, U are summed up. The only relevant non–oblique correction which affects the EWPT is the one–loop T_+ correction to the $Zb_{\mathrm{L}}\bar{b}_{\mathrm{L}}$ vertex, which has been evaluated in [37] and reads

$$\delta g_{\mathrm{L}}^{b\bar{b}} = \frac{g}{c_{\mathrm{W}}}\frac{\alpha_{\mathrm{W}}}{8\pi s_{\mathrm{W}}^2}\frac{m_{\mathrm{t}}^4 R^2}{m_{\mathrm{W}}^2 m_{T_+}^2}\log\frac{m_{T_+}^2}{m_{\mathrm{t}}^2}\,. \tag{4.27}$$

In this way, we reconstruct the total LHT contribution to electroweak observables following the EWPT parametrisation of [64], and perform a χ^2–scan in the (f, R) LHT parameter space. In particular, f is the $SU(5)/SO(5)$ symmetry breaking scale, while $R = \lambda_1/\lambda_2$ is the ratio of the two top–Yukawa couplings λ_1/λ_2, see eq. (3.116). From now on we will consider values of R within

$$0 < R \leq 3.3\,, \tag{4.28}$$

being the allowed range evaluated in [39] by estimating the tree–level unitarity limit of the scattering amplitudes within the coupled system of ($t\bar{t}$, $T\bar{T}$, $b\bar{b}$, WW, Zh). It should be noted that the remaining free parameter κ, which in the simplifying assumption of flavour–independent mirror quark sector parametrises the masses and couplings of the mirror fermions, see eq. (3.123), has been fitted during the χ^2 evaluation.

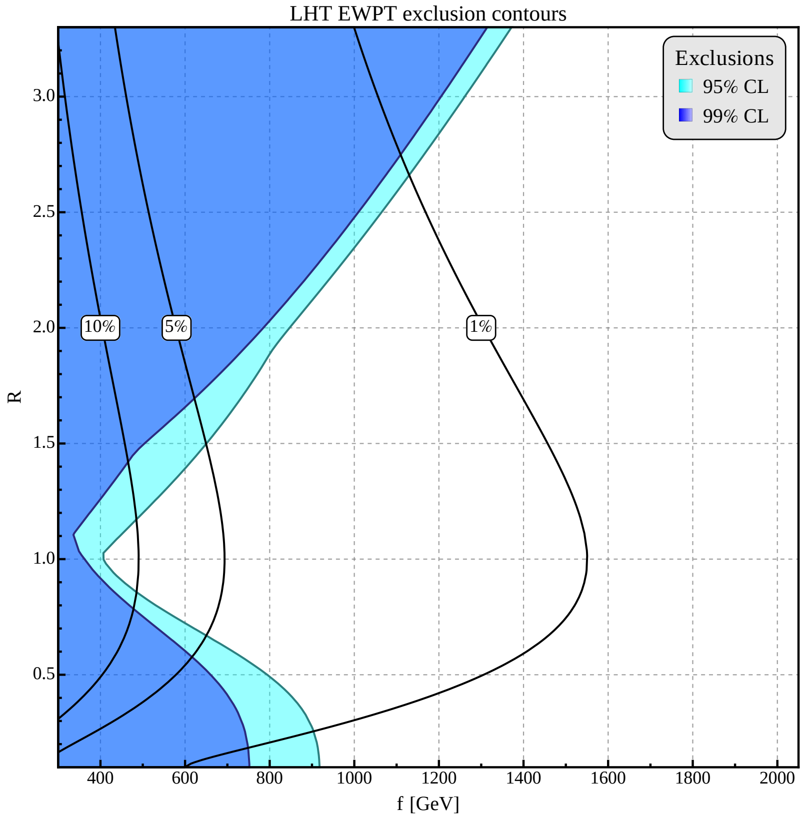

Figure 4.3: *Excluded LHT parameter space regions at 95% and 99% CL from EWPT. The thick black lines enclose regions of required fine–tuning (on the left–hand side of the lines).*

The resulting 95% and 99% CL exclusion contours are shown in figure 4.3: we obtain a lower bound on f at 95% CL of

$$(f_{\text{LHT}})_{\text{EWPT}} \gtrsim 405\,\text{GeV} \quad (95\%\,\text{CL})\,. \tag{4.29}$$

The dip in the exclusion contour around $R \sim 1.0$ arises due to a partial cancellation of the contributions to the T–parameter, as already observed in [37]. The required fine–tuning in the allowed region is observed to be of order $\mathcal{O}(5\%)$, still guaranteeing the status of “natural” SM extension to the LHT model.

4.2 Higgs Precision observables

4.2.1 Overview of LHC Higgs searches

On 4th July 2012, the ATLAS and CMS collaborations announced the discovery of a particle with mass of roughly 126 GeV compatible with the predicted SM Higgs boson [5,6]. This is a major step for particle physics, both to confirm the SM framework describing interactions of elementary particles, as well as to unveil the dynamics of Electroweak Symmetry Breaking at the TeV–scale.

Albeit no direct (tree–level) coupling of the Higgs boson to gluons is present in the SM, since the $SU(3)_{\mathrm{C}}$ symmetry of QCD is not spontaneously broken by the Higgs vacuum expectation value, the dominant Higgs production mechanism is via gluon fusion. The LHC is indeed usually referred to as a "gluon collider", and in spite of the expected suppression of the corresponding cross section by a one–loop factor $\left(g_S^2\lambda_t^2/16\pi^2\right)^2$, the gluon fusion turns out to be the dominant Higgs production process at the LHC [69–71]:

$$\sigma(pp\to h) = 14.89^{+7.1\%\,+7.6\%}_{-7.8\%\,-7.1\%}\ \mathrm{pb} \qquad \sqrt{s}=7\,\mathrm{TeV} \qquad m_h = 126.0\,\mathrm{GeV} \tag{4.30}$$

$$\sigma(pp\to h) = 18.97^{+7.2\%\,+7.5\%}_{-7.8\%\,-6.9\%}\ \mathrm{pb} \qquad \sqrt{s}=8\,\mathrm{TeV} \qquad m_h = 126.0\,\mathrm{GeV} \tag{4.31}$$

$$\sigma(pp\to h) = 48.80^{+7.5\%\,+7.2\%}_{-8.0\%\,-6.0\%}\ \mathrm{pb} \qquad \sqrt{s}=14\,\mathrm{TeV} \qquad m_h = 126.0\,\mathrm{GeV} \tag{4.32}$$

where the two uncertainties refer to the QCD scale and PDF uncertainties, respectively.

Another relevant Higgs production cross section is the vector boson fusion process, exploiting the large coupling of the Higgs to the weak gauge bosons, where two incoming quarks each radiate a W or a Z which merge and produce a Higgs boson. The vector boson fusion partonic cross section $qq\to qqh$ is proportional to the weak gauge coupling as g^6, and to an additional phase space factor for two additional jets in the final state: the total partonic cross section turns out to be comparable with the partonic gluon fusion cross section. On the other hand, a large difference in rate with respect to the gluon fusion production arises from the different quark and gluon luminosities: in particular, vector boson fusion probes high–x quark momentum fraction, while low–x gluon momentum fraction for the gluon fusion process. The vector boson fusion cross section amounts to [69–71]

$$\sigma(pp\to qqh) = 1.211^{+0.3\%\,+2.5\%}_{-0.3\%\,-2.1\%}\ \mathrm{pb} \qquad \sqrt{s}=7\,\mathrm{TeV} \qquad m_h = 126.0\,\mathrm{GeV} \tag{4.33}$$

$$\sigma(pp\to qqh) = 1.568^{+0.3\%\,+2.6\%}_{-0.1\%\,-2.8\%}\ \mathrm{pb} \qquad \sqrt{s}=8\,\mathrm{TeV} \qquad m_h = 126.0\,\mathrm{GeV} \tag{4.34}$$

$$\sigma(pp\to qqh) = 4.206^{+0.4\%\,+3.4\%}_{-0.4\%\,-3.4\%}\ \mathrm{pb} \qquad \sqrt{s}=14\,\mathrm{TeV} \qquad m_h = 126.0\,\mathrm{GeV} \tag{4.35}$$

where the two uncertainties refer to the QCD scale and PDF uncertainties, respectively.

Smaller contributions to the Higgs production arise from associated production with heavy SM particles, namely associated production with W/Z gauge bosons (also called Higgs–Strahlung process) $q\bar{q} \to Vh$, and associated production with a $t\bar{t}$ pair $gg \to ht\bar{t}$. At 14 TeV center of mass energy, the total contribution of these production mechanisms is roughly 3 pb [69–71]:

$$\sigma(pp \to Wh) = 1.485^{+0.8\%\,+3.2\%}_{-1.7\%\,-3.2\%}\ \text{pb} \qquad \sqrt{s} = 14\,\text{TeV} \qquad m_h = 126.0\,\text{GeV} \tag{4.36}$$

$$\sigma(pp \to Zh) = 0.9465^{+4.1\%\,+3.5\%}_{-3.9\%\,-3.5\%}\ \text{pb} \qquad \sqrt{s} = 14\,\text{TeV} \qquad m_h = 126.0\,\text{GeV} \tag{4.37}$$

$$\sigma(pp \to ht\bar{t}) = 0.5969^{+5.9\%\,+8.9\%}_{-9.3\%\,-8.9\%}\ \text{pb} \qquad \sqrt{s} = 14\,\text{TeV} \qquad m_h = 126.0\,\text{GeV} \tag{4.38}$$

where the two uncertainties refer to the QCD scale and PDF uncertainties, respectively. It should be noted that even if these processes contribute with a low production cross section, the peculiar final state topologies are suitable for otherwise hopeless analyses dealing with e.g. huge QCD backgrounds, if only relying on the dominant gluon fusion process.

Regarding possible decays of the Higgs boson, we can consider ourselves lucky with an observed Higgs mass around 126 GeV: this mass point allows us to observe the largest number of different Higgs decays, while still having a reasonably high production cross section.

At tree–level all decay rates of the Higgs in the SM are proportional to the mass of the final state particles, because of the EWSB mechanism. The Higgs decays thus preferably to the heaviest particles allowed by phase space: for a 126 GeV Higgs the dominant branching ratio is given by the decay into a pair of bottom quarks.

On the other hand, once the off–shell decay to WW^* is allowed, it dominates over the other decay rates, being comparable with the decay into bottom pairs for masses around 126 GeV (only a factor of three smaller). Because of the small mass difference between the W and Z bosons, the decay to ZZ pairs is smaller compared to the decay into a pair of W bosons, because of the exchange symmetry for two identical final state particles. Finally, loop–induced decays can be sizable as well: in particular, the loop–induced decay to two photons turned out to be crucial for the Higgs discovery.

In table 4.3 we collect part of the SM Higgs branching ratios for $m_h = 126.0\,\text{GeV}$ and total width of $\Gamma_h = 4.21 \cdot 10^{-3}\ {}^{+3.87\%}_{-3.83\%}\ \text{GeV}$ [69–71].

Despite the lower values of branching ratios, the Higgs boson has been first discovered (with more than 5σ significance) in the search channels $h \to \gamma\gamma$ (focussing both on gluon

Higgs decay	BR
$h \to b\bar{b}$	$5.61 \cdot 10^{-1}\,{}^{+3.31\%}_{-3.36\%}$
$h \to c\bar{c}$	$2.83 \cdot 10^{-2}\,{}^{+12.19\%}_{-12.20\%}$
$h \to s\bar{s}$	$2.39 \cdot 10^{-4}\,{}^{+4.82\%}_{-4.88\%}$
$h \to \tau^+\tau^-$	$6.16 \cdot 10^{-2}\,{}^{+5.62\%}_{-5.59\%}$
$h \to \mu^+\mu^-$	$2.14 \cdot 10^{-4}\,{}^{+5.86\%}_{-5.85\%}$
$h \to WW^*$	$2.31 \cdot 10^{-1}\,{}^{+4.14\%}_{-4.08\%}$
$h \to ZZ^*$	$2.89 \cdot 10^{-2}\,{}^{+4.14\%}_{-4.08\%}$
$h \to \gamma\gamma$	$2.28 \cdot 10^{-3}\,{}^{+4.88\%}_{-4.80\%}$
$h \to gg$	$8.48 \cdot 10^{-2}\,{}^{+10.13\%}_{-9.90\%}$
$h \to Z\gamma$	$1.62 \cdot 10^{-3}\,{}^{+8.84\%}_{-8.84\%}$

Table 4.3: *Theoretical predictions for the SM Higgs branching ratios with* $m_h = 126.0$ *GeV [69–71]*

fusion and vector boson fusion production modes) and in the "golden channel" $h \to ZZ^* \to 4\ell$, because of the possibility of full mass reconstruction of the Higgs boson and an easier background suppression. The combined best fit mass for the Higgs boson has been reported to be [72, 73]

$$m_h = 125.36 \pm 0.37\,(\text{stat}) \pm 0.18\,(\text{syst})\ \text{GeV} \qquad \text{ATLAS} \tag{4.39}$$

$$m_h = 125.03 \pm 0.27\,(\text{stat}) \pm 0.14\,(\text{syst})\ \text{GeV} \qquad \text{CMS}\,. \tag{4.40}$$

Together with these channels with high mass resolution, other important channels in which the ATLAS and CMS collaborations have been focusing to determine the properties of the Higgs boson are $h \to WW^* \to 2\ell\,2\nu$, $h \to b\bar{b}$ (exploiting especially the associated production with gauge bosons) and $h \to \tau^+\tau^-$.

Experimental collaborations usually express the results of Higgs searches in terms of a signal strength modifier, being the factor by which the SM Higgs signal is modified, given a particular assumption on the Higgs mass. In particular, the signal strength modifier can be defined for each Higgs decay channel i being analysed experimentally. It is defined as the ratio of observed signal events in the channel i, denoted by $n_{\rm S}^i$, divided by the expected number of events as predicted in the SM, denoted by $n_{\rm S}^{{\rm SM},\,i}$, after the analysis–dependent selection cuts, namely

$$\mu^i = \frac{n_{\rm S}^i}{n_{\rm S}^{{\rm SM},\,i}} = \frac{n_{\rm S}^i}{\sum\limits_p \sigma_p^{\rm SM}\,{\rm BR}_i^{\rm SM}}\,. \tag{4.41}$$

In particular, $\sigma_p^{\rm SM}$ is the value of a specific SM Higgs production cross section p, while $\mathrm{BR}_i^{\rm SM}$ the branching ratio of the corresponding decay i. The ATLAS and CMS collaborations report the best–fit value $\hat{\mu}^i$ for a given hypothesis on m_h, and a 1σ significance range of consistency around the best–fit value. We display in figure 4.4 an example of the signal strength best fits provided by ATLAS and CMS with up to $25\,\mathrm{fb}^{-1}$ of integrated luminosity collected at $\sqrt{s} = 7,\, 8\,\mathrm{TeV}$ [72, 73].

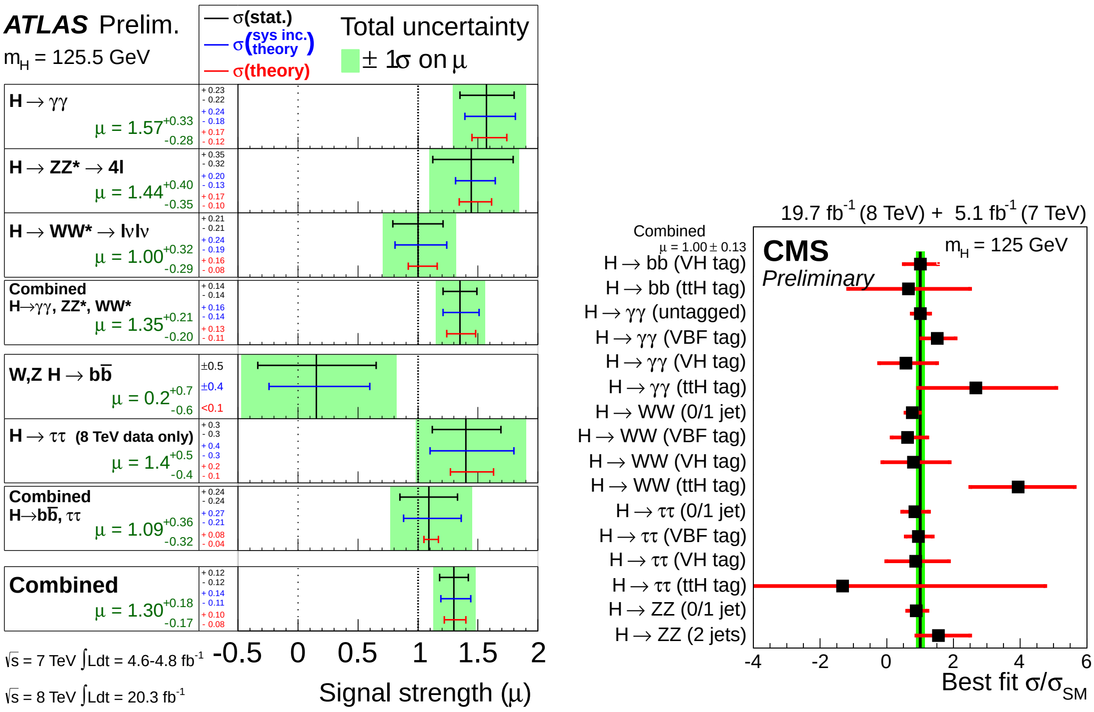

Figure 4.4: *ATLAS and CMS signal strength modifier best fits for different search channels up to* $25\,fb^{-1}$ *of integrated luminosity collected at* $\sqrt{s} = 7,\, 8\,TeV$ *[72, 73].*

Furthermore, the collaborations usually report the composition of the signal events in terms of the different production modes, namely

$$n_{\rm S}^i = n_{{\rm S},p}^i \, \zeta_p^i \,, \qquad \sum_p \zeta_p^i = 1 \,, \tag{4.42}$$

such that eq. (4.41) becomes

$$\mu^i = \sum_p \frac{n_{{\rm S},p}^i \; \zeta_p^i}{\sigma_p^{\rm SM}\, \mathrm{BR}_i^{\rm SM}} \,. \tag{4.43}$$

Let us now assume that each Higgs production cross section within the underlying model can be expressed as a rescaling of the corresponding SM cross section, namely

$$\sigma_p = c_p \, \sigma_p^{\rm SM} \qquad \forall \, p \,. \tag{4.44}$$

In this way, we can further simplify the signal strength definition of eq. (4.43) to

$$\mu^i = \left(c_g \, \zeta_g^i + c_{\mathrm{V}}^2 \, \zeta_{\mathrm{V}}^i + c_{\mathrm{t}}^2 \, \zeta_{\mathrm{t}}^i\right) \frac{\mathrm{BR}_i}{\mathrm{BR}_i^{\mathrm{SM}}}\,, \tag{4.45}$$

where c_g, c_{V}^2, c_{t}^2 parametrise the rescaling of the gluon fusion, of the vector boson fusion, and of the $t\bar{t}$–Higgs production cross sections, respectively, and where BR_i is the branching ratio of the Higgs decay i evaluated within the underlying model.

New physics effects can generate modifications of the production cross sections, namely $c_p \neq 1$, as well as of the branching ratios BR_i. One can predict the signal strength modifier μ^i as a function of the free parameters of a BSM model, and constrain them to a consistent region from the reported best fit values $\hat{\mu}^i$. In the next section we will thoroughly present the predictions of the different c_p and BR_i within the considered Little Higgs models.

The increasing integrated luminosity up to $25\,\mathrm{fb}^{-1}$ has allowed to reduce the total uncertainties on the best fit values of the signal strength modifiers to such an extent, that it is not far–fetched to say that a new era of Higgs precision measurements has already begun. In other words, besides electroweak constraints, flavour measurements, and direct searches for new particles, the Higgs sector has nowadays become a useful framework to test the validity of BSM models.

4.2.2 Little Higgs modifications to Higgs observables

Generically, there are three possible modifications from BSM physics which can affect the prediction of the Higgs signal strength modifiers: modifications of Higgs tree–level couplings with respect to their SM values, additional contributions to loop–induced processes involving the Higgs, and possible new Higgs decay channels if kinematically accessible.

Higgs–gauge bosons couplings

The interaction terms of the Higgs boson with electrically charged gauge bosons arise from the expansion of the kinetic term of the sigma fields Σ, involving the covariant derivatives of the different gauge groups: see eq. (3.36) and eq. (3.61) for the explicit expressions within the considered models. These interaction terms can be generically parametrised as

$$\mathcal{L}_\Sigma \supset 2\,\frac{m_{\mathrm{W}}^2}{v}\, y_{\mathrm{W}}\, W^{+\,\mu}\, W_\mu^-\, h + 2\,\frac{m_{\mathrm{V_H}}^2}{v}\, y_{\mathrm{V_H}}\, V_{\mathrm{H}}^{+\,\mu}\, V_{\mathrm{H}\,\mu}^-\, h\,, \tag{4.46}$$

where $V_{\mathrm{H}}^{\pm}$ corresponds to the additional (heavy) gauge bosons predicted within the different models with a non–vanishing interaction to the Higgs boson. In particular, the dimensionless coefficients y_V can be obtained up to a specific order in the v/f expansion of the kinetic terms:

$$y_\text{V} = \begin{cases} 1 + \mathcal{O}\left(\dfrac{v^2}{f^2}\right) & \text{for } y_\text{W} \\ \mathcal{O}\left(\dfrac{v^2}{f^2}\right) & \text{for } y_{\text{V}_\text{H}} \,. \end{cases} \tag{4.47}$$

The absence of a zeroth–order v/f interaction between the heavy gauge bosons and the Higgs boson from the expansion of the sigma fields, reflects the fact that the mass of the heavy gauge bosons is generated at the scale f from the G/H spontaneous symmetry breaking, with only a sub–leading v^2/f^2 contribution generated via EWSB. On the other hand, the SM gauge boson mass is entirely generated via EWSB. Clearly, $y_\text{W} = 1$ corresponds to the predicted SM value, while v^2/f^2 corrections are a genuine effect of the Composite/Little Higgs structure.

We can equivalently express the Higgs–SM gauge bosons coupling by replacing the vacuum expectation value v with its expression in terms of the SM vacuum v_SM as e.g. in eq. (3.42) and eq. (3.70):

$$c_\text{V} \equiv \frac{y_\text{V}}{v}\, v_\text{SM} = 1 + \mathcal{O}\left(\frac{v^2}{f^2}\right) \qquad V \equiv W^\pm, Z\,, \tag{4.48}$$

such that we can express the corresponding Lagrangian term of eq. (4.46) as

$$\mathcal{L}_\Sigma \supset 2\, \frac{m_\text{W}^2}{v_\text{SM}}\, c_\text{V}\, W^{+\,\mu}\, W^-_\mu\, h\,. \tag{4.49}$$

The rescaling factor c_V of the SM–like Lagrangian of eq. (4.49), where the SM prediction is recovered for $c_\text{V} = 1$, yields a tree–level modification of the vector boson fusion and Higgs–Strahlung production cross sections as

$$\frac{\sigma(pp \to qqh)}{\sigma(pp \to qqh)_\text{SM}} = \frac{\sigma(pp \to Vh)}{\sigma(pp \to Vh)_\text{SM}} = c_\text{V}^2\,, \tag{4.50}$$

since the new vertex normalisation can be factorised out of the amplitude of the process. Analogously, the modified Higgs decay width into SM gauge bosons turns out to be

$$\frac{\Gamma(h \to VV^*)}{\Gamma(h \to VV^*)_\text{SM}} = c_\text{V}^2\,. \tag{4.51}$$

We evaluated the explicit expressions of y_W, y_{V_H} and c_V within the different considered models [7,61,62], and summarised the results up to $\mathcal{O}(v^2/f^2)$ in table 4.4.

Besides the usual tree–level decays of the Higgs boson into SM gauge bosons, other Higgs decays into new gauge bosons might be kinematically accessible in particular regions of parameter space.

	$y_{\rm W}$	$y_{\rm V_H}$	$c_{\rm V}$
SLH	$1-\frac{1}{6}\frac{v^2}{f^2}\frac{t_\beta^4-t_\beta^2+1}{t_\beta^2}$	$y_{\rm X^\pm}=-\frac{1}{2}\frac{v^2}{f^2}$	$1-\frac{1}{4}\frac{v^2}{f^2}\frac{t_\beta^4-t_\beta^2+1}{t_\beta^2}$
L^{2}H	$1+\frac{v^2}{f^2}\left[-\frac{1}{6}-\frac{1}{4}\left(c^2-s^2\right)^2\right]$	$y_{\rm W_H}=-s^2\,c^2\,\frac{v^2}{f^2}$	$1+\frac{1}{8}\frac{v^2}{f^2}\left[-3+x^2-2\left(c^2-s^2\right)^2\right]$
LHT	$1-\frac{1}{6}\frac{v^2}{f^2}$	$y_{\rm W_H}=-\frac{1}{4}\frac{v^2}{f^2}$	$1-\frac{1}{4}\frac{v^2}{f^2}$

Table 4.4: *Contributions to Higgs–gauge bosons couplings within different Little Higgs models.*

Since EWPT already force the scale f in the range of several TeV for models without a custodial symmetry or T–parity, see eq. (4.19) and eq. (4.20), no tree–level decays of the Higgs into new gauge bosons are kinematically accessible for the SLH and L^{2}H models.

The situation is completely different for the LHT model, where the presence of T–parity reduces the constraint on the scale f to only $\mathcal{O}(500)$ GeV. For such a small value of f, the heavy photon $A_{\rm H}$ might be light enough to allow for a tree–level decay $h\to A_{\rm H}\,A_{\rm H}$. In particular, the partial width of the latter decay has been calculated to be [61]

$$\Gamma(h\to A_{\rm H}\,A_{\rm H})=\frac{g_{\rm hAA}^2\,m_h^3}{128\pi m_{A_{\rm H}}^4}\sqrt{1-x_{A_{\rm H}}}\left(1-x_{A_{\rm H}}+\frac{3}{4}x_{A_{\rm H}}^2\right)\qquad \text{if } x_{A_{\rm H}}<1\,, \tag{4.52}$$

where $g_{\rm hAA}=-g'^2\,v/2$, and $x_{A_{\rm H}}=4m_{A_{\rm H}}^2/m_h^2$. If kinematically allowed, the Higgs decay into two heavy photons acquires a significant branching ratio: the Higgs phenomenology is thus extremely different in the corresponding parameter space regions.

Higgs–fermions couplings

Interaction terms of the Higgs boson to all fermions arise from the expansion of the Yukawa Lagrangians, and can be generically parametrised as

$$\mathcal{L}_Y\supset-\frac{m_\psi}{v}\,y_\psi\,\bar\psi\,\psi\,h-\frac{m_{\psi_{\rm H}}}{v}\,y_{\psi_{\rm H}}\,\bar\psi_{\rm H}\,\psi_{\rm H}\,h\,, \tag{4.53}$$

where ψ is a collective index for the SM fermions, while $\psi_{\rm H}$ for the model–dependent new heavy fermions present in the different spectra (with a non–negligible coupling to the Higgs boson). As for the gauge sector, the v/f expansion of the Yukawa Lagrangians yields the following dimensionless coefficients

$$y_\Psi=\begin{cases}1+\mathcal{O}\left(\dfrac{v^2}{f^2}\right) & \text{for } y_\psi\\[2ex] \mathcal{O}\left(\dfrac{v^2}{f^2}\right) & \text{for } y_{\psi_{\rm H}}\,.\end{cases} \tag{4.54}$$

In particular, $y_\psi=1$ corresponds to the predicted SM value, and the v^2/f^2 corrections are a genuine effect of the Composite/Little Higgs structure.

A privileged role is dedicated to the third generation top and top–partner(s), because of their role in the tuning of the Higgs mass. We evaluated the explicit expressions of y_t and y_{T} within the different considered models [7,61,62], and summarised the results up to $\mathcal{O}(v^2/f^2)$ in table 4.5.

	y_t	y_{T}
SLH	$1-\frac{1}{6}\left[\frac{\left(1+t_\beta\right)^2\left(R^4-R^2t_\beta^2+t_\beta^4\right)}{t_\beta^2\left(t_\beta^2+R^2\right)^2}\right]$	$-\frac{1}{2}\frac{v^2}{f^2}R^2\left(\frac{t_\beta^2+1}{t_\beta^2+R^2}\right)^2$
$\mathrm{L^2H}$	$1-\frac{v^2}{f^2}\left[\frac{2R^4+R^2+2}{3\left(1+R^2\right)^2}+\frac{x^2}{4}-\frac{x}{2}\right]$	$-\frac{R^2}{\left(1+R^2\right)^2}\frac{v^2}{f^2}$
LHT	$1-\frac{v^2}{f^2}\left(\frac{2R^4+R^2+2}{3\left(1+R^2\right)^2}\right)$	$y_{T_+}=-\frac{R^2}{\left(1+R^2\right)^2}\frac{v^2}{f^2}$ $y_{u_-}=-\frac{1}{4}\frac{v^2}{f^2}$

Table 4.5: *Contributions to Higgs–top/top partner couplings within different Little Higgs models.*

Note that for the LHT model more quark partners have relevant couplings to the Higgs boson, namely the T–even top partner T_+, which is the "cancellon" field responsible for the vanishing of dangerous quadratic divergences at one–loop, see eq. (3.116), and the up–type T–odd mirror quarks u_-, c_-, t_-, whose couplings to the Higgs arise from eq. (3.123). On the other hand, the down–type mirror fermions of eq. (3.123), as well as the T–odd partner T_- arising from eq. (3.116), have no direct coupling to the Higgs of the form given by eq. (4.53).

Furthermore, at order v/f one would expect the presence of a Higgs coupling even with the other two charge $-1/3$ heavy fermion partners in the anomaly–free embedding of the SLH model, namely D, S. However, as discussed in [29], these terms exactly vanish at this order if the down– and strange–quark masses are neglected. For this reason, we will not consider these couplings.

Similarly to the gauge sector, we can express the rescaling factor y_ψ of eq. (4.53), which determines the couplings of the Higgs to the SM fermions, by replacing the vacuum expectation value v with its expression in terms of the SM vacuum v_{SM}:

$$c_\psi \equiv \frac{y_\psi}{v}\,v_{\mathrm{SM}} = 1+\mathcal{O}\left(\frac{v^2}{f^2}\right). \tag{4.55}$$

In this way we can express the corresponding Lagrangian term of eq. (4.53) as

$$\mathcal{L}_Y \supset -\frac{m_\psi}{v_{\mathrm{SM}}}\,c_\psi\,\bar\psi\,\psi\,h\,, \tag{4.56}$$

and evaluating a tree–level modification of the Higgs decay width into SM fermions as

$$\frac{\Gamma(h\to \bar{f}f)}{\Gamma(h\to \bar{f}f)_{\rm SM}} = c_\psi^2\,. \tag{4.57}$$

A tree–level rescaling of the SM $t\bar{t}$–Higgs associated production is analogously possible by considering the modification of the corresponding Yukawa coupling:

$$\frac{\sigma(pp\to ht\bar{t})}{\sigma(pp\to ht\bar{t})_{\rm SM}} = c_t^2\,. \tag{4.58}$$

We summarised our results up to $\mathcal{O}(v^2/f^2)$ in table 4.6, as in ref. [7,61,62].

	$c_u \quad (u\equiv u,c)$	$c_d \quad (d\equiv d,s,b,\ell)$
SLH	$1-\frac{1}{4}\frac{v^2}{f^2}\left(\frac{t_\beta^4+t_\beta^2+1}{t_\beta}\right)$	
L^{2}H	$1-\frac{1}{2}\frac{v^2}{f^2}\left(\frac{7}{4}+\frac{x^2}{4}-x\right)$	
LHT	$1-\frac{3}{4}\frac{v^2}{f^2}$	Case A: $1-\frac{1}{4}\frac{v^2}{f^2}$ Case B: $1-\frac{5}{4}\frac{v^2}{f^2}$

Table 4.6: *Contributions to Higgs–fermions couplings within different Little Higgs models.*

Higgs–scalar bosons couplings

The scalar sectors of the different Little Higgs models provide further modifications which have to be taken into account. As described in section 3.2.1, the scalar sectors are characterised by new quarticon fields responsible to overcome the quadratic sensitivity at one–loop of the Higgs mass: in particular, the SLH model predicts a new real pseudo–scalar field η, while the L^{2}H/LHT models include a complex scalar triplet in the spectrum.

The mass of the pseudo–scalar η is fixed by the free–parameter μ introduced in eq. (3.45): for particular values of μ, new Higgs decays involving η might be kinematically allowed, in particular [30,32]

$$\Gamma(h\to\eta\eta) = \frac{m_\eta^4}{8\pi v^2\, m_h}\sqrt{1-x_\eta}\,, \qquad \text{if } x_\eta<1\,, \tag{4.59}$$

$$\Gamma(h\to Z\eta) = \frac{m_h^3}{32\pi f^2}\left(\frac{t_\beta^2-1}{t_\beta}\right)^2\left[\lambda\left(1,\frac{m_Z^2}{m_h^2},\frac{m_\eta^2}{m_h^2}\right)\right]^{3/2}\,, \tag{4.60}$$

where $x_i = 4m_i^2/m_h^2$, and $\lambda(1,x,y) = (1-x-y)^2-4xy$.

The complex triplet scalar predicted by the L^{2}H/LHT models is parametrically heavier than the Higgs boson, see eq. (3.79). Therefore, no tree–level decay of the Higgs involving the triplet scalar is kinematically allowed. Higgs couplings to the charged components of scalar triplet are generated at order v/f in the CW radiative potential, and can be parametrised as

$$V_{\text{eff}} \supset 2\frac{m_\Phi^2}{v}\, y_{\phi^+}\, \phi^+\, \phi^-\, h + 2\frac{m_\Phi^2}{v}\, y_{\phi^{++}}\, \phi^{++}\, \phi^{--}\, h\,, \tag{4.61}$$

where we have evaluated the relative coefficients to be [7,61,62]

$$y_{\phi^+} = \frac{v^2}{f^2}\left(-\frac{1}{3}+\frac{x^2}{4}\right)\,, \qquad y_{\phi^{++}} = \mathcal{O}\left(\frac{v^4}{f^4}\right)\,. \tag{4.62}$$

One–loop processes

Finally, one–loop induced processes get additional contributions from new degrees of freedom. One can express the decay widths of the Higgs boson into two gluons and into two photons, respectively, as

$$\Gamma(h\to gg) = \frac{\alpha_{\text{S}}^2\, m_h^3}{32\,\pi^3\, v^2}\left|\sum_\Psi -\frac{1}{2}F_{1/2}(x_\Psi)\, y_\Psi\right|^2\,, \tag{4.63}$$

$$\Gamma(h\to \gamma\gamma) = \frac{\alpha_{\text{W}}^2\, m_h^3}{256\,\pi^3\, v^2}\left|\sum_\Psi \frac{4}{3}F_{1/2}(x_\Psi)\, y_\Psi + \sum_{\text{V}} F_1(x_{\text{V}})\, y_{\text{V}} + \sum_{\text{S}} F_0\, y_{\text{S}}\right|^2\,, \tag{4.64}$$

where the following functions have been defined to parametrise the one–loop vertices [74,75]

$$F_0(x) = x\left[1 - x\, f(x)\right]\,, \tag{4.65}$$

$$F_{1/2}(x) = -2x\left[1 + (1-x)\, f(x)\right]\,, \tag{4.66}$$

$$F_1(x) = 2 + 3x + 3x(2-x)\, f(x)\,, \tag{4.67}$$

$$f(x) = \begin{cases} \left(\sin\dfrac{1}{\sqrt{x}}\right)^{-1/2} & \text{for } x \equiv \dfrac{4\,m^2}{m_h^2} \geq 1 \\ -\dfrac{1}{4}\left(\log\dfrac{1+\sqrt{1-x}}{1-\sqrt{1-x}} - i\pi\right)^2 & \text{for } x \equiv \dfrac{4\,m^2}{m_h^2} < 1\,. \end{cases} \tag{4.68}$$

In particular, for Little Higgs models the sum of eq. (4.63) is extended over all possible coloured fermionic particles Ψ included in the loop, while the sums within eq. (4.64) are extended over all electrically charged fermionic, vector or scalar particles running in the loop. For comparison, in Supersymmetry one should instead include in eq. (4.63) the contribution from scalar coloured particles, which in Little Higgs models are usually not present. As previously defined in this section, y_Ψ, y_{V}, y_{S} represent the dimensionless couplings to the Higgs boson of the corresponding fermionic, vector or scalar particles.

Through eq. (4.63) and (4.64) we have been able to evaluate the Little Higgs predictions of the corresponding widths of the one–loop processes. Moreover, we have been also able to evaluate the modification induced to the gluon fusion production mechanism. In the narrow–width approximation one can relate the partonic gluon fusion cross section to the Higgs decay width into two gluons:

$$\hat{\sigma}(gg \to h) = \frac{\pi^2}{8\, m_h^3}\, \Gamma(h \to gg)\,, \tag{4.69}$$

such that we can approximate the prediction for the hadronic cross section by exploiting the modification of the Higgs decay width into two gluons, namely

$$\frac{\sigma(pp \to h)}{\sigma(pp \to h)_{\rm SM}} \sim \frac{\Gamma(h \to gg)}{\Gamma(h \to gg)_{\rm SM}} \equiv c_g\,. \tag{4.70}$$

Summary and Results

In summary, we showed how to obtain (approximate) predictions within the considered Little Higgs models for the following observables:

- gluon fusion production cross section, eq. (4.70)
- vector boson fusion production cross section, eq. (4.50)
- Higgs–Strahlung production cross section, eq. (4.50)
- associated $t\bar{t}$–Higgs production cross section, eq. (4.58)
- Higgs decay widths into light SM fermions, eq. (4.57)
- Higgs decay widths into SM gauge bosons, eq. (4.51), (4.63) and (4.64)
- possible new Higgs decays, eq. (4.52), (4.59) and (4.60).

These predictions can be tested with the observed best fits of the signal strength modifiers as defined in eq. (4.45). As for the EWPT, we performed a χ^2 analysis within each considered model, taking into account the most up–to–date experimental results made public by the ATLAS and CMS collaborations as of the summer of 2013, with up to $25\,\text{fb}^{-1}$ of integrated luminosity at 7 and 8 TeV. By including the EWPT observables in the χ^2 analysis, we could obtain also a combined exclusion contours [7–9]. We catalogue in tables B.2 and B.3 the explicit values of the signal strength modifiers best fits and the corresponding uncertainties used in our analysis.

As mentioned before, for the SLH and L^{2}H models the scale f is already driven in the range of several TeV by the EWPT due to the absence of a custodial symmetry or T–parity, see eq. (4.19) and eq. (4.20). Therefore, in this “extreme” region of parameter space, the v^2/f^2 modifications to the Higgs sector observables compared to their SM values are negligible: we will call this large–f region as the SM–limit. Since the reported measurements of the Higgs properties are consistent with the SM hypothesis within the current uncertainties, the net effect of the inclusion of the Higgs data in our χ^2 analysis in the SM–limit region is to reduce the χ^2 per degree of freedom. Therefore, it should not surprise that the combined exclusion contours from EWPT and current Higgs data allow for a smaller consistent value for f compared to the inclusion of EWPT only:

$$(f_{\mathrm{SLH}})_{\mathrm{EWPT+Higgs}} \gtrsim 3.3\,\mathrm{TeV} \quad (95\%\,\mathrm{CL})\,, \tag{4.71}$$

$$(f_{\mathrm{L^2H}})_{\mathrm{EWPT+Higgs}} \gtrsim 4.0\,\mathrm{TeV} \quad (95\%\,\mathrm{CL})\,. \tag{4.72}$$

The corresponding 95% and 99% CL exclusion contours are shown in figure 4.5.

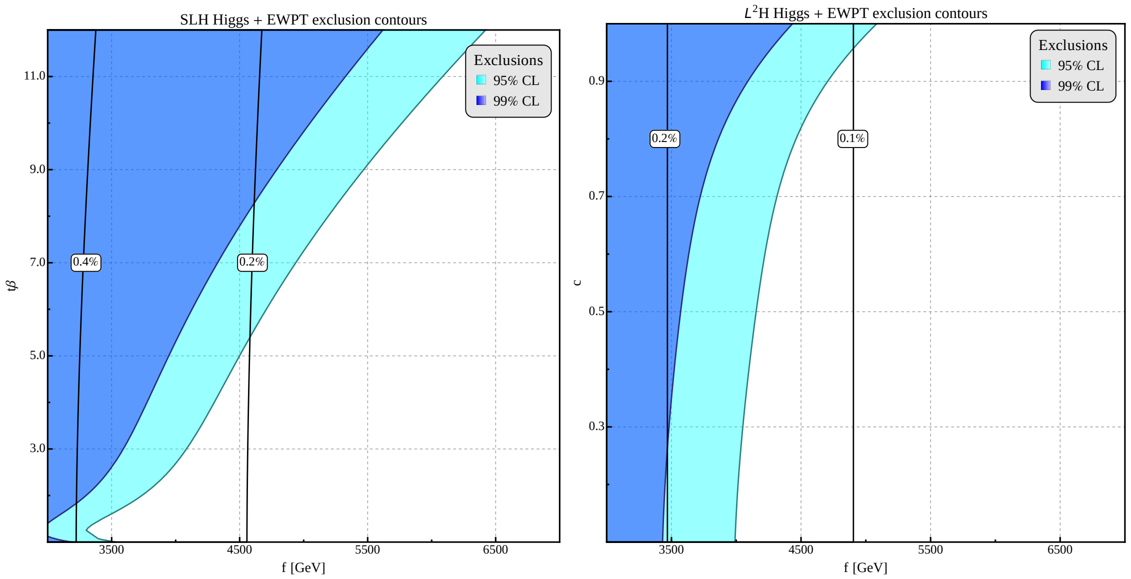

Figure 4.5: *Excluded SLH (left plot) and L^2H (right plot) parameter space regions at 95% and 99% CL from the combination of EWPT and Higgs searches data. The thick black lines enclose regions of required fine–tuning (on the left–hand side of the lines).*

A further reduction of the uncertainties of the Higgs sector observables will increase the sensitivity of the χ^2 analysis in the SM–limit region: we expect that the inclusion of Higgs measurements from forthcoming measurements at the LHC with higher integrated luminosities, and possibly at linear colliders, will guarantee a stronger exclusion of the parameter space of the SLH and L^{2}H models.

The situation is different if we consider the LHT model. Here, a much smaller value of the scale f is consistent with EWPT, see eq. (4.29), and for smaller values of f the modifications to Higgs observables yield a sizable effect to the total χ^2. In the following we will present the results for the LHT model, distinguishing between the two implementations of the down–type Yukawa Lagrangian, namely Case A and Case B.

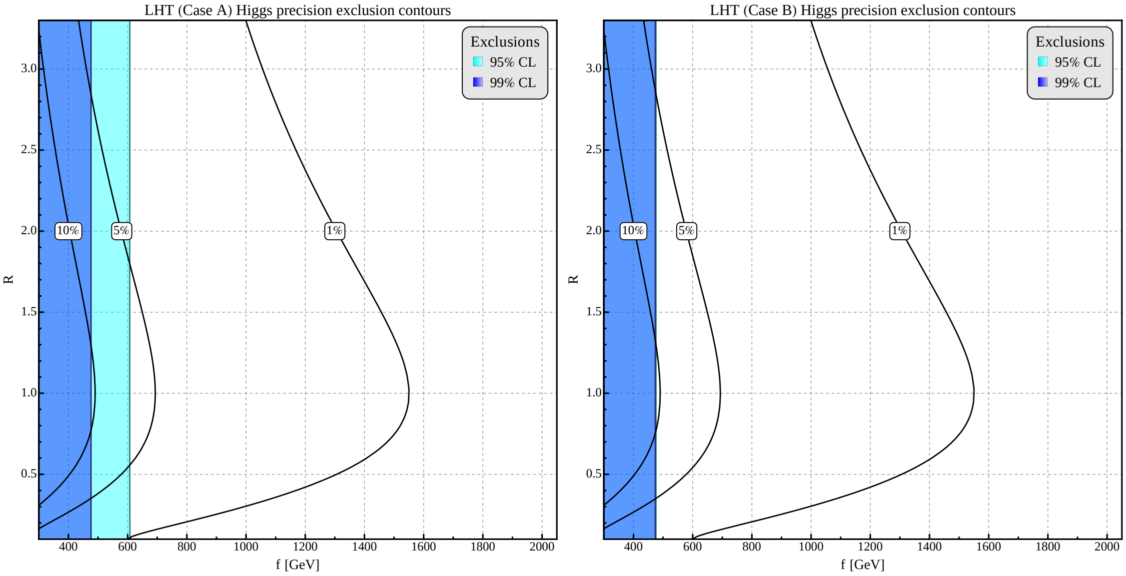

Figure 4.6: *Excluded LHT parameter space regions at 95% and 99% CL from Higgs searches data. The thick black lines enclose regions of required fine–tuning (on the left–hand side of the lines). The left plot corresponds to the down–type Yukawa implementation called Case A, the right plot to Case B.*

By including only the Higgs data in our χ^2 analysis, we obtain lower limits on f as:

$$(f_{\rm LHT,\,A})_{\rm Higgs} \gtrsim 607\,{\rm GeV} \quad (95\%\,{\rm CL})\,, \tag{4.73}$$

$$(f_{\rm LHT,\,B})_{\rm Higgs} \gtrsim 476\,{\rm GeV} \quad (95\%\,{\rm CL})\,. \tag{4.74}$$

A slightly smaller excluded region is observed for Case B, see figure 4.6. This is due to the different suppression of the down–type Yukawa coupling with respect to the SM value: in particular, for fixed f, a smaller Higgs/down–quark coupling is predicted for Case B, see table 4.6, which in turn yields a bigger suppression of the Higgs branching ratio into two bottom quarks and an enhancement of all other decay rates. This is more aligned with the reported Higgs results especially by the ATLAS collaboration, where a generic enhancement in the non–fermionic decays of the Higgs is observed.

In both cases, the results are driven by the presence of the kinematically accessible invisible decay for the Higgs at lower values of f, namely the decay into two stable heavy photons $A_{\rm H}$, see eq. (4.52). This two–body decay is indeed open for $f \lesssim 473\,{\rm GeV}$ at $m_h = 125\,{\rm GeV}$, with a dominant branching ratio compared to the other SM–like decays. As a consequence, all other SM–like decay rates are highly reduced for $f \lesssim 473\,{\rm GeV}$, in contrast with the current observations. An enhancement in the Higgs production cross sections would compensate this reduction in the branching ratios, but this is not the case since we observe a generic suppression of all Higgs production modes within the LHT parameter space.

It is interesting to notice that the LHT exclusion region from Higgs data does not depend on the parameter R, namely on the particular value of the couplings in the top sector. As described in [7] and references therein, this can be understood by looking at the effective one–loop vertices of the Higgs, which are the only quantities potentially sensible to the top sector couplings, as one can see from the explicit formulae reported before. The effective one–loop vertices exhibit the following behaviour in terms of the mass matrices of the particles running in the loops in the background of the Higgs field:

$$\mathcal{L}_{\text{eff}} \sim \frac{\partial}{\partial v} \log \left(\det M(h)^\dagger M(h) \right)_{\langle h \rangle} . \tag{4.75}$$

One can show that Composite and Little Higgs models generically predict a fermion mass matrix with a factorisation between the non–linear sigma model expansion parameter v/f and the other couplings of the fermion sector, namely

$$\det M(\Sigma)^\dagger M(\Sigma) = F\left(\frac{v}{f}\right) \times P(\lambda_i,\, f) . \tag{4.76}$$

By substituting eq. (4.76) into eq. (4.75), we see that $\mathcal{L}_{\text{eff}}$ is independent of $P(\lambda_i,\, f)$: this factorisation prevents the Higgs one–loop effective vertices to depend on the details of the Composite and Little Higgs top sectors. In the specific LHT example one can easily show, using the top–sector mass matrix M_{t} of eq. (3.109), that

$$\det M_{\text{t}}(\Sigma)^\dagger M_{\text{t}}(\Sigma) = \frac{1}{2}\, \lambda_1^2\, \lambda_2^2\, f^4\, \sin \frac{\sqrt{2}\, v}{f} . \tag{4.77}$$

By combining in the χ^2 analysis the Higgs data with the EWPT measurements, we obtain a stronger bound on f:

$$(f_{\text{LHT, A}})_{\text{EWPT+Higgs}} \gtrsim 694\,\text{GeV} \quad (95\%\,\text{CL}) \tag{4.78}$$

$$(f_{\text{LHT, B}})_{\text{EWPT+Higgs}} \gtrsim 560\,\text{GeV} \quad (95\%\,\text{CL})\,. \tag{4.79}$$

The resulting 95% and 99% CL exclusion contours are shown in figure 4.7.

Based on fine–tuning arguments, we can conclude that our analysis confirmed how models without a mechanism to prevent dangerous contributions to oblique parameters are in huge tension with the collected EWPT data. Only large values of f might accommodate

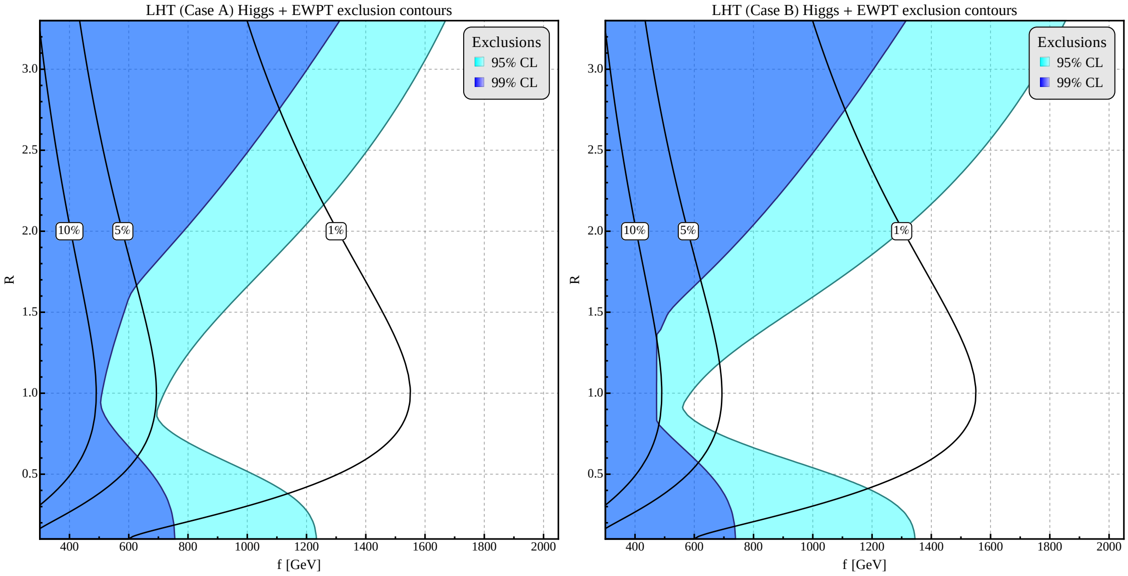

Figure 4.7: *Excluded LHT parameter space regions at 95% and 99% CL from the combination of EWPT and Higgs searches data. The thick black lines enclose regions of required fine–tuning (on the left–hand side of the lines). The left plot corresponds to the down–type Yukawa implementation called Case A, while the right plot corresponds to Case B.*

the experimental results, which in turn yield large masses for the new particles and a substantial required fine–tuning as defined in eq. (4.13), of order 0.1% for both the SLH and L^2H models. Models with T–parity, or similar custodial–symmetry preserving mechanisms, still allow large portions of parameter space which are consistent with the observed data, requiring only a mild degree of 5–10% fine–tuning.

Furthermore, we showed that the inclusion of Higgs data represents a fundamental ingredient to extensively analyse the consistency of the BSM predictions: our analysis showed that an increased precision in the Higgs observables should be highly sought after to probe parameter space regions where the modifications from BSM physics might be more difficult to observe.

4.3 Direct searches for new particles

Beyond the Higgs discovery, the ATLAS and CMS collaborations have put great effort during the 7 and 8 TeV LHC runs to realise dedicated search analyses to discover possible signals of new particles above the known SM backgrounds. In particular, no relevant discrepancies compared to the SM predictions have been observed within many different search strategies, yet, and limits on the parameter space on certain BSM models have been consistently set. The ATLAS and CMS collaborations have usually interpreted the direct searches results in terms of specific SUSY scenarios, e.g. the cMSSM, or more generic simplified models. However, the same information can be used to probe the parameter space of different models which have not taken into account by the experimental collaborations when interpreting the results. Therefore, it is of great interest to scrutinise the public experimental results to make sure that no information might be overlooked.

The aim of this section is to describe our analysis of refs. [8, 9], where we systematically re–interpreted recent ATLAS and CMS public results of searches for BSM particles, assuming an LHT signal. This represents an important and complementary information with respect to the Electroweak Precision and Higgs Observables analyses of sections 4.1 and 4.2, and can be used to obtain a further constraint on the LHT parameter space.

We focussed only on the LHT model because it guarantees the consistency of a rather small value of f with EWPT and Higgs searches: since the masses of the new particles are proportional to the scale f, one might thus expect production cross sections which are not severely suppressed at $\sqrt{s} = 8\,\text{TeV}$ center–of–mass energy. A possible LHT signature detectable via direct searches for new particles is therefore plausible.

Before turning our attention to the results of the recasting procedure, it is worth to detail some more phenomenological aspects of the considered LHT model. In this way, we will emphasise how the free parameters of the model affect the mass spectrum and different decay branching ratios, giving rise to particular final state signatures which might be captured by the analysed direct searches.

4.3.1 Phenomenology of the Littlest Higgs with T–parity

Within the gauge and scalar sectors, the mass spectrum is completely determined by the mass scale f. In particular, the heavy photon A_H is always the lightest T–odd gauge boson, and can be generically considered the lightest T–odd particle for most of the parameter space, apart from an “extreme” region where the mirror fermions are lighter than A_H. This happens for the mirror fermion mass parameter $\kappa \lesssim 0.1$. However, we will not consider this region since it can safely be considered as excluded, given the experimental constraints on coloured stable particles from the LHC and from cosmological observations [76, 77].

From now on, the heavy photon $A_{\rm H}$ will always be the lightest T–odd particle in the spectrum: because of T–parity conservation, no decay of the heavy photon into (T–even) SM particles is allowed. This is not the case if T–parity is broken by anomalies [58], but we will not consider this possibility in our study. As a consequence, only (pairs) of heavy photons $A_{\rm H}$ are allowed to appear at the end of decay chains of processes involving LHT T–odd particles, and possibly detected from final state transverse momentum imbalance measurements. The other heavy gauge boson partners $W_{\rm H}$, $Z_{\rm H}$ are degenerate up to corrections of order v^2/f^2, and lighter than the different components of the scalar complex triplet Φ.

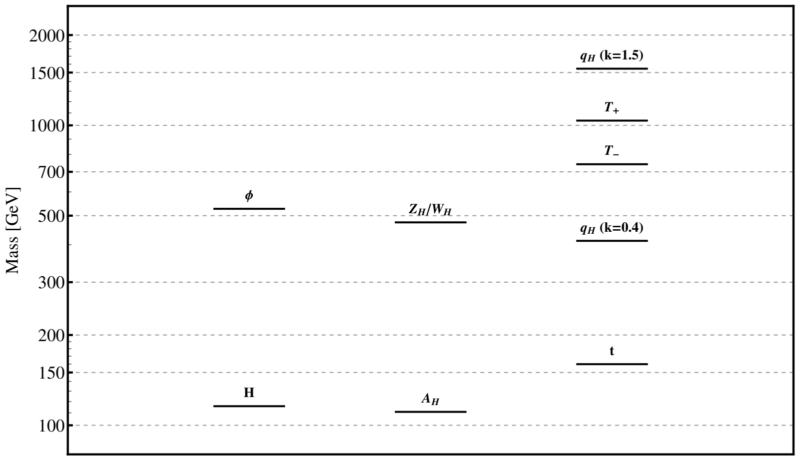

Figure 4.8: *Mass spectrum of LHT new particles: the effect of the free parameter κ, making the mirror fermions heavier or lighter than the gauge boson partners, has the biggest impact defining possible final state topologies to be scrutinised. We use as reference values $f = 800\, GeV$, $R = 1.0$ and $\kappa = 0.4$ or $\kappa = 1.5$, as in [8, 9].*

On the other hand, the spectrum of the fermion sector depends on the parameters R and κ besides the mass scale f. Generically, both the cancellon top partner T_+ and its T–parity partner T_- are always heavier than all gauge boson partners, if we restrict ourselves to the considered parameter space region defined in eq. (4.28). Furthermore, the T–even T_+ partner is heavier than the T–odd T_-, see eq. (3.119), with the mass splitting proportional to R.

The T–odd partners of all SM quarks (mirror quarks $q_- \equiv q_{\rm H}$) have masses proportional to the free parameter κ, see eq. (3.125). For $\kappa \gtrsim 0.45$ the mirror quarks are heavier than all gauge boson partners, opening up e.g. the two–body decays $q_{\rm H} \to V_{\rm H}\, q$ ($V_{\rm H} \equiv W^{\pm}_{\rm H}, Z_{\rm H}, A_{\rm H}$). For values $\kappa < 0.45$, only the decay $q_{\rm H} \to A_{\rm H}\, q$ is kinematically accessible. For the region $0.1 \lesssim \kappa \lesssim 0.2$ the mass difference between $q_{\rm H}$ and $A_{\rm H}$ is rather small: we will refer to this region as the "compressed spectrum" region, where most of the direct searches for new particles are not feasible. As mentioned before, the region $\kappa \lesssim 0.1$, where the mirror quarks become the lightest T–odd particles in the spectrum, is highly disfavoured by experimental observations and will not be considered in the following.

In figure 4.8 we plot a typical mass spectrum of the new particles introduced in the LHT model, with reference values of $f = 800\,\text{GeV}$, $R = 1.0$ and $\kappa = 0.4$ or $\kappa = 1.5$, as in [8,9]: while all masses explicitly depend on these three parameters, the general pattern of mass relations is altered only by different values of κ, as explained in the text.

We can now discuss the major production modes of LHT particles at the LHC. First of all, one should notice that due to T–parity, only the T–even cancellon T_{+} can be singly–produced in association with a SM particle. All other new particles have to be either pair–produced, or singly–produced in association with another LHT partner, highly reducing the available phase space with increasing masses.

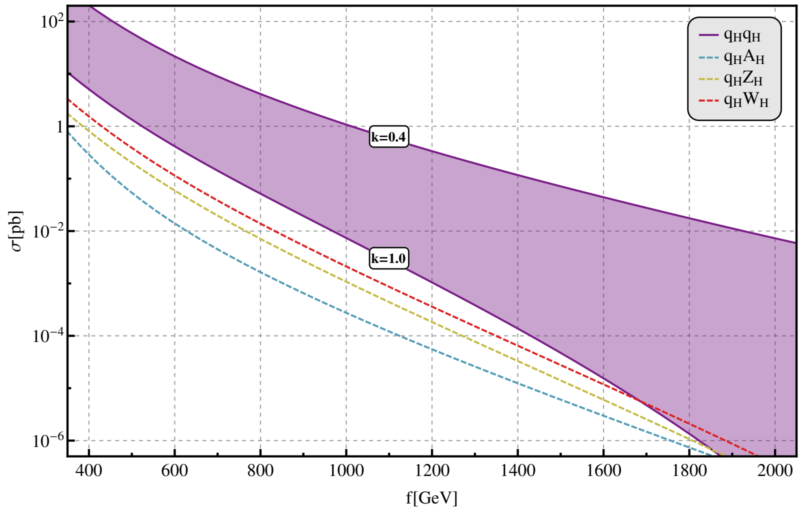

Figure 4.9: *Possible production cross section of LHT mirror quarks q_H at the LHC with $\sqrt{s}$ = 8 TeV, as a function of f with reference values $R = 1.0$ and $\kappa = 1.0$. The width of the pair production line corresponds to values of $\kappa \in [0.4, 1.0]$.*

Among the possible production cross sections of LHT partners, the pair production of mirror quarks $q_{\rm H}$ could be the most significant due to PDF enhancement, especially if their masses are not too large: their production is dominated by QCD processes, but also EW processes with a t-channel heavy gauge boson diagram might significantly contribute. Furthermore, associated production with a heavy gauge boson provide additional production channels for the mirror quarks. In figure 4.9 we show, as in [8, 9], the possible pair– and associated–production cross sections of the mirror quarks at the LHC with $\sqrt{s} = 8\,\text{TeV}$ as a function of f, with reference values $R = 1.0$ and $\kappa = 1.0$. To emphasise the effect of the parameter κ, we display the variation of the pair production cross section for $\kappa \in [0.4, 1.0]$ with the width of the corresponding cross–section line.

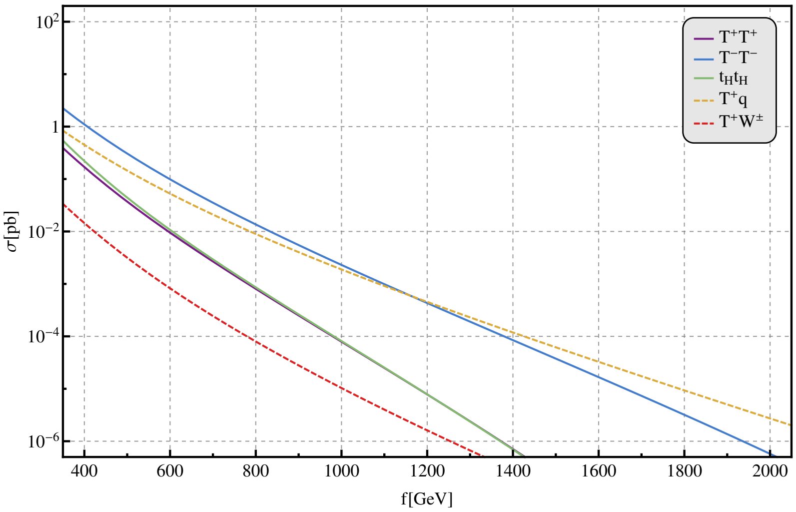

Figure 4.10: *Possible production cross section of LHT top partners at the LHC with* $\sqrt{s} = 8$ *TeV, as a function of* f *with reference values* $R = 1.0$ *and* $\kappa = 1.0$.

Among the top sector quarks, the T–odd T_- has the largest pair production cross section, unless the mirror top t_{H} is lighter, namely unless $\kappa \lesssim 0.6$. For large values of f, the single production of the T–even T_+ in association with a light quark, through a diagram involving a t–channel SM W with an initial state bottom quark, becomes comparable in size or even larger than the T_- pair production, due to phase space suppression of the latter process. This pattern can be observed in figure 4.10, where we plot, as in [8, 9], possible top–partner cross sections as a function of the scale f.

Production cross sections of pairs of gauge boson partners as a function of f are shown in figure 4.11: the dependence on the parameters R and κ is milder compared to the dependence on f, since the former might affect only the masses of the exchanged t–channel fermion partners. The gauge boson pair production is indeed generated via s–channel exchange of SM gauge bosons or via t–channel exchange of fermion partners.

Finally, in table 4.7 we list an overview of decay modes and branching ratios of the LHT new particles, with reference values $f = 1\,\text{TeV}$ and $R = 1.0$. We can observe e.g. the different decay pattern of the mirror quarks q_{H} depending on the particular value of κ.

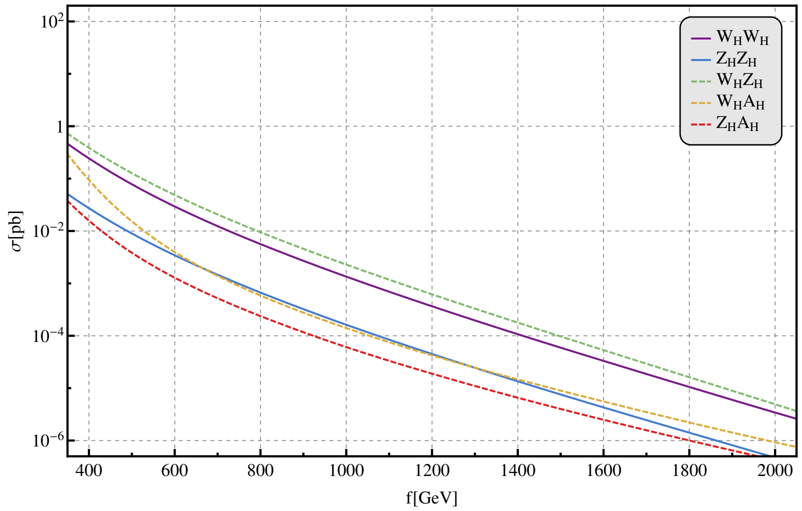

Figure 4.11: *Possible production cross section of LHT gauge boson partners at the LHC with* $\sqrt{s} = 8$ *TeV, as a function of* f *with reference values* $R = 1.0$ *and* $\kappa = 1.0$.

Particle	Decay	BR$_{\kappa=1.0}$	BR$_{\kappa=0.4}$
$d_{\rm H}$	$W_{\rm H}^-\ u$	63%	0%
	$Z_{\rm H}\ d$	31%	0%
	$A_{\rm H}\ d$	6%	100%
$u_{\rm H}$	$W_{\rm H}^+\ d$	61%	0%
	$Z_{\rm H}\ u$	30%	0%
	$A_{\rm H}\ u$	9%	100%
T_+	$W^+\ b$	46%	46%
	$Z\ t$	22%	22%
	$H\ t$	21%	21%
	$T_-\ A_{\rm H}$	11%	11%
T_-	$A_{\rm H}\ t$	100%	100%
ϕ^0	$A_{\rm H}\ Z$	100%	100%
ϕ^P	$A_{\rm H}\ H$	100%	100%

Particle	Decay	BR$_{\kappa=1.0}$	BR$_{\kappa=0.4}$
$\phi^\pm$	$A_{\rm H}\ W^\pm$	100%	100%
$\phi^{\pm\pm}$	$A_{\rm H}\ W^\pm\ W^\mp$	99%	96%
$A_{\rm H}$	stable		
$W_{\rm H}^\pm$	$A_{\rm H}\ W^\pm$	100%	2%
	$u_{\rm H}\ d$	0%	44%
	$d_{\rm H}\ u$	0%	27%
	$l_{\rm H}^\pm\ \nu$	0%	13.5%
	$\nu_{\rm H}\ l^\pm$	0%	13.5%
$Z_{\rm H}$	$A_{\rm H}\ H$	100%	2%
	$d_{\rm H}\ d$	0%	40%
	$u_{\rm H}\ u$	0%	30%
	$l_{\rm H}^\pm\ l^\mp$	0%	14%
	$\nu_{\rm H}\ \nu$	0%	14%

Table 4.7: *Overview of the decay modes with the corresponding branching ratios of the LHT new particles, with reference values* $f = 1$ *TeV and* $R = 1.0$. *We emphasise two possible scenarios, namely with the mirror quarks* q_H *either lighter* ($\kappa = 0.4$) *or heavier* ($\kappa = 1.0$) *than the gauge boson partners. The heavy leptons decay analogously to the heavy quarks and the decays involving generic up or down quarks have to be considered as summed over all flavours.*

4.3.2 Comparison with experimental results

In a cut–and–count based analysis, several signal regions are defined with different selection cuts, optimised for a particular signal topology to be tested. These selection cuts allow for a high suppression of the otherwise dominant SM backgrounds, together with only a mild suppression of the hypothesised BSM signal, such that an optimised signal over background ratio (S/B) might be achieved.

If no deviation from the SM background is observed, namely if the number of observed events is consistent within the uncertainties with the SM predicted number of events, the experimental collaborations provide through a statistical procedure the 95% CL upper limit on the possible additional signal events $n_{\mathrm{UL}}^{95\%}$. At this point, $n_{\mathrm{UL}}^{95\%}$ is still independent of the particular BSM signal to be tested: it is a measure of how much a generic BSM signal might contribute above the SM prediction in order to be consistent with the observed number of events within the uncertainties.

Given the integrated luminosity $\mathcal{L}$ of the analysed data, $n_{\mathrm{UL}}^{95\%}$ can be translated into the so–called visible cross section upper limit, namely

$$\sigma_{\mathrm{vis}}^{95\%,\,i} = \frac{n_{\mathrm{UL}}^{95\%,\,i}}{\mathcal{L}}\,, \tag{4.80}$$

where the index i refers to a particular signal region. The upper limit has to be compared with the visible cross section contribution of the considered BSM model. This is given by the cross section of all possible BSM processes contributing to the desired final state topology scrutinised in the analysis, collectively denoted as σ_{BSM}, re–weighted by the corresponding efficiency of the analysis–dependent selection cuts ϵ^i, namely

$$\sigma_{\mathrm{vis}}^{i} = \sigma_{\mathrm{BSM}} \cdot \epsilon^i\,. \tag{4.81}$$

One can exclude at 95% CL every BSM signal which would yield a visible cross section above the observed experimental upper limit, i.e. if

$$\sigma_{\mathrm{vis}}^{i} > \sigma_{\mathrm{vis}}^{95\%,\,i}\,. \tag{4.82}$$

This is indeed the procedure used by the collaborations to constrain specific SUSY scenarios or simplified models. It should be noted that the final exclusion contours depend on the particular assumption of the BSM signal, while the upper bound on the visible cross section is a model–independent quantity, which can be re–interpreted within different hypotheses.

The exclusion contours of parameter space points can then be directly translated as lower bounds on the possible masses of new particles predicted within the assumed BSM

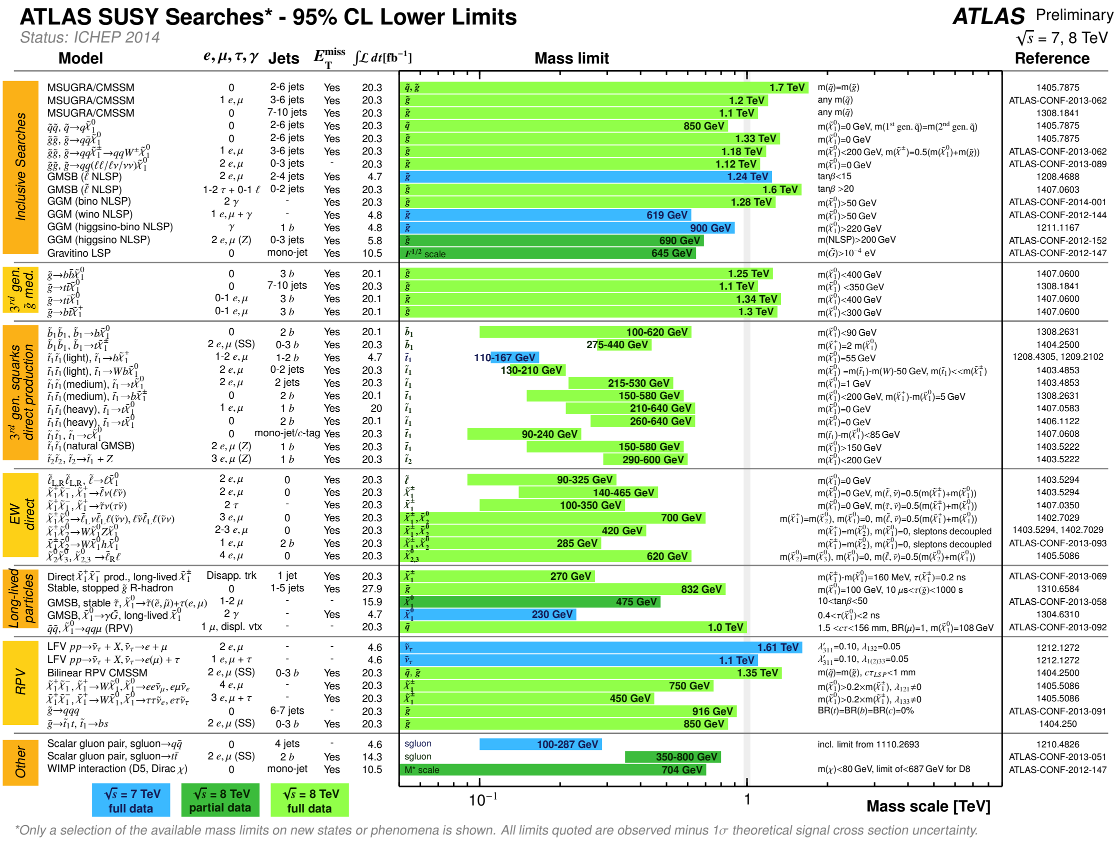

Figure 4.12: *95% CL mass limits on SUSY particles from the* $7-8$ *TeV ATLAS searches with up to* $20\,fb^{-1}$ *of integrated luminosity.*

model: for example, in figure 4.12 we can see the 95% CL mass limits on different SUSY particles from the 7 and 8 TeV ATLAS searches with up to $20\,\text{fb}^{-1}$ of integrated luminosity.

Therefore, it is crucial to evaluate the visible cross section of a BSM model, given a particular parameter space point to be probed. The production cross section might be calculated up to a desired precision using dedicated tools: in particular, for SUSY cross sections several public softwares are available, e.g. Prospino [78]. In our case, where we want to test a possible LHT signal against the direct search results, we first implemented the LHT model in FeynRules [79] combining the Feynman rules presented in [35, 36, 40] (focusing in particular on the *Case A* implementation of the down–type Yukawa Lagrangian), in order to obtain a viable model file with the UFO interface [80] for different Monte Carlo (MC) generators. This model file has been validated, using e.g. the MC generator Whizard [81–83], by reproducing the production cross sections and branching ratios of the new LHT particles as known in literature.

We used MadGraph 1.5 [84] to evaluate the LO cross section of the considered LHT topologies, given a parameter space point which we are free to modify. The efficiency can be estimated via a MC event simulation, too: if we call $N_{\rm MC}$ the total number of independently generated events, and N_i the number of events passing the cuts of the signal region i, the efficiency is given by

$$\epsilon^i = \lim_{N_{\rm MC}\to\infty} \frac{N_i}{N_{\rm MC}} \,, \qquad 0 \leq \epsilon^i \leq 1 \,. \tag{4.83}$$

We can imagine the evaluation of the efficiency as a result of a counting experiment, governed by a Poisson probability density function with mean value N_i: in this way, we can express a relative statistical uncertainty on the efficiency using the Poisson coefficient of variation, namely

$$\delta\epsilon^i \,\% = \frac{1}{\sqrt{N_i}}\,\% \,. \tag{4.84}$$

From eq. (4.84) it is clear that in order to obtain a realistic evaluation of the cut efficiencies, a large number of MC events has to be generated. The generation of large enough background samples to obtain a small relative uncertainty on the cut efficiencies represents the most time–consuming part of the recasting procedure.

MadGraph 1.5 is used to generate parton level events, subsequently processed through the Pythia 6.42 parton shower [85]. The output has been further analysed via Delphes 3.0 [86] for a fast simulation of either the ATLAS or CMS detector, depending on the specifications of the considered analysis. A dedicated tool has been developed to evaluate the different cut efficiencies, namely by evaluating the fraction of generated events satisfying the signal–region dependent cuts, when applied on the reconstructed objects of each event.

For each analysis to be recasted, we need to identify the possible LHT production modes yielding a possible final state topology matching the necessary requirements. This is followed by the evaluation of the process cross sections and efficiencies as described before in the text, given a particular point in the LHT parameter space.

We can then discriminate the consistency of the chosen parameter space point at 95% CL by comparing the evaluated visible cross section with the corresponding upper bound, see eq. (4.82). Exclusion limits can finally be presented as contours either in the (f, κ) or (f, R) plane. Since the mirror quarks posses the largest cross section among LHT new particles, with only a mild dependence on the parameter R as described in section 4.3.1, we will present exclusion contours from our recasting analysis in (f, κ) planes, fixing the value of R to a reference value $R = 1.0$.

Since most of the LHT final states mimick supersymmetric final states, due to the presence of an “invisible” particle at the end of most decay chains with a significant transverse momentum, namely the heavy photon $A_{\rm H}$, we analysed only experimental searches requiring a large fraction of missing transverse energy ($\not{E}_{\rm T}$) in the final state. Among those, we can distinguish three different classes of analyses: monojets plus $\not{E}_{\rm T}$, multijets plus $\not{E}_{\rm T}$, and multijets plus leptons and $\not{E}_{\rm T}$. In the following, we will present the details of the different analyses and the results of our recasting procedure.

Monojet plus $\not{E}_{\rm T}$ searches

The first class of direct searches we are going to discuss requires a low multiplicity of hard jets in the final state, together with a large cut on $\not{E}_{\rm T}$. Both ATLAS and CMS analysed 8 TeV data specifically for final states containing exactly no isolated leptons, one hard jet, a large fraction of $\not{E}_{\rm T}$, and at most another second slightly hard jet with $p_{\rm T} > 30\,{\rm GeV}$ [87,88]. Different requirements on the $p_{\rm T}$ of the leading jet and on the total $\not{E}_{\rm T}$ define specific signal regions within the analyses.

The most severe SM background is represented by QCD multijet processes, where part of the jet momenta are mismeasured or not reconstructed, yielding a non–negligible imbalance in the total transverse momentum. In order to discriminate against this QCD background, ATLAS requires the azimuthal separation between the $\not{E}_{\rm T}$ direction and the second leading jet, if present, to be greater than 0.5, while CMS only keeps two–jet events if the azimuthal separation between the jets is less than 2.5.

Monojet plus $\not{E}_{\rm T}$ searches are suitable for two LHT production modes with large cross sections, namely pair production of mirror quarks $p\,p \to q_{\rm H}\,q_{\rm H}$, and single production of mirror quarks in association with the heavy photon $p\,p \to q_{\rm H}\,A_{\rm H}$, in particular with subsequent decay $q_{\rm H} \to A_{\rm H}\,q$. Other possible decays of $q_{\rm H}$ into the gauge boson partners $W_{\rm H}$, $Z_{\rm H}$ would yield a larger multiplicity of final state hard jets: the efficiency for these production modes is therefore negligible. For this reason, monojet plus $\not{E}_{\rm T}$ searches guarantee the highest exclusion power in the low–κ region $0.2 \lesssim \kappa \lesssim 0.6$, where the mirror quarks $q_{\rm H}$ are lighter than $W_{\rm H}$, $Z_{\rm H}$. On the other hand, for higher values of κ, the branching ratio of the decay $q_{\rm H} \to A_{\rm H}\,q$ is highly suppressed, see table 4.7.

In the absence of any deviation from the SM prediction, both experimental collaborations report the 95% CL upper limit on the visible cross section. As anticipated, the highest exclusion power of these searches lies in the low–κ region: we are able to exclude nearly the whole range $0.2 \lesssim \kappa \lesssim 0.5$ up to $f = 1200\,{\rm GeV}$, as can be seen in figure 4.13.

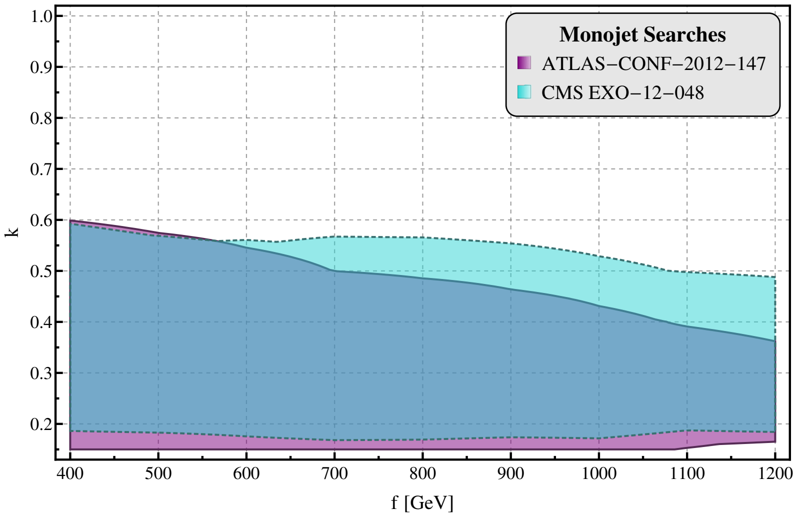

Figure 4.13: *Exclusion contours in the (f, κ) plane at 95% CL from monojet plus $\not{E}_T$ searches at LHC8, corresponding to different recasted ATLAS and CMS analyses.*

Multijets plus $\not{E}_{\mathrm{T}}$ searches

A second class of direct searches we have analysed is dedicated to final states with a high multiplicity of hard jets, together with a large cut on $\not{E}_{\mathrm{T}}$. Numerous analyses within this category have been interpreted by ATLAS and CMS using 7 and 8 TeV data, in particular in terms of supersymmetric decay chains with all–hadronic decays of squarks and gluinos. The recasting of these searches guarantees a good discrimination power in the region of larger κ values, too, where the decay of the mirror quarks into gauge boson partners W_{H}, Z_{H} allows for high multiplicity final state hard jets when considering all–hadronic final states.

The ATLAS search published in [89] is optimised for squark and gluino production. Together with a requirement on the multiplicity of final state hard jets, different cuts are introduced to discriminate against e.g. QCD background: as with the monojet plus $\not{E}_{\mathrm{T}}$ searches, a large azimuthal separation between the $\not{E}_{\mathrm{T}}$ direction and the hard jets is required, as well as a stringent cut on the fraction of missing transverse momentum with respect to the hadronic transverse momenta within each event.

The ATLAS search published in [90] is on the other hand optimised for stop pair production processes, where each stop decays into a hadronically decaying top and the lightest supersymmetric particle. At least six hard jets are required in the final state, of which at least two have to be tagged as b–jets. This search exploits the presence of intermediate top quarks in the decay chain: besides the presence of at least two b–jets, it is required that the invariant mass of two trijet systems should reconstruct the top mass. As usual, a requirement on the azimuthal separation between the $\not{E}_{\mathrm{T}}$ direction and the three hardest jets is required, as well as a large cut on the missing transverse momentum itself. Finally, to discriminate against the $t\bar{t}$ SM background, the transverse mass m_{T} between the $\not\!\!E_{\mathrm{T}}$ and the b–tagged jet closest in $\Delta\phi$ to the $\not\!\!E_{\mathrm{T}}$ direction is required to be greater that 175 GeV. For this analysis, the LHT topologies yielding the highest sensitivity are pair production of the T–odd mirror fermion t_{H} with subsequent stop–like decay, and the decay $q_{\mathrm{H}} \to q\, Z_{\mathrm{H}}$, with $Z_{\mathrm{H}} \to h\, A_{\mathrm{H}}$ and q_{H} either associated or pair produced.

Finally, the CMS search published in [91] looks generically at squark, sbottom and gluino production. Different signal regions are defined depending on the particular multiplicity of final state hard jets and b–jets required. Additional cuts on the transverse momenta of the jets are included to reduce possible SM backgrounds, as well as a cut on a dedicated variable called α_{T}, which guarantees a good discrimination power against QCD background with jet energy mismeasurements. For a two–jet event, the α_{T} variable is defined as the ratio of the transverse momentum of the less energetic jet over the transverse mass of the dijet system. QCD events are usually measured with $\alpha_{\mathrm{T}} \lesssim 0.5$, while jets recoiling against significant, genuine $\not\!\!E_{\mathrm{T}}$ yield α_{T} values larger than 0.5. A generalisation of the definition to multi–jet events can be found in [91].

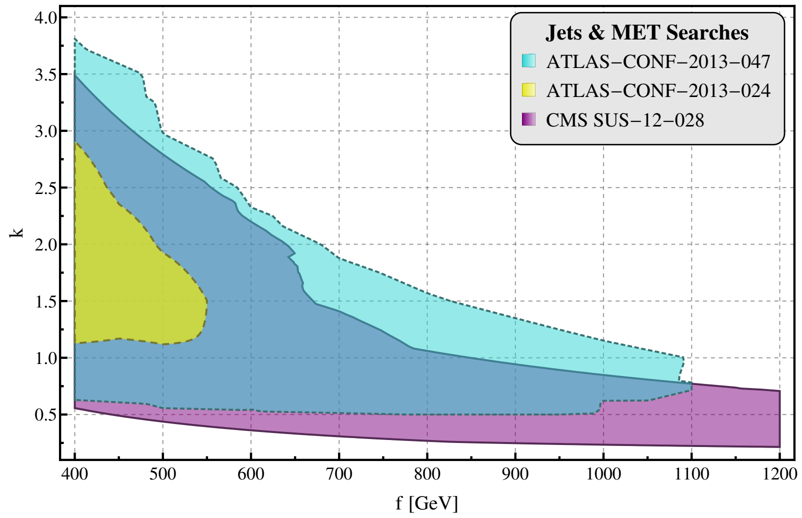

Figure 4.14: *Exclusion contours in the (f, κ) plane at 95% CL from multijet plus $\not\!\!E_T$ searches at LHC8, corresponding to different recasted ATLAS and CMS analyses.*

As anticipated, multijet plus $\not\!\!E_{\mathrm{T}}$ searches guarantee a good discrimination power for $\kappa \gtrsim 0.5$ in the LHT parameter space, providing an important complementary information compared to searches requiring a small multiplicity of final state hard jets. The results of our recasting analysis for multijet plus $\not\!\!E_{\mathrm{T}}$ searches are shown in figure 4.14.

Multijets plus leptons and $\not{E}_T$ searches

Finally, we consider searches dedicated to final states with high multiplicity hard jets, plus additional tagged isolated leptons and $\not{E}_T$. It turns out that the requirement of leptons in the final state does not increase the exclusion power for the LHT parameter space: for completeness we will report here the results of the recasting analysis, even if the exclusion contour will not be extended compared to all–hadronic analyses described before.

In particular, the ATLAS analyses published in [92, 93] both require: the presence of exactly one isolated lepton; at least four reconstructed hard jets; a large cut on the missing transverse momentum $\not{E}_T$ as well as a large cut on the scalar sum of the momenta of all the reconstructed jets; a cut on the transverse mass m_T between the $\not{E}_T$ and the isolated lepton. Furthermore, since the analysis [93] focuses on stop pair production, with the stop either decaying into a top quark and a neutralino, or into a bottom quark plus the lightest chargino, additional requirements on final state tagged b–jets and a cut on the variable m_{T2} are included. The latter to suppress dangerous $t\bar{t}$ backgrounds. Among matching LHT topologies, we consider mirror quark production with subsequent decays to gauge boson partners W_H, Z_H generating exactly one single charged lepton in the final state: if b–jets are required, particularly important are processes including $Z_H \to h\,A_H$ or $t_H \to t\,A_H$ decays.

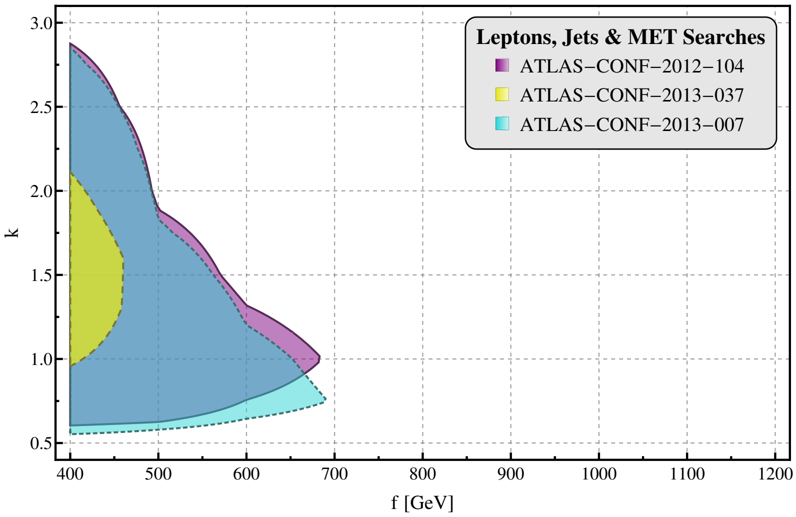

Figure 4.15: *Exclusion contours in the (f, κ) plane at 95% CL from multijet, leptons plus $\not{E}_T$ searches at LHC8. The different contours represent the exclusions limits from the recasted ATLAS analyses.*

On the other hand, the ATLAS analysis [94], originally optimised for gluino pair production, looks for exactly two same–sign leptons in combination with at least three jets and significant missing transverse momentum in the final state. For this analysis, same charge mirror quarks pair production with subsequent leptonic decay $q_{\rm H} \to q' \, W_{\rm H}$, $W_{\rm H} \to W^{\pm} \, A_{\rm H}$, represents an LHT topology which can be tested accordingly.

A similar CMS analysis [95] turns out to be inefficient for the considered LHT topology because of the large number of required tagged b–jets in the final state.

In figure 4.15 we show the result of the recasting procedure of the described analyses: as mentioned before, the exclusion power is smaller than the all–hadronic final state searches, see figure 4.14.

Effective operator bound

Before showing the combined limit from the different recasted analyses, it is important to mention another available constraining information which we have taken into account. The T–odd mirror fermions can generate four–fermion operators via diagrams involving the exchange of Goldstone bosons χ and η, as first described in [37]. By power–counting, it is easy to see that, after integrating out the intermediate mirror fermions of the box diagram, a four–fermion operator proportional to κ^2 is generated, see [37]:

$$\mathcal{O}^{\rm LHT}_{\text{4–ferm}} = -\frac{\kappa^2}{128\pi^2 f^2} \bar{\psi}_{\rm L} \, \gamma^{\mu} \, \psi_{\rm L} \, \bar{\psi}'_{\rm L} \, \gamma_{\mu} \, \psi'_{\rm L} + \mathcal{O}\left(g/\kappa\right) \tag{4.85}$$

where ψ, ψ' are distinct SM fermions. An upper bound on the allowed coefficient of possible four–fermion operators might constrain κ within a certain range, given a particular value f. The possibility to set an upper bound on κ will be crucial to set a global limit on f together with the results from the direct searches, the latter providing instead an exclusion for lower values of κ.

Possible constrains on four–fermion operators at the LHC arise from operators involving four quarks, for example searches in the angular distribution of dijets [96, 97]. However, the most stringent bounds on four–fermion operators are still from LEP searches: given a four–fermion operator of the form

$$\mathcal{O}_{\text{4–ferm}} = \frac{2\pi}{\Lambda^2_{\text{4–ferm}}} \bar{\psi}_{\rm L} \, \gamma^{\mu} \, \psi_{\rm L} \, \bar{\psi}'_{\rm L} \, \gamma_{\mu} \, \psi'_{\rm L} \, , \tag{4.86}$$

the strongest constraint comes from the *eedd* operator [37], namely $\Lambda_{\text{4–ferm}} \gtrsim 26.4\,\text{TeV}$. This is turn yields the following upper bound for κ

$$\kappa^2 < 256 \, \pi^3 \frac{f^2}{\Lambda^2_{\text{4–ferm}}} \, . \tag{4.87}$$

Combined exclusion limits

It is now possible to superimpose the different exclusion regions obtained from the recasting of direct searches, as well as from constraints on four–fermion operators. The result of our findings is shown in figure 4.16, as published in [8, 9].

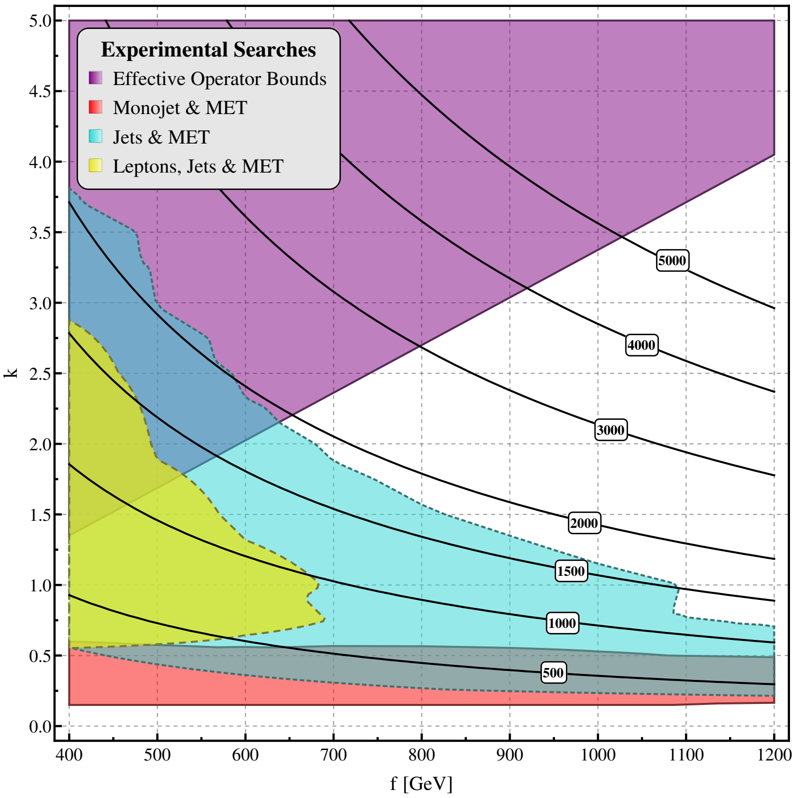

Figure 4.16: *Exclusion contours in the (f, κ) plane at 95% CL from different recasted ATLAS and CMS direct searches at LHC8, as well as from constraints on four–fermion operators. The black lines display the value of the masses of the mirror quarks in GeV.*

From the combined result of figure 4.16 we can extract a global lower bound on f:

$$(f_{\mathrm{LHT,\ A}})_{\text{direct–search.}} \gtrsim 638\,\mathrm{GeV} \quad (95\%\,\mathrm{CL})\,, \tag{4.88}$$

which is comparable with the current bound obtained from EWPT and Higgs observables, see eq. (4.78), although not pushing the limit much beyond. However, it is clear that direct searches for new particles cover interesting regions of the LHT parameter space, and we expect that further experimental analyses at higher center of mass energies, but most of all with an increased integrated luminosity, might help to extend the current limits.

4.3.3 Towards LHT–optimised direct searches

The setup of the direct searches we have analysed so far has been optimised by the experimental collaboration for specific assumptions on the possible underlying BSM signal. Supersymmetric signatures involving squarks, gluinos and neutralinos are usually considered. The question we will try now to answer in this section is whether an optimisation of the current setups might be possible with a different assumption on the underlying signal, discussing the results published in refs. [8, 9]. In particular, we want to define new optimised signal regions to increase the sensitivity of direct searches to Little Higgs parameter space regions not constrained by the existing setup.

However, such an optimisation is sensible only to the particular kinematic signatures of the underlying signal, e.g. different mass gaps between particles in the decay chains, since no angular observables have been taken into account in the recasted analyses. On the other hand, angular observables represent an important discriminant tool for the exclusion (or discovery) of Little Higgs signals, given the different spin structure compared to supersymmetric spectra: we expect thus a boost for possible dedicated analyses for Little Higgs signals involving angular observables, especially in the context of future linear colliders.

The optimisation method proceeds as follows. We first generate LHT event samples for some benchmark points in the (f, κ) parameter space, together with SM background samples, assuming a center–of–mass energy of $\sqrt{s} = 8\,\text{TeV}$. We then vary the values of the selection cuts of the most constraining recasted analyses within sensible domains, evaluating the corresponding efficiencies for both signal and backgrounds as a function of the kinematic cuts. In this way, we can obtain a map of the $S/\sqrt{B}$ ratio as a function of the cut values: a maximisation of this ratio allows us to identify optimised cut values, which guarantee the highest exclusion power for the chosen signal benchmark point.

Assuming an integrated luminosity as reported in the experimental papers, we obtain the 95% CL upper bound on the visible cross section[1] using a standard CLs frequentist approach [98]. The upper bounds on the visible cross sections are then finally translated into exclusion regions in the (f, κ) plane.

In the following we will discuss possible optimisations of monojet plus $\not{E}_\text{T}$ and multijets plus $\not{E}_\text{T}$ direct searches.

---

[1] In particular, we evaluate the *expected* upper bound, namely assuming that the would–be observed number of events is equal to the predicted SM background events.

Monojet plus $\not{E}_{\mathrm{T}}$ searches

The dominant backgrounds for monojet plus $\not{E}_{\mathrm{T}}$ searches are $Z(\to \nu\nu)+$jets and $W+$jets, with smaller contributions from $Z/\gamma^*(\to \ell^+\ell^-)$ + jets, QCD multijet, $t\bar{t}$ and diboson (WW, ZZ, WZ) processes. Events for all these processes have been generated via the Monte Carlo generation chain described in section 4.3.2, applying the detector specifications given in the experimental papers.

Benchmark	f [GeV]	κ
BM1	1600	0.2
BM2	2000	0.4
BM3	600	0.8

Table 4.8: *Benchmark points for the optimisation of monojet plus $\not{E}_T$ searches.*

Remembering that monojet plus $\not{E}_{\mathrm{T}}$ searches are mostly constraining for lower values of $\kappa \lesssim 0.6$, we identify three possible benchmark (f, κ) scenarios, as listed in table 4.8.

Cut	Range
$\not{E}_{\mathrm{T}}$	$[120, 600]$ GeV
$p_{\mathrm{T}}(j_1)$	$[100, 600]$ GeV
$p_{\mathrm{T}}(j_2)$	$[0, 450]$ GeV

Table 4.9: *Cut ranges scanned to identify an optimised monojet plus $\not{E}_T$ analysis.*

We then scan within sensible ranges different values of three selection cuts required in the monojet plus $\not{E}_{\mathrm{T}}$ searches, namely the transverse momentum of the two leading jets, and the total amount of missing transverse momentum: the specific ranges are summarised in table 4.9. In particular, the possible presence of a second hard jet is not included in the original experimental searches: this requirement has been included since our assumed signal mostly consists of two jets in the final state. In table 4.10 we report the optimised cuts for the three different signal benchmark points, as well as one of the signal regions of both ATLAS and CMS analyses [87, 88], for comparison.

In general, we observe that the $\not{E}_{\mathrm{T}}$ and the p_{T} cuts increase together with the mass gap between the mirror quark and the heavy photon, which scales with κ: the larger the mass gap, the larger the acquired transverse momenta of the decay products of $q_{\mathrm{H}} \to q\, A_{\mathrm{H}}$.

Cut	BM1	BM2	BM3	ATLAS	CMS
$\not{E}_{\mathrm{T}}$	170 GeV	520 GeV	370 GeV	120	250
$p_{\mathrm{T}}(j_1)$	120 GeV	470 GeV	250 GeV	120	110
$p_{\mathrm{T}}(j_2)$	80 GeV	310 GeV	180 GeV	✗	✗
Lepton veto	✓	✓	✓	✓	✓
Two–jet veto	✓	✓	✓	✓	✓
$\Delta\phi(\not{E}_{\mathrm{T}}, j_2) \geq$	0.5	0.5	0.5	0.5	✗
$\Delta\phi(j_1, j_2) \leq$	2.5	2.5	2.5	✗	2.5
$\mathrm{S}^{95}_{\mathrm{exp}}$	1745	8.4	99.9	45136	3694

Table 4.10: *Optimised monojet plus $\not{E}_T$ cuts for three LHT benchmark points as in table 4.8. In particular, the lepton veto rejects any event with an isolated electron ($p_T > 10$ GeV), muon ($p_T > 10$ GeV) or tau ($p_T > 20$ GeV) in the final state. The two–jet veto rejects events with more than two jets satisfying $p_T > 30$ GeV and $|\eta| < 4.5$. The last two columns show one of the signal regions of the recasted ATLAS and CMS analysis [87, 88]. S^{95}_{exp} represents the (expected) upper bound on the number of signal events.*

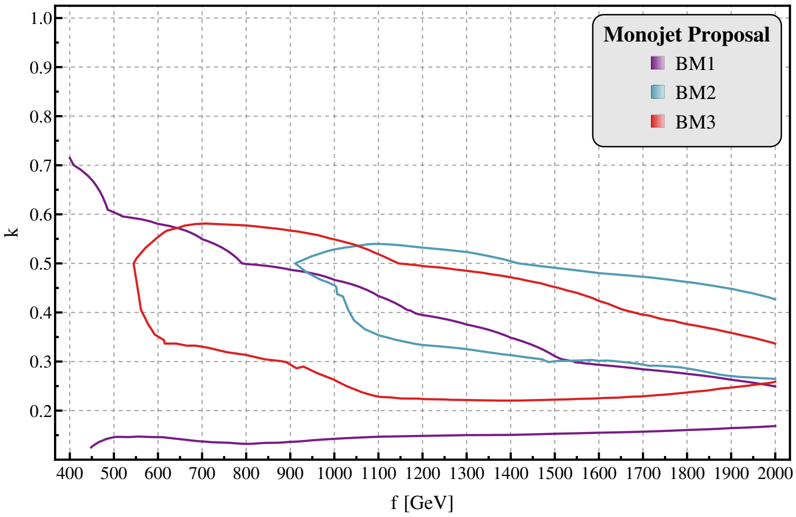

Figure 4.17: 95% *CL exclusion contours using the optimised selection cuts summarised in table 4.10 at LHC8 with 20 fb^{-1}. The different contours correspond to the three considered signal regions.*

After extracting the expected upper bound on the visible cross section, we can obtain the excluded regions within the LHT parameter space. In particular, in figure 4.17 we show the exclusion limits for each considered signal region, while in figure 4.18 we show the corresponding combination together with the exclusion from the original ATLAS and CMS analysis, for comparison.

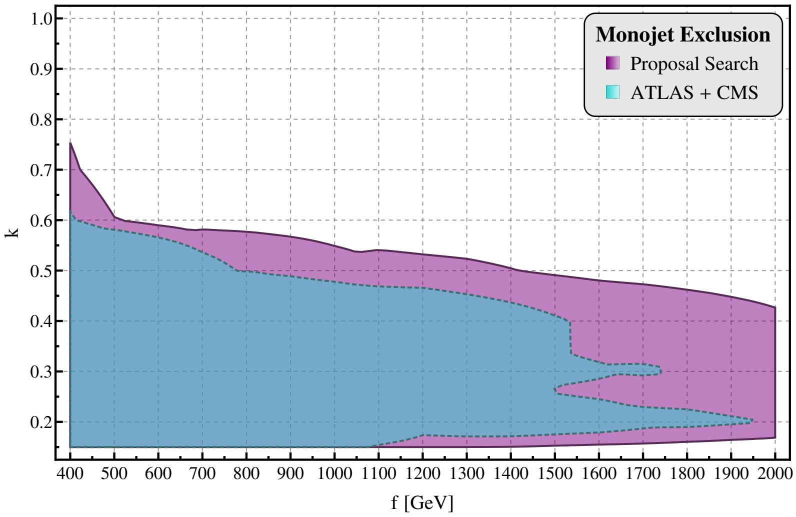

Figure 4.18: *Comparison between the optimised monojet plus $\not{E}_T$ exclusion limits and the limits from the recasting of the ATLAS and CMS [87, 88] analyses.*

As expected, the optimised searches are mostly discriminant in the low–κ range, as the original experimental searches: as detailed in section 4.3.2, for higher values of κ the branching ratio of the interesting decay $q_{\rm H} \to q\, A_{\rm H}$ is too much suppressed, together with a reduced cross section due to the higher $q_{\rm H}$ mass. Furthermore, we can observe that the optimised set of selection cuts obtained from our analysis does expand the excluded region, especially for larger values of the scale f. This suggests that a dedicated analysis focussing on particular kinematic regimes of the LHT model might indeed be conceivable.

Multijets plus $\not{E}_{\rm T}$ searches

The dominant background for multijet plus $\not{E}_{\rm T}$ searches are W+jets, Z+jets, $t\bar{t}$, single top, QCD multijet and diboson (WW, ZZ, WZ) processes. As with the monojet plus $\not{E}_{\rm T}$ analysis, events for all these processes have been generated applying the detector specifications of the ATLAS analysis [89].

In this case, we choose benchmark parameter space points with higher values of κ, in order to maximise the exclusion power for the parameter space regions where multijet final states are accessible with higher production cross sections. In particular, we choose three benchmark scenarios as summarised in table 4.11.

Benchmark	f [GeV]	κ
BM1	600	1.0
BM2	700	2.0
BM3	1000	1.0

Table 4.11: *Benchmark points for the optimisation of multijet plus* $\not{E}_T$ *searches.*

We then scan within sensible ranges different values of the selection cuts used in the ATLAS analysis [89]: in its original setup, this analysis provided the most stringent limit among the considered analyses, as shown in section 4.3.2 and figure 4.14. We focus in particular on the ATLAS signal regions requiring at least three and at least four hard jets in the final state, respectively.

Cut	Range
n_{jets}	3 or 4
$\not{E}_{\mathrm{T}}$	$[100, 500]$ GeV
$p_{\mathrm{T}}(j_1)$	$[100, 400]$ GeV
$p_{\mathrm{T}}(j_n)$	$[40, 100]$ GeV
m_{eff}	$[1.2, 3.0]$ TeV

Table 4.12: *Cut ranges scanned to identify an optimised multijet plus* $\not{E}_T$ *analysis.*

To identify optimised selection cuts, we scan the values of the total missing transverse momentum, the p_{T} of the two leading jets, and of the scalar sum of the transverse momenta of all reconstructed objects in the event (m_{eff}): the range of our scan is listed in table 4.12. Together with the optimised cuts, we include in our analysis a lepton veto and a cut on the azimuthal separation of the leading three (four) jets with respect to the direction of the $\not{E}_{\mathrm{T}}$, in order to reduce QCD background, as in the original ATLAS setup. The optimised cuts for the three different signal benchmark points are given in table 4.13, for both the 3–jets and 4–jets final state.

We can observe that the optimised cut on the effective mass m_{eff} increases with both f and κ, as indeed the mass gap between the mirror quarks q_{H} and the heavy photon becomes larger: $m_{\text{eff}} \sim 2(m_{q_{\mathrm{H}}} - m_{A_{\mathrm{H}}})$ for pair production of mirror quarks. Analogously, the optimised value for $\not{E}_{\mathrm{T}}$ increases with the mass gap between q_{H} and A_{H}.

Cut	$\mathrm{BM1}_{3j}$	$\mathrm{BM2}_{3j}$	$\mathrm{BM3}_{3j}$	$\mathrm{BM1}_{4j}$	$\mathrm{BM2}_{4j}$	$\mathrm{BM3}_{4j}$
Lepton veto	✓					
n_{jets}	3			4		
$\not{E}_\mathrm{T}$	200 GeV	340 GeV	400 GeV	200 GeV	300 GeV	400 GeV
$p_\mathrm{T}(j_1)$	120 GeV	380 GeV	180 GeV	140 GeV	320 GeV	180 GeV
$p_\mathrm{T}(j_n)$	100 GeV	100 GeV	100 GeV	70 GeV	80 GeV	100 GeV
$\Delta\phi(j_{1,2,3}, \not{E}_\mathrm{T}) \geq$	0.4					
m_eff	1.2 TeV	2.8 TeV	2.1 TeV	1.2 TeV	2.6 TeV	2.1 TeV
$\mathrm{S}^{95}_{\mathrm{exp}}$	298	3.5	11.3	154	3.5	4.2

Table 4.13: *Optimised multijets plus $\not{E}_T$ cuts for the three LHT benchmark points as in table 4.11, for both the 3–jet and 4–jet final states. The lepton veto rejects any event with an electron (muon) with $p_T > 20$ (10) GeV and $|\eta| < 2.8$ (2.4). S^{95}_{exp} represents the (expected) upper bound on the number of signal events.*

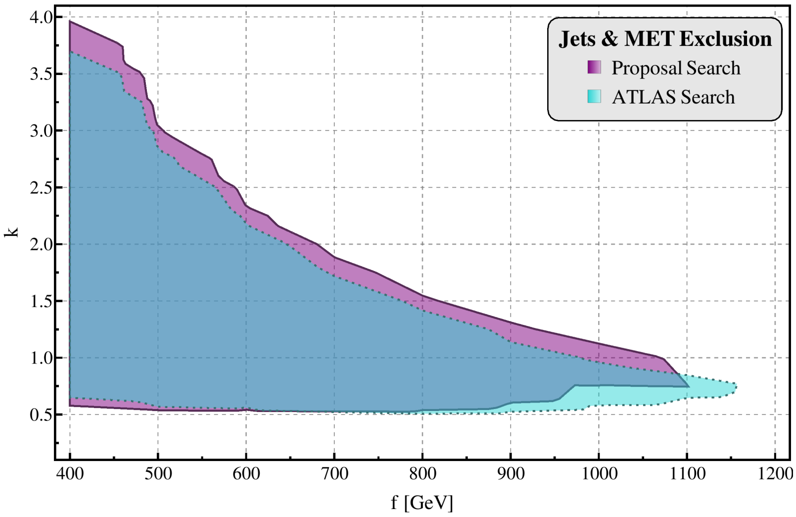

Figure 4.19: *Comparison between the optimised multijet plus $\not{E}_T$ exclusion limits and the limits from the recasting of the ATLAS [89] analysis.*

With the extracted upper bounds on the visible cross section for each signal region denoted in table 4.13, we are finally able to obtain the exclusion contours and compare them with the original ATLAS setup. The result is shown in figure 4.19, where we combine the exclusion from all optimised signal regions. In particular, we see that with the current setup of the analysis there is only small room for improvement in searches with multijet plus $\not{E}_{\mathrm{T}}$ final state topologies. The improvement with our proposed optimised signal region can be estimated to be roughly 50 GeV for fixed value of κ.

	SR BM	SR BT	SR CM	SR CT	SR D
ATLAS analysis [89]					
Total bkg	33 ± 7	2.4 ± 1.4	210 ± 40	1.6 ± 1.4	15 ± 5
$\mathrm{S}^{95}_{\mathrm{exp}}$	$17.0^{+6.6}_{-4.6}$	$5.8^{+2.9}_{-1.8}$	$72.9^{+23.6}_{-18.0}$	$3.3^{+2.1}_{-1.2}$	$13.6^{+5.1}_{-3.5}$
Recasting procedure					
Total bkg	30.2 ± 9.1	3.2 ± 1.6	218.5 ± 43.7	2.4 ± 1.2	15.2 ± 4.5
$\mathrm{S}^{95}_{\mathrm{exp}}$	21.0	5.4	90.2	4.3	12.2

Table 4.14: *Validation of the recasting procedure, event generation and statistical tools by comparing the published experimental results [89] and our findings. The labels BM, BT, CM, CT and D refer to specific signal regions (SR) defined in [89]. In particular, the total number of background events and the corresponding* 95% *CL expected upper bound on BSM signal events (S^{95}_{exp}) are shown.*

Finally, we want to comment about the validation of our statistical procedure to extract the upper bounds on the visible cross section, and of the recasting procedure in general. By applying the recasted selection cuts of the original ATLAS analysis [89] on the generated background samples, we are able to compare the expected number of background events with the published numbers from the experimental paper, as well as the expected upper bounds on possible BSM events. The result of the comparison is shown in table 4.14: our findings are clearly consistent within the reported uncertainties.

Chapter 5

Prospects for LHC run II

This chapter details the results of my research work concerning the proposal of dedicated analyses for particular BSM signatures at the foreseen $\sqrt{s} = 13$, 14 *TeV LHC run II. The corresponding publications are [10, 11]. Different discovery strategies and mass measurement methods have been developed. In particular, on the one side I have been focusing on the discovery of a possible top partner signal: in a first section of this chapter I will present the motivation for a dedicated top partner experimental analysis, the theoretical framework in the context of different Composite– and Little Higgs models, and the proposed analysis involving top–tagging techniques and optimised selection cuts accounting for the particular kinematics of the considered process. A possible measurement of the top partner invariant mass is furthermore described, in a final state without missing transverse momentum.*

In a second section of this chapter I will present the results for a possible mass measurement from a BSM signature involving a large fraction of missing transverse momentum in the final state. In particular, the minimum symmetric event topology is considered, namely X *pair production followed by* $X \to \ell N$*, where* X *and* N *are unknown particles with the masses to be measured, and* N *is an invisible particle, focusing on the case where* X *is pair produced from a resonance. After presenting a method to identify the kinematically allowed mass regions in the* (m_N, m_X) *plane, I will define kinematical variables on the boundary of the allowed mass region which can be used in measuring the unknown masses. As a case study, the process* $pp \to A \to \tilde{\chi}_1^+ \tilde{\chi}_1^-$*, followed by* $\tilde{\chi}_1^\pm \to \ell^\pm \tilde{\nu}_\ell$ *in the Minimal Supersymmetric Standard Model has been considered. The main resources used for this chapter are refs. [10, 11, 99–102].*

5.1 Top Partner Discovery in the $T \to tZ$ channel at the LHC

In this section we will discuss our results concerning the analysis presented in ref. [10], where we propose a direct search for a charge–2/3, spin–1/2, vector–like top partner T at the LHC with $\sqrt{s} = 13\,\mathrm{TeV}$ and $300\,\mathrm{fb}^{-1}$ of integrated luminosity. In particular, we are interested in the top partner decay $T \to t\,Z \to (q\,q'\,b)\;(\ell^+\ell^-)$. This is a process that has been ignored in the literature up to now. However, it is quite interesting as it allows a possible full reconstruction of the invariant mass of the on–shell top partner.

We will exploit top–tagging techniques capturing the particular boosted kinematics of the top partner decay products, as well as optimised selection cuts, in order to reduce potentially dangerous SM background processes while retaining a large fraction of signal events.

In the following, we will first motivate why direct searches for new particles should focus on possible BSM top partner signals, further reviewing the current experimental status and the proposed analyses from the theoretical community. Details about jet substructure methods, specifically top–tagging algorithms, will be discussed as well. Furthermore, we will present examples of possible top partners arising in different strongly coupled models, even if we decided to use a simplified–model approach regarding the assumption on the underlying BSM model. A recipe to match the free parameters used in our analysis to specific BSM models will be described.

We will then detail the selection cuts of our proposed analysis, and explain the procedure to fully reconstruct the four–momenta of the candidate Z and t of our signal process. In this way, we will obtain a possible measurement of the top partner invariant mass, and discuss a systematic procedure to evaluate the statistical significance of the top partner signal evidence above the SM backgrounds.

5.1.1 Top partners and top tagging

General motivation

Direct searches for Supersymmetry have pushed the limit on the masses of supersymmetric particles in simplified models above the TeV threshold. However, these limits apply to partners of the gluons and of the light quarks, which are abundantly produced at the LHC. On the other hand, direct limits on the top superpartners, and on the partners of the W and Z bosons, are still below the TeV scale due to the smaller production rates, and the more involved final states from the experimental point of view.

Light partners of the top and of the gauge bosons are a key ingredient for the naturalness argument of different BSM models, in order to cut off the quadratic UV–sensitivity of the Higgs mass squared parameter: we have seen in section 3.2.3 the example of Little Higgs models, but this is a common feature for generic Supersymmetric and Composite Higgs models.

Contrary to sequential fourth generation quarks, which are heavily constrained already from Higgs boson searches, since they would yield a large impact e.g. in the one–loop induced processes like gluon fusion production and diphoton decay of the Higgs, indirect bounds on vector–like quarks are much weaker. Their effect on the Higgs observables is indeed less dramatic than fourth generation quarks, since their vector–like nature allow to obtain a large Dirac mass without introducing a large Yukawa coupling to the Higgs.

Both the ATLAS and CMS collaborations have recently performed dedicated searches for top partners [42, 103–108]. Depending on the particular branching ratio under investigation, the actual limits on the top partner mass, at $\sqrt{s} = 8\,\text{TeV}$ and with up to $20\,\text{fb}^{-1}$ of integrated luminosity, do not exceed $700 - 800\,\text{GeV}$. Most of these experimental searches assume the new heavy quarks to be pair produced: however, searches combining pair production with single production through EW interactions will become an important feature in the future. Present limits from the LHC start indeed to enter the region in which single production becomes comparable to pair production due to the smaller phase space suppression, even if an EW coupling is involved.

Tagging the boosted regime

Let us now focus on the kinematics of a possible top partner decay. For masses much heavier than the top quark, the top partner decay products are produced with large spatial separation (back–to–back decay). Furthermore, for large center–of–mass energies, these "first generation" top partner decay products are necessarily boosted, namely with transverse momentum p_T which considerably exceeds their rest mass: this means that the subsequent decay products are highly collimated in one area of the detector. As a rule of thumb, the decay products of a highly boosted particle of mass m and transverse momentum $p_\text{T} \gg m$ are collimated within a cone of radius

$$\Delta R \sim 2\,\frac{m}{p_\text{T}}\,, \tag{5.1}$$

such that e.g. the hadronic decays of a boosted SM top with $p_\text{T} \sim 250\,\text{GeV}$ are collimated within a detector region of radius $\Delta R \lesssim 1.4$.

In this kinematical regime, conventional reconstruction algorithms that rely on a jet–to–parton assignment are often "inappropriate". Crucial ingredients for high center–of–mass searches involving massive particles are the so called substructure methods [109,110], to identify the top partner decay products within large "fat" jets. Generically, focusing on hadronic decays of boosted objects, these substructure methods first reconstruct jets with a much larger radius parameter, in order to capture the energy of the complete hadronic decay in a single jet; then use method–dependent discriminating variables to analyse the internal structure of the fat jets, to separate boosted objects from the large QCD background. Jet–substructure methods which are dedicated to the identification of possible boosted tops are generically called *top–taggers*.

A review on top–taggers can be found e.g. in [111]. Among possible available algorithms, the two most commonly exploited are the John Hopkins top–tagger [112] ("JHTopTagger") and the Heidelberg–Eugene–Paris top–tagger [110] ("HEPTopTagger"). Similar to the BDRS jet substructure method for boosted Higgs [109], the JHTopTagger clusters the decay products and relevant radiations of the decaying boosted top using a large cone radius, and then de–clusters the candidate top jet with a dedicated algorithm to find a suitable trijet system. If the invariant mass of the trijet system satisfies criteria involving m_t and m_{W}, the fat–jet is tagged as top–jet.

The HEPTopTagger has been developed to capture moderately boosted tops. First, the Cambridge–Aachen clustering algorithm with large cone radius $R = 1.5$ is applied to reconstruct possible fat–jets: as seen in eq. (5.1), such large R allows to access top quarks down to $p_{\mathrm{T}} \sim 200\,\mathrm{GeV}$. The HEPTopTagger unclusters the fat–jet using an iterative mass–drop criterion, and simultaneously employs a filtering procedure [109] to identify three suitable hard jets reconstructing the original top, further testing them with top kinematics. It turns out, see e.g. refs. [101, 104], that the HEPTopTagger can have a relatively better performance: therefore, in our analysis we will adopt the HEPTopTagger to tag boosted top quarks in the considered signal events.

In particular, top tagging techniques are crucial not only to reduce the huge SM QCD and $t\bar{t}$ backgrounds, exploiting the particular kinematical feature of the boosted decay products, but also to avoid combinatorics in the reconstruction of the top four momentum from high multiplicity final state jets. In this way, fully–hadronic top decays with a larger branching ratio compared to leptonic final states, can be systematically exploited for searches involving top partners.

Models comprising top partners

All differences on the underlying top–partner model depend on the choice of the representation of the new quarks and on the assignment of the quantum numbers. We have already discussed the example of an $SU(2)$ singlet top partner within the LHT model, see section 3.3.2. Another relevant class of models predicting light spin–1/2 vector–like top partners is the class of minimal Composite Higgs Models [99, 113–119]. We will briefly discuss now for comparison some examples of top partners in the context of minimal Composite Higgs Models.

The main guiding principle of minimal Composite Higgs Models is the fact that the decays and single production of the new partners are generated via mixing with the standard quarks, induced by Yukawa interactions with the Higgs. Similarly to Little Higgs models, the Higgs is a pseudo–Goldstone boson associated to the breaking of a global symmetry due to a strongly interacting dynamics. In the minimal Composite Higgs scenario, the coset structure is $SO(5)/SO(4)$. In particular, only the right–handed top quark $t_{\rm R}$ is a fully composite state belonging to a complete multiplet (singlet) of the unbroken $SO(4)$ group, while the (elementary) left–handed doublet $q_{\rm L}$ is assumed to be coupled linearly to the strong sector, and embedded into an incomplete $SO(5)$ multiplet.

The possible vector–like top partners are introduced as composite bound states belonging to a complete multiplet Ψ of the unbroken group $SO(4)$: two cases are usually considered, namely $\Psi \sim \mathbf{4}$ or $\Psi \sim \mathbf{1}$ under $SO(4)$. We will refer to these two implementations as $\mathbf{M4_5}$ and $\mathbf{M1_5}$, respectively. In the $\mathbf{M4_5}$ case, the multiplet Ψ includes two charge–2/3 top partners $X_{2/3}$, T, one exotic charge–5/3 top partner $X_{5/3}$, and a charge–1/3 bottom partner B: under the SM group, the four components of Ψ decompose into two SM doublets (T, B) and ($X_{5/3}$, $X_{2/3}$) of hypercharge 1/6 and 7/6, respectively. In the $\mathbf{M1_5}$ case, only one $SU(2)$–singlet charge–2/3 top partner $\tilde{T}$ is introduced.

Assuming an embedding of the elementary doublet $q_{\rm L}$ into an incomplete fundamental representation $Q^{\mathbf{5}}_L \sim \mathbf{5}$ of $SO(5)$, the following interactions involving the top partners can be written down [99]:

$$\mathcal{L}^{\mathbf{M4_5}} \supset i\, c_1 \left(\bar{\Psi}_{\rm R}\right)_i \gamma^\mu d^i_\mu\, t_{\rm R} + y\, f \left(\bar{Q}^{\mathbf{5}}_{\rm L}\right)^I U_{I\,i}\, \Psi^i_{\rm R} + y\, c_2\, f \left(\bar{Q}^{\mathbf{5}}_{\rm L}\right)^I U_{I\,5}\, t_{\rm R} + \text{h.c.} \tag{5.2}$$

$$\mathcal{L}^{\mathbf{M1_5}} \supset y\, f \left(\bar{Q}^{\mathbf{5}}_{\rm L}\right)^I U_{I\,5}\, \Psi_{\rm R} + y\, c_2\, f \left(\bar{Q}^{\mathbf{5}}_{\rm L}\right)^I U_{I\,5}\, t_{\rm R} + \text{h.c.}\,, \tag{5.3}$$

where d_μ is the symbol defined in the CCWZ formalism as in section 2.1.1, U is the 5×5 Goldstone boson matrix, y is a Yukawa coupling controlling the mixing between the composite and elementary states, c_1, c_2 are $\mathcal{O}(1)$ parameters associated with the interactions of t_R, and f is the usual symmetry breaking scale of the strong sector. For the model $\mathbf{M1_5}$, a direct coupling of Ψ with t_R like the first term in eq. (5.2) can be removed with a field redefinition. Note that the operators proportional to y explicitly break the $SO(5)$ symmetry, since q_L is embedded into an incomplete $SO(5)$ multiplet, giving rise to the leading contribution to the Higgs potential triggering EWSB.

It turns out that the couplings of the top partners to the Goldstone bosons ($\phi^\pm$, ϕ^0), which in the high energy limit correspond to the longitudinal components of the gauge bosons (Equivalence Theorem), and to the Higgs h, are proportional to linear combinations of the couplings y, c [99]:

$$\mathbf{M4_5} : \begin{cases} \phi^+\, \bar{X}_{5/3\,\mathrm{L}}\, t_\mathrm{R} & : \ \sqrt{2}\, c_1\, g_\Psi \\ \left(h + i\phi^0\right) \bar{X}_{2/3\,\mathrm{L}}\, t_\mathrm{R} & : \ c_1\, g_\Psi \\ \left(h - i\phi^0\right) \bar{T}_\mathrm{L}\, t_\mathrm{R} & : \ -c_1\sqrt{y^2 + g_\Psi^2} + \dfrac{c_2\, y^2}{\sqrt{2}\sqrt{y^2 + g_\Psi^2}} \\ \phi^-\, \bar{B}_\mathrm{L}\, t_\mathrm{R} & : \ c_1\sqrt{2}\sqrt{y^2 + g_\Psi^2} - \dfrac{c_2\, y^2}{\sqrt{y^2 + g_\Psi^2}} \end{cases} \tag{5.4}$$

$$\mathbf{M1_5} : \begin{cases} \left(h + i\phi^0\right) \bar{\tilde{T}}_\mathrm{R}\, t_\mathrm{L} & : \ \dfrac{y}{\sqrt{2}} \\ \phi^+ \bar{\tilde{T}}_\mathrm{R}\, b_\mathrm{L} & : \ y\,, \end{cases} \tag{5.5}$$

where $g_\Psi = M_\Psi/f$, M_Ψ being the Dirac mass of the top partner multiplet.

These couplings govern the associated production of the different top partners. In particular we see that the $SU(2)$–singlet top partner $\tilde{T}$ can be copiously produced in association with a b–quark: from eq. (5.5), its coupling to the W boson is given by

$$\left(\frac{m_\mathrm{W}}{M_{\tilde{\mathrm{T}}}}\right) \cdot \mathrm{coeff}(\phi^+\, \bar{\tilde{T}}_\mathrm{R}\, b_\mathrm{L}) = \left(\frac{m_\mathrm{W}}{M_{\tilde{\mathrm{T}}}}\right) y \equiv \frac{g\, g^*}{\sqrt{2}}\,, \tag{5.6}$$

with y of order $\mathcal{O}(1)$ to reproduce the SM top mass.

Furthermore, we can easily read off from eq. (5.4) and (5.5) the different branching ratios of all top partners. For example, in the decoupling limit of $m_\Psi \to \infty$, the branching ratios of the $\mathbf{M1_5}$ $SU(2)$ singlet top partner $\tilde{T}$ are

$$\begin{aligned} BR(\tilde{T} \to W\, b) &\sim 0.5\,, \\ BR(\tilde{T} \to Z\, t) &\sim 0.25\,, \\ BR(\tilde{T} \to h\, t) &\sim 0.25\,. \end{aligned} \tag{5.7}$$

while the branching ratios of the charge–2/3 top partners of $\mathbf{M4_5}$ are given by

$$\begin{aligned} BR(X_{2/3} \to Z\,t) \sim BR(T \to Z\,t) \sim 0.5\,, \\ BR(X_{2/3} \to h\,t) \sim BR(T \to h\,t) \sim 0.5\,. \end{aligned} \tag{5.8}$$

We can now compare these results with the $SU(2)$–singlet top–partner T_+ arising in the LHT model. In particular, the EW coupling to the W boson which governs the associated production of T_+ with a b–quark, is given by [40]

$$\text{coeff}\left(W^+ \bar{T}_{+\,\mathrm{R}}\, b_{\mathrm{L}}\right) = \frac{g}{\sqrt{2}} \frac{R^2}{1+R^2} \frac{v}{f} + \mathcal{O}\left(\frac{v^2}{f^2}\right) \equiv \frac{g\,g^*}{\sqrt{2}}\,, \tag{5.9}$$

expressed in the same form as eq. (5.6). The T_+ decay branching ratios are given in table 4.7 for two benchmark scenarios: in particular, it shares the 2:1:1 ratio for the decays into SM particles as in eq. (5.7), but allows for a further decay channel involving the T–odd partner T_- and the heavy photon A_{H} with a non–negligible rate.

It is then clear that charge–2/3 vector–like top partners share similar final state topologies, with different branching ratios and single production couplings depending on the particular underlying model. However, when looking for possible dedicated searches for top partners at the LHC, it is important to look for mostly model independent searches, involving for example only the mass of the top partner and its “single production” coupling as free parameters.

Model independent parametrisation

Recently, a generic parametrisation of an effective Lagrangian for top partners has been proposed in [100], where the authors considered vector–like quarks embedded in different representations of the weak $SU(2)$ group, with other minimal assumptions regarding the structure of the couplings. In particular, vector–like quarks which can mix and decay directly into SM quarks of all generations are included. Particularly interesting for our purposes is the case in which the top partner is an $SU(2)$ singlet, with couplings only to the third generation of SM quarks. The Lagrangian parametrising the possible top partner interactions reads [100]

$$\mathcal{L}_{\mathrm{T}} \supset \frac{g^*}{\sqrt{2}} \left[\frac{g}{\sqrt{2}} \bar{T}_{\mathrm{L}}\, W^+_\mu \gamma^\mu\, b_{\mathrm{L}} + \frac{g}{2c_{\mathrm{W}}} \bar{T}_{\mathrm{L}}\, Z_\mu \gamma^\mu\, t_{\mathrm{L}} - \frac{M_{\mathrm{T}}}{v} \bar{T}_{\mathrm{R}}\, h\, t_{\mathrm{L}} - \frac{m_t}{v} \bar{T}_{\mathrm{L}}\, h\, t_{\mathrm{R}} \right] + \text{h.c.}\,, \tag{5.10}$$

where M_{T} is the top partner mass, and g^* parametrises the single production coupling in association with a b– or a top–quark. In the limit of $M_{\mathrm{T}} \gg m_t$, we have calculated the width of the top partner to be

$$\Gamma_{\rm T} \simeq \frac{(g\,g^*)^2\, M_{\rm T}^3}{64\,\pi\, m_{\rm W}^2} \left(1 + \frac{1}{2} + \frac{1}{2}\right) , \qquad (5.11)$$

where the three contributions in parentheses arise from the top partner decays to W, Z and Higgs, respectively. The different branching ratios are clearly the same as in eq. (5.7), since we are describing effectively the same type of top partner as in $\mathbf{M1_5}$.

For our proposed top partner search at the LHC we will exploit a simplified–model approach, assuming the interactions described by the Lagrangian of eq. (5.10), where the only free parameters will be the top partner mass $M_{\rm T}$ and its "single production" coupling g^*. In this way, our results will be straightforwardly mapped within the context of the $\mathbf{M1_5}$ minimal Composite Higgs Model, namely by identifying as in eq. (5.6)

$$y = \frac{g\,g^*}{\sqrt{2}}\,\frac{M_{\tilde{\rm T}}}{m_{\rm W}} \qquad (\mathbf{M1_5})\,. \qquad (5.12)$$

For comparison, with $y = 1$ and $M_{\tilde{\rm T}} = 1\,$TeV one obtains $g^* \sim 0.17$.

On the other hand, while an immediate map of g^* to the LHT parameters is straightforward from eq. (5.9), namely with

$$g^* = \sqrt{2}\,\frac{R^2}{1+R^2}\,\frac{v}{f} + \mathcal{O}\left(\frac{v^2}{f^2}\right) \qquad ({\rm LHT})\,, \qquad (5.13)$$

the Lagrangian of eq. (5.10) does not exactly reproduce the T_+ phenomenology because of the absence of the $T_+ \to T_-\, A_{\rm H}$ vertex. In particular, it should be remembered that the different branching ratios of the top partner described by eq. (5.10) slightly overestimate the actual branching ratios of the LHT T_+ partner. For comparison, fixing $R = 1.0$ and $f = 1\,$TeV yields $g^* \sim 0.17$.

On the other hand, we underestimate the branching ratios of the charge–2/3 top partners within the $\mathbf{M4_5}$ model, as in eq. (5.8): our results will be conservative in this case.

Overview over top partner searches

Many different theoretical analyses involving top partners have been recently proposed, some of them exploiting tagging techniques [99,101,102,120–132]. In particular:

- in ref. [102] the authors proposed a $\sqrt{s} = 8\,$TeV analysis for the $\mathbf{M1_5}$ top partner in the $T \to W\,b$ channel, focusing on the single production process and requiring exactly one isolated lepton in the final state.

- in ref. [120] the authors investigated both decay channels $T \to h\,t$ and $T \to W\,b$ of the **M1$_5$** top partner for a possible analysis at $\sqrt{s} = 8\,\mathrm{TeV}$. In particular, they designed an analysis for single production of the top quark, further requiring exactly one lepton in final state.

- in ref. [121] the author developed a search strategy for the **M1$_5$** top partner, focusing on its single production in association with a b–quark, and further decay $T \to h\,t$, with leptonic decay of the SM top. Both center–of–mass energies $\sqrt{s} = 8$, $14\,\mathrm{TeV}$ have been considered.

- in ref. [122] the authors investigated the discovery potential of searches for all–hadronic $T \to h\,t$ final states at $\sqrt{s} = 14\,\mathrm{TeV}$, with $\mathrm{BR}(h\,t) = 1.0$, making use of particular top–tagging (HEPTopTagger) and Higgs–tagging techniques. The same final state has been investigated in ref. [123] for a possible $\sqrt{s} = 8\,\mathrm{TeV}$ analysis.

- in ref. [99] different search strategies are discussed in the context of both **M1$_5$** and **M4$_5$** models. In particular, analyses for $B \to W\,t$, $T \to W\,b$ and $T \to Z\,t$ are presented with $\sqrt{s} = 8\,\mathrm{TeV}$. The $T \to Z\,t$ search is performed in the tri–lepton channel, without including top–tagging techniques.

- in ref. [124] the authors presented a dedicated analysis which can be sensitive to final states which are obtained by different top partner decays in the context of minimal Composite Higgs Models. In particular, exactly one single lepton, b–tagging and “top–veto” requirements are exploited, together with other optimised kinematic cuts, to improve the sensitivity of top partner searches at $\sqrt{s} = 8$, $14\,\mathrm{TeV}$. No top–tagging algorithms have been included in the analysis.

- in ref. [125] a systematic discussion of multi–lepton final states is presented, with final states accessible through many different production and decay channels involving top partners in the context of minimal Composite Higgs Models. The outcome is that single lepton final states provide the best discovery potential. No tagging techniques have been exploited.

- in ref. [126] the authors investigate pair and single production of the $X_{5/3}$ and B partners of the **M4$_5$** model, exploiting top–tagging (HEPTopTagger) and W–tagging in a single lepton plus jets final state.

- in refs. [127, 128] the authors scrutinised the particular same–sign lepton final state from the $X_{5/3}$ and B decays within the $\mathbf{M4_5}$ model, considering both pair and associated production. Mass reconstruction and observables to distinguish the nature of the decaying partner are thoroughly presented.

- in ref. [101] the authors developed a search strategy for a bottom partner, optimised for its pair production at $\sqrt{s} = 14\,\text{TeV}$ in the all–hadronic $B \to W\,t$ channel, with $\text{BR}(W\,t) = 1.0$. Top– and W–tagging techniques have been included.

- in ref. [129] the authors presented a search strategy for a top partner decay to a charged Higgs boson and a bottom quark, focusing on the case where the charged Higgs decays to third–generation quarks to yield a multi–b final state. This analysis is motivated e.g. by different Little Higgs scenarios featuring extended Higgs sectors.

From this we see that the top partner decay $T \to Z\,t$ has not been thoroughly explored yet, because it appears rather difficult at first glance. In particular, the all–hadronic final state suffers from huge SM backgrounds, making the alternative $T \to W\,b$ channel more suited for all–hadronic analyses due to the enhanced branching ratio and the possibility to exploit b–tagging. Furthermore, the channel involving a leptonic decay of the Z entails a large suppression from the Z leptonic branching ratio, namely $\text{BR}(Z \to \ell^+\ell^-) \sim 0.067$ ($\ell \equiv e,\, \mu$).

In order to test the nature of the top partner, it is important to develop search strategies which might cover all possible channels, especially for the foreseen LHC energy upgrade to 13 TeV. For this reason, we developed a search strategy tailored for a charge–2/3 top partner optimised for its decay channel $T \to t\,Z \to (q\,q'\,b)\,(\ell^+\ell^-)$, at the LHC with center–of–mass energy of $\sqrt{s} = 13\,\text{TeV}$ and integrated luminosity of $300\,\text{fb}^{-1}$. Our aim is to develop, with minimal assumptions on the underlying model as explained before, a method to discover a possible top partner signature with large statistical significance, together with a precise measurement of its invariant mass.

It is to be noted that a recent ATLAS analysis [103] presented a $\sqrt{s} = 8\,\text{TeV}$ search optimised for either pair or single production of a top partner, subsequently decaying as $T \to Z\,t$ with leptonic decay of the Z boson. This encouraged us to further analyse this rather unexplored process, in order to provide an effective search strategy for the forthcoming 13 TeV LHC runs.

5.1.2 Setup of the analysis

Event generation

As mentioned in section 5.1.1, we investigate processes involving a charge–2/3 vector–like top partner T, inclusively pair and associated produced, with subsequent decay

$$T \to t\, Z \to \left(q\, q'\, b\right)\, \left(\ell^+ \ell^-\right)\, . \tag{5.14}$$

The single production process is depicted in figure 5.1 together with our conditions on the cones of the boosted objects to be defined below.

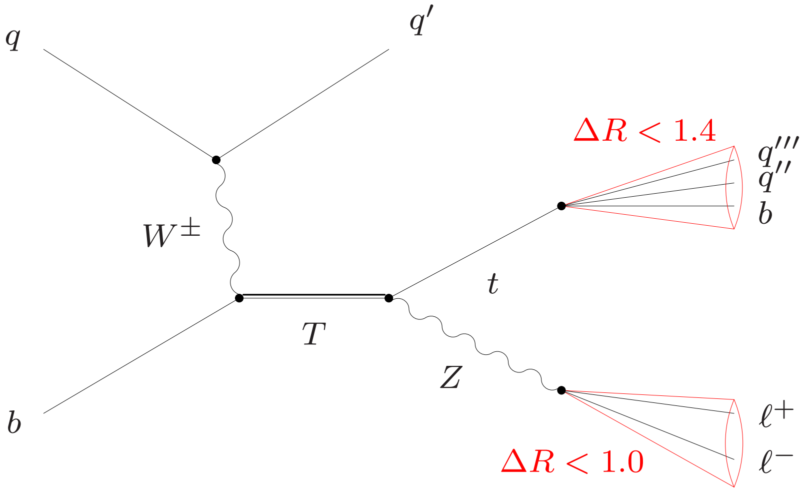

Figure 5.1: *Single production of a heavy top partner T with subsequent decay into tZ. The boosted decay products of the latter are collected inside cones of $\Delta R < 1.4$ and $\Delta R < 1.0$, respectively.*

We study a possible search strategy optimised for the LHC with center–of–mass energy of $\sqrt{s} = 13\,\text{TeV}$ and integrated luminosity of $300\,\text{fb}^{-1}$. The clean final state and the absence of missing transverse energy makes this channel promising for a possible mass reconstruction of the top partner, even if the possible SM backgrounds are rather huge.

Signal and background events have been simulated using MadGraph5_aMC@NLO v2.1 (MG5_aMC) [133] interfaced with Pythia 8.183 [134] for parton–shower and fragmentation, and further analysed via Delphes 3.1 [86] for a fast detector simulation following the specifications which we are going to detail in the following. In particular, an anti–k_t jet clustering algorithm with radius parameter of $R = 0.4$ is used to reconstruct jets, which in the following we will call *slim jets*. The same Pythia output is simultaneously analysed through FastJet 3.0.6 [135, 136] in order to cluster the hadronic activity using the Cambridge–Aachen algorithm with larger radius parameter of $R = 1.5$, reconstructing jets which in the following we will identify as *fat jets*.

The model file generating signal events according to the Lagrangian of eq. (5.10) [100], can be found in the dedicated FeynRules model database webpage ("Singlet T Model VLQ") [79, 80]. The corresponding free parameters are the top partner mass $M_{\rm T}$, the coupling g^* which governs the top partner EW single production involving a t–channel W, and the rate $R_{\rm L}$ of T decays into light quarks. We fix $R_{\rm L} = 0$ in order to force T to decay only to third generation SM quarks. For our analysis we consider values in the range

$$M_{\rm T} \in [850, 1450] \text{ GeV}\,, \qquad g^* \in [0.05, 0.5]\ . \tag{5.15}$$

In particular, our signal processes consist of pair and associated production of a charge–2/3 vector–like top partner T, with subsequent decay as in eq. (5.14): in the case of pair production we consider the inclusive decay of the second top partner according to the branching ratios reported in eq. (5.7). The LO signal cross section is calculated via MG5_aMC, depending on the particular choice of the free parameters which were consistently updated, together with the top partner width, before the event generation. We further rescale the signal cross section with a K–factor which we evaluate using Hathor 2.0 [137, 138]. In particular, we calculate the K–factors for both top pair (NNLO) and single productions (NLO) for different values of the top mass in the range (5.15), eventually choosing a minimal and conservative value of $K = 1.14$.

The main SM background processes turn out to be $Z +$ jets, associated Z production with a pair of top quarks ($t\bar{t}Z +$ jets), plus subleading contributions from associated Z production with single top ($t/\bar{t}\,Z +$ jets). All other potentially dangerous contributions like $t\bar{t} +$ jets, $t\bar{t}W^{\pm} +$ jets and $\gamma^* \to \ell^+\ell^- +$ jets turn out to be negligible by requiring exactly two opposite charge and same flavour leptons in the final state with invariant mass satisfying $|m_{\ell^+\ell^-} - m_{\rm Z}| < 10\,\text{GeV}$. Furthermore, the large $W^{\pm}Z+$ jets background becomes also negligible due to the smaller boost of the Z boson compared to the signal and the backgrounds involving the top quark, and by exploiting b- and top-tagging.

Large samples of background events are generated using MG5_aMC, requiring up to three, two or one additional hard jets at matrix element level for $Z +$ jets, $t/\bar{t}\,Z +$ jets and $t\bar{t}Z +$ jets processes, respectively. To avoid double counting of jets generated at matrix element level and jets radiated during the parton showering process, a CKKW–L merging procedure [139–141] is exploited. In particular, we interface, for each background sample, the corresponding parton level MG5_aMC outputs with different multiplicities of additional jets to Pythia 8.183 and its internally built–in routines for the CKKW–L merging, accordingly setting the merging scale value and the number of additional jets available from matrix element. This procedure guarantees a correct prediction for the (merged) cross section of the desired process.

bkg. process	K–factor	Ref.
Z + jets	1.20	[142]
$t\bar{t}\,Z$ + jets	1.30	[143]
$t\,Z$ + jets	1.11	[144]
$\bar{t}\,Z$ + jets	1.09	[144]

Table 5.1: *K–factors of the leading SM background processes for our analysis.*

We rescale the evaluated background cross sections with appropriate K–factors, summarising the values in table 5.1. It should be noted that the inclusive $t\bar{t}\,Z$+ jets K–factor as given in [143] is $K = 1.39$: however, this value is reduced for large top transverse momenta, as in our case. For this reason we conservatively set $K = 1.30$ as in table 5.1.

Reconstruction of physics objects

Final state objects reconstruction is performed mainly following the specifications detailed in [145]. An electron candidate is required to have a transverse momentum $p_{\mathrm{T}}^{e} \geq 20\,\mathrm{GeV}$ and $|\eta^{e}| < 2.47$. An isolation requirement is further applied, namely the total p_{T} of all charged particles q satisfying $p_{\mathrm{T}}^{q} > 1.0\,\mathrm{GeV}$ and $\Delta R(e, q) < 0.3$, should be less than 10% of p_{T}^{e}. A muon candidate is required to satisfy $p_{\mathrm{T}}^{\mu} \geq 10\,\mathrm{GeV}$ and $|\eta^{\mu}| < 2.5$. The isolation for the muon requires that the total p_{T} of all charged particles q satisfying $p_{\mathrm{T}}^{q} > 1.0\,\mathrm{GeV}$ and $\Delta R(\mu, q) < 0.4$, should be less than 6% of p_{T}^{μ}.

As mentioned before, slim jets are clustered from all final state particles with $|\eta| < 4.9$, except isolated leptons and neutrinos, using the anti–k_t algorithm with a radius parameter of $R = 0.4$ as implemented in Delphes 3.1. Only slim jets with $p_{\mathrm{T}}^{j} \geq 20\,\mathrm{GeV}$ are further considered. Slim jets are possibly identified as b–jets through the built–in Delphes 3.1 dedicated routines: in particular, we set the probability to tag b–jets (b–tag efficiency) to 70%, together with a charm quark misidentification probability of 10%. Tagged b–jets are further required to be reconstructed within $|\eta^{b}| < 2.5$.

Fat jets are clustered using FastJet 3.0.6 on the same final state particles with $|\eta| < 4.9$, except isolated leptons and neutrinos, using the Cambridge–Aachen algorithm with radius parameter of $R = 1.5$. Only fat jets with $p_{\mathrm{T}}^{j} \geq 20\,\mathrm{GeV}$ are further considered.

Cutflow

Events are required to contain in the final state at least two leptons with minimum transverse momentum $p_{\mathrm{T}}^{\ell} > 25\,\mathrm{GeV}$. Among all possible pairs of leptons, we require at least one pair to consist of opposite charge and same flavour leptons matching the invariant mass of the Z boson, namely such that the lepton–pair invariant mass $m_{\ell^+\ell^-}$ satisfies

$$|m_{\ell^+\ell^-} - m_{\mathrm{Z}}| < 10\,\mathrm{GeV}\,. \tag{5.16}$$

We further require that for at least one pair, the separation $\Delta R = \sqrt{\Delta\phi^2 + \Delta\eta^2}$ between the two candidate leptons reconstructing the Z mass should satisfy

$$\Delta R(\ell^+, \ell^-) < \Delta R(\ell^+, \ell^-)_{\max} = 1.0\,. \tag{5.17}$$

If more than one pair of leptons satisfies the previous requirements, we select the pair with invariant mass closest to the Z boson mass. This pair of leptons allows us to fully reconstruct the four–momentum of the candidate Z boson.

The cut of eq. (5.17) is particularly effective to suppress SM backgrounds containing a Z boson, since it captures the expected boosted kinematics of the Z boson from the top partner decay. According to eq. (5.1), we expect indeed highly collimated decay products from a boosted Z. On the other hand, SM processes do not provide a large transverse boost to the Z boson, guaranteeing a good discrimination power to eq. (5.17).

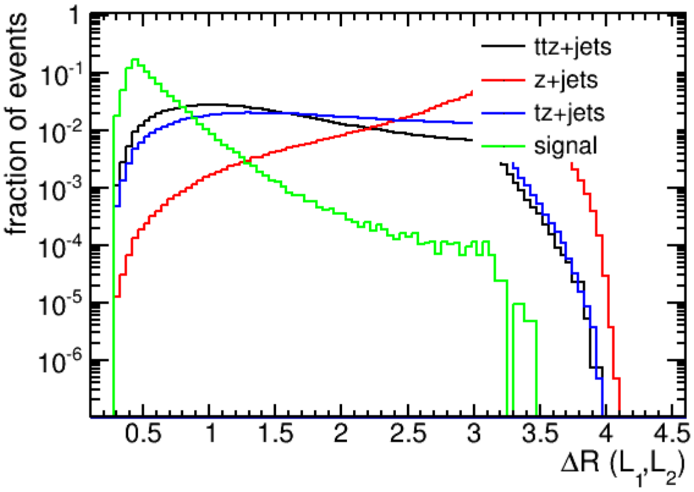

Figure 5.2: *Distribution of the ΔR variable evaluated among candidate leptons reconstructing the Z boson for different processes. The signal process assumes $M_T = 1$ TeV and $g^* = 0.1$.*

We show in figure 5.2 the distribution of the variable ΔR evaluated among candidate leptons reconstructing the Z boson, for the different background and signal processes: a peak at smaller values of ΔR is clearly visible for signal events. Note that the signal events used for all distribution plots shown in this section correspond to the benchmark point $M_{\rm T} = 1\,\rm TeV$ and $g^* = 0.1$.

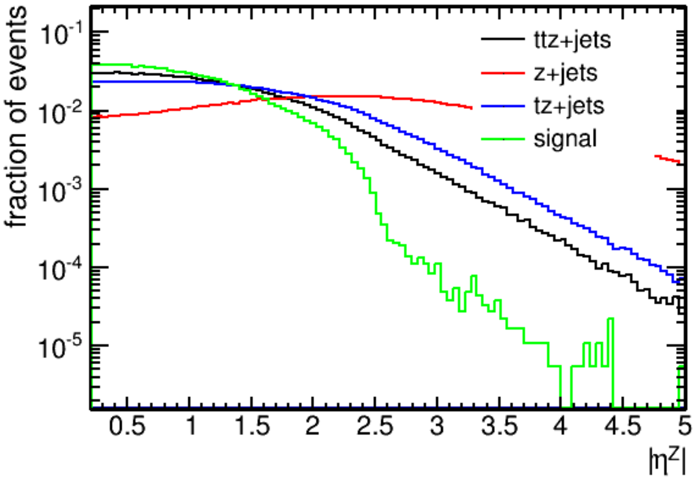

Figure 5.3: *Distribution of the psudorapidity $|\eta^Z|$ of the reconstructed candidate Z boson for different processes. The signal process assumes $M_T = 1$ TeV and $g^* = 0.1$.*

Further kinematic constraints are imposed on the candidate Z boson, again to exploit the boosted properties of the considered signal. In particular, we require a large transverse momentum of the candidate Z, namely

$$p_{\rm T}^{\rm Z} > p_{\rm T,\,min}^{\rm Z} = 225\,\rm GeV\,, \tag{5.18}$$

as well as requiring that the Z should be produced in the central region of the detector:

$$|\eta^{\rm Z}| < |\eta^{\rm Z}|_{\rm max} = 2.3\,. \tag{5.19}$$

The requirement of eq. (5.19) is useful in rejecting e.g. the SM $Z+$ jets background, the latter being mostly produced via a Drell–Yan process with the initial quarks yielding a forward boost to the produced Z boson, as can be seen in figure 5.3.

In figure 5.4 we show the distribution of the transverse momentum of reconstructed Z boson candidates as described in the text. Larger transverse momenta are observed for the (boosted) Z from the signal process.

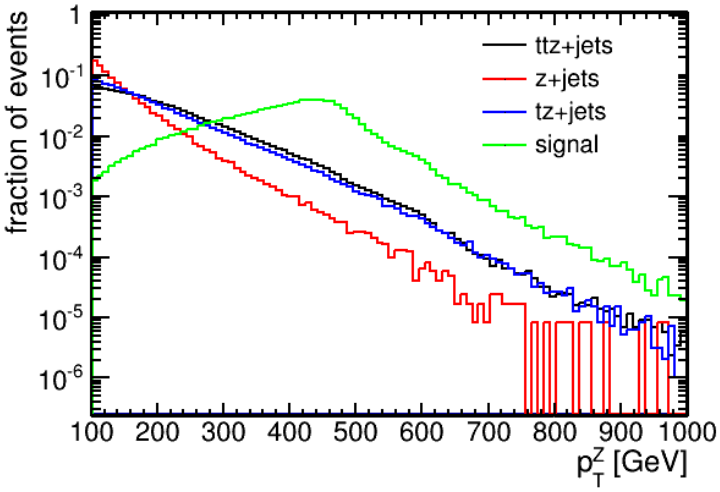

Figure 5.4: *Distribution of the transverse momentum p_T^Z of the reconstructed candidate Z boson for different processes. The signal process assumes $M_T = 1$ TeV and $g^* = 0.1$.*

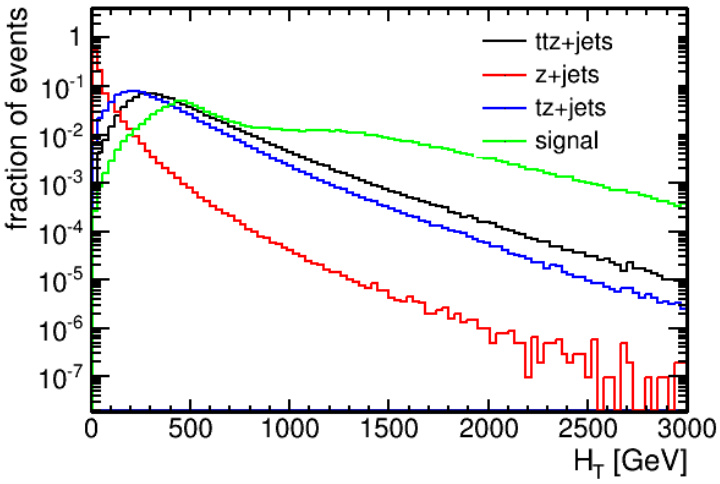

Figure 5.5: *Distribution of the scalar sum of the transverse momenta H_T of the clustered* slim jets *for different processes. The signal process assumes $M_T = 1$ TeV and $g^* = 0.1$.*

In the next step, the hadronic activity is considered for additional selection cuts. In order to account for the large boost of the top quark, we expect the final state jets to possess a large amount of transverse momentum. Therefore, we evaluate the H_T variable, namely the scalar sum of the transverse momenta of the reconstructed slim jets with $p_\mathrm{T}^j > 30\,\mathrm{GeV}$

and within $|\eta^j| < 3.0$, requiring each event to satisfy

$$H_{\rm T} > H_{\rm T,\,min} = 400\,{\rm GeV}\,. \tag{5.20}$$

In figure 5.5 we show the $H_{\rm T}$ distribution for the different considered processes. The signal distribution has a considerable tail for larger values of $H_{\rm T}$ compared to background events, confirming the good discrimination power of eq. (5.20). It is also worth noticing that the $H_{\rm T}$ distribution for the signal in figure 5.5 displays two different visible peaks, at $\mathcal{O}(500\,{\rm GeV})$ and at $\mathcal{O}(1.3\,{\rm TeV})$: these correspond to the top partner single and pair production components of the signal, respectively.

Among the reconstructed final state slim jets, we further require the presence of at least one tagged b–jet with

$$p_{\rm T}^b > p_{\rm T,\,min}^b = 40\,{\rm GeV}\,. \tag{5.21}$$

We then turn our attention to the reconstructed fat jets in the final state: our aim is to identify one reconstructed fat jet as our top candidate. At least one fat jet is required to be reconstructed among final state particles, satisfying the definition of fat jets given before, and with an additional requirement on its transverse momentum being

$$p_{\rm T}^J > p_{\rm T,\,min}^J = 200\,{\rm GeV}\,. \tag{5.22}$$

Most importantly, we require at least one fat jet to be HEPTop–tagged: the presence of a boosted SM top from the decay of a heavier resonance is indeed one of the main features of the signal. As mentioned in section 5.1.1, top tagging is crucial not only as a discriminant against SM backgrounds, but also to effectively deal with the combinatorics in the top reconstruction from high multiplicity final state jets. If more than one fat jet is identified as a (boosted) top jet via the HEPTopTagger algorithm, we identify our candidate top as the fat jet mostly back–to–back with respect to the previously reconstructed candidate Z direction, as we would expect from the signal topology.

To account for its boosted kinematics, we require that the transverse momentum of the candidate top should satisfy the cut

$$p_{\rm T}^t > p_{\rm T,\,min}^t = 250\,{\rm GeV}\,. \tag{5.23}$$

The $p_{\rm T}^t$ distribution of signal and background processes, after applying the cut of eq. (5.23), is shown in figure 5.6: a large fraction of signal events is observed for higher values of $p_{\rm T}^t$.

Finally, to ensure that at least one of the tagged b–jets is originating from the candidate top, and not from additional radiation or as decay product of another involved particle,

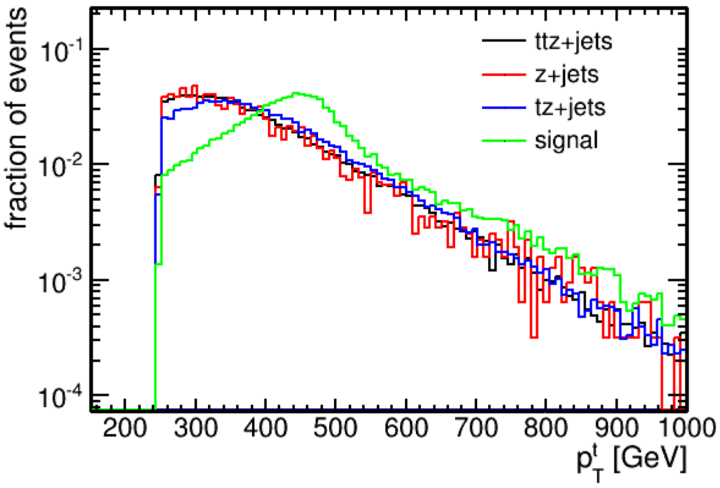

Figure 5.6: *Distribution of the transverse momentum p_T^t of the reconstructed candidate top for different processes. The signal process assumes $M_T = 1$ TeV and $g^* = 0.1$.*

we require that the spatial separation between the candidate top and at least one of the slim jets tagged as b–jet should satisfy

$$\Delta R(t, b) < \Delta R(t, b)_{\max} = 0.8\,. \tag{5.24}$$

In other words, this cut ensures that at least one (slim) b–jet lies within the decay–cone of the candidate (fat jet) top.

To summarise the applied cuts, in table 5.2 we categorise them according to the reconstructed object on which they are applied. It should be noted that the actual values of $\Delta R(\ell^+, \ell^-)_{\max}$, $p^{\mathrm{Z}}_{\mathrm{T,\,min}}$, $|\eta^{\mathrm{Z}}|_{\max}$, $H_{\mathrm{T,\,min}}$, $p^{b}_{\mathrm{T,\,min}}$ are identified using an optimisation procedure similar as the one described in section 4.3.3: in particular, we scan the aforementioned cut values within appropriate ranges and evaluate the corresponding signal and background efficiencies for each possible configuration, obtaining a signal over background (S/B) map as a function of the cut values. We then identify the optimal cut configuration yielding the highest S/B ratio, assuming $M_{\mathrm{T}} = 1$ TeV and $g^* = 0.1$ for the signal, and making sure that the total number of events after applying the cuts would remain reasonably large for $300\,\mathrm{fb}^{-1}$ of integrated luminosity.

	selection cuts
reconstructed Z	$n_{\ell^+\ell^-} \geq 1$ $\lvert m_{\ell^+\ell^-} - m_{\mathrm{Z}} \rvert < 10\,\mathrm{GeV}$ $\Delta R(\ell^+, \ell^-) < 1.0$ $p_{\mathrm{T}}^{\mathrm{Z}} > 225\,\mathrm{GeV}$ $\lvert \eta^{\mathrm{Z}} \rvert < 2.3$
slim jets	$H_{\mathrm{T}} > 400\,\mathrm{GeV}$ $n_b \geq 1$, $p_{\mathrm{T}}^b > 40\,\mathrm{GeV}$
fat jets	$n_J \geq 1$, $p_{\mathrm{T}}^J > 200\,\mathrm{GeV}$ HEPTop $n_t \geq 1$ $p_{\mathrm{T}}^t > 250\,\mathrm{GeV}$ $\Delta R(t, b) < 0.8$

Table 5.2: *Summary of the selection cuts of the proposed analysis, sorted per type of reconstructed object on which the cut is applied.*

5.1.3 Results

The procedure detailed in section 5.1.2 has a double benefit, namely largely improving the S/B ratio from one side, and uniquely determining the four momenta of the reconstructed top and Z boson candidates satisfying the possible kinematics of a top partner decay.

We finally plot the distribution of the invariant mass of the $(t$–$Z)$ system, which we expect to peak at the invariant mass of the on–shell top partner for the signal process, while described by a smoothly descending distribution for the different backgrounds, since the reconstructed top and Z in the latter events do not originate from an on–shell decay.

We show the result in figure 5.7, where we rescale the different distributions with the visible cross section of the corresponding processes, times an assumed integrated luminosity of $300\,\mathrm{fb}^{-1}$. The different contributions are stacked in the plot. In this way, figure 5.7 shows a realistic amount of events which could be observed at the LHC with $\sqrt{s} = 13\,\mathrm{TeV}$ and $300\,\mathrm{fb}^{-1}$ of integrated luminosity. For the signal we fixed $M_{\mathrm{T}} = 1\,\mathrm{TeV}$ and $g^* = 0.1$.

A peak in the bins around $M_{\mathrm{T}} = 1\,\mathrm{TeV}$, fixing the bin width to $50\,\mathrm{GeV}$, is clearly visible above the background distribution, with up to 25 total events in the most significant bin. The result of the analysis is therefore encouraging, and we support the experimental

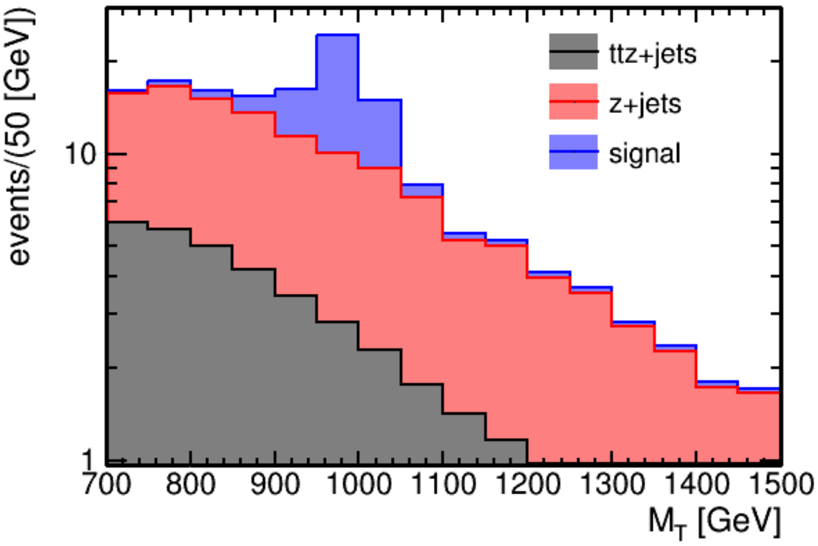

Figure 5.7: *Stacked distribution plot of the invariant mass* M_T *of the reconstructed top partner for different processes. All distributions have been rescaled with the visible cross section of the corresponding processes, times an integrated luminosity of* $300\,fb^{-1}$*. The signal process assumes* $M_T = 1$ *TeV and* $g^* = 0.1$*. Other possible SM background processes are not shown in the plot since their contribution turned out to be negligible.*

collaborations to further analyse the discussed channel: clearly, in a real experimental search the background estimation would be more robust and precise, e.g. via the inclusion of reconstructed fake leptons.

It is very important to estimate the significance of the signal peak above the SM background, in order to consistently claim the evidence for or the discovery of a top partner signal. In particular, the hypothesis testing procedure is carried out using the public BumpHunter code [146]. This code operates on datasets that are binned in some a–priori fixed set of bins: in our case, the input datasets correspond to the total number of signal+background and background–only events observed in M_T–bins of 50 GeV as in figure 5.7. The BumpHunter scans the input–given data using a window of varying width, and identifies the window with biggest excess compared to the background: the dedicated test statistic is indeed designed to be sensitive to local excesses of data[1].

---

[1] We setup the code to look for bumps in up to three consecutive bins, namely the possible mass resolution is at worst ± 75 GeV around the central value.

The same scanning procedure is further applied to pseudo–data sampled from the expectation of the background input[2], in order to reconstruct the “expected” distribution of the test statistic. The p–value of the test is calculated, being the probability that the test statistic will be equal to, or greater than the test statistic obtained by comparing the actual data to the background hypothesis. In other words, the p–value might be interpreted as a false–discovery probability. When the distribution of the test statistic is estimated using pseudo–experiments, as in our case, then the p–value is calculated as a binomial success probability.

An equivalent formulation in terms of Gaussian significance is straightforwardly obtained: it is common to claim that *evidence* for a new signal beyond the SM background is observed if the p–value of the peak corresponds to at least 3.0σ of Gaussian significance, while it is common to claim a *discovery* if the p–value corresponds to at least 5.0σ of Gaussian significance.

By running the BumpHunter on the datasets summarised in figure 5.7, the most significant peak is observed in the $[900, 1050]$ GeV range, with an equivalent Gaussian significance of $2.6^{+1.0}_{-0.9}\,\sigma$. The uncertainties on the Gaussian significance of the peak are estimated by applying a 20% uncertainty on both the signal and background event yields, which might account for up to 30% possible further non-statistical uncertainties which we have not taken into account.

Different hypotheses on the underlying BSM signal would alter the shape of the signal distribution of figure 5.7. However, we expect that our analysis, although being optimised for the signal values $M_{\mathrm{T}} = 1\,\mathrm{TeV}$ and $g^* = 0.1$, should still display a peak in the M_{T} distribution even for different choices of the free parameters. In particular, a higher statistical significance of the peak might be achieved for different signal hypotheses. For this reason, we generate a grid of signal points for $M_{\mathrm{T}} \in [850, 1450]\,\mathrm{GeV}$ in steps of $150\,\mathrm{GeV}$, and for $g^* \in [0.05, 0.5]$ in steps of 0.05, and for each combination we evaluate the corresponding significance of the peak, if observed.

Our results are displayed in figure 5.8, where regions of possible *evidence* (3.0σ) or *discovery* (5.0σ) of a top partner signal above the SM background are identified, assuming

---

[2] In our case, we choose to model the background expectation by a Poisson distribution with the mean value distributed according to a Gamma distribution. The latter Gamma distribution is defined by fixing its mean value to the actual background bin value, and variance to the squared background bin error, as suggested in the BumpHunter manual. A total number of 10^8 pseudo–experiments is generated accordingly.

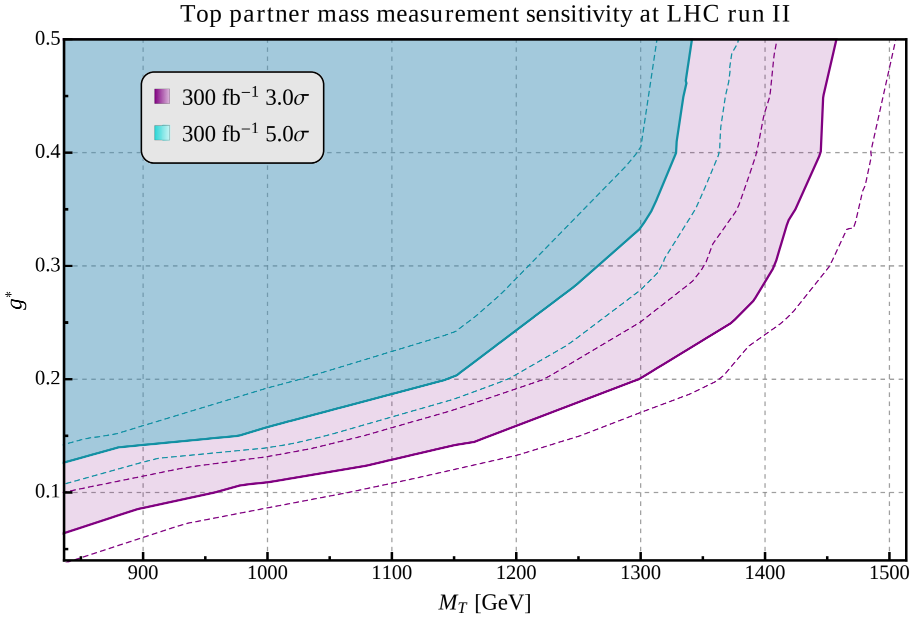

Figure 5.8: *Parameter space regions of possible* evidence *(3.0σ) or* discovery *(5.0σ) of a top partner signal above the SM background, assuming the described analysis at the LHC with $\sqrt{s} = 13\,TeV$ and $300\,fb^{-1}$ of integrated luminosity. Also shown are bands representing the effect of a possible further non-statistical 30% uncertainty on the visible cross section of the involved processes. If a signal peak is observed above the SM background, a possible mass measurement of the top partner invariant mass M_T is possible with a mass resolution of at worst $\pm 75\,GeV$ around the central value.*

a dedicated LHC analysis as discussed in the text. Also shown are bands representing the effect of a possible total 30% uncertainty as discussed before. We observe that a large fraction of the considered parameter space might be probed using our proposed analysis; in particular, the top partner mass might be measured via the described BumpHunter procedure, with a mass resolution in our setup of at worst $\pm 75\,$GeV around the central value. The mass resolution might also be improved in a dedicated experimental setup.

5.2 Mass determination of semi–invisibly decaying particles

In the previous section, we developed a mass determination method focusing on a possible final state without a large fraction of missing transverse momentum. The possibility of fully reconstructing the four–momenta of the final state particles allowed us to reconstruct the invariant masses of the intermediate on–shell particles, among which the top partner with a–priori unknown mass.

In the context of top partner searches, a big effort was also dedicated to analyse top partner channels yielding missing transverse momentum in the final state. The missing transverse momentum is measured as imbalance in the total transverse momentum of an event: all transverse momenta of the final state particles should indeed sum up to zero ideally, namely in the limit of perfect detector resolution, since the incoming initial state partons possess only a longitudinal momentum component in very good approximation.

Sources of missing transverse momentum are particles which are not detected within the different components of the detector, such that no measurement of their four–momenta is possible: for this reason one usually refers to them as the "invisible" final state particles. It is to be noted that if more than one invisible particle is present in the final state, the individual transverse momenta are in principle indistinguishable, since the missing transverse momentum corresponds only to the vector sum of their transverse momenta. An example of invisible particles are the neutrinos of the SM: top partner decay channels with a leptonically–decaying W boson are a corresponding example.

It is very common for many BSM models to predict additional invisible particles in their spectra, namely because a discrete parity like R–parity in Supersymmetry or T–parity in the LHT model is introduced as unbroken symmetry of the Lagrangian, yielding a stable particle as lightest parity–odd state. These particles might represent viable candidates for Dark Matter. Prime examples are the lightest neutralino $\tilde{\chi}_1^0$ in supersymmetric theories, and the heavy photon A_{H} in the LHT model.

The mass determination of BSM invisible particles has been always very challenging, because they are usually pair produced at the end of BSM decay chains due to their odd parity, and because the mass of other intermediate on–shell BSM particles is also unknown. Therefore, a method to simultaneously measure the invariant mass of different BSM particles involved in a decay chain is of great interest, at least for some specific final state topologies.

In the following, we will propose a possible mass measurement method from a signal consisting of pair production of a BSM particle X further decaying as $X \to \ell N$, where both masses $(m_{\mathrm{N}}, m_{\mathrm{X}})$ are a–priori unknown, and N is an invisible particle, yielding a final state with a large fraction of missing transverse momentum. In particular, we will focus on the case where X is pair produced from a resonance.

This mass determination method, as presented in ref. [11], relies on the identification of particular observables defined on the boundary of the kinematically allowed mass region in the $(m_{\rm N}, m_{\rm X})$ plane: these observables will be used in measuring the unknown masses. A specific example in the context of the Minimal Supersymmetric Standard Model (MSSM) will be discussed as well, showing that the proposed method might provide a precise measurement of the chargino and sneutrino masses at the LHC with $\sqrt{s} = 14\,{\rm TeV}$ and $300\,{\rm fb}^{-1}$ of integrated luminosity.

5.2.1 Kinematical constraints and consistent mass regions

As just anticipated, let us now consider the pair production of a BSM particle X, which then further decays to a SM lepton plus an invisible particle N, namely $X \to \ell N$. Suppose that both masses $m_{\rm X}$ and $m_{\rm N}$ are a–priori unknown.

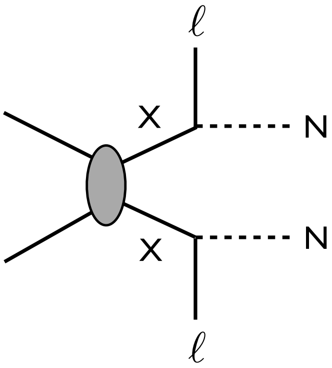

Figure 5.9: *One–step decay chain of a pair produced and semi–invisibly decaying particle X.*

For this rather short (one–step) decay chain, as depicted in figure 5.9, simultaneously measuring the two unknown masses is particularly challenging. At a hadron collider, this event topology yields a “minimal” set of constraints given by the measured visible leptonic four–momenta $p^\mu_{\ell_1}, p^\mu_{\ell_2}$ and the measured missing transverse momentum $\not{p}^{\rm T}$ [147–149]:

$$\Phi_{\rm min} \;:\; \begin{cases} \tilde{m}^2_{\rm X} = (p^\mu_{\ell_1} + p^\mu_{\rm N_1})^2 = (p^\mu_{\ell_2} + p^\mu_{\rm N_2})^2 \\ \tilde{m}^2_{\rm N} = p^2_{\rm N_1} = p^2_{\rm N_2} \\ \not{p}^{\rm T} = p^{\rm T}_{\rm N_1} + p^{\rm T}_{\rm N_2} \end{cases} \tag{5.25}$$

where $(\tilde{m}_{\rm X}, \tilde{m}_{\rm N})$ need not coincide with the true unknown mass values $(m_{\rm X}, m_{\rm N})$. These constraints represent six equations for a total of eight unknown components of $(p^\mu_{\rm N_1}, p^\mu_{\rm N_2})$: no unique solution for a given $(\tilde{m}_{\rm X}, \tilde{m}_{\rm N})$ pair is possible. In other words, for this kind of one–step decay chains it is impossible to determine both $(m_{\rm X}, m_{\rm N})$ by the constraints obtained from a single event.

Longer decay chains, where additional kinematical constraints might be introduced, can possibly yield a simultaneous $(m_{\rm X}, m_{\rm N})$ measurement, see e.g. ref. [147], where the authors considered a two–step decay chain from pair production of MSSM squarks decaying as

$$\tilde{q} \to q\, \tilde{\chi}_2^0 \to q\, \left(\ell^\pm \tilde{\ell}^\mp\right) \to q\, \ell^\pm\, \left(\ell^\mp\, \tilde{\chi}_1^0\right)\,, \tag{5.26}$$

where in our previous notation $\tilde{\ell} \equiv X$ and $\tilde{\chi}_1^0 \equiv N$. One can distinguish the cases in which X is produced on– or off–shell, and for both cases the authors provided a method to simultaneously measure $(m_{\rm X}, m_{\rm N})$.

Returning to our one–step decay chain with minimal kinematic constrains $\Phi_{\rm min}$, it is anyway possible to restrict the values of $(\tilde{m}_{\rm X}, \tilde{m}_{\rm N})$ to a *kinematically consistent region* on an event–by–event basis. Namely, the $(\tilde{m}_{\rm X}, \tilde{m}_{\rm N})$ hypotheses providing a physical solution for $\Phi_{\rm min}$ (real momenta and positive energy) are called the kinematically consistent region.

Particularly interesting is the boundary curve of the allowed region in the $(\tilde{m}_{\rm X}, \tilde{m}_{\rm N})$ plane: if the system is boosted in the transverse direction by e.g. hard initial state radiation, one can collect the boundary curves of the allowed mass regions from different events. It turns out that a collection of these boundary curves from a large number of events exhibits a cusp structure at the true mass point [147, 150–152].

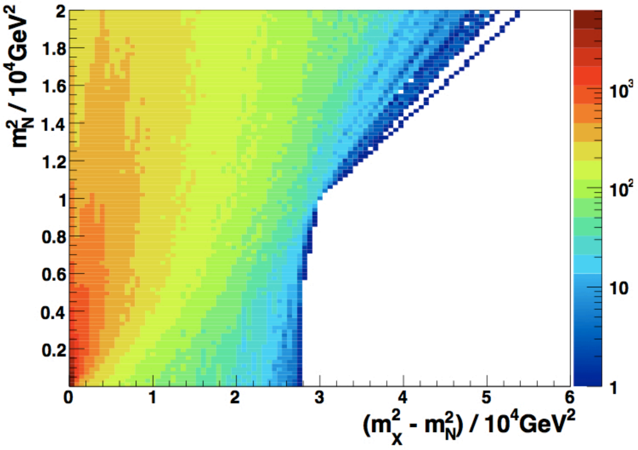

Figure 5.10: *Density plot of* $\Phi_{\rm min}$ *boundary curves for* $pp \to \tilde{q}\tilde{q}^* \to \tilde{\chi}_1^+ \tilde{\chi}_1^- q\bar{q} \to (e^+ \tilde{\nu}_e)\, (e^- \tilde{\bar{\nu}}_e)\, q\bar{q}$ *at the LHC with* $\sqrt{s} = 14$ *TeV. We set* $(m_{\tilde{q}}, m_{\tilde{\chi}_1^\pm}, m_{\tilde{\nu}}) = (1500, 200, 100)$ *GeV. Parton–level momenta are used, and no detector simulation has been included. The z–axis shows the number of boundary curves passing through* $(0.06\; GeV^2) \times (0.02\; GeV^2)$ *bins in* 10^4 *events.*

As an explicit example, we show in figure 5.10 the density of the boundary curves projected onto the $(\tilde{m}_{\rm X}^2 - \tilde{m}_{\rm N}^2, \tilde{m}_{\rm N}^2)$ plane for the process $pp \to \tilde{q}\tilde{q}^*$, $\tilde{q} \to q\, \tilde{\chi}_1^+$, $\tilde{\chi}_1^+ \to \ell^+ \tilde{\nu}_\ell$, with $(m_{\tilde{q}}, m_{\tilde{\chi}_1^\pm}, m_{\tilde{\nu}}) = (1500, 200, 100)\,\mathrm{GeV}$, neglecting finite width effects and detector resolution. It should be noted that the right–hand side white region in figure 5.10 represents the intersection of all kinematically consistent regions from the different events. A cusp structure is observed at the true mass point.

However, the density of boundary curves around the cusp is very low, and if we further consider realistic effects like momentum mismeasurement and potential background contamination, it is clear that a precise mass measurement from the position of the cusp is not reliable [153, 154].

Maximal extension of Φ_{min}

A key observation is that additional constraints besides Φ_{min} would further restrict the kinematically allowed mass region, therefore sharpening the cusp structure at the true mass point, and leading to a possible simultaneous measurement of $(m_{\mathrm{X}}, m_{\mathrm{N}})$. In refs. [148, 149], the authors studied the effect of introducing the following constraints:

$$\Phi_{\mathrm{s}}: \ s = (p^\mu_{\ell_1} + p^\mu_{\mathrm{N}_1} + p^\mu_{\ell_2} + p^\mu_{\mathrm{N}_2})^2 \tag{5.27}$$

$$\Phi_{\mathrm{z}}: \ \not{p}^z = p^z_{\mathrm{N}_1} + p^z_{\mathrm{N}_2}\,, \tag{5.28}$$

namely assuming that the invariant mass of the process, as well as the longitudinal component of the missing transverse momentum, could be experimentally measured. We will call this set of constraints as $\Phi_{\mathrm{max}} \equiv \Phi_{\mathrm{min}} + \Phi_{\mathrm{s}} + \Phi_{\mathrm{z}}$. This situation might be possible in a central exclusive process (CEP) with forward proton tagging at the LHC, or in the case of lepton colliders. It is to be noted that while at a lepton collider the invariant mass of the process is fixed by the center–of–mass energy of the collision, in the CEP case it is not a–priori fixed but measured via proton tagging detectors.

For comparison, we show in figure 5.11 the density plot of boundary curves of kinematically consistent mass regions as evaluated from a semi–invisible decay process at the ILC, namely $e^+e^- \to \tilde{e}^+\tilde{e}^- \to \left(e^+\,\tilde{\chi}^0_1\right)\left(e^-\,\tilde{\chi}^0_1\right)$ with $(\sqrt{s}, m_{\tilde{e}}, m_{\tilde{\chi}^0_1}) = (500, 200, 100)\,\mathrm{GeV}$. This process corresponds to the kinematical constraints defined for the Φ_{max} case. The global allowed region reduces to a straight line between the true mass point $(m^2_{\mathrm{X}} - m^2_{\mathrm{N}}, m^2_{\mathrm{N}})$ and $(m^2_{\mathrm{X}} - m^2_{\mathrm{N}}, 0)$: a simultaneous $(m_{\mathrm{X}}, m_{\mathrm{N}})$ measurement might thus be possible.

Let us now briefly review the method developed in refs. [148, 149] for an explicit $(m_{\mathrm{X}}, m_{\mathrm{N}})$ mass determination in the Φ_{max} case.

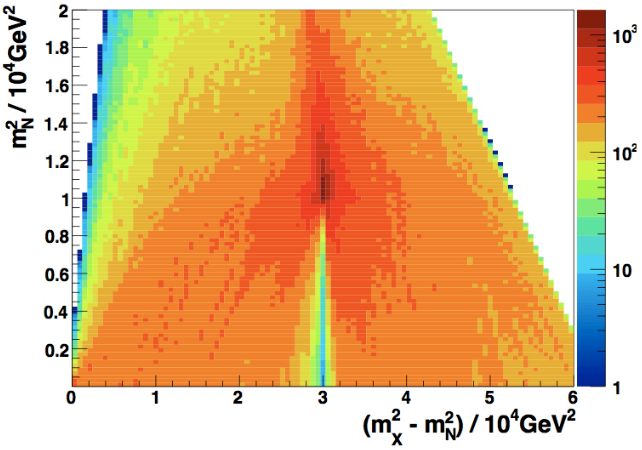

Figure 5.11: *Density plot of* $\Phi_{\rm max}$ *boundary curves for* $e^+e^- \to \tilde{e}^+\tilde{e}^- \to \left(e^+\tilde{\chi}_1^0\right)\left(e^-\tilde{\chi}_1^0\right)$ *at the ILC. We set* $(\sqrt{s}, m_{\tilde{e}}, m_{\tilde{\chi}_1^0}) = (500, 200, 100)\,\mathrm{GeV}$. *Parton–level momenta are used, and no detector simulation has been included. The z–axis shows the number of boundary curves passing through* $(0.06\ GeV^2) \times (0.02\ GeV^2)$ *bins in* 10^4 *events.*

In general, any $p^\mu_{\rm N_1}$ and $p^\mu_{\rm N_2}$ satisfying $\not{p}^\mu = p^\mu_{\rm N_1} + p^\mu_{\rm N_2}$ can be parametrised as

$$p^\mu_{\rm N_1/N_2} = \frac{1 \mp a}{2}\,\not{p}^\mu \pm \frac{b}{2}\,p^\mu_{\ell_1} \mp \frac{c}{2}\,p^\mu_{\ell_2} \pm d\,P^\mu\,, \tag{5.29}$$

where a, b, c, d are dimensionless constants, and $P_\mu \equiv \epsilon_{\mu\nu\rho\sigma}\not{p}^\nu p^\rho_{\ell_1} p^\sigma_{\ell_2}$ is a space–like vector. The $\Phi_{\rm max}$ constraints can then be expressed as

$$\Phi_{\rm max}\ :\ \begin{cases} p^\mu_{\rm X_1} = p^\mu_{\rm N_1} + p^\mu_{\ell_1} \\ p^\mu_{\rm X_2} = p^\mu_{\rm N_2} + p^\mu_{\ell_2} \\ \tilde{m}^2_{\rm X} = p^2_{\rm X_1} = p^2_{\rm X_2} \\ \tilde{m}^2_{\rm N} = p^2_{\rm N_1} = p^2_{\rm N_2} \end{cases} \tag{5.30}$$

where again $(\tilde{m}_{\rm X}, \tilde{m}_{\rm N})$ are test mass values which need not coincide with the true masses $(m_{\rm X}, m_{\rm N})$. For a given $(\tilde{m}_{\rm X}, \tilde{m}_{\rm N})$, the above conditions uniquely determine the coefficients a, b, c in eq. (5.29), together with an equation which has to be imposed to obtain the remaining coefficient d, namely

$$\lambda_{\rm N} = \frac{c_a}{4\mathcal{M}}\lambda_\Delta^2 + \frac{c_b}{2\mathcal{M}}\lambda_\Delta + \frac{c_c}{4\mathcal{M}} + d^2\lambda_P^2\,. \tag{5.31}$$

In eq. (5.31) the coefficients c_a, c_b, c_c and $\mathcal{M}$ are functions of the measured momenta p_{ℓ_1}, p_{ℓ_2} and $\not{p}$, and one explicitly has $\lambda_N \equiv \tilde{m}^2_{\rm N}/(p_{\ell_1}\cdot p_{\ell_2})$, $\lambda_\Delta \equiv (\tilde{m}^2_{\rm X} - \tilde{m}^2_{\rm N})/(p_{\ell_1}\cdot p_{\ell_2})$, see refs. [148, 149].

A hypothesis $(\tilde{m}_{\rm X}, \tilde{m}_{\rm N})$ is called consistent if eq. (5.31) leads to a solution for d with $d^2 > 0$, in order to obtain four–momenta p_i^μ with real components in eq. (5.29). In other words, the $(\tilde{m}_{\rm X}, \tilde{m}_{\rm N})$ hypotheses leading to $d^2 > 0$ represent the kinematically consistent mass region of the event, while the corresponding boundary is identified from eq. (5.31) by setting $d = 0$. Furthermore, one can show that the shape of the boundary curve is a parabola with negative curvature, containing the true mass point $(m_{\rm X}, m_{\rm N})$ below its apex in the $(\tilde{m}_{\rm X}^2 - \tilde{m}_{\rm N}^2, \tilde{m}_{\rm N}^2)$ plane.

One can then define possible observables along the boundary curve of the kinematically consistent region. In particular, analytic expressions for the global maxima of $\tilde{m}_{\rm X}$ and $\tilde{m}_{\rm N}$ along the boundary have been obtained in [148, 149] as

$$\left[\tilde{m}^{\rm max}_{\rm X;\,\Phi_{max}}\right]^2 = \frac{p_{\ell_1} \cdot p_{\ell_2}}{4\mathcal{M}}\left[c_c - \frac{(c_b + 2\mathcal{M})^2}{c_a}\right] \tag{5.32}$$

$$\left[\tilde{m}^{\rm max}_{\rm N;\,\Phi_{max}}\right]^2 = \frac{p_{\ell_1} \cdot p_{\ell_2}}{4\mathcal{M}}\left[c_c - \frac{c_b^2}{c_a}\right]. \tag{5.33}$$

In ref. [11] we have further obtained the analytic expressions of new possible variables defined along the boundary, in particular the extremal values of $\tilde{m}_{\rm X}$ along the boundary for a given hypothesis on $\tilde{m}_{\rm N}$, denoted as $\tilde{m}^{\rm max/min}_{\rm X;\,\Phi_{max}}(\tilde{m}_{\rm N})$:

$$\left[\tilde{m}^{\rm max/min}_{\rm X;\,\Phi_{max}}(\tilde{m}_{\rm N})\right]^2 = \frac{p_{\ell_1} \cdot p_{\ell_2}}{c_a}\left[C_{\rm X} \pm \sqrt{D_{\rm X}}\right]. \tag{5.34}$$

In eq. (5.34), we have defined

$$C_{\rm X} = c_a \lambda_N - c_b, \tag{5.35}$$

$$D_{\rm X} = c_b^2 + c_a(4\mathcal{M}\lambda_N - c_c) \tag{5.36}$$

$$\lambda_{\rm X} \equiv \tilde{m}_{\rm X}^2/(p_{\ell_1} \cdot p_{\ell_2}). \tag{5.37}$$

The consistent mass region of a typical event and the kinematic variables as defined in eq. (5.32) (5.33) and (5.34), are shown in figure 5.12. The interesting feature is that, by definition, the aforementioned boundary variables satisfy the following relations:

$$\begin{cases} \tilde{m}^{\rm max}_{\rm X;\,\Phi_{max}} \geq \tilde{m}^{\rm max}_{\rm X;\,\Phi_{max}}(m_{\rm N}) \geq m_{\rm X} \\ \tilde{m}^{\rm min}_{\rm X;\,\Phi_{max}}(m_{\rm N}) \leq m_{\rm X} \\ \tilde{m}^{\rm max}_{\rm N;\,\Phi_{max}} \geq m_{\rm N}\,. \end{cases} \tag{5.38}$$

Using the results of eq. (5.38), the authors of refs. [148, 149] showed that the distributions of $\tilde{m}^{\rm max}_{\rm X;\,\Phi_{max}}$ and $\tilde{m}^{\rm max}_{\rm N;\,\Phi_{max}}$ exhibit a sharp endpoint structure at the corresponding true masses $(m_{\rm X}, m_{\rm N})$ when considering examples of CEP and e^+e^- processes, allowing thus for a simultaneous $(m_{\rm X}, m_{\rm N})$ measurement.

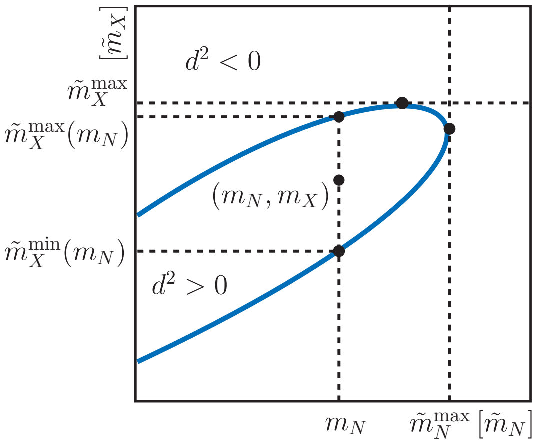

Figure 5.12: *Kinematically consistent $(\tilde{m}_X, \tilde{m}_N)$ region ($d^2 > 0$ in eq. (5.31)) for a "typical" event, defined by the four–momenta $(p_{\ell_1}, p_{\ell_2}, \not{p})$, as published in [149]. The consistent mass region contains by definition the true mass point (m_N, m_X). $\tilde{m}_N^{\max}$ is the global maximum $\tilde{m}_N$ value, while $\tilde{m}_X^{\min}(m_N)$ is the minimal value of $\tilde{m}_X$ given m_N. Analogously for the other shown variables.*

Relaxing one of the hypotheses

We can now turn our attention to our results published in ref. [11]. In particular, the aim is to extend the mass determination method presented in refs. [148, 149], relaxing one of the kinematical hypothesis defining the $\Phi_{\max}$ constraints, to reflect a more realistic LHC scenario. At the LHC, a significant and unknown proportion of the energy of the incoming hadrons in each event escapes down the beam pipe: therefore, the longitudinal and energy components of the missing four–momentum are not determined. In this way, the Φ_z constraint of eq. (5.28) cannot be imposed to identify the kinematically consistent mass region.

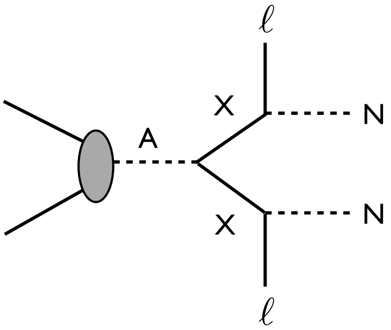

Figure 5.13: *Pair production of a particle X from an s–channel particle A, followed by semi–invisible X decays.*

On the other hand, the Φ_s constraint of eq. (5.27) can still be included, if the particles X are e.g. pair produced from an s–channel particle A of mass m_A. In this case, the invariant mass of the process is fixed to m_A^2. Therefore, as in ref. [11], we focus now on the $\Phi_\mathrm{min} + \Phi_\mathrm{s}$ case, developing a mass measurement method of $(m_\mathrm{X}, m_\mathrm{N})$ for event samples with the topology shown in figure 5.13. As a specific example, we investigate the process $pp \to A \to \tilde{\chi}_1^+ \tilde{\chi}_1^- \to (\ell^+ \tilde{\nu}_\ell)\,(\ell^- \tilde{\bar{\nu}}_\ell)$ at the LHC, with A the MSSM CP–odd Higgs boson.

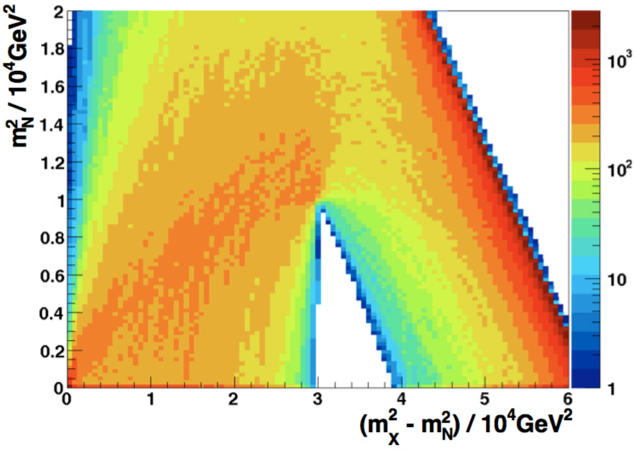

Figure 5.14: *Density plot of the* $\Phi_\mathrm{min} + \Phi_\mathrm{s}$ *boundary curves for* $pp \to A \to \tilde{\chi}_1^+ \tilde{\chi}_1^- \to (\ell^+ \tilde{\nu}_\ell)\,(\ell^- \tilde{\bar{\nu}}_\ell)$ *at the LHC with* $\sqrt{s} = 14$ *TeV. We set* $(m_A, m_{\tilde{\chi}_1^\pm}, m_{\tilde{\nu}}) = (500, 200, 100)$ *GeV. Parton–level momenta are used, and no detector simulation has been included. The z–axis shows the number of boundary curves passing through* $(0.06\ GeV^2) \times (0.02\ GeV^2)$ *bins in* 10^4 *events.*

For comparison, we show in figure 5.14 the density plot of boundary curves of kinematically consistent mass regions for the aforementioned process. In particular, we imposed $(m_\mathrm{A}, m_{\tilde{\chi}_1^\pm}, m_{\tilde{\nu}}) = (500, 200, 100)$ GeV. One can see that the kinematically allowed region, given by the lower white triangle, is more restricted with respect to the Φ_min case of figure 5.10: the cusp structure at the true mass point is more pronounced and more easily identified, reflecting the additional kinematical information which has been included.

In order to obtain possible expressions of the observables defined on the boundary of the kinematically allowed mass region for the $\Phi_\mathrm{min} + \Phi_\mathrm{s}$ case, we proceed as follows. Since the analytical expressions of the desired observables, as defined for the Φ_max case in eq. (5.32) (5.33) and (5.34), are functions of the now unknown $\not{p}^0$ and $\not{p}^z$, we scan the corresponding expressions over values of $\not{p}^0$ and $\not{p}^z$ satisfying the constraint Φ_s. In doing so we define

$$\tilde{m}_\mathrm{X}^\mathrm{max}(\tilde{m}_\mathrm{N}) = \max_{\{\not{p}^0,\not{p}^z\};\,\Phi_\mathrm{s}} \left[\tilde{m}^\mathrm{max}_{\mathrm{X};\,\Phi_\mathrm{max}}(\tilde{m}_\mathrm{N})\right] \tag{5.39}$$

$$\tilde{m}_\mathrm{X}^\mathrm{min}(\tilde{m}_\mathrm{N}) = \min_{\{\not{p}^0,\not{p}^z\};\,\Phi_\mathrm{s}} \left[\tilde{m}^\mathrm{min}_{\mathrm{X};\,\Phi_\mathrm{max}}(\tilde{m}_\mathrm{N})\right] \tag{5.40}$$

$$\tilde{m}_\mathrm{X}^\mathrm{max} = \max_{\{\not{p}^0,\not{p}^z\};\,\Phi_\mathrm{s}} \left[\tilde{m}^\mathrm{max}_{\mathrm{X};\,\Phi_\mathrm{max}}\right] \tag{5.41}$$

$$\tilde{m}_\mathrm{N}^\mathrm{max} = \max_{\{\not{p}^0,\not{p}^z\};\,\Phi_\mathrm{s}} \left[\tilde{m}^\mathrm{max}_{\mathrm{N};\,\Phi_\mathrm{max}}\right] . \tag{5.42}$$

By analogous relations to eq. (5.38), we can conclude that

$$\begin{cases} \tilde{m}_\mathrm{X}^\mathrm{max} \geq \tilde{m}_\mathrm{X}^\mathrm{max}(m_\mathrm{N}) \geq m_\mathrm{X} \\ \tilde{m}_\mathrm{X}^\mathrm{min}(m_\mathrm{N}) \leq m_\mathrm{X} \\ \tilde{m}_\mathrm{N}^\mathrm{max} \geq m_\mathrm{N} \, . \end{cases} \tag{5.43}$$

In particular, we will show how the observables $\tilde{m}_\mathrm{X}^\mathrm{max}(m_\mathrm{N})$ and $\tilde{m}_\mathrm{N}^\mathrm{max}$ possess the highest sensitivity for a simultaneous $(m_\mathrm{X}, m_\mathrm{N})$ mass measurement in the $\Phi_\mathrm{min} + \Phi_\mathrm{s}$ case.

5.2.2 Results

The mass measurement method presented in section 5.2.1 is independent of the particular underlying model. However, to illustrate its main features, we consider as a case study the MSSM pair production of charginos $\tilde{\chi}_1^\pm$ from an on–shell CP–odd Higgs boson A, in association with two initial state radiation b–jets. To match the desired final state topology as in figure 5.13, we consider the decay of the charginos into a SM lepton plus a sneutrino. The diagram of the considered process is shown in figure 5.15.

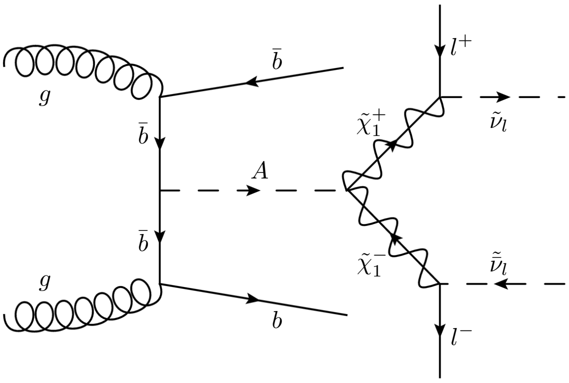

Figure 5.15: *Feynman diagram for the MSSM* $p\,p \to A b\bar{b} \to \tilde{\chi}_1^+ \tilde{\chi}_1^- \, b\bar{b} \to (\ell^+ \tilde{\nu}_\ell)\,(\ell^- \bar{\tilde{\nu}}_\ell)\, b\bar{b}$ *process considered in our analysis as a case study.*

Event generation

As a benchmark MSSM parameter space point for the BSM event generation, we fix $m_{\mathrm{A}} = 800\,\mathrm{GeV}$, $m_{\tilde{\chi}_1^{\pm}} = 350\,\mathrm{GeV}$ and $m_{\tilde{\nu}} = 200\,\mathrm{GeV}$. Furthermore, we have chosen the values $\tan\beta = 50$ and $\mu = 400\,\mathrm{GeV}$, the former to increase the production cross section of the CP–odd Higgs for a given mass, the latter to increase its branching ratio to two charginos. It is to be noted that the CP–odd Higgs dominantly decays into two bottom quarks, but we assume that its mass m_{A} has already been measured within 10% uncertainty from a dedicated study of the $A \to \tau^+\tau^-$ channel, as in [155].

Background contamination from SM and other MSSM processes are taken into account. In particular, the dominant processes consist of MSSM direct $\tilde{\chi}_1^+\tilde{\chi}_1^-$ + jets production, and SM $t\bar{t}$ and W^+W^- + jets, with leptonic decays of the W bosons. The corresponding cross sections are calculated as follows, for the foreseen LHC runs at $\sqrt{s} = 14\,\mathrm{TeV}$. Regarding the MSSM processes, the associated CP–odd Higgs cross section is evaluated via FeynHiggs 2.9.5 [156], while for the $\tilde{\chi}_1^+\tilde{\chi}_1^-$ + jets process we use the $\tilde{\chi}_1^+\tilde{\chi}_1^-$ LO cross section evaluated via MadGraph 1.5 [84] plus up to two matrix–element additional hard partons, matched to the Pythia 6.42 parton shower via MLM merging scheme implemented in the MadGraph5–Pythia 6.42 interface [84, 85]. The cross sections for the considered SM processes are given in [157, 158] at order NLO+NNLL for $t\bar{t}$, and NLO for WW. We summarise the cross section values in table 5.3.

	$Ab\bar{b}$	$\tilde{\chi}_1^+\tilde{\chi}_1^-$+ jets	$t\bar{t}$	WW+ jets
$\sigma \cdot \mathrm{BR}\,[\mathrm{pb}]$	0.023	0.079	40.92	5.80

Table 5.3: *Cross sections at LHC14 for the considered signal and background processes.*

We further set the branching ratio of the chargino to a SM charged lepton and MSSM sneutrino to 1.0: we do not consider chargino decays either to a SM W plus a neutralino, or to a charged slepton plus a neutrino, since these topologies would be categorised in the $\Phi_{\min}$ case. It should be noted that our procedure is valid for both a long–lived sneutrino, or for the case in which the sneutrino decays to invisible particles.

A set of selection cuts is chosen to reduce the background contamination while retaining a large fraction of signal events. In particular, each event should consist of exactly two opposite sign leptons within $|\eta^{\ell}| < 2.5$, and two tagged b–jets satisfying $p_{\mathrm{T}}^{b} > 20\,\mathrm{GeV}$ and $|\eta^{b}| < 2.5$. Furthermore, we exploit large cuts on the total missing transverse momentum

($\not{E}_{\rm T} > 130\,{\rm GeV}$), on the $p_{\rm T}$ of the two leptons ($p_{\rm T}^{\ell_1} > 80\,{\rm GeV}$, $p_{\rm T}^{\ell_2} > 40\,{\rm GeV}$), and on the m_{T2} variable [159][3] ($m_{T2} > 120\,{\rm GeV}$), too.

MadGraph 1.5 is used to generate all parton–level events, further interfaced with the Pythia 6.42 parton shower. The Pythia output is then analysed via Delphes 3.0 [86] for a fast simulation of the ATLAS detector, following the specifications as in [155].

The generated signal and background events, corresponding to an integrated luminosity of $300\,{\rm fb}^{-1}$ and passing the described selection cuts, are then used as input for the mass measurement method described in section 5.2.1, as we will detail in the following.

Mass determination method at work

Given the relations of eq. (5.43), we claim that a possible measurement of the invisible mass $m_{\rm N}$ is possible by measuring the endpoint of the $\tilde{m}_{\rm N}^{\rm max}$ distribution, namely identifying $m_{\rm N}^{\rm exp} = [\tilde{m}_{\rm N}^{\rm max}]^{\rm endpoint}$. Analogously, we can simultaneously determine the chargino mass $m_{\rm X}$ by measuring the endpoint of the $\tilde{m}_{\rm X}^{\rm min}(m_{\rm N}^{\rm exp})$ distribution, identifying $m_{\rm X}^{\rm exp} = \left[\tilde{m}_{\rm X}^{\rm min}(m_{\rm N}^{\rm exp})\right]^{\rm endpoint}$.

We developed a numerical procedure to evaluate the endpoints of the considered distributions, for details see ref. [11]. In particular, the aim of the numerical procedure is to minimise any potential bias in extracting the endpoints. Besides the position of the endpoint, this procedure allows us to determine an estimate of the steepness of the slope of any distribution at its endpoint: this information will become crucial for our attempt to measure the mass of the intermediate particle A, too.

In figure 5.16 we show typical distributions of the aforementioned variables defined on the boundary of the kinematically consistent mass region. In particular, in the left plot we show the $\tilde{m}_{\rm N}^{\rm max}$ distribution from a simulated LHC14 event generation with $300\,{\rm fb}^{-1}$ of integrated luminosity: the left–hand side endpoint corresponds to the “experimental” measure of $m_{\rm N}^{\rm exp}$. By simulating 100 independent LHC measurements, we obtain an averaged $m_{\rm N}^{\rm exp}$ value, and estimate a statistical uncertainty as standard deviation from the 100 measurements: the result is remarkably close to the true value $m_{\rm N} = 200\,{\rm GeV}$, namely

$$m_{\rm N}^{\rm exp} = 195.9 \pm 2.5\,{\rm GeV}\,. \tag{5.44}$$

On the other hand, in the right plot of figure 5.16 we show the $\tilde{m}_{\rm X}^{\rm min}(m_{\rm N}^{\rm exp})$ distribution from a simulated LHC14 event generation with $300\,{\rm fb}^{-1}$ of integrated luminosity, where we

---

[3] We used the public code described in ref. [147] to evaluate m_{T2} for each event.

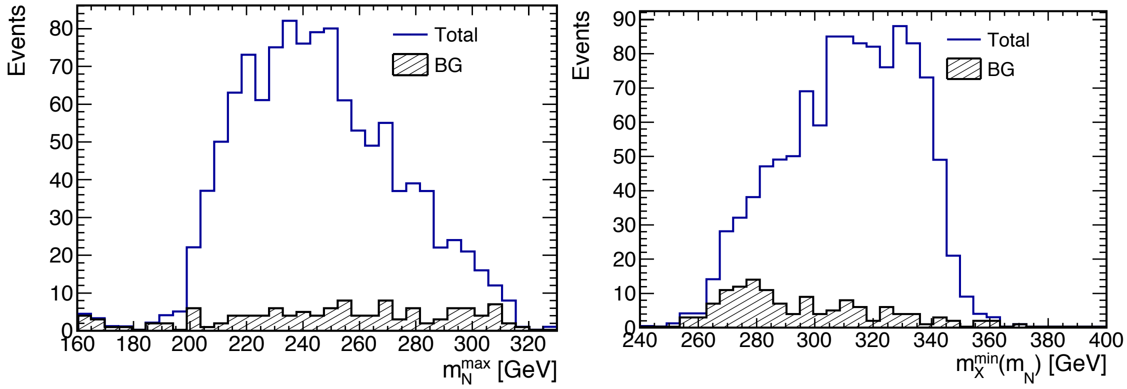

Figure 5.16: *Distribution plots of boundary observables evaluated on a single full simulation at the LHC with* $\sqrt{s} = 14\,TeV$ *and* $300\,fb^{-1}$ *of integrated luminosity. The label "Total" refers to the signal plus background event sample, while the label "BG" refers to the distribution of only background events. We set* $m_A = 800\,GeV$, $m_{\tilde{\chi}_1^\pm} = 350\,GeV$ *and* $m_{\tilde{\nu}} = 200\,GeV$*. In particular, the left plot shows the distribution of the* $\tilde{m}_N^{\max}$ *variable, while the right plot shows the distribution of the* $\tilde{m}_X^{\min}(m_N^{\exp})$ *variable, for which we have fixed* $m_N^{\exp}$ *as in eq. (5.44).*

fixed $m_{\rm N}^{\rm exp}$ to its measured value as in eq. (5.44). In this case, the right–hand side endpoint corresponds to the "experimental" measure of $m_{\rm X}^{\rm exp}$. By simulating 100 independent LHC measurements, we obtain a result again close to the true value $m_X = 350\,$GeV:

$$m_{\rm X}^{\rm exp} = 362.0 \pm 4.6\,{\rm GeV}\,. \tag{5.45}$$

From eq. (5.44) and eq. (5.45), we observe a slight offset of the measured endpoints compared to the true mass values. This might be traced back to detector effects and to background contamination, which tend to smear the endpoints of the distributions, as well as to possible limitations of the developed edge–finding method. This small effect might anyway be corrected for in a dedicated experimental analysis, by comparing the measured endpoint values with the corresponding simulation.

Including uncertainties on $m_{\rm A}$

In a realistic collider analysis, the mass of the intermediate s–channel particle A might be known only within a certain uncertainty. In the mass determination method we have discussed so far, $m_{\rm A}$ has been fixed to the ideal value as used in the event generation, namely $m_{\rm A} = 800\,$GeV. We are now interested to understand how an experimental uncertainty on $m_{\rm A}$ might affect the endpoint determination for the observables $\tilde{m}_{\rm N}^{\rm max}$ and $\tilde{m}_{\rm X}^{\rm min}(m_{\rm N}^{\rm exp})$.

This effect is studied by changing the input value of $m_{\rm A}$ in the analytical relations of

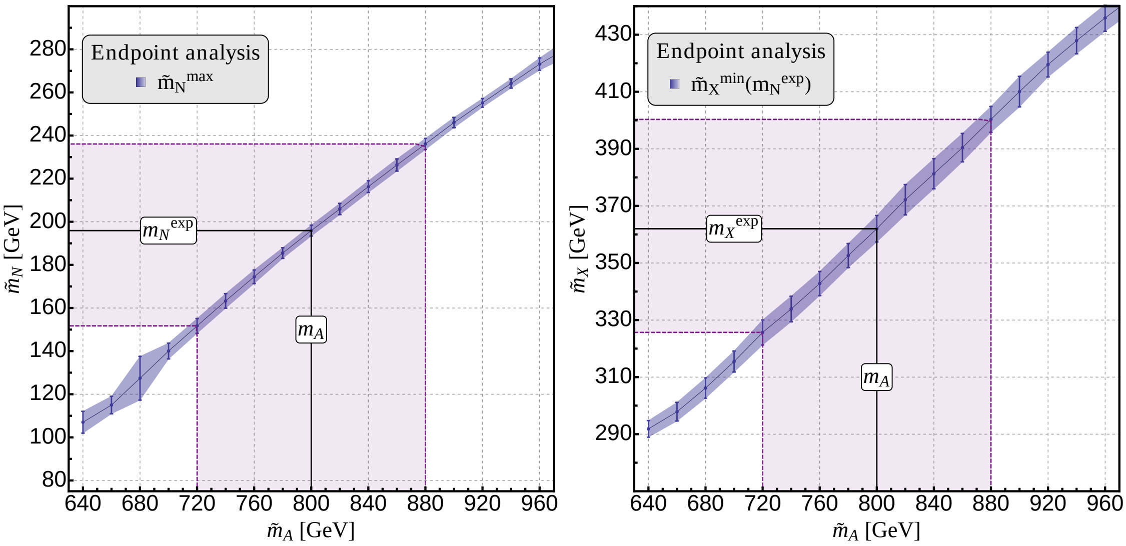

Figure 5.17: *Endpoint measurements of the* $\tilde{m}_N^{\max}(\tilde{m}_A)$ *distribution (left plot) and of the* $\tilde{m}_X^{\min}(\tilde{m}_A, m_N^{\text{exp}})$ *distribution (right plot) for different* $\tilde{m}_A$ *hypotheses. The uncertainties on the single endpoints correspond to the standard deviations from 100 different LHC simulations. A band showing the effect of a 10% uncertainty on* m_A *is also shown.*

eq. (5.40) and eq. (5.42): the used mass hypothesis will be called $\tilde{m}_{\text{A}}$, in order to distinguish it from the true value m_{A}.

The endpoints of the $\tilde{m}_{\text{N}}^{\max}(\tilde{m}_{\text{A}})$ and $\tilde{m}_{\text{X}}^{\min}(\tilde{m}_{\text{A}}, m_{\text{N}}^{\text{exp}})$ distributions, as evaluated for different hypotheses on the input value $\tilde{m}_{\text{A}}$, are shown in figure 5.17, in the left and right plot, respectively. On both plots, it is shown how a 10% uncertainty on m_{A} might affect the two endpoint measurements, namely introducing a 20% uncertainty.

The uncertainty on a single endpoint value corresponds to the standard deviation from 100 different LHC simulations. Furthermore, we illustrate the position of the measured $m_{\text{N}}^{\text{exp}}$ and $m_{\text{X}}^{\text{exp}}$, as given by eq. (5.44) and (5.45), respectively.

Finally, let us discuss a method to infer a possible measurement for the s–channel mass m_{A} as well. The key observation is that if a “wrong” value for m_{A} is used as input for the determination of the boundary observables, then the Φ_{s} constraint no longer corresponds to the correct event kinematics, and one cannot expect the different distributions to display a sharp endpoint structure.

For example, one would expect the slope of $\tilde{m}_{\text{N}}^{\max}(\tilde{m}_{\text{A}})$ at the endpoint to become steeper as the input $\tilde{m}_{\text{A}}$ value approaches the true value m_{A}, where one expects a sharper endpoint structure. Therefore, it is interesting to plot the steepness of the $\tilde{m}_{\text{N}}^{\max}(\tilde{m}_{\text{A}})$

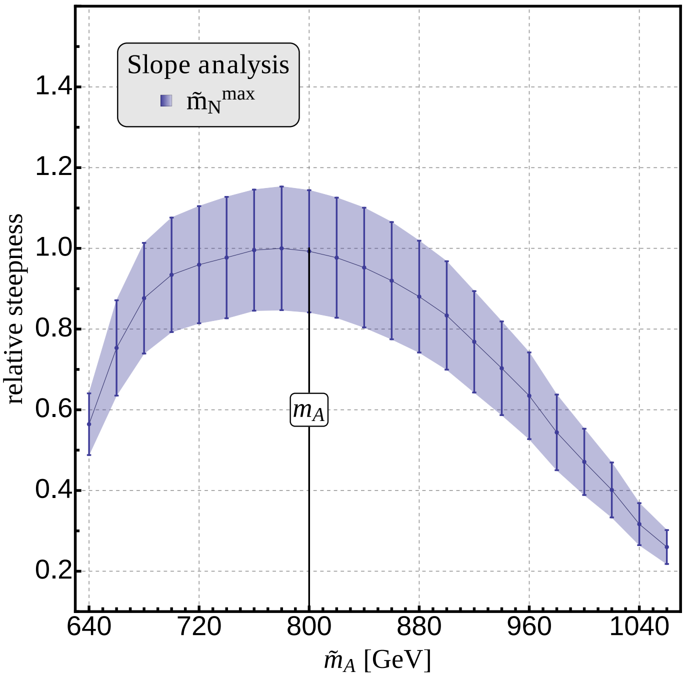

Figure 5.18: *Slope measurement at the endpoint of the $\tilde{m}_N^{\max}(\tilde{m}_A)$ distribution, for different values of $\tilde{m}_A$. The values are normalised to the largest measured steepness. Note that the maximum of the distribution is observed near $\tilde{m}_A = m_A$.*

distribution at the corresponding endpoint, as a function of $\tilde{m}_{\mathrm{A}}$.

In figure 5.18 we show the corresponding distribution of the "endpoint steepness" as a function of $\tilde{m}_{\mathrm{A}}$, normalised to the largest measured steepness. A possible measure of $m_{\mathrm{A}}^{\mathrm{exp}}$ might therefore be identified with the $\tilde{m}_{\mathrm{A}}$ hypothesis yielding the largest endpoint steepness: by averaging over the 100 different event simulations we obtain

$$m_A^{\mathrm{exp}} = 776.4 \pm 34.3\,\mathrm{GeV}\,. \tag{5.46}$$

The relatively large statistical uncertainty on the central value indicates that this method should be used only as a guide to infer the mass of the particle A, although a more precise procedure in evaluating the steepness of the distribution might reduce the uncertainty.

Chapter 6

Conclusions

Exclusion limits on Little Higgs parameter space

Together with the huge quantity of collected and analysed LHC data by the experimental collaborations, the physics community should always try to develop new tools to gain the highest sensitivity to possible new physics signals, as well as being able to scrutinise the available information in such a way that no evidence of new physics could possibly be overlooked. This has been our motivation to thoroughly investigate the compatibility of the parameter space of different Little Higgs models using the available experimental collider data.

Many observables are altered by the Little Higgs structure: Higgs couplings to SM particles are generically modified with respect to their SM values, and completely new Higgs couplings to new particles are present, yielding possible additional Higgs decay channels or changes in its production rates. Furthermore, electroweak and low–energy observables, measured with high precision, are hugely sensitive to new physics contributions. Generically, the aforementioned modifications scale as powers of v/f: large values of f allow to recover the SM predictions, but the large–f limit represents a "decoupling" regime where one cannot consider the BSM model as a natural SM extension anymore. A rather large fine–tuning is reintroduced to obtain the correct Higgs mass. Therefore, it is of high interest to identify the lower bound on the scale f consistent with experimental results, in order to define the left–over degree of naturalness of the considered model.

In Chapter 4 we considered three well–known implementations of the Little Higgs paradigm, namely the Littlest Higgs (L^{2}H), the Littlest Higgs with T–parity (LHT) and the Simplest Little Higgs (SLH) models, and explicitly evaluated the modifications to specific observables which might be probed with the current collider data. We then set a lower bound on the symmetry breaking scale f within the considered models, up to a certain degree of compatibility with the data. In particular, we performed a χ^2 analysis including the best fit values of the Higgs signal strength modifiers as measured by both ATLAS and CMS collaboration, and 21 different electroweak and low–energy precision observables. For the Higgs observables, we have considered the most up–to–date experimental results as of the summer of 2013, with 7 and 8 TeV center–of–mass energies and up to $25\,\mathrm{fb}^{-1}$ of integrated luminosity. We obtained at 95% confidence level the following lower bounds:

$$
\begin{aligned}
(f_{\mathrm{SLH}})_{\mathrm{EWPT+Higgs}} &\gtrsim 3.3\ \mathrm{TeV} \\
(f_{\mathrm{L^2H}})_{\mathrm{EWPT+Higgs}} &\gtrsim 4.0\ \mathrm{TeV} \\
(f_{\mathrm{LHT,\ A}})_{\mathrm{EWPT+Higgs}} &\gtrsim 694\ \mathrm{GeV} \\
(f_{\mathrm{LHT,\ B}})_{\mathrm{EWPT+Higgs}} &\gtrsim 560\ \mathrm{GeV}\,.
\end{aligned}
$$

These bounds are among the major findings of this thesis, and represent the most up–to–date results in literature concerning the consistency of the aforementioned models in light of LHC data. These constraints have been considered as new reference values for many different phenomenological analyses performed by the Little Higgs community, as well as for an experimental CMS analysis involving $\mathrm{L^2H}$ topologies.

Furthermore, we have confirmed that models not providing a custodial symmetry, or another type of cancellation of additional contributions to oblique parameters, are in tension with the observed data, with the symmetry breaking scale pushed into the multi–TeV regime. On the other hand, the LHT model with both implementations of the down–Yukawa Lagrangian Case A and B, is found to be still consistent with the collected data down to values of f of $\mathcal{O}(500\,\mathrm{GeV})$, requiring thus only a rather small amount of fine–tuning to accommodate a naturally light Higgs boson.

We expect that these bounds will be further probed by the forthcoming LHC upgrade to higher center–of–mass energies and higher values of integrated luminosity. An even stronger exclusion potential will be guaranteed by reduced relative uncertainties on e.g. the best fit signal strength modifiers.

The consistency of a rather small value of f with EWPT and Higgs searches provides the possibility to study the phenomenology of LHT partners not only through indirect effects to precision observables, but also as possible signatures detectable via direct searches for new particles. Since the masses of these new particles are proportional to the scale f, one might indeed still expect production cross sections which are not severely suppressed even at $\sqrt{s} = 8\,\text{TeV}$ center–of–mass energy.

For this reason, in Chapter 4 we identified three main types of direct searches which can be matched onto LHT signal topologies, namely monojet with $\not{E}_{\rm T}$, multijet with $\not{E}_{\rm T}$, and multijet, leptons with $\not{E}_{\rm T}$. For each of these final state topologies we recasted the most recent ATLAS and CMS analyses as of the summer of 2013 with up to $20\,\text{fb}^{-1}$ of integrated luminosity, originally tailored for supersymmetric processes, reinterpreting the results assuming an LHT signal. By comparing the experimental upper bounds on the visible cross section with the LHT yields, we have been able to identify regions of parameter space which are excluded up to a certain confidence level. In particular, by combining the different direct search results, we obtained at 95% confidence level the following lower bound on the scale f:

$$(f_{\rm LHT,\,A})_{\rm direct\text{-}search.} \gtrsim 638\,\text{GeV}\,.$$

We see that with the current amount of collected data, direct searches are starting to become competitive with analyses involving only precision observables. This gives us the confidence that the forthcoming LHC runs will be crucial in probing the parameter space of the LHT model, even for particular kinematic configurations in certain regions of the parameter space. Therefore, we concluded Chapter 4 with a proposal of possible optimisations of the considered direct searches, in order to increase the sensitivity to LHT signatures. In particular, we have showed that there is room for a possible improvement within the current setups especially for the monojet plus $\not{E}_{\rm T}$ topology.

Dedicated analyses for LHC run II

After focusing on the *exclusion*–information gathered from collected data, we turned our attention to the proposal of possible *discovery* methods for the foreseen experimental searches starting in 2015. In particular, if a signal of a new BSM particle will be observed, one of the first measured properties will be its mass. The mass measurement method will depend on the considered final state topology: a big discriminant for different methods will be represented by the possible presence of large fractions of missing transverse momentum. In Chapter 5 we developed two possible dedicated LHC run II analyses with $300\,\text{fb}^{-1}$ of integrated luminosity, aiming for mass measurements of BSM particles in final states yielding large or negligible fractions of missing transverse momentum, respectively.

First we considered the production and decay of a possible BSM top partner into a final state involving a hadronically–decaying SM top plus a leptonically–decaying SM Z

boson at $\sqrt{s} = 13\,\text{TeV}$, exploiting a simplified–model approach. We have identified this final state because of its clean topology for a possible mass measurement. Both pair and single production of the top partner have been considered. Free parameters of our study are the mass of the top partner, and a dimensionless parameter g^* governing the rate of the single production cross section, namely the top partner coupling to SM bosons.

The main peculiarity of the considered signal topology is the highly boosted kinematics of the top partner decay products, namely the SM top and Z boson, in contrast to the SM background processes for which a large transverse boost for the top and Z is not expected. Jet–substructure methods and optimised kinematic selection cuts have been exploited to identify and reconstruct the candidate top partner from signal events, together with a large suppression of the otherwise dominant background processes. We showed that a large portion of parameter space of our simplified model, namely up to masses of 1450 GeV, can be probed to claim possible evidence or discovery of a top partner signal. Within our setup we evaluated the resolution of the mass measurement to be at worst $\pm 75\,\text{GeV}$, but a dedicated experimental analysis including additional sources of systematic uncertainties might realise more precise and robust results. Our study is indeed to be intended as a possible guideline for an actual experimental analysis, showing the feasibility of a possible top partner discovery and mass measurement.

In the second proposed analysis of Chapter 5 we discussed a mass determination method for the minimum symmetric event topology, namely pair production of a particle X with unknown mass, followed by its semi–invisible decay $X \to \ell\, N$, where ℓ is a SM charged lepton, and N is an invisible particle with a–priori unknown mass. As a specific topology, we considered the case in which X is pair produced from the decay of an s–channel particle.

By considering the boundary of the kinematically consistent mass region identified by the experimentally measured final state momenta, we defined kinematic variables which can be used in measuring the unknown m_{X}, m_{N} masses. We applied the discussed method to the specific example of a Minimal Supersymmetric Standard Model process, namely $pp \to A \to \tilde{\chi}_1^+ \tilde{\chi}_1^-$ followed by $\tilde{\chi}_1^\pm \to \ell^\pm \tilde{\nu}_\ell$, where A is the s–channel CP-odd Higgs decaying into a pair of lightest charginos $\tilde{\chi}_1^\pm$. In particular, we showed that our method provides a precise measurement of the chargino and sneutrino masses considering a possible LHC analysis with $\sqrt{s} = 14\,\text{TeV}$ and $300\,\text{fb}^{-1}$ of integrated luminosity, with the mass of the s–channel particle A as the only additional kinematic information to be included besides the measured final state momenta.

Summary and Outlook

In this thesis we have systematically analysed the consistency of different Little Higgs models in light of the recent data collected in collider experiments. The lack of specific analyses by the experimental collaborations within the framework of Little Higgs models motivated us to reinterpret the results to either strengthen the existing exclusion limits on the parameter space of the models, or to develop additional optimised searches. This gave us the opportunity to propose tailored analyses aiming at the discovery of specific new signals beyond the SM background.

From our results, many observations and questions arise. First of all, it is clear how the foreseen LHC runs with higher center–of–mass energy and integrated luminosity will boost the sensitivity to different "unexplored" regions of BSM parameter spaces, such that a semi–definitive conclusion on the naturalness of the considered models will be achieved. We have indeed shown that already 8 TeV searches are constraining the models without custodial symmetry protection to high fine–tuning regimes. In this regard, Higgs searches and direct searches are quickly becoming competitive with respect to existing limits from electroweak precision observables, making thus our analysis particularly attractive for forthcoming LHC measurements. The lack of indications of possible BSM signals should also motivate broader model–independent searches. However, it is still unclear how to uniquely associate a possible discovered BSM signal at the LHC to a specific model: studies involving angular observables will most probably be needed to disentangle different signal hypotheses, but their effective use within specific LHC analyses has to be clarified.

Appendix A

Additional topics

A.1 Coleman–Weinberg potential

We will discuss now an alternative way of presenting the hierarchy problem, which tuns out to be useful in order to show how different BSM implementations might represent viable natural extensions of the SM. Consider a quantum field theory of a scalar field ϕ, in the presence of an external source $J(x)$. One can define [160] the generating functional of connected correlation functions $W[J]$ by

$$\begin{aligned} Z[J] = e^{iW[J]} &= \int \mathcal{D}\phi \, \exp\left[i \int d^4x \, (\mathcal{L}[\phi] + J\phi)\right] \\ &\equiv \int \mathcal{D}\phi \, \exp\left[i \left(S[\phi] + J\phi\right)\right] . \end{aligned} \tag{A.1.1}$$

The functional derivative of $W[J]$ with respect to the auxiliary function $J(x)$ in different points x, y produces e.g. the connected correlator for the field ϕ between the points x, y

$$\frac{\delta^2 W[J]}{\delta J(x)\, \delta J(y)} = -i \langle \phi(x) \phi(y) \rangle_{\text{conn}} \, . \tag{A.1.2}$$

The functional derivative of $W[J]$ with respect to a single auxiliary function $J(x)$ produces on the other hand the vacuum expectation value of the field ϕ in the presence of a non–zero source $J(x)$:

$$\frac{\delta W[J]}{\delta J(x)} = -i \langle \phi(x) \rangle_{\text{J}} \equiv \phi_{\text{cl}}(x) \tag{A.1.3}$$

where $\phi_{\text{cl}}(x)$ is called the classical field, representing a weighted average of the quantum field $\phi(x)$ over all possible fluctuations.

Given a functional $W[J]$ we can perform a Legendre transform to obtain a functional

$\Gamma\left[\phi_{\rm cl}\right]$ known as the effective action

$$\begin{aligned}\Gamma\left[\phi_{\rm cl}\right] &= W[J] - \int d^4x\, J(x)\, \phi_{\rm cl}(x) \equiv W[J] - J\,\phi_{\rm cl} = \\ &= \int d^4x \left[-V_{\rm eff}\left(\phi_{\rm cl}\right) + Z(\phi_{\rm cl})\left(\partial\phi_{\rm cl}\right)^2 + \dots\right] \end{aligned} \qquad \text{(A.1.4)}$$

where in the last equality we have expanded the effective action in powers of derivatives with respect to the classical field. In the absence of an external source $J(x)$, one can show that the x–independent vacuum expectation value of $\phi(x)$, namely $\phi_{\rm cl}$, can be determined by minimizing $V_{\rm eff}\left(\phi_{\rm cl}\right)$:

$$\frac{\partial}{\partial\phi_{\rm cl}} V_{\rm eff} = 0\,. \qquad \text{(A.1.5)}$$

For this reason $V_{\rm eff}$ is called the *effective potential* of our quantum field theory, where all–order quantum contributions are included.

Now, all of these formal manipulations are not worth much if we cannot evaluate $W[J]$ and therefore $V_{\rm eff}$. In most cases we can only evaluate $Z[J]$ (A.1.1) in the steepest descent approximation, namely by expanding around the $\phi_{\rm s}(x)$ solution of

$$\frac{\delta\left(S[\phi] + J\phi\right)}{\delta\phi(x)}\Big|_{\phi_{\rm s}} = \frac{\delta S[\phi]}{\delta\phi(x)}\Big|_{\phi_{\rm s}} + J(x) = 0\,. \qquad \text{(A.1.6)}$$

By writing the integration variable in (A.1.1) as $\phi = \phi_{\rm s} + \tilde\phi$, and expanding to quadratic order in $\tilde\phi$ one obtains (re–introducing the $\hbar$–dependence)

$$\begin{aligned} Z[J] &\sim \int \mathcal{D}\tilde\phi\, \exp\frac{i}{\hbar}\left[\left(S(\phi_{\rm s}) + J\phi_{\rm s}\right) + \frac{\delta\left(S[\tilde\phi] + J\tilde\phi\right)}{\delta\tilde\phi(x)}\Big|_{\phi_{\rm s}}\tilde\phi + \frac{1}{2}\frac{\delta^2 S[\tilde\phi]}{\delta\tilde\phi(x)\delta\tilde\phi(y)}\Big|_{\phi_{\rm s}}\tilde\phi^2\right] \\ &= \left(\exp\frac{i}{\hbar}\left[S(\phi_{\rm s}) + J\phi_{\rm s}\right]\right)\int\mathcal{D}\tilde\phi\,\exp\frac{i}{\hbar}\left[\frac{1}{2}\frac{\delta^2 S[\tilde\phi]}{\delta\tilde\phi(x)\delta\tilde\phi(y)}\tilde\phi^2\right] \\ &= \left(\exp\frac{i}{\hbar}\left[S(\phi_{\rm s}) + J\phi_{\rm s}\right]\right)\det\left[\frac{\delta^2 S[\tilde\phi]}{\delta\tilde\phi(x)\delta\tilde\phi(y)}\right]^{-\frac{1}{2}} \\ &= \exp\left(\frac{i}{\hbar}\left[S(\phi_{\rm s}) + J\phi_{\rm s}\right] - \frac{1}{2}\,{\rm Tr}\,\log\left[\frac{\delta^2 S[\tilde\phi]}{\delta\tilde\phi(x)\delta\tilde\phi(y)}\right]\right)\,. \end{aligned} \qquad \text{(A.1.7)}$$

From eq. (A.1.7) we thus have (writing for simplicity ϕ instead of $\tilde\phi$)

$$\begin{aligned} W[J] &= S(\phi_{\rm s}) + J\phi_{\rm s} + \frac{i\hbar}{2}\,{\rm Tr}\,\log\left[\frac{\delta^2 S[\phi]}{\delta\phi(x)\delta\phi(y)}\right] + \mathcal{O}(\hbar^2) \\ &= S(\phi_{\rm cl}) + J\phi_{\rm cl} + \frac{i\hbar}{2}\,{\rm Tr}\,\log\left[\frac{\delta^2 S[\phi]}{\delta\phi(x)\delta\phi(y)}\right] + \mathcal{O}(\hbar^2) \end{aligned} \qquad \text{(A.1.8)}$$

where in the last equality we observed that $\phi_{\rm cl} = \phi_{\rm s} + \mathcal{O}(\hbar)$. Finally, from eq. (A.1.4) we obtain

$$\begin{aligned} \Gamma[\phi_{\rm cl}] = W[J] - J\,\phi_{\rm cl} = S(\phi_{\rm cl}) + \frac{i\hbar}{2}\,\mathrm{Tr}\,\log\left[\frac{\delta^2 S[\phi]}{\delta\phi(x)\delta\phi(y)}\right] + \mathcal{O}(\hbar^2) = \\ = \int d^4x\,\left[-V_{\rm eff}(\phi_{\rm cl}) + \ldots\right] \end{aligned} \tag{A.1.9}$$

and it is straightforward to conclude that the effective potential can be written as

$$V_{\rm eff}(\phi) = V(\phi) - \frac{i\hbar}{2}\,\mathrm{Tr}\,\log\left[\frac{\delta^2 S[\phi]}{\delta\phi(x)\delta\phi(y)}\right] + \mathcal{O}(\hbar^2) \tag{A.1.10}$$

known as the *Coleman–Weinberg* effective potential [161]. What we have computed is the order $\hbar$ correction to the classical tree–level potential $V(\phi)$.

For a scalar field ϕ with Lagrangian $\mathcal{L} = \frac{1}{2}\left(\partial\phi\right)^2 - V(\phi)$ one can evaluate the effective potential (A.1.10), after a proper Wick–rotation, as

$$V_{\rm eff}(\phi) = V(\phi) - \frac{i\hbar}{2}\int\frac{d^4\,k}{(2\pi)^4}\log\left[\frac{k^2 - V''(\phi)}{k^2}\right] + \mathcal{O}(\hbar^2)\,. \tag{A.1.11}$$

This divergent integral can be calculated using a momentum cut–off Λ, obtaining

$$\begin{aligned} V_{\rm eff}(\phi) &= V_{\rm tree}(\phi) + \hbar\,V_{\rm 1\text{–}loop}(\phi) + \mathcal{O}(\hbar^2) \\ &= V(\phi) + \hbar\left(\frac{\Lambda^2}{32\pi^2}V''(\phi) - \frac{[V''(\phi)]^2}{64\pi^2}\log\frac{e^{\frac{1}{2}}\Lambda^2}{V''(\phi)}\right) + \mathcal{O}(\hbar^2)\,. \end{aligned} \tag{A.1.12}$$

This result can be extended by considering a generic field ψ which couples to the scalar ϕ with an interaction term like $M(\phi)\bar{\psi}\,\psi$, where $M(\phi)$ is a model–dependent function of the scalar field:

$$V_{\rm 1\text{–}loop}(\phi) = \frac{\Lambda^2}{64\pi^2}\,\mathrm{Str}\left[M^\dagger(\phi)\,M(\phi)\right] - \frac{1}{64\pi^2}\,\mathrm{Str}\left[\left(M^\dagger(\phi)\,M(\phi)\right)^2\right]\log\frac{\Lambda^2}{\mu^2} \tag{A.1.13}$$

where the super–trace Str is defined as the sum over the contributions of particles with spin s, weighted by $(2s+1)\cdot(-1)^{2s}$.

Let us consider the top–Yukawa coupling in the SM as an example. The Lagrangian term is given by

$$\mathcal{L}_{\rm H} \supset \frac{Y_t}{\sqrt{2}}\,\bar{t}_L\,t_R\,H + \text{ h.c.} \quad\Rightarrow\quad M(H) = \begin{pmatrix} 0 & H\frac{Y_t}{\sqrt{2}} \\ H\frac{Y_t}{\sqrt{2}} & 0 \end{pmatrix} \tag{A.1.14}$$

from which we can evaluate the contribution of the top loop to the Higgs potential using eq. (A.1.13) to be

$$V_{\rm 1\text{–}loop}(H) \supset N_c\cdot 2\cdot(-1)\,\mathrm{Tr}\left[\mathbb{1}\frac{Y_t^2}{2}H^2\right]\frac{\Lambda^2}{64\pi^2} = -\frac{3}{32\pi^2}Y_t^2\Lambda^2 H^2\,. \tag{A.1.15}$$

The Higgs potential therefore has a quadratic sensitivity in the momentum cut–off once we consider the one–loop correction given by the top Yukawa. Including the one–loop contributions generated by the diagrams in figure 2.6 one can finally obtain the total Λ^2 contribution to the Higgs potential as

$$V_{\text{1–loop}}(H) \supset \frac{1}{2}\left[\frac{1}{4}\left(9g' + 3g'^2\right) - 6\,Y_t^2 + 6\,\lambda\right]\frac{3}{32\pi^2}\Lambda^2 H^2\,. \tag{A.1.16}$$

which needs to be highly fine–tuned against the bare mass term of the Higgs in order to correctly reproduce the experimental value, if we assume a large cut–off scale Λ above the electroweak scale.

Appendix B

Experimental Data

B.1 Electroweak Precision data

Observable	Experimental value	SM prediction	Description
Γ_Z [GeV]	2.4952 ± 0.0023	2.4961 ± 0.0010	total Z width
$\sigma_{\rm had}$ [nb]	41.541 ± 0.037	41.477 ± 0.009	$\sigma(e^+e^- \to f\bar{f})$ at Z pole
R_e	20.804 ± 0.050	20.744 ± 0.011	$\Gamma(Z \to {\rm had})/\Gamma(Z \to e^+e^-)$
R_μ	20.785 ± 0.033	20.744 ± 0.011	$\Gamma(Z \to {\rm had})/\Gamma(Z \to \mu^+\mu^-)$
R_τ	20.764 ± 0.045	20.789 ± 0.011	$\Gamma(Z \to {\rm had})/\Gamma(Z \to \tau^+\tau^-)$
R_b	0.21629 ± 0.00066	0.21576 ± 0.00004	$\Gamma(Z \to b\bar{b})/\Gamma(Z \to {\rm had})$
R_c	0.1721 ± 0.0030	0.17227 ± 0.00004	$\Gamma(Z \to c\bar{c})/\Gamma(Z \to {\rm had})$
$A^e_{\rm FB}$	0.0145 ± 0.0025	0.01633 ± 0.00021	F/B asymm. in $e^+e^- \to e^+e^-$
$A^\mu_{\rm FB}$	0.0169 ± 0.0013	0.01633 ± 0.00021	F/B asymm. in $e^+e^- \to \mu^+\mu^-$
$A^\tau_{\rm FB}$	0.0188 ± 0.0017	0.01633 ± 0.00021	F/B asymm. in $e^+e^- \to \tau^+\tau^-$
$A^b_{\rm FB}$	0.0992 ± 0.0016	0.1034 ± 0.0007	F/B asymm. in $e^+e^- \to b\bar{b}$
$A^c_{\rm FB}$	0.0707 ± 0.0035	0.0739 ± 0.0005	F/B asymm. in $e^+e^- \to c\bar{c}$
$A_{\rm LR}$	0.15138 ± 0.00216	0.1475 ± 0.0010	L/R asymm. in $e^+e^- \to e^+e^-$
$A_{\rm pol}(\tau)$	0.1439 ± 0.0043	0.1475 ± 0.0010	τ–polarization asymmetry
$A_e(P_\tau)$	0.1498 ± 0.0049	0.1475 ± 0.0010	joint FB/LR asymmetry
m_W [GeV]	80.420 ± 0.031	80.381 ± 0.014	pole W mass
g_L^2	0.3009 ± 0.0028	0.3040 ± 0.0002	$(\nu\, N \to \nu\, X)$ scattering
g_R^2	0.0328 ± 0.0030	0.03001 ± 0.00002	$(\nu\, N \to \nu\, X)$ scattering
$g_V^{\nu e}$	-0.040 ± 0.015	-0.0398 ± 0.0003	$(\nu\, e \to \nu\, e)$ scattering
$g_A^{\nu e}$	-0.507 ± 0.014	-0.5064 ± 0.0001	$(\nu\, e \to \nu\, e)$ scattering
$Q_W({\rm Cs})$	-73.20 ± 0.35	-73.23 ± 0.02	atomic parity violation in Cs

Table B.1: *Experimental and SM values of 21 EW and low–energy precision observables [22].*

B.2 Higgs Precision data: ATLAS

Channel	$\hat{\mu}$ (7 TeV)	$\zeta_i^{(\mathrm{g,V,t})}$ (%)	$\hat{\mu}$ (8 TeV)	$\zeta_i^{(\mathrm{g,V,t})}$ (%)	Refs.
$b\bar{b}$ (VH)	combination	—	$-0.42^{+1.05}_{-1.05}$	$(0, 100, 0)$	[162]
$b\bar{b}$ (ttH)	3.81 ± 5.78	$(0, 30, 70)$	—	—	[163]
$\tau\tau$	combination	—	$0.7^{+0.7}_{-0.7}$	$(20, 80, 0)$	[164]
$WW\,(0j)$	0.06 ± 0.60	inclusive	$0.92^{+0.63}_{-0.49}$	inclusive	[165]
$WW\,(1j)$	$2.04^{+1.88}_{-1.30}$	inclusive	$1.11^{+1.20}_{-0.82}$	inclusive	
$WW\,(2j)$	—	—	$1.79^{+0.94}_{-0.75}$	$(20, 80, 0)$	
ZZ	combination	—	$1.7^{+0.5}_{-0.4}$	inclusive	[166]
$\gamma\gamma_{(\mathrm{L})}$ (uc|ct)	$0.53^{+1.37}_{-1.44}$	$(93, 7, 0)$	$0.86^{+0.67}_{-0.67}$	$(93.7, 6.2, 0.2)$	
$\gamma\gamma_{(\mathrm{H})}$ (uc|ct)	$0.17^{+1.94}_{-1.91}$	$(67, 31, 2)$	$0.92^{+1.1}_{-0.89}$	$(79.3, 19.2, 1.4)$	
$\gamma\gamma_{(\mathrm{L})}$ (uc|ec)	$2.51^{+1.66}_{-1.69}$	$(93, 7, 0)$	$2.51^{+0.84}_{-0.75}$	$(93.2, 6.6, 0.1)$	
$\gamma\gamma_{(\mathrm{H})}$ (uc|ec)	$10.39^{+3.67}_{-3.67}$	$(65, 33, 2)$	$2.69^{+1.31}_{-1.08}$	$(78.1, 20.8, 1.1)$	
$\gamma\gamma_{(\mathrm{L})}$ (c|ct)	$6.08^{+2.59}_{-2.63}$	$(93, 7, 0)$	$1.37^{+1.02}_{-0.88}$	$(93.6, 6.2, 0.2)$	
$\gamma\gamma_{(\mathrm{H})}$ (c|ct)	$-4.40^{+1.80}_{-1.76}$	$(67, 31, 2)$	$1.99^{+1.50}_{-1.22}$	$(78.9, 19.6, 1.5)$	
$\gamma\gamma_{(\mathrm{L})}$ (c|ec)	$2.73^{+1.91}_{-2.02}$	$(93, 7, 0)$	$2.21^{+1.13}_{-0.95}$	$(93.2, 6.7, 0.1)$	
$\gamma\gamma_{(\mathrm{H})}$ (c|ec)	$-1.63^{+2.88}_{-2.88}$	$(65, 33, 2)$	$1.26^{+1.31}_{-1.22}$	$(77.7, 21.2, 1.1)$	[167]
$\gamma\gamma$ (c|trans.)	$0.35^{+3.56}_{-3.60}$	$(89, 11, 0)$	$2.80^{+1.64}_{-1.55}$	$(90.7, 9.0, 0.2)$	[168]
$\gamma\gamma$ (dijet)	$2.69^{+1.87}_{-1.84}$	$(23, 77, 0)$	—	—	
$\gamma\gamma$ (m_{jj} high loose)	—	—	$2.76^{+1.73}_{-1.35}$	$(45, 54.9, 0.1)$	
$\gamma\gamma$ (m_{jj} high tight)	—	—	$1.59^{+0.84}_{-0.62}$	$(23.8, 76.2, 0)$	
$\gamma\gamma$ (m_{jj} low)	—	—	$0.33^{+1.68}_{-1.46}$	$(48.1, 49.9, 1.9)$	
$\gamma\gamma$ ($E_{\mathrm{T}}^{\mathrm{miss}}$)	—	—	$2.98^{+2.70}_{-2.15}$	$(4.1, 83.8, 12.1)$	
$\gamma\gamma$ (lepton tag)	—	—	$2.69^{+1.95}_{-1.66}$	$(2.2, 79.2, 18.6)$	

Table B.2: *ATLAS best fits on signal strength modifier μ with signal compositions ζ_i^p (if provided) for gluon (g), vector (V), and top (t) initiated production. If* inclusive *is denoted, the cut efficiencies have been neglected when evaluating μ, see [8, 9, 169], while if* combination *is denoted, only the 7+8 TeV combined result is available.*

B.3 Higgs Precision data: CMS

Channel	$\hat{\mu}$ (7 TeV)	$\zeta_i^{(\mathrm{g,V,t})}$ (%)	$\hat{\mu}$ (8 TeV)	$\zeta_i^{(\mathrm{g,V,t})}$ (%)	Refs.
$b\bar{b}$ (VBF)	—	—	$0.7^{+1.4}_{-1.4}$	$(0, 100, 0)$	[170]
$b\bar{b}$ (VH)	combination	—	$1.0^{+0.5}_{-0.5}$	$(0, 100, 0)$	[171]
$b\bar{b}$ (ttH)	$-0.81^{+2.05}_{-1.75}$	$(0, 30, 70)$	—	—	[172]
$\tau\tau$ $(0/1j)$	combination	—	$0.74^{+0.49}_{-0.52}$	inclusive	[173]
$\tau\tau$ (VBF)	combination	—	$1.38^{+0.61}_{-0.57}$	$(0, 100, 0)$	
$\tau\tau$ (VH)	combination	—	$0.76^{+1.48}_{-1.43}$	$(0, 100, 0)$	
WW $(0/1j)$	combination	—	$0.76^{+0.21}_{-0.21}$	inclusive	[174]
WW $(2j)$	combination	—	$-0.05^{+0.73}_{-0.56}$	$(17, 83, 0)$	
WW (VH)	combination	—	$-0.31^{+2.24}_{-1.96}$	$(0, 100, 0)$	
ZZ (untagged)	combination	—	$0.84^{+0.32}_{-0.26}$	$(95, 5, 0)$	[175]
ZZ (dijet tag)	—	—	$1.22^{+0.84}_{-0.57}$	$(80, 20, 0)$	
$\gamma\gamma$ (no tag 0)	$3.78^{+2.01}_{-1.62}$	$(61.4, 35.5, 3.1)$	$2.12^{+0.92}_{-0.78}$	$(72.9, 24.6, 2.6)$	[176]
$\gamma\gamma$ (no tag 1)	$0.15^{+0.99}_{-0.92}$	$(87.6, 11.8, 0.5)$	$-0.03^{+0.71}_{-0.64}$	$(83.5, 15.5, 1.0)$	
$\gamma\gamma$ (no tag 2)	$-0.05^{+1.21}_{-1.21}$	$(91.3, 8.3, 0.3)$	$0.22^{+0.46}_{-0.42}$	$(91.7, 7.9, 0.4)$	
$\gamma\gamma$ (no tag 3)	$1.38^{+1.66}_{-1.55}$	$(91.3, 8.5, 0.2)$	$-0.81^{+0.85}_{-0.42}$	$(92.5, 7.2, 0.2)$	
$\gamma\gamma$ (dijet)	$4.13^{+2.33}_{-1.76}$	$(26.8, 73.1, 0.0)$	—	—	
$\gamma\gamma$ (dijet loose)	—	—	$0.75^{+1.06}_{-0.99}$	$(46.8, 52.8, 0.5)$	
$\gamma\gamma$ (dijet tight)	—	—	$0.22^{+0.71}_{-0.57}$	$(20.7, 79.2, 0.1)$	
$\gamma\gamma$ (MET)	—	—	$1.84^{+2.65}_{-2.26}$	$(0.0, 79.3, 20.8)$	
$\gamma\gamma$ (Electron)	—	—	$-0.70^{+2.75}_{-1.94}$	$(1.1, 79.3, 19.7)$	
$\gamma\gamma$ (Muon)	—	—	$0.36^{+1.84}_{-1.38}$	$(21.1, 67.0, 11.8)$	

Table B.3: *CMS best fits on signal strength modifier* μ *with signal compositions* ζ_i^p *(if provided) for gluon (*g*), vector (*V*), and top (*t*) initiated production [169]. If* inclusive *is denoted, the cut efficiencies have been neglected when evaluating* μ*, see [8, 9, 169], while if* combination *is denoted, only the* 7+8 *TeV combined result is available.*

Bibliography

[1] F. Englert and R. Brout, *Broken Symmetry and the Mass of Gauge Vector Mesons*, *Phys.Rev.Lett.* **13** (1964) 321–323.

[2] G. Guralnik, C. Hagen, and T. Kibble, *Global Conservation Laws and Massless Particles*, *Phys.Rev.Lett.* **13** (1964) 585–587.

[3] P. W. Higgs, *Broken Symmetries and the Masses of Gauge Bosons*, *Phys.Rev.Lett.* **13** (1964) 508–509.

[4] P. W. Higgs, *Broken symmetries, massless particles and gauge fields*, *Phys.Lett.* **12** (1964) 132–133.

[5] **CMS Collaboration**, S. Chatrchyan et al., *Observation of a new boson at a mass of 125 GeV with the CMS experiment at the LHC*, *Phys.Lett.* **B716** (2012) 30–61, [`arXiv:1207.7235`].

[6] **ATLAS Collaboration**, G. Aad et al., *Observation of a new particle in the search for the Standard Model Higgs boson with the ATLAS detector at the LHC*, *Phys.Lett.* **B716** (2012) 1–29, [`arXiv:1207.7214`].

[7] J. Reuter and M. Tonini, *Can the 125 GeV Higgs be the Little Higgs?*, *JHEP* **1302** (2013) 077, [`arXiv:1212.5930`].

[8] J. Reuter, M. Tonini, and M. de Vries, *Little Higgs Model Limits from LHC - Input for Snowmass 2013*, `arXiv:1307.5010`.

[9] J. Reuter, M. Tonini, and M. de Vries, *Littlest Higgs with T-parity: Status and Prospects*, *JHEP* **1402** (2014) 053, [`arXiv:1310.2918`].

[10] J. Reuter and M. Tonini, *Top Partner Discovery in the $T \to tZ$ channel at the LHC*, `arXiv:1409.6962`.

[11] L. A. Harland-Lang, C.-H. Kom, K. Sakurai, and M. Tonini, *Sharpening m_{T2} cusps: the mass determination of semi-invisibly decaying particles from a resonance*, *JHEP* **1406** (2014) 175, [arXiv:1312.5720].

[12] R. Contino, *New Physics at the LHC: Strong versus Weak symmetry breaking*, *Nuovo Cim.* **C32N3-4** (2009) 11–18, [arXiv:0908.3578].

[13] R. Contino, *The Higgs as a Composite Nambu-Goldstone Boson*, arXiv:1005.4269.

[14] T. Plehn, *Lectures on LHC Physics*, *Lect.Notes Phys.* **844** (2012) 1–193, [arXiv:0910.4182].

[15] D. Buttazzo, *Implications of the discovery of a Higgs boson with a mass of 125 GeV*, arXiv:1403.6535.

[16] D. Curtin, *Model building and collider physics above the weak scale*, PhD Thesis.

[17] M. Schmaltz and D. Tucker-Smith, *Little Higgs review*, *Ann.Rev.Nucl.Part.Sci.* **55** (2005) 229–270, [hep-ph/0502182].

[18] S. R. Coleman, J. Wess, and B. Zumino, *Structure of phenomenological Lagrangians. 1.*, *Phys.Rev.* **177** (1969) 2239–2247.

[19] J. Callan, Curtis G., S. R. Coleman, J. Wess, and B. Zumino, *Structure of phenomenological Lagrangians. 2.*, *Phys.Rev.* **177** (1969) 2247–2250.

[20] A. Manohar and H. Georgi, *Chiral Quarks and the Nonrelativistic Quark Model*, *Nucl.Phys.* **B234** (1984) 189.

[21] **LEP, ALEPH, DELPHI, L3, OPAL, LEP EWWG, SLD EW, SLD Heavy Flavor Collaborations**, *A Combination of preliminary electroweak measurements and constraints on the standard model*, hep-ex/0312023.

[22] **Particle Data Group**, J. Beringer et al., *Review of Particle Physics (RPP)*, *Phys.Rev.* **D86** (2012) 010001.

[23] M. E. Peskin and T. Takeuchi, *Estimation of oblique electroweak corrections*, *Phys.Rev.* **D46** (1992) 381–409.

[24] R. Barbieri, A. Pomarol, R. Rattazzi, and A. Strumia, *Electroweak symmetry breaking after LEP-1 and LEP-2*, *Nucl.Phys.* **B703** (2004) 127–146, [hep-ph/0405040].

[25] H. Georgi, *Effective field theory and electroweak radiative corrections*, *Nucl.Phys.* **B363** (1991) 301–325.

[26] M. Perelstein, *Little Higgs models and their phenomenology*, *Prog.Part.Nucl.Phys.* **58** (2007) 247–291, [`hep-ph/0512128`].

[27] M. Schmaltz and J. Thaler, *Collective Quartics and Dangerous Singlets in Little Higgs*, *JHEP* **0903** (2009) 137, [`arXiv:0812.2477`].

[28] J. Kearney, A. Pierce, and J. Thaler, *Exotic Top Partners and Little Higgs*, *JHEP* **1310** (2013) 230, [`arXiv:1306.4314`].

[29] T. Han, H. E. Logan, and L.-T. Wang, *Smoking-gun signatures of little Higgs models*, *JHEP* **0601** (2006) 099, [`hep-ph/0506313`].

[30] K. Cheung and J. Song, *Light pseudoscalar eta and $H \to \eta\eta$ decay in the simplest little Higgs mode*, *Phys.Rev.* **D76** (2007) 035007, [`hep-ph/0611294`].

[31] F. del Aguila, J. I. Illana, and M. D. Jenkins, *Lepton flavor violation in the Simplest Little Higgs model*, *JHEP* **1103** (2011) 080, [`arXiv:1101.2936`].

[32] W. Kilian, D. Rainwater, and J. Reuter, *Pseudo-axions in little Higgs models*, *Phys.Rev.* **D71** (2005) 015008, [`hep-ph/0411213`].

[33] W. Kilian, D. Rainwater, and J. Reuter, *Distinguishing little-Higgs product and simple group models at the LHC and ILC*, *Phys.Rev.* **D74** (2006) 095003, [`hep-ph/0609119`].

[34] W. Kilian and J. Reuter, *The Low-energy structure of little Higgs models*, *Phys.Rev.* **D70** (2004) 015004, [`hep-ph/0311095`].

[35] T. Han, H. E. Logan, B. McElrath, and L.-T. Wang, *Phenomenology of the little Higgs model*, *Phys.Rev.* **D67** (2003) 095004, [`hep-ph/0301040`].

[36] J. Hubisz and P. Meade, *Phenomenology of the littlest Higgs with T-parity*, *Phys.Rev.* **D71** (2005) 035016, [`hep-ph/0411264`].

[37] J. Hubisz, P. Meade, A. Noble, and M. Perelstein, *Electroweak precision constraints on the littlest Higgs model with T parity*, *JHEP* **0601** (2006) 135, [`hep-ph/0506042`].

[38] C.-R. Chen, K. Tobe, and C.-P. Yuan, *Higgs boson production and decay in little Higgs models with T-parity*, *Phys.Lett.* **B640** (2006) 263–271, [hep-ph/0602211].

[39] A. Belyaev, C.-R. Chen, K. Tobe, and C.-P. Yuan, *Phenomenology of littlest Higgs model with T-parity: including effects of T-odd fermions*, *Phys.Rev.* **D74** (2006) 115020, [hep-ph/0609179].

[40] M. Blanke, A. J. Buras, A. Poschenrieder, S. Recksiegel, C. Tarantino, et al., *Rare and CP-Violating K and B Decays in the Littlest Higgs Model with T-Parity*, *JHEP* **0701** (2007) 066, [hep-ph/0610298].

[41] **ATLAS Collaboration**, *Search for heavy top-like quarks decaying to a Higgs boson and a top quark in the lepton plus jets final state in pp collisions at* $\sqrt{s} = 8$ *TeV with the ATLAS detector*, tech. rep., ATLAS-CONF-2013-018, ATLAS-COM-CONF-2013-024, 2013.

[42] **ATLAS Collaboration**, *Search for pair production of heavy top-like quarks decaying to a high-*p_{T} *W boson and a b quark in the lepton plus jets final state in pp collisions at* $\sqrt{s} = 8$ *TeV with the ATLAS detector*, tech. rep., ATLAS-CONF-2013-060, ATLAS-COM-CONF-2013-066, 2013.

[43] **ATLAS Collaboration**, *Search for pair production of new heavy quarks that decay to a Z boson and a third generation quark in pp collisions at* $\sqrt{s} = 8$ *TeV with the ATLAS detector*, tech. rep., ATLAS-CONF-2013-056, ATLAS-COM-CONF-2013-070, 2013.

[44] **ATLAS Collaboration**, *Search for anomalous production of events with same-sign dileptons and b jets in 14.3* fb^{-1} *of pp collisions at* $\sqrt{s} = 8$ *TeV with the ATLAS detector*, tech. rep., ATLAS-CONF-2013-051, ATLAS-COM-CONF-2013-055, 2013.

[45] **ATLAS Collaboration**, *Search for high-mass dilepton resonances in 20* fb^{-1} *of pp collisions at* $\sqrt{s} = 8$ *TeV with the ATLAS experiment*, tech. rep., ATLAS-CONF-2013-017, ATLAS-COM-CONF-2013-010, 2013.

[46] **ATLAS Collaboration**, *Search for high-mass states with one lepton plus missing transverse momentum in pp collisions at* $\sqrt{s} = 8$ *TeV with the ATLAS detector*, tech. rep., ATLAS-CONF-2014-017, ATLAS-COM-CONF-2014-017, 2014.

[47] N. Arkani-Hamed, A. G. Cohen, and H. Georgi, *Electroweak symmetry breaking from dimensional deconstruction*, *Phys.Lett.* **B513** (2001) 232–240, [hep-ph/0105239].

[48] N. Arkani-Hamed, A. G. Cohen, T. Gregoire, and J. G. Wacker, *Phenomenology of electroweak symmetry breaking from theory space*, *JHEP* **0208** (2002) 020, [hep-ph/0202089].

[49] N. Arkani-Hamed, A. Cohen, E. Katz, and A. Nelson, *The Littlest Higgs*, *JHEP* **0207** (2002) 034, [hep-ph/0206021].

[50] S. Chang, *A "Littlest Higgs" model with custodial SU(2) symmetry*, *JHEP* **0312** (2003) 057, [hep-ph/0306034].

[51] D. E. Kaplan and M. Schmaltz, *The Little Higgs from a simple group*, *JHEP* **0310** (2003) 039, [hep-ph/0302049].

[52] M. Schmaltz, *The Simplest little Higgs*, *JHEP* **0408** (2004) 056, [hep-ph/0407143].

[53] H.-C. Cheng and I. Low, *TeV symmetry and the little hierarchy problem*, *JHEP* **0309** (2003) 051, [hep-ph/0308199].

[54] H.-C. Cheng and I. Low, *Little hierarchy, little Higgses, and a little symmetry*, *JHEP* **0408** (2004) 061, [hep-ph/0405243].

[55] D. Pappadopulo and A. Vichi, *T-parity, its problems and their solution*, *JHEP* **1103** (2011) 072, [arXiv:1007.4807].

[56] I. Low, W. Skiba, and D. Tucker-Smith, *Little Higgses from an antisymmetric condensate*, *Phys.Rev.* **D66** (2002) 072001, [hep-ph/0207243].

[57] M. Schmaltz, D. Stolarski, and J. Thaler, *The Bestest Little Higgs*, *JHEP* **1009** (2010) 018, [arXiv:1006.1356].

[58] C. T. Hill and R. J. Hill, *Topological Physics of Little Higgs Bosons*, *Phys.Rev.* **D75** (2007) 115009, [hep-ph/0701044].

[59] O. C. Kong, *A Completed chiral fermionic sector model with little Higgs*, hep-ph/0307250.

[60] O. C. Kong, *Flavor and little Higgs*, *J.Korean Phys.Soc.* **45** (2004) S404–S409, [hep-ph/0312060].

[61] L. Wang and J. M. Yang, *The LHC di-photon Higgs signal predicted by little Higgs models*, *Phys.Rev.* **D84** (2011) 075024, [arXiv:1106.3916].

[62] B. Yang, G. Mi, and N. Liu, *Higgs couplings and Naturalness in the littlest Higgs model with T-parity at the LHC and TLEP*, *JHEP* **1410** (2014) 47, [arXiv:1407.6123].

[63] R. Barbieri, B. Bellazzini, V. S. Rychkov, and A. Varagnolo, *The Higgs boson from an extended symmetry*, *Phys.Rev.* **D76** (2007) 115008, [arXiv:0706.0432].

[64] C. Burgess, S. Godfrey, H. Konig, D. London, and I. Maksymyk, *Model independent global constraints on new physics*, *Phys.Rev.* **D49** (1994) 6115–6147, [hep-ph/9312291].

[65] G. Marandella, C. Schappacher, and A. Strumia, *Little-Higgs corrections to precision data after LEP2*, *Phys.Rev.* **D72** (2005) 035014, [hep-ph/0502096].

[66] C. Csaki, J. Hubisz, G. D. Kribs, P. Meade, and J. Terning, *Big corrections from a little Higgs*, *Phys.Rev.* **D67** (2003) 115002, [hep-ph/0211124].

[67] J. Berger, J. Hubisz, and M. Perelstein, *A Fermionic Top Partner: Naturalness and the LHC*, *JHEP* **1207** (2012) 016, [arXiv:1205.0013].

[68] M. Asano, S. Matsumoto, N. Okada, and Y. Okada, *Cosmic positron signature from dark matter in the littlest Higgs model with T-parity*, *Phys.Rev.* **D75** (2007) 063506, [hep-ph/0602157].

[69] LHC Higgs Cross Section Working Group, S. Dittmaier, C. Mariotti, G. Passarino, and R. Tanaka (Eds.), *Handbook of LHC Higgs Cross Sections: 1. Inclusive Observables*, *CERN-2011-002* (CERN, Geneva, 2011) [arXiv:1101.0593].

[70] LHC Higgs Cross Section Working Group, S. Dittmaier, C. Mariotti, G. Passarino, and R. Tanaka (Eds.), *Handbook of LHC Higgs Cross Sections: 2. Differential Distributions*, *CERN-2012-002* (CERN, Geneva, 2012) [arXiv:1201.3084].

[71] LHC Higgs Cross Section Working Group, S. Heinemeyer, C. Mariotti, G. Passarino, and R. Tanaka (Eds.), *Handbook of LHC Higgs Cross Sections: 3. Higgs Properties*, *CERN-2013-004* (CERN, Geneva, 2013) [arXiv:1307.1347].

[72] **ATLAS Collaboration**, G. Aad et al., *Measurement of the Higgs boson mass from the* $H \to \gamma\gamma$ *and* $H \to ZZ^* \to 4\ell$ *channels with the ATLAS detector using 25* fb^{-1} *of pp collision data*, arXiv:1406.3827.

[73] **CMS Collaboration**, *Precise determination of the mass of the Higgs boson and studies of the compatibility of its couplings with the standard model*, tech. rep., CMS-PAS-HIG-14-009, 2014.

[74] J. F. Gunion, H. E. Haber, G. L. Kane, and S. Dawson, *The Higgs Hunter's Guide*, *Front.Phys.* **80** (2000) 1–448.

[75] J. F. Gunion, H. E. Haber, G. L. Kane, and S. Dawson, *Errata for the Higgs hunter's guide*, hep-ph/9302272.

[76] **ATLAS Collaboration**, G. Aad et al., *Searches for heavy long-lived sleptons and R-Hadrons with the ATLAS detector in pp collisions at* $\sqrt{s} = 7$ *TeV*, *Phys.Lett.* **B720** (2013) 277–308, [arXiv:1211.1597].

[77] R. Barbieri, C. Berat, M. Besancon, M. Chemtob, A. Deandrea, et al., *R-parity violating supersymmetry*, *Phys.Rept.* **420** (2005) 1–202, [hep-ph/0406039].

[78] W. Beenakker, R. Hopker, and M. Spira, *PROSPINO: A Program for the production of supersymmetric particles in next-to-leading order QCD*, hep-ph/9611232.

[79] N. D. Christensen and C. Duhr, *FeynRules - Feynman rules made easy*, *Comput.Phys.Commun.* **180** (2009) 1614–1641, [arXiv:0806.4194].

[80] C. Degrande, C. Duhr, B. Fuks, D. Grellscheid, O. Mattelaer, et al., *UFO - The Universal FeynRules Output*, *Comput.Phys.Commun.* **183** (2012) 1201–1214, [arXiv:1108.2040].

[81] M. Moretti, T. Ohl, and J. Reuter, *O'Mega: An Optimizing matrix element generator*, hep-ph/0102195.

[82] W. Kilian, T. Ohl, and J. Reuter, *WHIZARD: Simulating Multi-Particle Processes at LHC and ILC*, *Eur.Phys.J.* **C71** (2011) 1742, [arXiv:0708.4233].

[83] N. D. Christensen, C. Duhr, B. Fuks, J. Reuter, and C. Speckner, *Introducing an interface between WHIZARD and FeynRules*, *Eur.Phys.J.* **C72** (2012) 1990, [arXiv:1010.3251].

[84] J. Alwall, M. Herquet, F. Maltoni, O. Mattelaer, and T. Stelzer, *MadGraph 5 : Going Beyond*, *JHEP* **1106** (2011) 128, [arXiv:1106.0522].

[85] T. Sjoestrand, S. Mrenna, and P. Z. Skands, *PYTHIA 6.4 Physics and Manual*, *JHEP* **0605** (2006) 026, [hep-ph/0603175].

[86] **DELPHES 3**, J. de Favereau et al., *DELPHES 3, A modular framework for fast simulation of a generic collider experiment*, *JHEP* **1402** (2014) 057, [arXiv:1307.6346].

[87] **ATLAS Collaboration**, *Search for New Phenomena in Monojet plus Missing Transverse Momentum Final States using 10 fb^{-1} of pp Collisions at $\sqrt{s} = 8$ TeV with the ATLAS detector at the LHC*, tech. rep., ATLAS-CONF-2012-147, 2012.

[88] **CMS Collaboration**, *Search for new physics in monojet events in pp collisions at $\sqrt{s} = 8$ TeV*, tech. rep., CMS-PAS-EXO-12-048.

[89] **ATLAS Collaboration**, *Search for squarks and gluinos with the ATLAS detector in final states with jets and missing transverse momentum and 20.3 fb^{-1} of $\sqrt{s} = 8$ TeV proton-proton collision data*, tech. rep., ATLAS-CONF-2013-047, 2013.

[90] **ATLAS Collaboration**, *Search for direct production of the top squark in the all-hadronic ttbar + etmiss final state in 21 fb^{-1} of pp collisions at $\sqrt{s} = 8$ TeV with the ATLAS detector*, tech. rep., ATLAS-CONF-2013-024, 2013.

[91] **CMS Collaboration**, S. Chatrchyan et al., *Search for supersymmetry in hadronic final states with missing transverse energy using the variables α_T and b-quark multiplicity in pp collisions at $\sqrt{s} = 8$ TeV*, arXiv:1303.2985.

[92] **ATLAS Collaboration**, *Search for supersymmetry at $\sqrt{s} = 8$ TeV in final states with jets, missing transverse momentum and one isolated lepton*, tech. rep., ATLAS-CONF-2012-104, 2012.

[93] **ATLAS Collaboration**, *Search for direct top squark pair production in final states with one isolated lepton, jets, and missing transverse momentum in* $\sqrt{s} = 8$ *TeV pp collisions using 21 fb*$^{-1}$ *of ATLAS data*, tech. rep., ATLAS-CONF-2013-037, 2013.

[94] **ATLAS Collaboration**, *Search for strongly produced superpartners in final states with two same sign leptons with the ATLAS detector using 21 fb*$^{-1}$ *of proton-proton collisions at* $\sqrt{s} = 8$ *TeV.*, tech. rep., ATLAS-CONF-2013-007, 2013.

[95] **CMS Collaboration**, S. Chatrchyan et al., *Search for new physics in events with same-sign dileptons and b jets in pp collisions at* $\sqrt{s} = 8$ *TeV*, *JHEP* **1303** (2013) 037, [arXiv:1212.6194].

[96] **ATLAS Collaboration**, G. Aad et al., *ATLAS search for new phenomena in dijet mass and angular distributions using pp collisions at* $\sqrt{s} = 7$ *TeV*, *JHEP* **1301** (2013) 029, [arXiv:1210.1718].

[97] **CMS Collaboration**, S. Chatrchyan et al., *Search for quark compositeness in dijet angular distributions from pp collisions at* $\sqrt{s} = 7$ *TeV*, *JHEP* **1205** (2012) 055, [arXiv:1202.5535].

[98] G. Cowan, K. Cranmer, E. Gross, and O. Vitells, *Asymptotic formulae for likelihood-based tests of new physics*, *Eur.Phys.J.* **C71** (2011) 1554, [arXiv:1007.1727].

[99] A. De Simone, O. Matsedonskyi, R. Rattazzi, and A. Wulzer, *A First Top Partner Hunter's Guide*, *JHEP* **1304** (2013) 004, [arXiv:1211.5663].

[100] M. Buchkremer, G. Cacciapaglia, A. Deandrea, and L. Panizzi, *Model Independent Framework for Searches of Top Partners*, *Nucl.Phys.* **B876** (2013) 376–417, [arXiv:1305.4172].

[101] S. Yang, J. Jiang, Q.-S. Yan, and X. Zhao, *Hadronic* b' *search at the LHC with top and W taggers*, arXiv:1405.2514.

[102] N. G. Ortiz, J. Ferrando, D. Kar, and M. Spannowsky, *Reconstructing singly produced top partners in decays to* Wb, arXiv:1403.7490.

[103] **ATLAS Collaboration**, *Search for pair and single production of new heavy quarks that decay to a Z boson and a third generation quark in pp collisions at* $\sqrt{s} = 8$

TeV with the ATLAS detector, tech. rep., ATLAS-CONF-2014-036, ATLAS-COM-CONF-2014-055, 2014.

[104] **CMS Collaboration**, *Boosted Top Jet Tagging at CMS*, tech. rep., CMS-PAS-JME-13-007, 2014.

[105] **CMS Collaboration**, S. Chatrchyan et al., *Inclusive search for a vector-like T quark with charge $\frac{2}{3}$ in pp collisions at $\sqrt{s} = 8$ TeV*, *Phys.Lett.* **B729** (2014) 149–171, [arXiv:1311.7667].

[106] **CMS Collaboration**, *Search for vector-like top quark partners produced in association with Higgs bosons in the diphoton final state*, tech. rep., CMS-PAS-B2G-14-003, 2014.

[107] **CMS Collaboration**, *Search for top-Higgs resonances in all-hadronic final states using jet substructure methods*, tech. rep., CMS-PAS-B2G-14-002, 2014.

[108] **CMS Collaboration**, *Search for Vector-Like b' Pair Production with Multilepton Final States in pp collisions at sqrt(s) = 8 TeV*, tech. rep., CMS-PAS-B2G-13-003, 2013.

[109] J. M. Butterworth, A. R. Davison, M. Rubin, and G. P. Salam, *Jet substructure as a new Higgs search channel at the LHC*, *Phys.Rev.Lett.* **100** (2008) 242001, [arXiv:0802.2470].

[110] T. Plehn, M. Spannowsky, M. Takeuchi, and D. Zerwas, *Stop Reconstruction with Tagged Tops*, *JHEP* **1010** (2010) 078, [arXiv:1006.2833].

[111] T. Plehn and M. Spannowsky, *Top Tagging*, *J.Phys.* **G39** (2012) 083001, [arXiv:1112.4441].

[112] D. E. Kaplan, K. Rehermann, M. D. Schwartz, and B. Tweedie, *Top Tagging: A Method for Identifying Boosted Hadronically Decaying Top Quarks*, *Phys.Rev.Lett.* **101** (2008) 142001, [arXiv:0806.0848].

[113] D. B. Kaplan and H. Georgi, *SU(2) × U(1) Breaking by Vacuum Misalignment*, *Phys.Lett.* **B136** (1984) 183.

[114] D. B. Kaplan, H. Georgi, and S. Dimopoulos, *Composite Higgs Scalars*, *Phys.Lett.* **B136** (1984) 187.

[115] D. B. Kaplan, *Flavor at SSC energies: A New mechanism for dynamically generated fermion masses*, *Nucl.Phys.* **B365** (1991) 259–278.

[116] R. Contino, T. Kramer, M. Son, and R. Sundrum, *Warped/composite phenomenology simplified*, *JHEP* **0705** (2007) 074, [`hep-ph/0612180`].

[117] K. Agashe, R. Contino, and A. Pomarol, *The Minimal composite Higgs model*, *Nucl.Phys.* **B719** (2005) 165–187, [`hep-ph/0412089`].

[118] R. Contino, L. Da Rold, and A. Pomarol, *Light custodians in natural composite Higgs models*, *Phys.Rev.* **D75** (2007) 055014, [`hep-ph/0612048`].

[119] M. S. Carena, E. Ponton, J. Santiago, and C. Wagner, *Electroweak constraints on warped models with custodial symmetry*, *Phys.Rev.* **D76** (2007) 035006, [`hep-ph/0701055`].

[120] J. Li, D. Liu, and J. Shu, *Towards the fate of natural composite Higgs model through single t' search at the 8 TeV LHC*, *JHEP* **1311** (2013) 047, [`arXiv:1306.5841`].

[121] N. Vignaroli, *Early discovery of top partners and test of the Higgs nature*, *Phys.Rev.* **D86** (2012) 075017, [`arXiv:1207.0830`].

[122] M. Endo, K. Hamaguchi, K. Ishikawa, and M. Stoll, *Reconstruction of Vector-like Top Partner from Fully Hadronic Final States*, `arXiv:1405.2677`.

[123] S. Beauceron, G. Cacciapaglia, A. Deandrea, and J. D. Ruiz-Alvarez, *Fully hadronic decays of a singly produced vector-like top partner at the LHC*, `arXiv:1401.5979`.

[124] B. Gripaios, T. Mueller, M. Parker, and D. Sutherland, *Search Strategies for Top Partners in Composite Higgs models*, `arXiv:1406.5957`.

[125] J. Aguilar-Saavedra, *Identifying top partners at LHC*, *JHEP* **0911** (2009) 030, [`arXiv:0907.3155`].

[126] A. Azatov, M. Salvarezza, M. Son, and M. Spannowsky, *Boosting Top Partner Searches in Composite Higgs Models*, *Phys.Rev.* **D89** (2014) 075001, [`arXiv:1308.6601`].

[127] R. Contino and G. Servant, *Discovering the top partners at the LHC using same-sign dilepton final states*, *JHEP* **0806** (2008) 026, [`arXiv:0801.1679`].

[128] J. Mrazek and A. Wulzer, *A Strong Sector at the LHC: Top Partners in Same-Sign Dileptons*, *Phys.Rev.* **D81** (2010) 075006, [`arXiv:0909.3977`].

[129] J. Kearney, A. Pierce, and J. Thaler, *Top Partner Probes of Extended Higgs Sectors*, *JHEP* **1308** (2013) 130, [`arXiv:1304.4233`].

[130] C. Han, A. Kobakhidze, N. Liu, L. Wu, and B. Yang, *Constraining Top partner and Naturalness at the LHC and TLEP*, `arXiv:1405.1498`.

[131] S. Gopalakrishna, T. Mandal, S. Mitra, and G. Moreau, *LHC Signatures of Warped-space Vectorlike Quarks*, *JHEP* **1408** (2014) 079, [`arXiv:1306.2656`].

[132] G. Brooijmans, R. Contino, B. Fuks, F. Moortgat, P. Richardson, et al., *Les Houches 2013: Physics at TeV Colliders: New Physics Working Group Report*, `arXiv:1405.1617`.

[133] J. Alwall, R. Frederix, S. Frixione, V. Hirschi, F. Maltoni, et al., *The automated computation of tree-level and next-to-leading order differential cross sections, and their matching to parton shower simulations*, `arXiv:1405.0301`.

[134] T. Sjoestrand, S. Mrenna, and P. Z. Skands, *A Brief Introduction to PYTHIA 8.1*, *Comput.Phys.Commun.* **178** (2008) 852–867, [`arXiv:0710.3820`].

[135] M. Cacciari, G. P. Salam, and G. Soyez, *FastJet User Manual*, *Eur.Phys.J.* **C72** (2012) 1896, [`arXiv:1111.6097`].

[136] M. Cacciari and G. P. Salam, *Dispelling the N^3 myth for the k_t jet-finder*, *Phys.Lett.* **B641** (2006) 57–61, [`hep-ph/0512210`].

[137] M. Aliev, H. Lacker, U. Langenfeld, S. Moch, P. Uwer, et al., *HATHOR: HAdronic Top and Heavy quarks crOss section calculatoR*, *Comput.Phys.Commun.* **182** (2011) 1034–1046, [`arXiv:1007.1327`].

[138] P. Kant, O. Kind, T. Kintscher, T. Lohse, T. Martini, et al., *HATHOR for single top-quark production: Updated predictions and uncertainty estimates for single top-quark production in hadronic collisions*, `arXiv:1406.4403`.

[139] S. Catani, F. Krauss, R. Kuhn, and B. Webber, *QCD matrix elements + parton showers*, *JHEP* **0111** (2001) 063, [`hep-ph/0109231`].

[140] L. Loennblad, *Correcting the color dipole cascade model with fixed order matrix elements*, *JHEP* **0205** (2002) 046, [hep-ph/0112284].

[141] L. Loennblad and S. Prestel, *Matching Tree-Level Matrix Elements with Interleaved Showers*, *JHEP* **1203** (2012) 019, [arXiv:1109.4829].

[142] S. Catani, L. Cieri, G. Ferrera, D. de Florian, and M. Grazzini, *Vector boson production at hadron colliders: a fully exclusive QCD calculation at NNLO*, *Phys.Rev.Lett.* **103** (2009) 082001, [arXiv:0903.2120].

[143] A. Kardos, Z. Trocsanyi, and C. Papadopoulos, *Top quark pair production in association with a Z-boson at NLO accuracy*, *Phys.Rev.* **D85** (2012) 054015, [arXiv:1111.0610].

[144] J. Campbell, R. K. Ellis, and R. Roetsch, *Single top production in association with a Z boson at the LHC*, *Phys.Rev.* **D87** (2013), no. 11 114006, [arXiv:1302.3856].

[145] **ATLAS Collaboration**, G. Aad et al., *Search for anomalous production of prompt like-sign lepton pairs at $\sqrt{s} = 7$ TeV with the ATLAS detector*, *JHEP* **1212** (2012) 007, [arXiv:1210.4538].

[146] G. Choudalakis, *On hypothesis testing, trials factor, hypertests and the BumpHunter*, arXiv:1101.0390.

[147] H.-C. Cheng and Z. Han, *Minimal Kinematic Constraints and m(T2)*, *JHEP* **0812** (2008) 063, [arXiv:0810.5178].

[148] L. Harland-Lang, C. Kom, K. Sakurai, and W. Stirling, *Measuring the masses of a pair of semi-invisibly decaying particles in central exclusive production with forward proton tagging*, *Eur.Phys.J.* **C72** (2012) 1969, [arXiv:1110.4320].

[149] L. Harland-Lang, C. Kom, K. Sakurai, and W. Stirling, *Mass Shell Technique for Measuring Masses of a Pair of Semi-Invisibly Decaying Particles*, *Phys.Rev.Lett.* **108** (2012) 181805, [arXiv:1202.0047].

[150] W. S. Cho, K. Choi, Y. G. Kim, and C. B. Park, *Gluino Stransverse Mass*, *Phys.Rev.Lett.* **100** (2008) 171801, [arXiv:0709.0288].

[151] W. S. Cho, K. Choi, Y. G. Kim, and C. B. Park, *Measuring superparticle masses at hadron collider using the transverse mass kink*, *JHEP* **0802** (2008) 035, [`arXiv:0711.4526`].

[152] A. J. Barr, B. Gripaios, and C. G. Lester, *Weighing Wimps with Kinks at Colliders: Invisible Particle Mass Measurements from Endpoints*, *JHEP* **0802** (2008) 014, [`arXiv:0711.4008`].

[153] P. Konar, K. Kong, K. T. Matchev, and M. Park, *Superpartner Mass Measurement Technique using 1D Orthogonal Decompositions of the Cambridge Transverse Mass Variable* M_{T2}, *Phys.Rev.Lett.* **105** (2010) 051802, [`arXiv:0910.3679`].

[154] T. Cohen, E. Kuflik, and K. M. Zurek, *Extracting the Dark Matter Mass from Single Stage Cascade Decays at the LHC*, *JHEP* **1011** (2010) 008, [`arXiv:1003.2204`].

[155] **ATLAS Collaboration**, G. Aad et al., *Search for the neutral Higgs bosons of the Minimal Supersymmetric Standard Model in pp collisions at* $\sqrt{s} = 7$ *TeV with the ATLAS detector*, *JHEP* **1302** (2013) 095, [`arXiv:1211.6956`].

[156] T. Hahn, S. Heinemeyer, W. Hollik, H. Rzehak, and G. Weiglein, *FeynHiggs 2.7*, *Nucl.Phys.Proc.Suppl.* **205-206** (2010) 152–157, [`arXiv:1007.0956`].

[157] M. Cacciari, M. Czakon, M. Mangano, A. Mitov, and P. Nason, *Top-pair production at hadron colliders with next-to-next-to-leading logarithmic soft-gluon resummation*, *Phys.Lett.* **B710** (2012) 612–622, [`arXiv:1111.5869`].

[158] J. M. Campbell, R. K. Ellis, and C. Williams, *Vector boson pair production at the LHC*, *JHEP* **1107** (2011) 018, [`arXiv:1105.0020`].

[159] C. Lester and D. Summers, *Measuring masses of semiinvisibly decaying particles pair produced at hadron colliders*, *Phys.Lett.* **B463** (1999) 99–103, [`hep-ph/9906349`].

[160] M. E. Peskin and D. V. Schroeder, *An Introduction to quantum field theory.* 1995.

[161] S. R. Coleman and E. J. Weinberg, *Radiative Corrections as the Origin of Spontaneous Symmetry Breaking*, *Phys.Rev.* **D7** (1973) 1888–1910.

[162] **ATLAS Collaboration**, *Search for the Standard Model Higgs boson produced in association with a vector boson and decaying to bottom quarks with the ATLAS detector*, tech. rep., ATLAS-CONF-2012-161, 2012.

[163] **ATLAS Collaboration**, *Search for the Standard Model Higgs boson produced in association with top quarks in proton-proton collisions at* $\sqrt{s} = 7$ *TeV using the ATLAS detector*, tech. rep., ATLAS-CONF-2012-135, 2012.

[164] **ATLAS Collaboration**, *Search for the Standard Model Higgs boson in H-> tau tau decays in proton-proton collisions with the ATLAS detector*, tech. rep., ATLAS-CONF-2012-160, 2012.

[165] **ATLAS Collaboration**, *Measurements of the properties of the Higgs-like boson in the* $WW^{(*)} \to \ell\nu\ell\nu$ *decay channel with the ATLAS detector using 25* fb^{-1} *of proton-proton collision data*, tech. rep., ATLAS-CONF-2013-030, 2013.

[166] **ATLAS Collaboration**, *Measurements of the properties of the Higgs-like boson in the four lepton decay channel with the ATLAS detector using 25* fb^{-1} *of proton-proton collision data*, tech. rep., ATLAS-CONF-2013-013, 2013.

[167] **ATLAS Collaboration**, *Observation of an excess of events in the search for the Standard Model Higgs boson in the gamma-gamma channel with the ATLAS detector*, tech. rep., ATLAS-CONF-2012-091, 2012.

[168] **ATLAS Collaboration**, *Measurements of the properties of the Higgs-like boson in the two photon decay channel with the ATLAS detector using 25* fb^{-1} *of proton-proton collision data*, tech. rep., ATLAS-CONF-2013-012, 2013.

[169] A. Azatov and J. Galloway, *Electroweak Symmetry Breaking and the Higgs Boson: Confronting Theories at Colliders*, *Int.J.Mod.Phys.* **A28** (2013) 1330004, [`arXiv:1212.1380`].

[170] **CMS Collaboration**, *Search for the standard model Higgs boson produced in vector boson fusion, and decaying to bottom quarks*, tech. rep., CMS-PAS-HIG-13-011, 2013.

[171] **CMS Collaboration**, *Search for the standard model Higgs boson produced in association with W or Z bosons, and decaying to bottom quarks*, tech. rep., CMS-PAS-HIG-13-012, 2013.

[172] **CMS Collaboration**, *Search for Higgs boson production in association with top quark pairs in pp collisions*, tech. rep., CMS-PAS-HIG-12-025, 2012.

[173] **CMS Collaboration**, *Search for the Standard-Model Higgs boson decaying to tau pairs in proton-proton collisions at* $\sqrt{s} = 7$ *and* 8 *TeV*, tech. rep., CMS-PAS-HIG-13-004.

[174] **CMS Collaboration**, *Evidence for a particle decaying to W+W- in the fully leptonic final state in a standard model Higgs boson search in pp collisions at the LHC*, tech. rep., CMS-PAS-HIG-13-003.

[175] **CMS Collaboration**, *Properties of the Higgs-like boson in the decay H to ZZ to 4l in pp collisions at* $\sqrt{s} = 7$ *and* 8 *TeV*, tech. rep., CMS-PAS-HIG-13-002.

[176] **CMS Collaboration**, *Updated measurements of the Higgs boson at 125 GeV in the two photon decay channel*, tech. rep., CMS-PAS-HIG-13-001.